# Exploring new routes to decoherence-free quantum computing; and quantum thermodynamics for fermions

by

Marvellous Onuma-Kalu

A thesis
presented to the University of Waterloo
in fulfillment of the
thesis requirement for the degree of
Doctor of Phyilosophy
in
Physics

Waterloo, Ontario, Canada, 2020

**Examining Committee Membership**

The following served on the Examining Committee for this thesis. The decision of the Examining Committee is by majority vote.

| | |
|---|---|
| External Examiner | Karl-Peter Marzlin,<br>Professor, Department of Physics<br>St Francis Xavier University |
| Supervisor | Robert Mann<br>Professor, Department of Physics and Astronomy<br>University of Waterloo |
| Committee member | Kevin Resch,<br>Professor, Department of Physics and Astronomy<br>University of Waterloo |
| Committee member | Eduardo Martín-Martínez<br>Assitant Professor, Department of Applied Mathematics<br>University of Waterloo |
| Internal/External examiner | Achim Kempf<br>Professor, Department of Applied Mathematics<br>University of Waterloo |

## Author's Declaration

The thesis consist of material all of which I authored or co-authored: see Statement of Contributions included in the thesis. This is a true copy of the thesis, including any required final revisions, as accepted by my examiners.

I understand that my thesis may be made electronically available to the public.

## Statement of Contribution

Two sections in Chapter 4 consist of material produced in different collaborations. The first 4.2 consists of materials from the paper [33], co-authored with Paulina Corona-Ugalde and Robert Mann. The second 4.3 consists of material from the paper [89], co-authored with Kae Nemoto, W. J. Munro, and Robert Mann.

Chapter 6 consists of material from the paper [96], co-authored with Robert Mann.

Chapter 7 consists of material from the paper [95], co-authored with Daniel Grimmer, Robert Mann and Eduardo Martín-Martínez.

## Abstract

This thesis has two parts; the first part is a contribution to the research field of quantum measurement in quantum optics while the second part focuses on quantum thermodynamics for fermionic systems.

The aim of the research on quantum optics is to detect and subsequently characterize quantum states of light. Specifically, we focus on characterizing 1) entanglement between a two-level atom and superposition of coherent states (known as Bell cat state) 2) quantum superposition of coherent states (Schrödinger cat states). The photon is the particle of light which carries quantum information; it is usually lost (destroyed) while being detected. Many physical implementations of quantum logic gate aim to encode quantum information processing into large registers of entangled qubits. However for these larger much distinguishable states, creating and preserving entanglement becomes difficult due to rapid onset of decoherence. Encoding quantum information on Schrodinger's cat states take advantage of a cavity resonators much larger Hilbert space, as compared with that of a two-level system. This architecture allows redundant qubit encodings that can simplify the operations needed to initialize, manipulate and measure the encoded information. For such a system to be viable as a quantum computing platform, efficient measurement of such encoded qubit observables must be possible.

The concept of quantum non demolition measurement was introduced to evade the problem of decoherence. Researchers now know through quantum theory that it is indeed possible to count photons in a given state of light without destroying them. This nondestructive measurement scheme is coined in the term "quantum non-demolition measurement". We can extend the ideas of quantum nondemolition measurement scheme to detect a system made up of two or more quantum states (not necessarily states of light) that are combined based on the superposition principle. An example is the Schrödinger's cat state which is a superposition of two coherent states of light of equal amplitudes but opposite phase. At this point, one is not only interested in counting photons, but in understanding the nature of the superposition, the possible problems and the different physical properties that follow. Ways to detect the Schrödinger cat states and subsequently a Bell cat state (Schrödinger cat entangled with a qubit) without significantly perturbing them are discussed. The method analyzed is the mode-invisibility measurement scheme earlier proposed to detect single Fock states and coherent states of light. The method gives a new insight to the known properties of Schrödinger cat states and contributes to our understanding of the quantum-classical boundary problem.

The second part of the thesis falls in the research field of quantum thermodynamics and open quantum systems. Most problems in quantum thermodynamics have been explored in

bosonic systems with little or less done in fermionic systems. Therefore the aim of this part of the thesis is to explore related quantum thermodynamical problems in fermionic systems. I begin by considering the problem of work extraction from noninteracting fermionic systems. For work to be extracted from the state of a quantum system, a unitary operation on the state must act to reduce the average energy of the system. Passive states are those states whose energy cannot be reduced through unitary transformation, that is work cannot be extracted via unitary transformations given only a single copy of the system. It follows that some passive states may have extractable work if several copies of the system is processed. Passive states for which no work can be extracted, no matter the number of available copies, are called completely passive states. An example is the thermal Gibbs state. Here, the limit for which multiple copies of passive states in fermionic systems can be activated for work extraction is studied. It was observed for $n \geq 3$ fermionic modes at the same frequency, the product state of $n$ thermal states with different temperatures is not passive. This in principle implies that the construction of a heat engine in fermionic systems need access to three thermal baths at different temperature. This is unlike the bosonic system, where access to only two thermal baths are required.

On the other hand, while the product state of three thermal states of three fermionic modes at the same frequency but different temperatures is not passive, the unitary transformation required to extract work from the state is difficult to realize. A set of operations that are easier to realize are Gaussian unitaries which are generated by Hamiltonian that are at most quadratic in the system's operators. One may consider extracting work via the restricted class of Gaussian unitaries. Hence fermionic Gaussian passive states for which energy cannot be extracted using only Gaussian operations are characterized.

The last problem I investigate is that of understanding the dynamics of an open Markovian non-interacting fermionic system. I introduce a classification scheme for the generators of open fermionic Gaussian dynamics and simultaneously partition the dynamics along the following four lines: 1) unitary vs. non-unitary, 2) active vs. passive, 3) state-dependent vs. state-independent, and 4) single-mode vs. multi-mode. Unlike in the bosonic case where only eleven of these sixteen types of dynamics turn out to be possible, one observe only nine types of dynamics in the fermionic setting. Using this partition I discuss the consequences of imposing complete positivity on fermionic Gaussian dynamics. In particular, I show that completely positive dynamics must be either unitary (and so can be implemented without a quantized environment) or active (and so must involve particle exchange with an environment).

**Acknowledgements**

I would like to acknowledge the University of Waterloo, for hosting this project. My profound gratitude goes out to all Research Fund and the government agency; "Natural Sciences and Engineering Research Council (NSERC)", for helping and providing the funding for the work. Without your funding; this project could not have reached its goal.

To my supervisor, Professor Robert Mann: his qualities are beyond compare. I am grateful for his continuous support, his patience, and immense knowledge. His guidance helped me in all the time of research and writing this thesis. I could not have imagined having a better advisor and mentor for my graduate studies.

I wish to appreciate my PhD/thesis committee: Professors' Karl-Peter Marzlin, Achim Kempf, Kevin Resch and Eduardo Martín-Martínez, for their insightful comments and recommendations which from various perspectives helped me widen my research and improved the writing of this thesis. I also acknowledge Professor Kae Nemoto of the National Institute of Informatics (NII), Tokyo, Japan, who provided me an opportunity to join her research group as intern. I also appreciate the helpful comments from Bill Munro, who made me see my theoretical research from an experimental view.

I wish to acknowledge a special woman, my landlady; Nancy Mann for her moral support, encouragement and understanding at all times. Living at her home was comforting, loving and peaceful. I am indebted to her for accommodating me.

Along the line during the Phd program, I started my family and had two children in the process. As a mother and graduate student, one could have imagined the possibility of completing my Phd program. Yes, it got tough and quite challenging trying to balance academic life and family. There were several days I felt like quitting, but for the amazing support from my fellow Nigerians in Waterloo whom I am indebted to and wish to acknowledge: Mr Okoli and family, Professor Felix Nwaishi and family, Dr Chike Okonkwo and family. And to my closest friends Dr Joachim Nsofini, Christian, Chukwuemeka, Fidelia, Chioma Emeka, Jessica Achebe, Mrs Jones, Joyce, and Liza, thank you for the love and immense support.

In memory of the dear ones who supported, encouraged and believed in me but are not here to see the completion of the program: my granddad, Benedict Duru; and father-in-law, Hilary Onwuka Alikeh. Thank you my fathers. To the one so dear to my heart, friend, sister and fellow physicist, late Dr Chiamaka Okoli; you were a blessing to me Chi. I sincerely miss your moral and emotional support in my life. May your souls continue to Rest In Peace.

Finally to my very large family whom I have dedicated this thesis to; “you all rock”! Thank you all for the laughter, joy, fervent prayers, belief, assistance and support. To my beautiful mother, Jacinta Onuma-Kalu Eleanya, you are a perfect description of a role-model, I appreciate your sacrifices mum; my sisters, Oleka Kalu-Onuma, your sacrifices-shuffling between Manchester, United Kingdom and Canada during your holidays to support my family and I, are highly appreciated; Mrs Elizabeth Izuchukwu-Iluoze, thank you for the constant reminder that it ‘only gets better’. I also acknowledge the encouragement from my mother-in-law Mrs Ann Alikeh, your prayers for me were answered mama, thank you. To my beloved husband-Oscar Michael Okechukwu Iheshiulor and dear children Michael Chinedu Okechukwu-Iheshiulor and Sarah Chizoba Okechukwu-Iheshiulor, thank you for your love, support motivation, understanding and corporation. “We did it!”

Most especially to my creator and advocate, the almighty God through whom all things were made possible and to whom I owe all, I am grateful.

## Dedication

To my family.

# Table of Contents

# List of Tables

# List of Figures

# Chapter 1

# Overview

## Part one

Quantum computing is essentially harnessing and exploiting the laws of quantum mechanics to process information. *What is this information? How is the information processed? What quantum mechanical laws are applicable? Why quantum mechanics instead of the traditional classical mechanics?* The mere act of answering these questions opens up new problems; new questions arise as researchers attempt to find answers and solutions to problems. Two central research directions come to play:

- *Experimental*: here the goal is to build quantum devices with specified behaviour
- *Theoretical*:
  - Designing algorithms that use quantum mechanical phenomena for computation
  - Designing protocols for transmitting and processing quantum information

In this thesis, we do not attempt to answer the above questions, but we will give insight concerning various issues relevant to these questions. Our direction is theoretical, proposing schemes for efficient quantum information processing. In processing information, natural questions arise, such as the following. How much memory do I need to store my information? What is the amount of time needed to process the information? What class of operations are possible? Can I reliably send a message through a noisy line?

Quantum information processing [93] is the act of processing information based on the principles of quantum physics that are not tractable by classical theories. By definition,

quantum theories describe nature at the microscopic scale while classical theories do so at the macroscopic scale. The resulting advantage of processing information based on quantum theories is that the quantum resources needed are proportionally much smaller than the associated classical resources.

The fundamental units of information such as the bits for classical information or qubits for quantum information can be described by what we know as states. A state is a property that encodes certain information about a system, such as a particle's motion or behaviour. While a classical bit (the basic unit of classical information) is limited to only two states, quantum physics allows a qubit (the basic unit of quantum information ) to exist in a *superposition* of states simultaneously [93]. One might wonder what this superposition implies as to quantum information processing. The existence of the qubit in a superposition provides advantage in that with smaller resources, it becomes possible to store more information in a quantum system. The superposition effectively offers a computational parallelism, where it becomes possible to perform computations at high speed and with greater efficiency. Intuitively, the future of quantum computing and communication technology relies on the principle of superposition to create quantum computers.

In spite of this potential, generating superpositions of states is experimentally and theoretically challenging. Quantum state superpositions can be very fragile: any interaction with the environment can perturb the state and cause it to rapidly decohere to a mere statistical mixture. In fact the difficulty in generating a macroscopic quantum state superposition is the basic reason why quantum computers are hard to build. A quantum computer will need to repeatedly alter the states of its qubits in the course of any computation it carries out. Without proper care, these alterations could act as a measurement processes that project out a particular part of the superposition, taking a quantum computer back to a classical one. Scientists need to realize ways to access the superposition states and manipulate them with suitable tools.

Interestingly, in addition to quantum superpositions, quantum physics also allows for the existence of entanglement (quantum correlations) [93] between macroscopic and microscopic objects. Hence a (macroscopic) quantum state superposition can be entangled with a (microscopic) atom through an interaction process. Such entanglement makes it possible to manipulate this superposition of states by manipulating the atom. The prototypical example is the Schrödinger's cat gedanken thought experiment [118], where a living cat is trapped together with a radioactive atom in a box. Two processes are possible in the box: either the atom decays and triggers a death mechanism that kills the cat, or the atom does not decay and the cat remains alive. In quantum physics, we say the atom's decay occurs at some time given by its half-life – at this time the atom has a 50% probability of decaying. Before observation, the atom is in a superposed state of decay or not; consequently,

the time of death of the cat is unknown until an observation is made (that is the box is opened). In principle, a measurement apparatus that is capable of measuring the state of the atom to be in superposition immediately projects the cat into a superposition of life and death. The observation thus transfers the superposition state of the microscopic atom into the macroscopic classical world.

This brings us to the phenomenon of entanglement. Now suppose that instead of a single cat in the box, we have two cats in two different boxes. Again applying the Schrödinger's cat experiment to this pair of cats, we expect one of four possible outcomes. Either both cats are alive, or both cats are dead, or one is alive and the other dead or vice versa, all with equal probability if this larger system is observed during at the half-life of the atom. Prior to observation we say the system of both cats is again in a superposition of states. Quantum mechanics tells us that it is possible, for example, to eliminate the outcome of the two cats being both alive or both dead from the superposition. We then have a two cat system such that the outcome would always be one cat alive and the other cat dead. The state of one cat becomes correlated with the state of the other, such as if one cat is measured to be alive, then the other cat is definitely dead. This phenomena is known as *quantum entanglement* [93] and has some amazing implications. An application of this includes secure transfer of information because any change in one particle (due to an eavesdropper, for example) would be seen in the other immediately.

The Schrödinger's cat thought experiment can actually be realized in an atom-cavity system by a superposition of coherent states (of light) that are macroscopically (classically) distinguishable. This entangled superposition state is known as a Schrödinger's cat state. Such states play an important role in understanding the classical to quantum boundary, and in quantum information tasks including quantum computation [108, 52], quantum teleportation [10], quantum error correction [11, 9], and precision measurements [92]. Just like other quantum state superpositions, generating a macroscopically distinguishable superposition of coherent states can be experimentally challenging. Macroscopic quantum state superpositions of coherent states will decohere to a statistical mixture of coherent states due to any interaction with the environment.

In generating quantum superpositions of coherent states, two things are required. 1) For fundamental tests of quantum field theory, we need cat states with large amplitudes (greater than or equal to 2). 2) For applications in quantum information processing, we require quantum superpositions of coherent states with high fidelity (greater than 0.99). Thanks to developments of the quantum theory of light, we have a better understanding of the nonclassical properties of superpositions of states [120, 119]. High quality cavities are now available to trap and manipulate microwave photons. In recent years, quantum superpositions of coherent states have been generated from an interaction of these trapped

photons with Rydberg atoms [68] crossing the cavity [120, 134]. Such interactions, which belong to the domain of cavity quantum electrodynamics (CQED) [12], represent fundamental aspects of measurement theory. While superpositions of coherent states have been generated in this way, only those with small amplitudes have been realized. Recently, a simple observation was made that small amplitudes such as $\alpha < 1.2$ are well approximated as squeezed single photons. On the other hand, squeezed single photons can be generated through addition and subtraction of photons from a squeezed vacuum state [85]. This motivated the generation of single-photon subtracted squeezed states that are close to superpositions of coherent states with small amplitudes ($\alpha \leq 1$). Today there are several proposals to generate squeezed superpositions of coherent states with large amplitudes Such states are more robust against decoherence than the regular quantum superposition of coherent states.

The first part of this thesis is aimed at measuring a superposition of squeezed coherent states. My aim is to propose a scheme that detects the two quantum superposition of states without significantly altering the state superposition or the entanglement structure. To go about this, I apply the recently proposed Mode Invisibility (MI) measurement scheme [97], which is based on the ideas of quantum nondemolition (QND) measurement [16, 35, 56]. The scheme makes use of methods in CQED; in an interferometric setting, a Fock state trapped in a cavity mode is detected by a resonant two-level atom crossing the cavity. By taking advantage of the cavity's geometry it was observed that a two-level atom in a resonant interaction with the cavity mode gains information about the cavity field. This idea was extended in [98] to detect coherent states of light. I will extend the MI measurement scheme to the measurement of quantum superpositions of coherent states. Intuitively, it is generally believed that I cannot observe quantum superpositions at macroscopic scale. I show through the MI measurement scheme that I can achieve distinguishability of the two coherent states even if their amplitudes are large. I exploit nonlinear effects to squeeze these superpositions of coherent states and find sensitivity to their quantum features (including phase and amplitude) as well as non-classical effects associated with their superposition. I show that the problem of decoherence inherent in measurement involving superposition of coherent states can be circumvented. Our research gives a new insight to the known properties of Schrödinger cat states and contributes to our understanding of the quantum-classical boundary problem.

I then proceed to apply the MI measurement scheme to detect an entangled superposition of coherent states, also known as a Bell cat state [134]. Investigating the dynamics of the system using a quantum 2-level probe, I demonstrate a way to non-destructively measure a number of properties of the Bell cat state including the amplitude of the coherent state, the location and relative excitation of the qubit, and the von Neumann entropy.

These results indicate a connection between this last quantity and the interferometric phase shift of the probe, thereby suggesting a possible way to experimentally measure entanglement non-destructively.

### Outline

The outline of the first part of the thesis is as follows. In chapter 2, I introduce the concepts of superposition and entanglement. Chapter 3 focuses on the background of our study. There we give a detailed discussion on two-level systems. I also presented the electromagnetic (EM) field and how they are quantized in a cavity. Next we described two important quantum states of EM field: the Bell cat state [134] and the Schrödinger's cat state [118] respectively. Finally I present the Unruh-deWitt model [87] for describing interactions between two-level atom and our relevant quantum states of the EM-field. I conclude this chapter with a brief review of the QND measurement idea [16, 49, 113], that characterizes a non-destructive measurement of quantum states of the EM field. Chapter 4 is devoted to my contributions to realizing a QND measurement for Bell-cat states and Schrödinger cat states respectively. I begin by reviewing the mode-invisibility (MI) measurement scheme [97, 98]. Then we present two papers from our theoretical study. The first paper [33] proposed using the MI scheme to characterize the Bell-cat states while the second paper 2 [95] is a proposal to characterize the Schrödinger's cat states. We present the results of the measurement proposals and discuss our findings.

## Part two

This part of the thesis investigates quantum thermodynamics for fermionic systems. In general, due to the complexity of the structure of fermionic systems, the bosonic system have being a common system where most quantum thermodynamical problems have been explored in recent years. Some of the problems which are of interest include work extraction from quantum systems [22] and dynamics of open quantum systems [58]. Hence it is my aim here to explore the case for fermionic systems.

In the quantum thermodynamical concept, work is said to be done if the average energy of the system is reduced by a unitary operation acting on the system. From the so-called passive states, no work can be extracted if only a single copy of the system is available. That is, given a single copy, the average energy of a passive state cannot be reduced by a unitary operation acting on it. However, some passive state may have extractable energy if

several copies of the system are processed together by a global unitary operation. Passive states for which no work can be extracted, no matter the number of available copies, are called completely passive states – an example is the thermal Gibbs state. This implies that any device for unitary work extraction must be out-of equilibrium. In the bosonic setting, the simplest out-of-equilibrium cycle engine for unitary work extraction is a heat engine which requires minimum access to two thermal baths at different temperatures. We will show that this is not the case for two fermionic modes. Instead the minimum number of baths required to construct a heat engine in the fermionic setting is three [96].

On the other hand, although work can be extracted from non-passive states the unitary transformation required for this process is difficult to realize. Given that Gaussian unitaries are easily generated, one may consider extracting work via the restricted class of Gaussian unitaries, this introduces us to the notion of Gaussian passivity [22].

The idea of Gaussian passivity is to extract work from quantum systems via Gaussian unitary transformations, which is believed to be easy to realize. In this context, bosonic Gaussian passive states (and non-Gaussian passive states), from which no (or maximal) work can be extracted using a Gaussian unitary transformation, were defined [22]. In this thesis I investigate the corresponding situation for fermionic systems. The main aim is to see how useful a fermionic system is for work extraction. I characterize general quantum states in fermionic systems according to their ability to yield work (or not) under such transformations.

Finally I direct my attention towards understanding the dynamics of open quantum systems. An open quantum system is one that is in constant interaction with its environment via exchange of energy or particles. As I have discussed earlier, physical quantum systems are subject to decoherence and dissipation as a result of their noisy interaction with the environment. This practically implies that the operation of any realistic quantum information devices (quantum computer for example) would be accompanied by noise and by loss of quantum information into the environment. Hence understanding the full dynamics of the system + environment and is challenging.

Gaussian quantum mechanics (GQM), offers a powerful tool for understanding the dynamics of an open system because of the simple mathematical structure. The basic tools of GQM are Gaussian states and the corresponding Gaussian operations. Using these tools, the dynamics of an open bosonic system has been investigated. We extend this tools to characterize the dynamics of open Markovian non-interacting fermionic system. I introduce a classification scheme for the generators of the open fermionic Gaussian dynamics. I simultaneously partition the dynamics along the following four dichotomies: 1) unitary vs. non-unitary depending 2) active vs. passive, 3) state-dependent vs. state-independent,

and 4) single-mode vs. multi-mode. Only nine of these sixteen types of dynamics turn out to be possible unlike in the bosonic case where eleven types of dynamics are possible.

## Outline

This part two of the thesis is structured as follows. In chapter 5, we present basic notations and the definition of fermionic systems, including the algebra associated with fermionic systems and their corresponding fermionic operators. Next Gaussian states and Gaussian operations which are the tools for GQM are presented. Finally an application of GQM for performing tasks such as energy extraction is discussed in chapter 6, and chapter 7 focuses on classification of Markovian fermionic Gaussian master equations. We close the thesis with conclusions discussing some future directions from the two parts.

# Part I

# Superposition, entanglement, and mode invisibility measurement.

# Chapter 2

# Quantum superposition and entanglement

## 2.1 Introduction

*The concept of linear superposition holds true for quantum particles but fails for classical particles. While we know that photon (a quantum particle of light) can simultaneously be in two possible states, a table (a classical object) is never found in two places at the same time. Why?*

Quantum particles are described by probabilities, which are complex numbers with phase and amplitude. A typical measurement on a quantum system will yield a probability amplitude that corresponds to partial amplitudes from different quantum states of the system. The partial amplitudes add to each other or cancel each other depending on their relative phases. This leads to interference effects; the characteristic property of microscopic systems that in a way describe the wave-like properties of quantum particles. Around the 19th century, the concept of wave-like properties in light was established. Louis de Broglie in his hypothesis related wavelength and momentum [37]:

$$\lambda = \frac{h}{p} \tag{2.1}$$

where $p$ is the momentum of light and $h$ is Planck's constant. His hypothesis was not generally accepted until 1801 when Thomas Young performed his double-slit interference

experiment with light [121]. In his experiment, a beam of light (with momentum $p$ and wavelength (2.1)) from a single source is fired at a screen with two narrow slits separated by a distance $a$, and each having a width of the order of the de Broglie wavelength (2.1). These slits define two distinct paths for the light. On a detection screen that records the impact of the incoming beam, an interference pattern was observed establishing the wave nature of light. This interference experiment has being reproduced with other quantum particles such as atoms, electrons and molecules, and light. A major concern in the interference experiment is that each particle crossing the double slit seemed to talk to each other. If one of the slit is closed, one does not observe the interference effect. A classical mind would ask the question, through which slit did a given atom cross the scree? A quantum description of this spooky action is that each particle crosses the screen in a quantum superposition of two states corresponding to each to a wave packet going through one of the slits.

Before the end of the 19th century, while scientists understood light to be made of waves, Max Planck and co workers in their study of the photoelectric effect [121] found that certain types of materials will eject electrons (photoelectrons) if light of certain frequency shines on them. Planck and coworkers could not find explanations for these observations, namely that there was a minimum wavelength of light that could eject electrons from the metal surfaces. Any wavelength of light above this minimum has no effect even if the intensity of light is increased. It was at this point that Albert Einstein proposed that light behaves as particles (or quanta) that he called photons. He observed that the photoelectric effect could be explained by associating the photon (a particle of light) with discrete energy

$$E_{\text{photon}} = h\nu \tag{2.2}$$

in an electric field, which the electrons in the metal absorb. Here the frequency of light $\nu$ is related to the energy $E$ of each individual photon via Planck's constant $h$.

However light also had wave-like properties, and soon the notion of wave-particle duality emerged. A natural consequence of the wave-particle duality was recognized by Heisenberg in what we now call the uncertainty principle: it is impossible to predict, measure, or know simultaneously the exact position and exact momentum of an object. Intuitively, the wave-like property of an object is associated with a very large region of space (no fixed position) with precise momentum, while the particle-like property of the same object is associated with a (fixed position) small region of physical space. Adding several waves of different frequencies yields a resultant wave which may be more localized (fixed position), however with unknown momentum. This is a paradox: the behaviour of a photon becomes unpredictable, and measurement of its properties is only possible with some particular

likelihood or probability. Hence a unified theory of wave-particle duality whereby the apparent paradox is resolved was sought for.

In an attempt to reconcile the wave-particle duality of light and explain the behaviour of atomic particles, Erwin Schrödinger proposed his probability wave theory, where he wrote down an equation (now called the Schrödinger wave equation) and its exact solutions. His work was in agreement with all known predictions on wave-particle duality. Using his wave equation, it became possible to determine with probability the location of an object in a region of space at any time.

Schrödinger's probabilistic theory of waves allows the existence of more than one wave and therefore of more than one particle. Since photons behave as waves, and since it is also possible to have a superposition of two or more waves, it is therefore possible to have a superposition of two or more photons. For example consider shining a beam of light through transparent glass. Photons are just as likely to pass through the glass (corresponding to one wave) as to bounce back (corresponding to another wave). Both waves can be in superposition, which leads to the possibility of a single photon being both reflected and transmitted, and therefore being on both sides of the glass simultaneously. The principle of quantum superposition has been verified for many quantum particles such as electrons [36], fermions [8] and even collections of particles such as Bose Einstein condensates [6, 31].

However, the superposition principle does not hold for macroscopically large objects. A possible explanation for the absence of superposition in macroscopic objects is decoherence. Quantum systems are not isolated from their environment and they lose their quantum properties at the slightest interaction with the outside world. An attempt to obtain knowledge of a quantum superpositions causes it to decohere, effectively destroying the superposition. Decoherence then results in the collapse of a wave function, its transition from quantum to classical world. We will come back to the topic of decoherence in Chapter 3.

Although Schrödinger's wave equation can be used to predict the results of measurement, with extraordinary accuracy and precision, it has the puzzling feature that it expresses motion in terms of probabilities, which is impossible to comprehend intuitively by our classical minds. Physicists consequently did not agree about the nature of the physical reality that Schrödinger's equation described. The founding fathers of physics at that time tried to come to terms with the philosophical implications of this. Their worries formed the basis of what we know today as the *Copenhagen interpretation* of quantum physics. In 1935, Erwin Schrödinger illustrated the concept of decoherence and in general the limitations of quantum mechanics by establishing his famous thought (or Gedanken) experiment (the Schrödinger's cat) where the life or death (the biological state) of a (macroscopic) cat

in a sealed box is entangled with the quantum state of a particular (microscopic) sub-atomic particle, resulting in a macroscopic quantum superposition state [118]. If the sub-atomic particle is in one state (for example a nucleus that has not decayed), the cat remains alive; but if it is in its orthogonal state (for example a nucleus that has decayed), the cat dies. The particle can be in a superposition of both states, and so the cat remains in a superposition of both dead and alive until the box is opened (that is until measurement has been made), and the cat is either dead or alive (that is the superposition would have collapsed into a single state). While the Schrödinger's cat idea is believed to provide answers to questions about the boundary between the quantum mechanical and classical world, many believe it highlights the mystery of the quantum world. We note that Schrödinger did not intend to elevate the quantum mystery into the classical world. In spite of this, the curiosity on identifying this boundary has led researchers to consider laboratory realizations of superpositions of macroscopically distinguishable quantum states.

Generating and observing superpositions between distinguishable quantum states is extremely difficult because any form of interaction with its environment decoheres the system thus resulting in the loss of superposition. In order to observe the superposition principle, one need to manipulate particles of matter or light in a much more gentle way. In quantum optics, the direct generation and detection of single quantum particles without destroying them has been successful and celebrated in two different studies [136, 59]. In [136], single atoms were trapped, then controlled and measured with light or photons while in [59, 60], photons were trapped and manipulated by sending atoms through a trap. These investigations opened the door to a new era of experimentation with quantum physics. For example, through a Ramsey interferometric setup it is possible to generate a version of Schrödinger's cat through the interaction between an atom and a coherent field trapped in an optical cavity [39]. The coherent field has a huge number of photons and negligible noise pattern and so behaves classically. Thus an ensemble of trapped microwave photons becomes an object of investigation to be observed and manipulated for fundamental tests and quantum information processing.

Measuring light in practice means the recording of photon statistics. Different states of light exhibit different photon statistics that characterize them. We can deduce from the corresponding photon statistics the nature of our quantum state of light – classical or non-classical – and what distinguishes a given quantum state of light from another. We can also learn about the features of light from a specific measurement result. For a coherent light field, a measurement result would include the amplitude and phase of the coherent field. Unfortunately we encounter difficulties and challenges when we want to experimentally measure light: It is almost impossible to measure light without significantly perturbing it. But as discussed in the previous paragraph, it is possible to trap light shielded from its

environment without destroying it [60].

Measuring non-classical states of trapped light requires cavities that prevent the escape of even single photons during the read out process [129, 60, 104]. Nowadays with advancement in solid state physics, optical cavities with long storage life are available where states of light can be trapped and shielded from their environment for more that a tenth of a second [59]. Various quantum states of light, including a superposition of coherent states, can be generated [39]. Nondemolition quantum detectors (usually in form of atoms) [68] are readily available and can be used as probes for light fields trapped in an optical cavity. With these experimental capabilities, quantum nondemolition (QND) schemes [24, 130, 47, 55, 16, 94, 35] have been designed to avoid the perturbation produced by a measurement. For an electromagnetic field mode, a version of QND consists in monitoring the photon number without changing it [94]. This may be achieved by coupling the field mode to a detector via a non-resonant interaction, excluding processes where photons are created and annihilated. The detector acquires a phase that is dependent on the state of the field [29]; therefore detecting the probe phase yields a QND measurement of the field mode.

The mode invisibility (MI) measurement idea was proposed to increase the sensitivity of the above QND method by coupling the detector to the field mode via a resonant interaction [97, 98, 33]. Although a resonant probe-field interaction includes photon absorption and annihilation processes, the cavity field modes have a geometrical property that allows one to probe the electromagnetic field without changing the field mode [97].

In the MI QND scheme, the detector travels in a superposition of states along the two paths of an atomic interferometric setup. Such an interferometric setup was first used to propose a scheme to detect the Unruh effect at low acceleration [87] and to build a quantum thermometer [86]. For applications in quantum optics, the interferometric setup includes two optical cavities that store electromagnetic fields. This setup has been used to propose a scheme to detect various quantum states of light including Fock states [97], squeezed coherent states [98], entangled superposition of coherent states with two-level atom [33] and a superposition of coherent states [95].

In detecting a superposition of quantum states, such as superposition of two coherent states of light, one must take note of the coherence properties of the states that distinguish them from an ordinary statistical mixture. The detection of quantum coherence, distinguishing between various superpositions of coherent states are the key issues when considering a measuring scheme for detecting a superposition of states.

## 2.2 Scope and Aim

In the context of generating and measuring quantum systems without destroying their quantum nature, our study in this part one of the thesis focuses on measuring Schrödinger cat states and Bell cat states, without destroying their quantum nature, that is their superposition and entanglement respectively. A Schrödinger's cat state and Bell cat state already generated and successfully trapped in an optical cavity will be our object of investigation to be observed and manipulated for quantum information processing.

The overall aim of this study is to propose a scheme that probes the two cat states without significantly destroying their quantum nature. Its specific objectives are:

- Demonstrate how one can detect a superposition of two coherent states, including the coherence between the individual coherent states that form the superposition, the amplitude, and phase of the individual coherent states. In defining a Schrödinger's cat state, three different types shall be employed: the even cat state, the odd cat state, and the Yuker-Stoller cat state (defined later). Our aim includes non-destructively distinguishing between these three various cat states.
- Investigate the entanglement structure in a Bell cat state (that is a quantum state of cat states entangled with two-level atoms).

# Chapter 3

# Background

In this chapter, we present the basic tools and concepts that we use in part 1. First, in Sec. 3.1, we talk about a detector in the form of two-level atom, which has been applied in quantum optics to create and directly probe quantum states of light. Then in Sec. 3.2, we give a description of an electromagnetic field in a cavity mode and show that it is equivalent to a quantum Harmonic oscillator. We then proceed in Sec. 3.3 with an overview of two important states of light: a superposition of two coherent states of equal amplitude and $\pi$ out of phase, commonly known as Schrödinger's cat states. We discuss the different non-classical properties that distinguish a superposition of coherent states from a mere statistical mixture of coherent states or the constituent coherent states.

The second quantum state of light we will discuss is an entangled state of light. Specifically we consider two kinds of entangled states: a) one made of two-level atoms and Schrödinger's cat states, known as Bell cat states [134] b) another made of two Schrödinger cat states.

## 3.1 Definition of two-level systems

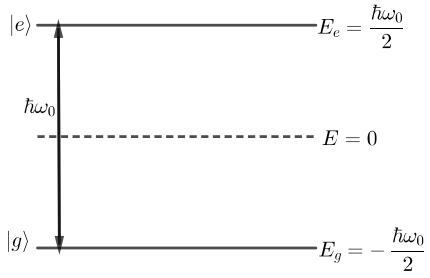


Figure 3.1: Pictorial representation of a two-level atomic system where the zero of energy ($E = 0$) is taken half way between the two energy levels $|e\rangle$ and $|g\rangle$.

### 3.1.1 The Hilbert space

Consider a two-dimensional linear vector space $\mathcal{H}$ defined by orthonormal basis vectors $\hat{e}_x$ and $\hat{e}_y$. In the column vector representation,

$$\hat{e}_y = \begin{pmatrix} 1 \\ 0 \end{pmatrix} \quad \text{and} \quad \hat{e}_x = \begin{pmatrix} 0 \\ 1 \end{pmatrix}. \tag{3.1}$$

We could also use the Dirac notation

$$\hat{e}_x = |g\rangle, \quad \hat{e}_y = |e\rangle \tag{3.2}$$

A two level-atom as shown in Fig. 3.1, is described by a two-dimensional Hilbert space represented by two orthonormal basis vectors $|g\rangle$ and $|e\rangle$ denoting the ground (lowest) energy state and excited (highest) energy state of the atom respectively;

$$\langle g|\, g\rangle = \langle e|\, e\rangle = 1, \qquad \langle g|\, e\rangle = \langle e|\, g\rangle = 0. \tag{3.3}$$

In vector notation,

$$|g\rangle = \begin{pmatrix} 0 \\ 1 \end{pmatrix} \quad \text{and} \quad |e\rangle = \begin{pmatrix} 1 \\ 0 \end{pmatrix}. \tag{3.4}$$

A general two-level atomic state $|\psi\rangle$ can be represented by the linear superposition

$$|\psi\rangle = c_e|e\rangle + c_g|g\rangle. \tag{3.5}$$

The normalization condition for the wave function $\langle\psi|\,\psi\rangle = 1$, where

$$\langle\psi|\,\psi\rangle = c_e c_g^*\langle g|e\rangle + c_g c_e^*\langle e|g\rangle + |c_e|^2\langle e|e\rangle + |c_g|^2\langle g|g\rangle \tag{3.6}$$

with $\rho = |\psi\rangle\,\langle\psi|$, entails that the complex coefficients $c_e$ and $c_g$ must satisfy

$$|c_e|^2 + |c_g|^2 = 1. \tag{3.7}$$

Here we use the orthonormality of $|e\rangle$ and $|g\rangle$: $\langle e|e\rangle = 1 = \langle g|g\rangle$ and $\langle g|e\rangle = 0 = \langle e|g\rangle$.

### 3.1.2 The Hamiltonian

In the absence of perturbation, the two-level atomic system with two energy eigenvalues $E_e$ and $E_g$ can be described by a constant time independent Hamiltonian $H_a$. We can write the eigenvalue equation of $H_a$ as

$$H_a|e\rangle = \frac{E_e}{2}|e\rangle, \quad H_a|g\rangle = -\frac{E_g}{2}|g\rangle \tag{3.8}$$

where $i = e, g$. Since $H_a$ is Hermitian, we can construct the matrix elements of $H_a$ in the $e, g$ basis using the completeness relation

$$H_a = \sum_{i,j} |i\rangle\,\langle i|\,H_a|j\rangle\,\langle j| = \sum_{i,j} \langle i|\,H_a|j\rangle \times |i\rangle\,\langle j| \tag{3.9}$$

$i, j = e, g$. So that in the $e, g$ basis, we have the matrix element

$$\langle i|\,H_a|j\rangle = \begin{pmatrix} H_a^{ii} & H_a^{ij} \\ H_a^{ji} & H_a^{jj} \end{pmatrix} \tag{3.10}$$

Assuming that $H_a$ is diagonal in the $|e\rangle$ and $|g\rangle$ basis, then we can associate it with the matrix

$$H_a = \begin{pmatrix} \frac{E_e}{2} & 0 \\ 0 & -\frac{E_g}{2} \end{pmatrix} \tag{3.11}$$

We note that this matrix elements can be constructed directly from the eigenvalue equation (3.8).

### 3.1.3 Representation of atomic operators

In principle, a measurement on the two level atomic state (3.5) collapses it to either a ground state with energy eigenvalue $E_g$ or an excited state with energy eigenvalue $E_e$. We will come back to this later, but before we proceed, let us now discuss the atomic operators that are responsible for transitions between one atomic state to the other. We can construct such operators from a combination of $|g\rangle$ and $|e\rangle$. For example

$$\hat{\sigma}_+ = |e\rangle\langle g|\,, \quad \hat{\sigma}_- = |g\rangle\langle e|\,,$$

with properties

$$\hat{\sigma}_+|g\rangle = |e\rangle, \quad \hat{\sigma}_-|e\rangle = |g\rangle, \quad \hat{\sigma}_+|e\rangle = 0 = \hat{\sigma}_-|g\rangle \tag{3.12}$$

where we note that $|e\rangle$ and $|g\rangle$ are orthonormal: $\langle e|e\rangle = 1 = \langle g|g\rangle$ and $\langle g|e\rangle = 0 = \langle e|g\rangle$. From (3.12), we see that the action of $\hat{\sigma}_-$ on the excited state $|e\rangle$ lowers it to the ground state $|g\rangle$ and is thus called the lowering operator, while $\hat{\sigma}_+$ on the ground state $|g\rangle$ raises it to the excited state $|e\rangle$; we call this the raising operator.

### 3.1.4 The Pauli matrices

We recall the definition of the Pauli matrices

$$\sigma_X = \begin{pmatrix} 0 & 1 \\ 1 & 0 \end{pmatrix}, \quad \sigma_Y = \begin{pmatrix} 0 & -\mathrm{i} \\ \mathrm{i} & 0 \end{pmatrix}, \quad \sigma_Z = \begin{pmatrix} 1 & 0 \\ 0 & -1 \end{pmatrix}.$$

We know that together with the identity operator $\mathbb{1} = \begin{pmatrix} 1 & 0 \\ 0 & 1 \end{pmatrix}$, the Pauli matrices form a basis ( $\mathbb{1}, \sigma_X, \sigma_Y, \sigma_Z$) of $2 \times 2$ matrices. That is, any $2 \times 2$ matrix can be expressed as a linear combination of $\mathbb{1}, \sigma_X, \sigma_Y$, and $\sigma_Z$ respectively.

#### *Atomic operators in terms of Pauli matrices*

The two-level atom operators can be associated to the matrix representation of the Pauli matrices. The atomic raising and lowering operators can also be expanded over the Pauli basis vectors as

$$\sigma_\pm = \frac{1}{2}\Big(\sigma_X \pm \mathrm{i}\sigma_Y\Big) \tag{3.13}$$

Equivalently,

$$\sigma_X = \sigma_+ + \sigma_-, \quad \sigma_Y = \mathrm{i}\big(\sigma_- - \sigma_+\big) \tag{3.14}$$

In contrast to the raising and lowering operators $\sigma_\pm$, the Pauli operators are Hermitian and form physical observables. To see how this works, we note that in terms of the ground and excited states of the two-level atom, Pauli matrices can be written as

$$\begin{aligned}
\mathbb{1} &= |e\rangle\langle e| + |g\rangle\langle g| \\
\sigma_X &= |e\rangle\langle g| + |g\rangle\langle e| \\
\sigma_Y &= \mathrm{i}(|g\rangle\langle e| - |e\rangle\langle g|) \\
\sigma_Z &= |e\rangle\langle e| - |g\rangle\langle g| \,.
\end{aligned}$$

and their action on the general atomic state (3.5) is given by

$$\begin{aligned}
\sigma_Z|\psi\rangle &= c_e|e\rangle - c_g|g\rangle \\
\sigma_X|\psi\rangle &= c_g|e\rangle + c_e|g\rangle \\
\sigma_Y|\psi\rangle &= -\mathrm{i}c_g|e\rangle + \mathrm{i}c_e|g\rangle
\end{aligned}$$

In particular, $\sigma_X$ swaps the two components $|e\rangle \Longrightarrow |g\rangle$ (spin flip) and $\sigma_Z$ inverts the sign of the $|g\rangle$ component (phase shift), while $\sigma_Y$ does both.

### *The Hamiltonian in terms of Pauli matrices*

We will now write the two-level atomic Hamiltonian (3.15) in this Pauli basis

$$\begin{aligned}
H_a =& E_e|e\rangle\langle e| + E_g|g\rangle\langle g| + \left(\frac{E_g}{2}|e\rangle\langle e| - \frac{E_g}{2}|e\rangle\langle e|\right) + \left(\frac{E_e}{2}|g\rangle\langle g| - \frac{E_e}{2}|g\rangle\langle g|\right) \\
=& \frac{E_e + E_g}{2} I + \frac{E_e - E_g}{2}\sigma_Z
\end{aligned}$$

Choosing the zero of energy as shown in Fig. 3.1 so that $E_e + E_g = 0$ , the unperturbed Hamiltonian in the Pauli basis is given by

$$H_a = \frac{\hbar\omega_{eg}}{2}\sigma_Z \tag{3.15}$$

where

$$\omega_{eg} = \frac{E_e - E_g}{\hbar} = \frac{2E_e}{\hbar} \tag{3.16}$$

is the transition frequency accounting for the energy difference between the two energy eigenstates $|e\rangle$ and $|g\rangle$.

### 3.1.5 The Bloch sphere

In other to relate unitary operations on a qubit state $|\rho\rangle$ to rotations on the Bloch sphere it turns out to be convenient to use the corresponding density operator $\rho = |\psi\rangle\langle\psi|$, so from the general two-level state (3.5),

$$\rho = |c_g|^2|g\rangle\langle g| + |c_e|^2|e\rangle\langle e| + c_g c_e^*|g\rangle\langle e| + c_e c_g^*|e\rangle\langle g| = \begin{pmatrix} |c_g|^2 & c_g c_e^* \\ c_e c_g^* & |c_e|^2 \end{pmatrix} \tag{3.17}$$

From this we can construct the matrix elements of the Pauli matrices in the $|e\rangle$ and $|g\rangle$ basis as follows

$$r_X = \langle\psi|\sigma_X|\psi\rangle = c_g c_e^* + c_e c_g^* \tag{3.18}$$

$$r_Y = \langle\psi|\sigma_Y|\psi\rangle = -\mathrm{i}\left(c_g c_e^* - c_e c_g^*\right) \tag{3.19}$$

$$r_Z = \langle\psi|\sigma_Z|\psi\rangle = |c_e|^2 - |c_g|^2 \tag{3.20}$$

The diagonal elements of the matrix $|c_e|^2$ and $|c_g|^2$ are the populations of the excited and ground states, respectively. The atomic inversion is given by (3.20), the expectation value of $\sigma_Z$. Grouping terms, the two-level atom density in the Pauli basis $\{\mathbb{1}, \sigma_X, \sigma_Y, \sigma_Z\}$, we have

$$\rho = \frac{1}{2}(\mathbb{1} + \mathbf{r}\cdot\sigma), \qquad \mathbf{r} = (r_X, r_Y, r_Z), \quad \sigma = (\sigma_X, \sigma_Y, \sigma_Z) \tag{3.21}$$

$\mathbf{r}$ is known as the Bloch vector defined later in the section.

#### *Rotation operator*

We can construct rotation operators by exponentiating the Pauli matrices. These operators rotate the Bloch vector $\mathbf{r}$ about the $x, y$ and $z$ axis accordingly.

$$R_x(\theta) = e^{-\mathrm{i}\frac{\theta}{2}\sigma_X} \equiv \cos\left(\frac{\theta}{2}\right)\mathbb{1}_2 - \mathrm{i}\sin\left(\frac{\theta}{2}\right)\sigma_X \tag{3.22a}$$

$$R_y(\theta) = e^{-\mathrm{i}\frac{\theta}{2}\sigma_Y} \equiv \cos\left(\frac{\theta}{2}\right)\mathbb{1}_2 - \mathrm{i}\sin\left(\frac{\theta}{2}\right)\sigma_Y \tag{3.22b}$$

$$R_z(\theta) = e^{-\mathrm{i}\frac{\theta}{2}\sigma_Z} \equiv \cos\left(\frac{\theta}{2}\right)\mathbb{1}_2 - \mathrm{i}\sin\left(\frac{\theta}{2}\right)\sigma_Z \tag{3.22c}$$

## 3.2 Electromagnetic field mode in a cavity

In this section, we discuss the physics of an electromagnetic wave inside a cavity (box). Electromagnetic field energy can be confined in a cavity in form of standing waves. This is because when an electromagnetic field encounters a boundary (perfectly reflecting surface), nearly all the energy in the wave is reflected from the surface and very little is transmitted into the boundary. Confining the field in a cavity allows us to gain control together with the advantage of having a close access to it for experimental purposes.

To treat such a cavity field-system, we start from Maxwell's equations, define a formalism that treats an electromagnetic field mode in free space and show that its classical energy is related to a harmonic oscillator [50]. These field modes can then be quantized and treated as quantum harmonic oscillators.

### 3.2.1 Maxwell's equations and wave equation

We start with a description of electromagnetic field in free space. Starting from Maxwell's equations for the electric field $\mathbf{E}$ and magnetic field $\mathbf{B}$, without any source of radiation (that is no free charges and current):

$$\nabla \cdot \mathbf{E} = 0, \tag{3.23}$$

$$\nabla \cdot \mathbf{B} = 0 \tag{3.24}$$

$$\nabla \times \mathbf{E} = -\frac{\partial \mathbf{B}}{\partial t} \tag{3.25}$$

$$\nabla \times \mathbf{B} = \mu\epsilon_0 \frac{\partial \mathbf{E}}{\partial t} \tag{3.26}$$

$\epsilon_0$ and $\mu_0$ are the permittivity and permeability of free space related to the speed of light $c = 1/\sqrt{\mu_0\epsilon_0}$. Maxwell showed that these equations could be rearranged to form a wave equation with propagation speed $c$. To see how this works, it is convenient to express the electric and magnetic fields in terms of the vector potential $\mathbf{A}(\mathbf{r}, t)$ which satisfies the Coulomb gauge condition

$$\nabla \cdot \mathbf{A}(\mathbf{r},t) = 0 \tag{3.27}$$

Thus

$$\mathbf{B}(\mathbf{r}, t) = \nabla \times \mathbf{A}(\mathbf{r}, t) \tag{3.28}$$

$$\mathbf{E}(\mathbf{r}, t) = -\frac{\partial \mathrm{A}(\mathbf{r}, t)}{\partial t} \tag{3.29}$$

We will now show that introducing the vector potential $\mathbf{A}(\mathbf{r},t)$ together with the Coulomb gauge condition (3.27) does not change the nature of the Maxwell's equations (3.23)-(3.26). First recall the vector identities for an arbitrary vector $\mathbf{F}$

$$\nabla \cdot (\nabla \times \mathbf{F}) = 0 \tag{3.30}$$

$$\nabla \times \nabla \mathbf{F} = 0 \tag{3.31}$$

$$\nabla \times \nabla \times \mathbf{F} = \nabla(\nabla \cdot \mathbf{F}) - \nabla^2 \mathbf{F} \tag{3.32}$$

With Eqn. (3.30) in mind, substituting (3.28) in (3.24), we obtain

$$\nabla \cdot \mathbf{B} = \nabla \cdot (\nabla \times \mathbf{A}) = 0 \tag{3.33}$$

Similarly, with the electric field written in the form in Eqn (3.29), we are sure that (3.25) is satisfied. To derive the wave equation for the vector potential, we now substitute Eqns (3.28) and (3.29) in (3.26):

$$\nabla \times \Big(\nabla \times \mathbf{A}\Big) = -\frac{1}{c^2}\frac{\partial^2 \mathbf{A}}{\partial t^2} \tag{3.34}$$

From the vector identity (3.32) we can re-write the left hand side so that the wave equation for the vector potential $\mathbf{A}(\mathbf{r},t)$ becomes

$$\nabla^2 \mathbf{A}(\mathbf{r},t) - \frac{1}{c^2}\frac{\partial^2 \mathbf{A}(\mathbf{r},t)}{\partial t^2} = 0 \tag{3.35}$$

We note that the Coulomb gauge condition (3.27) implies the longitudinal component of the vector potential is vanishing so that the wave equation (3.35) contains only the transverse component of the vector potential.

### 3.2.2 Mode expansion in a cavity

In this section, we look for solutions to the wave equation (3.35). To this end, we consider the EM waves confined in a cubic cavity of length $L$ as shown in FIG. 3.2. The idea of the cavity is to allow us impose a boundary condition on the faces of the cube. For example with the length of the cavity fixed at $L$, we can satisfy the boundary condition

$$\mathbf{A}(0,t) = \mathbf{A}(L,t) = 0, \quad \text{for all} \quad t. \tag{3.36}$$

with a general solution of the form

$$\mathbf{A}(\mathbf{r},t) = \sum_{\mathbf{k}} \sin(\mathbf{k}\cdot\mathbf{r})\Big(\mathbf{A}_{\mathbf{k}} e^{-\mathrm{i}\omega t} + \mathbf{A}_{\mathbf{k}}{}^{*} e^{-\mathrm{i}\omega t}\Big) \tag{3.37}$$

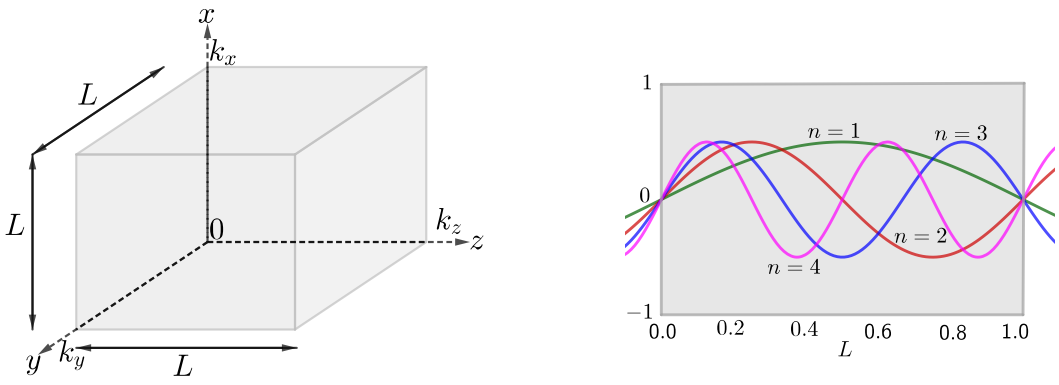


Figure 3.2: An EM-field confined in a cubic cavity (left image) and subjected to the Dirichlet boundary condition would have a standing wave produced in it (right image).

Here $\omega$ is the wave frequency and $\mathbf{k}$ is the wave vector with its magnitude $|\mathbf{k}| = \sqrt{k_x + k_y + k_z}$ called the wave number. $\omega$ and $\mathbf{k}$ are related by the dispersion relation

$$\omega = c|\mathbf{k}| \tag{3.38}$$

Our boundary condition (3.36) implies that only certain numbers of $\mathbf{k}$ give valid solutions. To see how this works, we see that at $\mathbf{r} = 0$, we have $\sin \mathbf{k} \cdot \mathbf{r} = 0$ hence $A(0, t) = 0$. The second boundary condition $A(L, t) = 0$ implies

$$\mathbf{A}(L, t) = \sum_{\mathbf{k}} \sin(\mathbf{k}L)\left(\mathbf{A_k} e^{-\mathrm{i}\omega t} + \mathbf{A_k}^* e^{\mathrm{i}\omega t}\right) = 0 \tag{3.39}$$

which is valid only for $\sin(\mathbf{k}L) = 0$. Thus we have the constraint on the components of $k$

$$k_x = \frac{\pi n_x}{L}, \quad k_y = \frac{\pi n_y}{L}, \quad k_z = \frac{\pi n_z}{L} \tag{3.40}$$

for any integer $n_x, n_y, n_z$ called mode numbers. Our solution thus looks like this

$$\mathbf{A}(\mathbf{r}, t) = \sum_{\mathbf{k}} \sin(\mathbf{kr})\left(\mathbf{A_k} e^{-\mathrm{i}(\omega t)} + \mathbf{A_k}^* e^{\mathrm{i}(\omega t)}\right) \tag{3.41}$$

with the wave vector $\mathbf{k} = (k_x, k_y, k_z)$ given as in (3.40) above.

From here we can find expressions for the electric field $\mathbf{E}(\mathbf{r},t)$ and magnetic field $\mathbf{B}(\mathbf{r},t)$ in the mode. The electric and magnetic field can be obtained from (3.37)

$$\mathbf{E}(\mathbf{r},t) = -\frac{\partial \mathbf{A}(\mathbf{r},t)}{\partial t} = \sum_{\mathbf{k}} \mathrm{i}\omega\Big(\mathbf{A}_{\mathbf{k}} e^{-\mathrm{i}\omega t} - \mathbf{A}_{\mathbf{k}}{}^{*} e^{\mathrm{i}(\omega t)}\Big)\sin(\mathbf{kr}) \tag{3.42}$$

Taking $\bigtriangledown \rightarrow \mathrm{i}\mathbf{k}$, the magnetic field becomes

$$\mathbf{B}(\mathbf{r},t) = \bigtriangledown \times \mathbf{A} = \sum_{\mathbf{k}} \mathrm{i}\mathbf{k} \times \Big(\mathbf{A}_{\mathbf{k}} e^{-\mathrm{i}\omega t} + \mathbf{A}_{\mathbf{k}}{}^{*} e^{\mathrm{i}(\omega t)}\Big)\sin(\mathbf{kr}) \tag{3.43}$$

Similarly, the total energy, that is the Hamiltonian stored in the mode can be derived from the expression

$$H_{\mathbf{k}} = \frac{1}{2}\int_V dV(\epsilon_0 \mathbf{E}_{\mathbf{k}}{}^2 + \mu_0^{-1}\mathbf{B}_{\mathbf{k}}{}^2) = \frac{1}{2}\int_V dV(\epsilon_0 \mathbf{E}_{\mathbf{k}}{}^2 + \mu_0^{-1}\frac{\mathbf{E}_{\mathbf{k}}{}^2}{c^2}) = \int_V dV \epsilon_0 \mathbf{E}_{\mathbf{k}}{}^2 \tag{3.44}$$

where the integral is taken over the entire volume of the cavity and $dV$ is the volume element. which gives [51]

$$\frac{1}{2}\int_V dV \epsilon_0 \mathbf{E}_{\mathbf{k}}{}^2 = \frac{1}{2}\int_V dV \epsilon_0 \sum_{\mathbf{k},\mathbf{k}'} \omega_{\mathbf{k}}\omega_{\mathbf{k}'} \sin(\mathbf{k}r)\sin(\mathbf{k}'r)\mathbf{A}_{\mathbf{k}} \cdot \mathbf{A}_{\mathbf{k}}{}^{*} \tag{3.45}$$

we have

$$\frac{1}{2}\int_V dV \sum_{\mathbf{k},\mathbf{k}'} \omega_{\mathbf{k}}\omega_{\mathbf{k}'} \sin(\mathbf{k}r)\sin(\mathbf{k}'r) = V\delta(\mathbf{k}-\mathbf{k}') \tag{3.46}$$

therefore,

$$H_{\mathbf{k}} = 2\epsilon_0 V \sum_{\mathbf{k}} \omega_k^2 \mathbf{A}_{\mathbf{k}} \cdot \mathbf{A}_{\mathbf{k}}{}^{*} \tag{3.47}$$

Later in this chapter, we will show that the total energy in a field mode (3.47) can be expressed as the energy of a Harmonic oscillator of unit mass and natural frequency $\omega_k$.

The mode variables can be replaced with a mode position coordinate and momentum coordinate

$$\mathbf{A}_{\mathbf{k}} = \sum_{\mathbf{k}} \frac{1}{\sqrt{4\epsilon_0 V \omega_k^2}}(\omega_k X_{\mathbf{k}} + \mathrm{i}P_{\mathbf{k}})\hat{\epsilon}_{\mathbf{k}} \tag{3.48}$$

$$\mathbf{A}_{\mathbf{k}}{}^{*} = \sum_{\mathbf{k}} \frac{1}{\sqrt{4\epsilon_0 V \omega_k^2}}(\omega_k X_{\mathbf{k}} - \mathrm{i}P_{\mathbf{k}})\hat{\epsilon}_{\mathbf{k}} \tag{3.49}$$

Here the vector nature is taken up by the unit polarization vector $\epsilon_{\mathbf{k}}$. Substituting these in the expression for the total energy in the modes (3.47), we obtain

$$H = \frac{1}{2}\sum_{\mathbf{k}}(P_{\mathbf{k}}^2 + \omega_{\mathbf{k}}^2 X_{\mathbf{k}}^2) \tag{3.50}$$

which is of the form of a harmonic oscillator of unit mass and natural frequency, $\omega_{\mathbf{k}}$.

### 3.2.3 Quantization of the electromagnetic fields modes

In this section, the main ideas and equations for quantized electromagnetic field are developed. The nature of the field Hamiltonian (3.50) suggests that we can treat electromagnetic field modes in a cavity as harmonic oscillators. We will now quantize the field modes following the same procedure as the quantization of harmonic oscillators. The Hamiltonian for the harmonic oscillator of unit mass is given as

$$H = \frac{1}{2m}(p^2 + \omega^2 x^2) \tag{3.51}$$

where $x$ and $p$ are the quantum mechanical operators for position and momentum and obey the commutation relation $[x, p] = \mathrm{i}\hbar$. Introducing the creation and annihilation operators $a$ and $a^\dagger$ respectively. defined as

$$a = \frac{1}{\sqrt{2\hbar\omega}}(\mathrm{i}p + \omega x) \tag{3.52}$$

$$a^\dagger = \frac{1}{\sqrt{2\hbar\omega}}(-\mathrm{i}p + \omega x) \tag{3.53}$$

Owing to the commutation of $x$ and $p$, we can obtain a commutation relation $a$ and $a^\dagger$ as follows

$$[a, a^\dagger] = 1 \tag{3.54}$$

The position and momentum coordinate are

$$q = \sqrt{\frac{\hbar}{2m\omega}}(a + a^\dagger) \tag{3.55}$$

$$p = \mathrm{i}\sqrt{\frac{\hbar m\omega}{2}}(a^\dagger - a) \tag{3.56}$$

The Hamiltonian becomes

$$H = \hbar\omega(\frac{1}{2} + a^\dagger a) \tag{3.57}$$

The number operator $n = a^\dagger a$ with property

$$[n, a] = [a^\dagger a, a] = [a^\dagger - a]a^\dagger = -a, \quad [n, a^\dagger] = [a^\dagger a, a^\dagger] = a^\dagger[a, a^\dagger] = a^\dagger \tag{3.58}$$

is the number operator that counts the number of quanta of excitation where $a$ destroys or removes a quanta and $a^\dagger$ adds or creates a quanta.

Now that we have shown that the energy of a classical electromagnetic field mode is in the form of a harmonic oscillator, we will proceed to quantization of the modes. To do this, we associate the classical variables with quantum mechanical operators. The quantized fields are thus

$$\begin{aligned}\mathbf{A}_\mathbf{k} &= \sum_\mathbf{k} \frac{1}{\sqrt{4\epsilon_0 V\omega_k^2}}(\omega_k X_\mathbf{k} + \mathrm{i}P_\mathbf{k})\hat{\epsilon}_\mathbf{k} \\ &\rightarrow \sum_\mathbf{k} \frac{1}{\sqrt{4\epsilon_\mathbf{k} V\omega_k^2}}(\omega_\mathbf{k} x_\mathbf{k} + \mathrm{i}p_\mathbf{k})\hat{\epsilon}_\mathbf{k} = \sum_\mathbf{k} \sqrt{\frac{\hbar}{2\epsilon_0 V\omega_k}} a_\mathbf{k}\hat{\epsilon}_\mathbf{k} \end{aligned} \tag{3.59}$$

$$\begin{aligned}\mathbf{A_k}^* &= \sum_\mathbf{k} \frac{1}{\sqrt{4\epsilon_0 V\omega_k^2}}(\omega_k X_\mathbf{k} - \mathrm{i}P_\mathbf{k})\hat{\epsilon}_\mathbf{k} \\ &\rightarrow \sum_\mathbf{k} \frac{1}{\sqrt{4\epsilon_0 V\omega_k^2}}(\omega_\mathbf{k} x_\mathbf{k} - \mathrm{i}p_\mathbf{k})\hat{\epsilon}_\mathbf{k} = \sum_\mathbf{k} \sqrt{\frac{\hbar}{2\epsilon_0 V\omega_k}} a_\mathbf{k}^\dagger\hat{\epsilon}_\mathbf{k} \end{aligned} \tag{3.60}$$

The operators obey the commutation relations

$$[x_\mathbf{k}, p_{\mathbf{k}'}] = \mathrm{i}\hbar\delta_{\mathbf{k},\mathbf{k}'}, \quad [x_\mathbf{k}, x_{\mathbf{k}'}] = 0, \quad [p_\mathbf{k}, p_{\mathbf{k}'}] = 0 \tag{3.61}$$

$$[a_\mathbf{k}, a_{\mathbf{k}'}^\dagger] = \delta_{\mathbf{k},\mathbf{k}'}, \quad [a_\mathbf{k}, a_{\mathbf{k}'}] = 0, \quad [a_\mathbf{k}^\dagger, a_{\mathbf{k}'}^\dagger] = 0 \tag{3.62}$$

where $\mathbf{k}$ and $\mathbf{k}'$ label the modes. Then the quantized vector potential is given as

$$\mathbf{A}_\mathbf{k} = \sum_\mathbf{k} \sqrt{\frac{\hbar}{V\epsilon_0\omega_\mathbf{k}}}\hat{\varepsilon}_\mathbf{k}(a_\mathbf{k}e^{-\mathrm{i}\omega_\mathbf{k}t} + a_\mathbf{k}^\dagger e^{\mathrm{i}\omega_\mathbf{k}t})\sin(\mathbf{k}r) \tag{3.63}$$

The electric and magnetic fields are given as

$$\mathbf{E}_\mathbf{k} = \sum_\mathbf{k} \mathrm{i}\sqrt{\frac{\hbar\omega_k}{2\epsilon_0 V}}\hat{\varepsilon}_\mathbf{k}\Big(ae^{-\mathrm{i}\omega_k t} - a^\dagger e^{\mathrm{i}\omega_k t}\Big)\sin(\mathbf{kr}) \tag{3.64}$$

$$\mathbf{B}_\mathbf{k} = \sum_\mathbf{k} \mathrm{i}\sqrt{\frac{\hbar}{2\epsilon_0\omega_k V}}\mathbf{k}\times\hat{\varepsilon}_\mathbf{k}\Big(ae^{-\mathrm{i}\omega_k t} - a^\dagger e^{\mathrm{i}\omega_k t}\Big)\sin(\mathbf{kr}) \tag{3.65}$$

Recalling the expression for the total field energy (3.50), we can write the quantized total field energy. For a single mode $\kappa$, the Hamiltonian is given as

$$H = -\sum \frac{1}{2}\frac{\hbar\omega_k}{2\epsilon_0 V}\epsilon_0 \int_V dV\Big(a_{\mathbf{k}}e^{-\mathrm{i}\omega_{\mathbf{k}}t} - a^\dagger_{\mathbf{k}}e^{\mathrm{i}\omega_k t}\Big)^2 \tag{3.66}$$

$$= -\frac{\hbar\omega_k}{4V}V\Big(-a_{\mathbf{k}}a^\dagger_{\mathbf{k}} - a^\dagger_{\mathbf{k}}a_{\mathbf{k}}\Big) = \frac{\hbar\omega_k}{2}(a^\dagger_{\mathbf{k}}a_{\mathbf{k}} + \frac{1}{2}) \tag{3.67}$$

The quantum mechanical operator for the total Hamiltonian in the field mode is given by the sum of the Hamiltonians for single modes

$$H_{\mathbf{k}} = \sum_{\mathbf{k}} \hbar\omega_k(a^\dagger_{\mathbf{k}}a_{\mathbf{k}} + \frac{1}{2}) \tag{3.68}$$

## 3.3 Quantum states of the electromagnetic field

We now present qubit systems using quantum states of the electromagnetic (EM) field. Quantum states of the electromagnetic field (light) often considered in terms of photons can be described in terms of waves by their amplitude and phase, or in the cartesian coordinates by their quadratures $X$ and $P$. In this section, we present different states of light which are of interest for our study.

### 3.3.1 Coherent states

Coherent states denoted as $|\alpha\rangle$, are important states of the electromagnetic field which are useful in many areas of theoretical and experimental physics [53]. A normalized coherent state can also be expressed as a linear superposition of number (or Fock) states $|n\rangle$

$$|\alpha\rangle = e^{-|\alpha|^2/2}\sum_{n=0}^{\infty}\frac{\alpha^n}{\sqrt{n!}}|n\rangle, \qquad n = 1, 2, 3, \cdots \tag{3.69}$$

where $n$ counts the number of photons in the field state. $\alpha = |\alpha|e^{\mathrm{i}\theta}$ is the complex amplitude of the coherent state with amplitude $|\alpha|$ and phase $\theta$. In principle, coherent states can be

created by a laser corresponding to a displacement operation on the vacuum state

$$\begin{aligned} D(\alpha)|0\rangle =& e^{\alpha a^\dagger - \alpha^* a}|0\rangle = e^{\alpha a^\dagger} e^{-\alpha^* a} e^{-\frac{1}{2}([\alpha a^\dagger, -\alpha^* a])}|0\rangle \\ =& e^{-\frac{|\alpha|^2}{2}} e^{\alpha a^\dagger}|0\rangle = e^{-\frac{|\alpha|^2}{2}} \sum_n^\infty \frac{\alpha^n}{n!} a^{\dagger n}|0\rangle \\ =& e^{-\frac{|\alpha|^2}{2}} \sum_n^\infty \frac{\alpha^n}{n!}\sqrt{n!}|n\rangle \\ \equiv& |\alpha\rangle \end{aligned} \tag{3.70}$$

where $a$ and $a^\dagger$ are related by the commutation relation (3.54). Here, $\alpha = |\alpha|e^{i\theta}$ is a complex amplitude, $\theta$ and $|\alpha|$ are respectively the phase and amplitude of the coherent states. $D(\alpha) = e^{\alpha a^\dagger - \alpha^* a}$ is a displacement operator; a unitary operator $D(-\alpha) = D^\dagger(\alpha)$ that acts as a displacement operator upon the field creation and annihilation amplitudes $\hat{a}^\dagger$ and $\hat{a}$ respectively.

$$D^\dagger(\alpha) a D(\alpha) = a + \alpha, \quad D^\dagger(\alpha) a^\dagger D(\alpha) = a^\dagger + \alpha^*$$

We can generalize this operation to squeezed states, that is we can write

$$S(r)D(\alpha)|0\rangle = |r, \alpha\rangle, \qquad S(r) = \exp[rK_+ - r^* K_-] \tag{3.71}$$

where $K_- = \frac{1}{2}aa$, $\quad K_+ = \frac{1}{2}a^\dagger a^\dagger$, $\quad K_0 = \frac{1}{2} + a^\dagger a$. $S(r)$ is known as the squeeze operator, we will come back to this operator later in the section.

Coherent states are equally described as eigenstates of the annihilation operator $\hat{a}$

$$\hat{a}|\alpha\rangle = \alpha|\alpha\rangle, \quad \text{and} \quad \langle\alpha|\, a^\dagger = \langle\alpha|\, \alpha^*, \qquad \langle\alpha|\, \alpha\rangle = 1. \tag{3.72}$$

This follows from (3.70). Since $a|0\rangle = 0$, we have

$$0 = D(\alpha)a|0\rangle \equiv D(\alpha)aD^\dagger(\alpha)D(\alpha)|0\rangle = (a - \alpha)D(\alpha)|0\rangle \tag{3.73}$$

***Properties of coherent states***

Coherent states of light have the following important properties

1. *Orthogonality and completeness relation*: The overlap between two quantum states $|m\rangle$ and $|n\rangle$ is given by the relation $\langle m|\, n\rangle = \delta(m - n)$. It follows that two coherent

states corresponding to different eigenstates $|\alpha\rangle$ and $|\beta\rangle$ are not orthogonal. Their overlap $\left|\langle\beta|\alpha\rangle\right|$ can be calculated

$$\begin{aligned}\langle\beta|\alpha\rangle &= \exp\Big\{-\frac{|\alpha|^2}{2}-\frac{|\beta|^2}{2}\Big\}\sum_{m,n=0}^{\infty}\frac{(\beta^*)^m\alpha^n}{\sqrt{m!n!}}\langle m|n\rangle \\ &= \exp\Big\{-\frac{|\beta|^2}{2}-\frac{|\alpha|^2}{2}+\beta^*\alpha\Big\}\end{aligned}$$

and the absolute magnitude of the scalar product (probability ) is

$$\left|\langle\beta|\alpha\rangle\right|^2 = \exp\{-|\alpha-\beta|^2\} \tag{3.74}$$

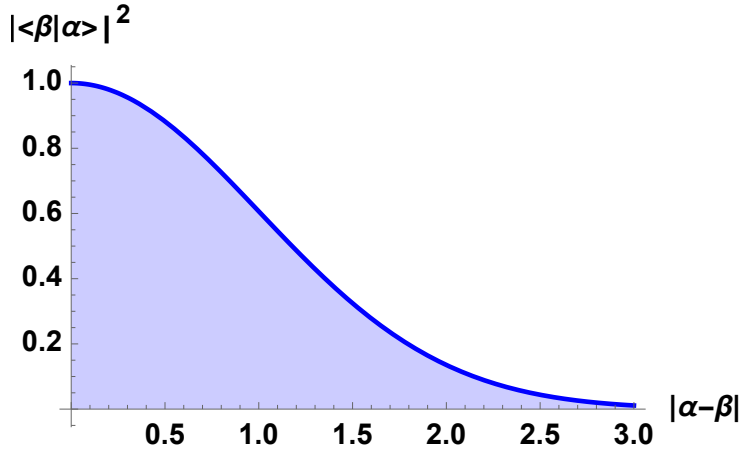


Figure 3.3: Overlap of two coherent states as a function of their distance in phase space.

Thus two coherent states are not orthogonal. Although the overlap between two coherent states is not strictly orthogonal, Fig 3.3 shows that their overlap decreases exponentially with their distance in phase space $|\alpha-\beta|$ and approaches zero (becomes orthogonal) when $|\alpha-\beta| \gg 1$. For example suppose $\beta=-\alpha$, so that the overlap is now given as $\left|\langle-\alpha|\alpha\rangle\right|^2 = e^{-4|\alpha|^2}$. Thus even for small values of $|\alpha|=2$, the overlap is $\approx 10^{-7} \approx 0$. In summary, two coherent states are macroscopically distinguishable (orthogonal) when they are well separated in phase space.

2. *Closure relation*: Coherent states satisfy the closure relation

$$\int \mathrm{d}^2\alpha\ |\alpha\rangle\langle\alpha| = \pi \tag{3.75}$$

and this can be easily shown:

$$\int \mathrm{d}^2\alpha \; |\alpha\rangle \langle\alpha| = \int \mathrm{d}^2\alpha \; e^{-|\alpha|^2} \sum_{n,m} \frac{\alpha^{*n}\alpha^m}{\sqrt{m!n!}} |m\rangle \langle n|$$

where we integrate over entire complex plane. We can express the equation in polar coordinates where

$$\alpha = re^{\mathrm{i}\theta} \qquad \Longrightarrow \qquad \mathrm{d}^2\alpha = r\mathrm{d}r\mathrm{d}\theta$$

and we get

$$\int \mathrm{d}^2\alpha e^{-|\alpha|^2}((\alpha^*)^n\alpha^m) = \int_0^\infty \mathrm{d}r \, r \, e^{-r^2} r^{m+n} \int_0^{2\pi} \mathrm{d}\theta e^{\mathrm{i}(m-n)\theta} \tag{3.76}$$

$$= 2\pi\delta_{m,n} \frac{1}{2} \int_0^\infty dr^2 (r^2)^m e^{-r^2} = \pi m! \delta_{m,n} \tag{3.77}$$

which finally gives

$$\int \mathrm{d}^2\alpha \; |\alpha\rangle \langle\alpha| = \int \mathrm{d}^2\alpha \; e^{-|\alpha|^2} \sum_{n,m} \frac{\alpha^{*n}\alpha^m}{\sqrt{m!n!}} |m\rangle \langle n| = \pi \sum_n |n\rangle \langle n| = \pi.$$

Since the overlap $|\langle\beta|\alpha\rangle| \neq 0$ for $\alpha \neq \beta$, we say coherent states $\{|\alpha\rangle\}$ form an overcomplete set and any quantum state can be decomposed in the coherent state basis.

3. *Mean photon number and variance*: the mean number of photons $\langle n\rangle$ is given by

$$\langle n\rangle = \langle\alpha| \, n|\alpha\rangle = \langle\alpha| \, a^\dagger a|\alpha\rangle = |\alpha|^2$$

and the variance in the photon number is

$$(\Delta n)^2 = \langle n^2\rangle - \langle n\rangle^2 = \langle a^\dagger a a^\dagger a\rangle - |\alpha|^4 = \langle a^\dagger a^\dagger a a\rangle - \langle a^\dagger a\rangle - |\alpha|^4 = |\alpha|^2$$

We have taken note of the property (3.54) to write the operators in normal ordering where all the $a$ terms are on the right and all the $a^\dagger$ terms on the left. The mean equals the variance in photon number, typical of a Poisson distribution.

We mention that the relative fluctuation of photon number in a coherent state is inversely proportional to the square root of its average. For large fields, we fall in the classical limit where this fluctuation becomes negligible as shown below

$$\frac{\Delta n}{\langle n\rangle} = \frac{1}{|\alpha|} = \frac{1}{\sqrt{n}} \tag{3.78}$$

4. *Photon number distribution:* coherent states do not have a definite photon number. The probability of finding $m$ photons in a coherent state $|\alpha\rangle$ is given by

$$P_m(\alpha) = \left|\langle m|\alpha\rangle\right|^2 = \left|e^{-\frac{|\alpha|^2}{2}} \sum_{k=0}^{\infty} \frac{\alpha^k}{\sqrt{k!}} \langle m|k\rangle\right|^2 = e^{-|\alpha|^2} \frac{|\alpha|^{2k}}{k!} \tag{3.79}$$

Noting that $|\alpha|^2 = \langle n\rangle = \overline{n}$, the mean photon number, then we see $P_c(\overline{n}) = e^{-\overline{n}} \frac{\overline{n}^k}{k!}$, a Poisson distribution in $\overline{n}$.

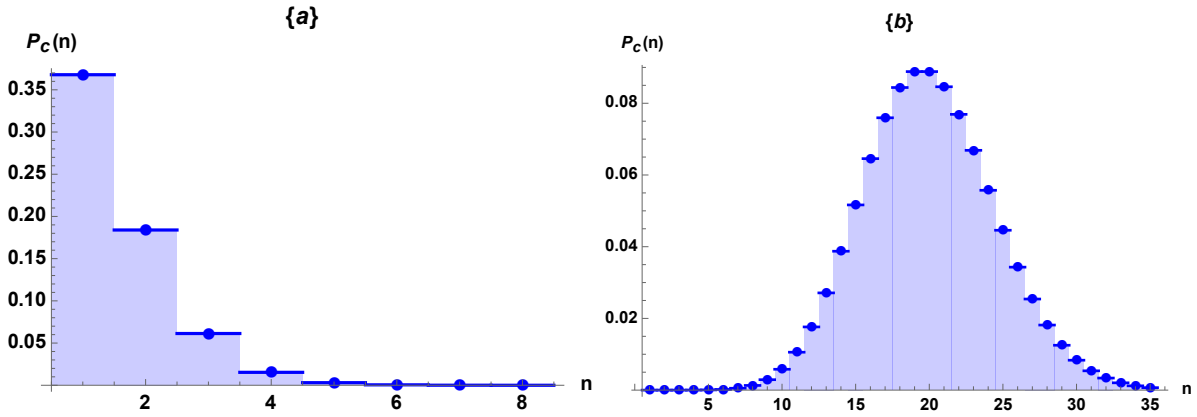


Figure 3.4: The probability of detecting $n$ photons, the photon number distribution for coherent states (a) $|\alpha|^2 = 1$ (b) $|\alpha|^2 = 20$

5. *Minimum Uncertainty*: Heisenberg uncertainty principle states that the more accurately we know the position of a particle (that is the smaller $\Delta x$ is), the less accurately we know the momentum (that is, the larger $\Delta p$ is) and vice versa. Mathematically,

$$\Delta X \Delta P \geq \frac{1}{2} \tag{3.80}$$

where $\Delta X$ and $\Delta P$ are uncertainties in position and momentum respectively. Let us now see what the minimum uncertainty principle says about coherent states.

The quadrature operators $X$ and $P$ are given as

$$X = \frac{1}{\sqrt{2}}(a + a^\dagger), \quad P = \frac{\mathrm{i}}{\sqrt{2}}(a^\dagger - a). \tag{3.81}$$

and obey the commutation relation $[X, P] = \mathrm{i}$. Recall the definition of coherent state $|\alpha\rangle$: $a|\alpha\rangle = \alpha|\alpha\rangle, \langle\alpha| a^\dagger = \langle\alpha| \alpha^*$. Thus

$$\langle X\rangle = \frac{1}{\sqrt{2}} \langle\alpha| a + a^\dagger|\alpha\rangle = \frac{1}{2}(\alpha + \alpha^*), \quad \langle P\rangle = \frac{\mathrm{i}}{\sqrt{2}} \langle\alpha| a^\dagger - a|\alpha\rangle = \frac{\mathrm{i}}{2}(\alpha^* - \alpha)$$

Similarly,

$$\langle X^2\rangle = \frac{1}{2} \langle\alpha| (a + a^\dagger)(a + a^\dagger)|\alpha\rangle = \frac{1}{2}\Big(\alpha^2 + (\alpha^*)^2 + 2\alpha^*\alpha + 1\Big) = \frac{1}{2}\Big[(\alpha + \alpha^*)^2 + 1\Big]$$
$$\langle P^2\rangle = -\frac{1}{2} \langle\alpha| (a^\dagger - a)(a^\dagger - a)|\alpha\rangle = -\frac{1}{2}\Big(\alpha^2 + (\alpha^*)^2 - 2\alpha\alpha^* - 1\Big) = -\frac{1}{2}\Big[(\alpha - \alpha^*) - 1\Big]$$

The fluctuations in these operators

$$(\Delta X)^2 = \langle\alpha| X^2|\alpha\rangle - (\langle\alpha| X|\alpha\rangle)^2 = \frac{1}{2},$$
$$(\Delta P)^2 = \langle\alpha| P^2|\alpha\rangle - (\langle\alpha| P|\alpha\rangle)^2 = \frac{1}{2}$$

Putting all these together, we have

$$\Delta X \Delta P = \frac{1}{2} \tag{3.82}$$

From Eq. (3.80), we see that all coherent states irrespective of the value of their amplitudes, are minimum uncertainty states.

### 3.3.2 Quantum superposition of coherent states

In the previous section, we discussed how two coherent states, although not strictly orthogonal, approach orthogonality when their amplitudes are large. By using coherent states with equal amplitudes and $\pi$ out of phase, one could produce a superposition of macroscopically distinguishable states known as the Schrödinger's cat state. In this section, we will discuss the Schrödinger's cat states and their quantum properties.

A superposition of two coherent states $|\alpha\rangle$ and $|\beta\rangle$ is given by

$$|\Psi\rangle = \frac{1}{\sqrt{\mathcal{N}}}(|\alpha\rangle + |\beta\rangle) \tag{3.83}$$

where $\mathcal{N}$ is the normalization constant. The coherent states are characterized by the complex amplitudes $\alpha = |\alpha|e^{\mathrm{i}\theta}$ and $\beta = |\beta|e^{\mathrm{i}\phi}$ . Now suppose the coherent states have

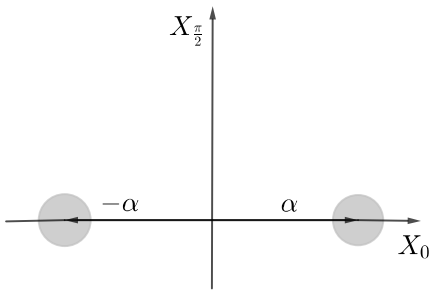


Figure 3.5: Pictorial representation of superposition of coherent states with equal amplitude and $\pi$ out of phase space. We see the two circles do not overlap.

equal amplitudes $|\alpha| = |\beta|$ but are $\pi$ - out of phase, that is $\phi = \theta + \pi$. In this case $\beta = -\alpha$ and we say that the two states are macroscopically distinguishable. In quantum optics, a Schrödinger's cat state is defined as a superposition of two coherent states with equal (large) amplitudes and $\pi$- out of phase. Mathematically it can be written as

$$|\Psi\rangle_{\text{cat}} = \frac{1}{\sqrt{\mathcal{N}}}(|\alpha\rangle + e^{\mathrm{i}\psi}|-\alpha\rangle) \tag{3.84}$$

The normalization factor $\mathcal{N}$ can be calculated by requiring that $\text{Tr}(\rho) = 1$ . This gives

$$\mathcal{N} = 2\,(1 + e^{-2|\alpha|^2}\cos\psi). \tag{3.85}$$

For $|\alpha| \gg 1$, we find $\mathcal{N} \approx 2$.

The density operator for the state is $\rho = |\Psi\rangle_{\text{cat}}\,\langle\Psi|_{\text{cat}}$

$$\rho = \frac{1}{\mathcal{N}}\Big[|\alpha\rangle\,\langle\alpha| + |-\alpha\rangle\,\langle-\alpha| + e^{-\mathrm{i}\psi}|\alpha\rangle\,\langle-\alpha| + e^{\mathrm{i}\psi}|-\alpha\rangle\,\langle\alpha|\,\Big] \tag{3.86}$$

The presence of the coherence terms $|\alpha\rangle\,\langle-\alpha|$ and $|-\alpha\rangle\,\langle\alpha|$ in (3.86) is due to quantum interference and gives the cat state its properties that distinguish it from a mere statistical mixture

$$\rho_{sm} = \frac{1}{2}(|\alpha\rangle\,\langle\alpha| + |-\alpha\rangle\,\langle-\alpha|) \tag{3.87}$$

and the different coherent states that make up the superposition. For example, the superposition (3.84) exhibits squeezing [27], higher order squeezing [63], sub-Poissonian photon statistics and oscillations in the photon number distribution [117, 27]. We need to be able to detect effects of coherence in other to observe these nonclassical properties.

As discussed in 3.3.1, if $|\alpha| \gg 1$, the two coherent states $|\alpha\rangle$ and $|-\alpha\rangle$ become orthogonal (that is macroscopically distinguishable) because their overlap approaches zero (see Fig. 3.3). This suggests that a Schrödinger's cat state can be produced by superposing coherent states. Thus a prototype of a Schrödinger's cat state is a superposition of coherent states with equal and large amplitudes and opposite phases. Recall the representation of coherent states in the number basis:

$$|\alpha\rangle = e^{-|\alpha|^2/2} \sum_{n=0}^{\infty} \frac{\alpha^n}{\sqrt{n!}} |n\rangle \tag{3.88}$$

and

$$|-\alpha\rangle = e^{-|-\alpha|^2/2} \sum_{n=0}^{\infty} \frac{(-\alpha)^n}{\sqrt{n!}} |n\rangle \tag{3.89}$$

Adding equations (3.88) and (3.89) we get

$$\begin{aligned} |\alpha\rangle + |-\alpha\rangle =& 2e^{-|\alpha|^2/2} \Big( \frac{\alpha^0}{\sqrt{0!}} |0\rangle + \frac{\alpha^2}{\sqrt{2!}} |2\rangle + \frac{\alpha^4}{\sqrt{4!}} |4\rangle + \cdots \Big) \\ =& e^{-|\alpha|^2/2} \sum_n \frac{1 + (-1)^n}{\sqrt{n!}} \alpha^n |n\rangle \end{aligned} \tag{3.90}$$

Here the odd terms cancel and we have only superposition of even number states. Similarly subtracting equation (3.89) from (3.88), we get

$$|\alpha\rangle - |-\alpha\rangle = 2e^{-|\alpha|^2/2} \Big( \frac{\alpha^1}{\sqrt{1!}} |1\rangle + \frac{\alpha^3}{\sqrt{3!}} |3\rangle + \frac{\alpha^5}{\sqrt{5!}} |5\rangle + \cdots \Big) \tag{3.91}$$

$$= e^{-|\alpha|^2/2} \sum_n \frac{1 - (-1)^n}{\sqrt{n!}} \alpha^n |n\rangle \tag{3.92}$$

Here, the even terms cancel out and we are left with superposition of only odd numbered states. The disappearance of the odd and even number states in (3.90) and (3.91) is the result of quantum interference.

Let us now introduce the three Schrödinger's cat states important for our study, defined according to our choice of $\psi$ in (3.84).

For $\psi = 0$ we obtain the even cat state,

$$|\psi\rangle_{\text{even}} = \frac{(|\alpha\rangle + |-\alpha\rangle)}{\sqrt{2 + 2e^{-2|\alpha|^2}}} \tag{3.93}$$

for $\psi = \pi$, the odd cat state

$$|\psi\rangle_{\text{odd}} = \frac{(|\alpha\rangle - |-\alpha\rangle)}{\sqrt{2 - 2e^{-2|\alpha|^2}}} \tag{3.94}$$

According to equations (3.90) and (3.91), the even and odd cat states [27, 42, 117] contain even and odd photon numbers respectively, which is why they are so called. The even and odd cat states can thus be discriminated by a photon parity measurement, which can be represented by [93]

$$O_{\Pi} = \sum_n (|2n\rangle \langle 2n| - |2n+1\rangle \langle 2n+1|) \tag{3.95}$$

Importantly, note that the even and odd cat states are orthogonal

$$\langle \psi_{\text{odd}} | \psi_{\text{even}} \rangle = \frac{1}{2\mathcal{N}_{\pm}} \Big( \langle \alpha | \, \alpha \rangle + \langle \alpha | -\alpha \rangle - \langle -\alpha | \, \alpha \rangle - \langle -\alpha | -\alpha \rangle \Big) = 0 \tag{3.96}$$

where the overlap

$$\langle \alpha | -\alpha \rangle = e^{-2|\alpha|^2} \tag{3.97}$$

according to equation (3.74). The orthogonality between the even and odd cat states implies that they are macroscopically distinguishable

Another important cat state in quantum optics is the Yuker-Stoler cat state, given when $\psi = \pi/2$. For $\psi = \frac{\pi}{2}$, the Yuker-Stoler cat states [138]

$$|\Psi\rangle_{\text{ys}} = \frac{1}{\sqrt{\mathcal{N}}} (|\alpha\rangle + \mathrm{i}|-\alpha\rangle) \tag{3.98}$$

The expectation value of $a$ and $a^\dagger$ in the cat states vanishes so that

$$\langle \Psi |_{\psi} \, X | \Psi \rangle_{\psi} = 0, \qquad \langle \Psi |_{\psi} \, P | \Psi \rangle_{\psi} = 0. \tag{3.99}$$

However the expectation values of a combination of the photon operators exist. The three cat states are normalized eigenstates of the operator $a^2$

$$a^2 |\Psi\rangle_{\psi} = \alpha^2 |\Psi\rangle_{\psi} \tag{3.100}$$

The mean number of photons in the cat states is given by $\overline{n} = \langle\Psi|_\psi\, a^\dagger a|\Psi\rangle_\psi$. For the even cat state, we have

$$\overline{n}_e = \frac{1 - e^{-(2|\alpha|^2)}}{1 + e^{(-2|\alpha|^2)}}|\alpha|^2 \tag{3.101}$$

For odd cat state, we have

$$\overline{n}_o = \frac{1 + e^{-(2|\alpha|^2)}}{1 - e^{(-2|\alpha|^2)}}|\alpha|^2 \tag{3.102}$$

For the Yuker-Stoler cat state, $\overline{n}_{ys} = |\alpha|^2$ similar to that of a coherent state and a statistical mixture.

Several successful attempts have been put forward to realize a superposition of macroscopically distinguishable states [34, 138, 79, 26, 134]. However realizing a superposition of the form (3.84) poses a challenge and such superpositions are never seen in our everyday world. Why not? The reason is partly because quantum systems are in constant interaction with their environment in a dissipative way. If we can somehow create a superposition of coherent states, it will quickly decohere into a statistical mixture (3.87) of coherent states [59]. We will address the issue of decoherence later. In the next section, we will discuss the nonclassical properties of a superposition of coherent states.

## Nonclassical properties of superpositions of coherent states

The nonclassical properties that classify a superposition of coherent state would be discussed here.

### *Photon number distribution*

The photon number distribution for the even and odd cat states can be calculated using the expansion in Fock basis (3.90) and (3.91)

$$P_n(|\Psi_\psi\rangle) = \Big|\langle n|\Psi_\psi\rangle\Big|^2$$

For even cat state, we obtain

$$P_n(|\psi\rangle_{\text{even}}) = \frac{e^{-|\alpha|^2}}{2(1 + e^{-|\alpha|^2})}\left|\frac{\alpha^n}{\sqrt{n!}} + \frac{(-1)^n\alpha^n}{\sqrt{n!}}\right|^2 = \frac{e^{-|\alpha|^2}}{1 + e^{-2|\alpha|^2}}\frac{|\alpha|^{2n}}{n!}(1 + (-1)^n)$$

For odd cat state

$$P_n(|\psi\rangle_{\text{odd}}) = \frac{e^{-|\alpha|^2}}{2(1-e^{-|\alpha|^2})}\left|\frac{\alpha^n}{\sqrt{n!}} - \frac{(-1)^n\alpha^n}{\sqrt{n!}}\right|^2 = \frac{e^{-|\alpha|^2}}{1-e^{-2|\alpha|^2}}\frac{|\alpha|^{2n}}{n!}(1-(-1)^n)$$

In summary for an even cat state, we obtain

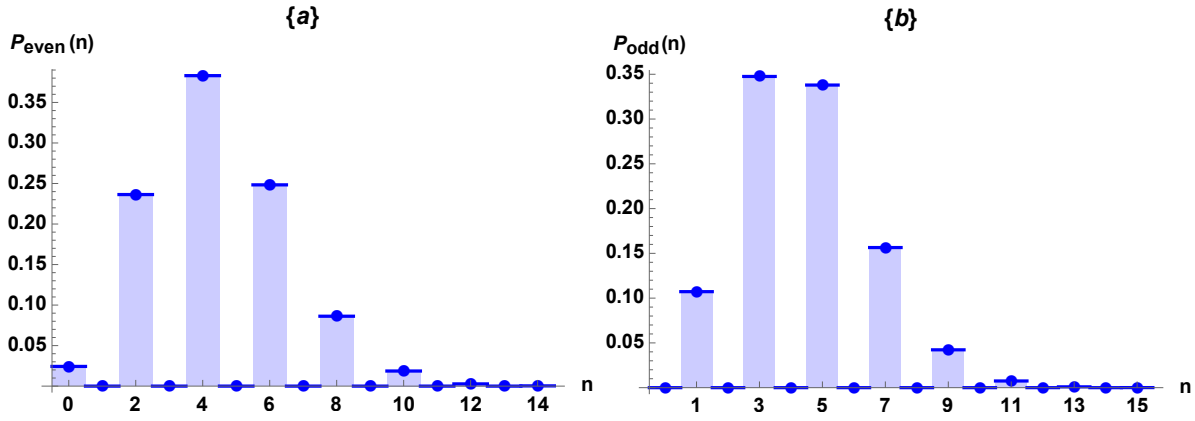


Figure 3.6: The probability of detecting $n$ photons, the photon number distribution for even cat state (a) and odd cat state (b) with $|\alpha| = 2.1$.

$$P_n = \begin{cases} \frac{2\exp(-|\alpha|^2)}{1+\exp(-2|\alpha|^2)}\ \frac{|\alpha|^{2n}}{n!} & n \text{ even} \\ 0 & n \text{ odd} \end{cases} \tag{3.103}$$

For odd cat state, we obtain

$$P_n = \begin{cases} 0 & n \text{ even} \\ \frac{2\exp(-|\alpha|^2)}{1-\exp(-2|\alpha|^2)}\ \frac{|\alpha|^{2n}}{n!} & n \text{ odd} \end{cases} \tag{3.104}$$

For Yuker-Stoler cat state, $P_n$ is just a Poisson distribution, identical to that of a coherent state (3.79) and a statistical mixture $\langle n|\rho_{sm}|n\rangle$. The oscillatory behaviour we see in Fig. 3.6 distinguishes the even and odd cat states from their statistical mixture (3.87).

***Mandel Q parameter***

Another nonclassical effect that describes a superposition of coherent states is the Mandel Q parameter [84] given by

$$Q = \frac{\langle a^{\dagger 2} a^2 \rangle - \langle a^\dagger a \rangle^2}{\langle a^\dagger a \rangle} = \frac{4\exp(-2|\alpha|^2)}{1 - \exp(-4|\alpha|^2)\cos^2(\psi)} |\alpha|^2 \cos\psi$$

Specifically, $Q$ describes the deviations from the Poisson character of the field. The states

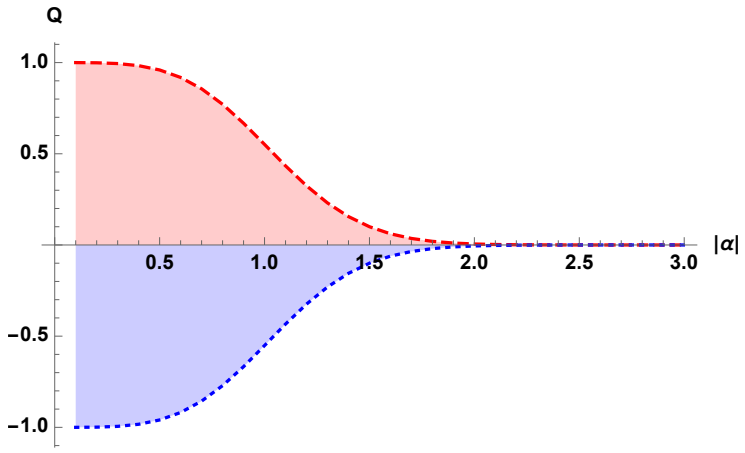


Figure 3.7: Mandel Q parameter as a function of coherent amplitude $|\alpha|$ for even cat state (red dashed curve) and odd cat state (blue dotted curve).

are called Poissonian, sub-Poissonian and super-Poissonian when $Q = 0, < 0$ and when $Q > 0$ respectively. For even cat state we obtain

$$Q = \frac{4\exp(-2|\alpha|^2)}{1 - \exp(-4|\alpha|^2)} |\alpha|^2 > 0 \tag{3.105}$$

For odd cat state, we obtain

$$Q = -\frac{4\exp(-2|\alpha|^2)}{1 - \exp(-4|\alpha|^2)} |\alpha|^2 < 0 \tag{3.106}$$

And $Q = 0$ for the Yuker-Stoller cat state for all values of $|\alpha|$. We note that for large values of $|\alpha| \geq 2$ (see Fig 3.7), $Q \to 0$ for both even and odd cat state.

***Quadrature Squeezing***

Another way to distinguish a superposition of coherent states from a statistical mixture of coherent states (3.87) is by looking at the quadrature squeezing via the quadrature operators $X$ and $P$ defined in (3.81). A quantized field is said to be squeezed [75] if the non commuting quadrature operators have any of their variances below their vacuum level. That is either $\Delta p < \frac{1}{4}$ or $\Delta x < \frac{1}{4}$. The variance of the $X$ and $P$ quadratures for a statistical mixture of coherent states (3.87) is given by

$$\langle(\Delta X)^2\rangle_{sm} = \mathrm{Tr}\Big[\rho_{sm}X^2\Big] - \mathrm{Tr}\Big[\rho_{sm}X\Big]^2 = \frac{1}{4}(\alpha^2 + (\alpha^*)^2 + 2|\alpha|^2 + 1),$$
$$\langle(\Delta P)^2\rangle_{sm} = \mathrm{Tr}\Big[\rho_{sm}P^2\Big] - \mathrm{Tr}\Big[\rho_{sm}P\Big]^2 = \frac{1}{4}(-\alpha^2 - (\alpha^*)^2 + 2|\alpha|^2 + 1),$$

where by definition, $X^2 = \frac{1}{4}(a^2 + a^{\dagger 2} + 2a^\dagger a + 1)$ and $P^2 = \frac{1}{4}(-a^2 - a^{\dagger 2} + 2a^\dagger a + 1)$. If we take the phase of the coherent state $\theta = \pi/2$, we obtain

$$\langle(\Delta X)^2\rangle_{sm} = \frac{1}{4} \tag{3.107}$$
$$\langle(\Delta P)^2\rangle_{sm} = \frac{1}{4} + |\alpha|^2 \tag{3.108}$$

Thus there's no squeezing in the quadratures. For an even cat state we get

$$\langle(\Delta X)^2\rangle_e = \langle\psi|\, X^2|\psi\rangle_{\text{even}} - (\langle\psi|\, X|\psi\rangle_{\text{even}})^2 \tag{3.109a}$$
$$\langle(\Delta P)^2\rangle_e = \langle\psi|\, P^2|\psi\rangle_{\text{even}} - (\langle\psi|\, P|\psi\rangle_{\text{even}})^2 \tag{3.109b}$$

The second terms vanish and so we obtain

$$\langle(\Delta X)^2\rangle = \langle\psi|\, X^2|\psi\rangle_{\text{even}} = \frac{1}{4} + \frac{1}{4}\Big[\alpha^2 + (\alpha^*)^2 + 2\overline{n}_e\Big] \tag{3.110a}$$
$$\langle(\Delta P)^2\rangle = \langle\psi|\, P^2|\psi\rangle_{\text{even}} = \frac{1}{4} - \frac{1}{4}\Big[\alpha^2 + (\alpha^*)^2 - 2\overline{n}_e\Big] \tag{3.110b}$$

where $\overline{n}_e$ is the average photon number in even cat state given by $\overline{n}_e = \frac{1-e^{-2|\alpha|^2}}{1+e^{-2|\alpha|^2}}|\alpha|^2$ (3.101). When we take the phase of the coherent state $\theta = \pi/2$, we obtain

$$\langle(\Delta X)^2\rangle_e = \frac{1}{4} - \frac{|\alpha|^2 e^{-2|\alpha|^2}}{1 + e^{-2|\alpha|^2}} \tag{3.111a}$$
$$\langle(\Delta P)^2\rangle_e = \frac{1}{4} + \frac{|\alpha|^2}{1 + e^{-2|\alpha|^2}} \tag{3.111b}$$

Recall the complex amplitude $\alpha = |\alpha|e^{i\theta}$ so that taking $\theta = \pi/2$ we obtain $\alpha = i|\alpha|$ and (3.111) follows from evaluating (3.110)

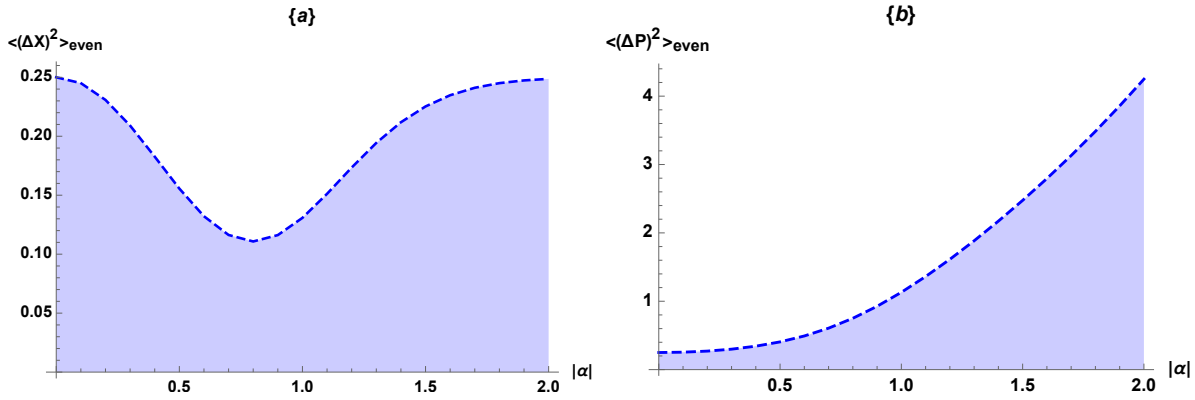


Figure 3.8: The uncertainty in $X$ quadrature amplitude (a) and $P$ quadrature amplitude (b) in even cat state

So reduced fluctuations appear in $X$ quadrature for small values of $\alpha$ evident in Fig. 3.8(a) where we see the curve has a minimum along the curve. We point out that most texts have assumed the complex parameter $\alpha$ to be real; in this context, reduced fluctuations would appear in the $P$ quadrature.

For odd cat state

$$\langle(\Delta X)^2\rangle_{\text{odd}} = \langle\psi|\, X^2|\psi\rangle_{\text{odd}} = \frac{1}{4} + \frac{1}{4}\Big[\alpha^2 + (\alpha^*)^2 + 2\overline{n}_o\Big] \tag{3.112a}$$

$$\langle(\Delta P)^2\rangle_{\text{odd}} = \langle\psi|\, P^2|\psi\rangle_{\text{odd}} = \frac{1}{4} - \frac{1}{4}\Big[\alpha^2 + (\alpha^*)^2 - 2\overline{n}_o\Big] \tag{3.112b}$$

where $\overline{n}_o$ is the average photon number in odd cat state given by $\overline{n}_o = \frac{1+e^{-2|\alpha|^2}}{1-e^{-2|\alpha|^2}}|\alpha|^2$ (3.101). When we take the phase of the coherent state $\theta = \pi/2$, we obtain

$$\langle(\Delta X)^2\rangle_o = \frac{1}{4} + \frac{|\alpha|^2 e^{-2|\alpha|^2}}{1 - e^{-2|\alpha|^2}} \tag{3.113}$$

$$\langle(\Delta P)^2\rangle_o = \frac{1}{4} + \frac{|\alpha|^2}{1 - e^{-2|\alpha|^2}} \tag{3.114}$$

and thus no squeezing is evident. For the Yuker-Stoler cat state, we obtain

$$\langle(\Delta X)^2\rangle_{ys} = \frac{1}{4} - |\alpha|^2 e^{-4|\alpha|^2} \tag{3.115}$$

$$\langle(\Delta P)^2\rangle_{ys} = \frac{1}{4} + |\alpha|^2 \tag{3.116}$$

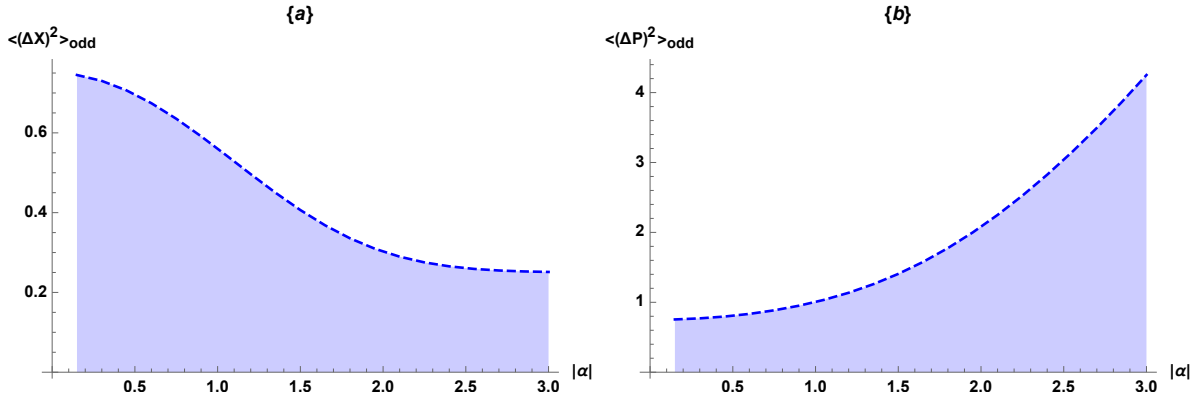


Figure 3.9: The uncertainty in $X$ quadrature amplitude (a) and $P$ quadrature amplitude (b) in odd cat state

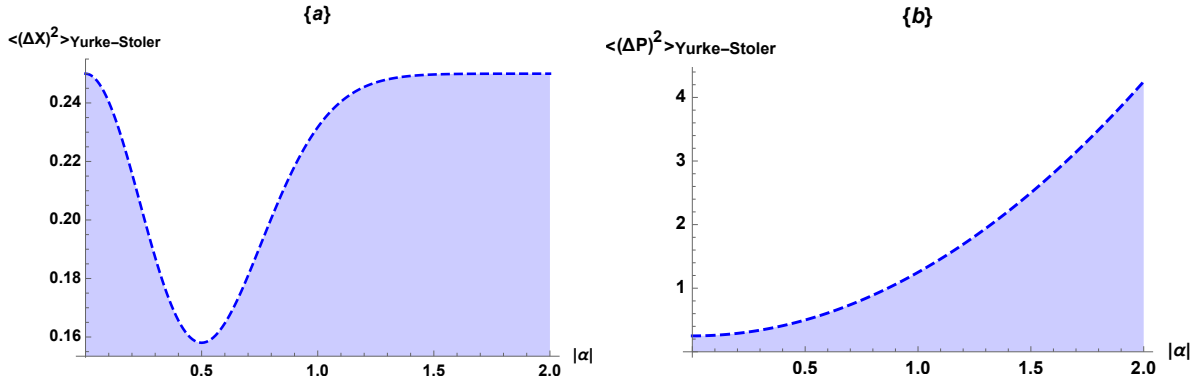


Figure 3.10: The uncertainty in $X$ quadrature amplitude (a) and $P$ quadrature amplitude (b) in Yuker-Stoler cat state

Having discussed the properties of the various Schrödinger's cat states, we are now ready to describe a method used to detect these properties in quantum optics. The method

involves an interaction between the field and a detector (usually in form of a two-level atom). Therefore we first describe the principle of atom-field interaction. Let us recall Schrödinger's thought experiment with a live cat and a radioactive atom, both inside a box. The decaying atom triggers a death mechanism that kills the cat. However without details of what happens inside the box, the atom and cat are in an entangled superposition of decayed-and-dead and undecayed-and-alive simultaneously.

The entangled Schrödinger's cat-atom system with the radioactive atom in a box is analogous to an entangled superposition of coherent states with a two-level atom

$$|\Psi\rangle_{\text{Bell-cat}} = \frac{1}{\sqrt{2}}(|g,\alpha\rangle + |e,-\alpha\rangle), \tag{3.117}$$

trapped in a cavity mode. What do we know about the entanglement of this state? How does the presence of the two-level atom affect the cat state? To answer these questions, we first discuss the interaction process between an atom and EM field in free space.

## 3.4 The atom-field interaction models

Combining the two-level system and a given state of the electromagnetic field in an interaction and in a controlled environment (example a cavity) gives birth to interesting phenomena [2] such as multimode squeezing [74, 78, 83, 122], superradiance [40], Rabi oscillations [5] and the corresponding so-called vacuum Rabi oscillations [70], collapse and revival [43, 109] and atom-field entanglement [13] and Schrödinger's cat [59, 25]. When the field and two-level atom states interact, the electron absorbs photon energy and make a transition into the higher energy level. On the other hand, the electron may also make a transition from the higher energy level to its ground energy level. The bipartite system of the two-level system and quantum field is described by a total Hamiltonian

$$H = H_0 + H_{\text{int}}. \tag{3.118}$$

$H_0$ is a time-independent Hamiltonian given by

$$H_0 = H_{\text{atom}} + H_{\text{field}}, \tag{3.119}$$

where $H_{\text{field}} = \hbar\omega a^\dagger a$ is the free field Hamiltonian, $a^\dagger(a)$ is the field's creation(annihilation) operator and $\omega$ is the cavity frequency. $H_{\text{atom}} = \hbar\Omega\sigma_z$ is the free atom Hamiltonian, $\sigma_z$ is the Pauli operator and $\Omega$ is the transition frequency between the excited and ground

state of the atom. We note that the spectrum of $H_0$ is known and $H_{\text{int}}$ acts as a perturbation. To describe the interaction process, two important models can be identified–The Jaynes-Cummings model and the Unruh deWitt-model. In this section, we will give a brief discussion on these models with focus on the Unruh DeWitt model.

### 3.4.1 The Jaynes-Cummings model

The Jaynes-Cummings (JC) model [70] is the simplest model describing light-matter interaction where a single two-level atom interacts with a single mode quantized EM field inside a highly reflective cavity. As we have discussed earlier, for the case of a free EM field (plane waves), an atom would interact with infinite number of modes, thus the dynamics is not well described. By trapping the field inside the cavity (example the optical cavities, microwave cavities), we confine the field to a space where their dynamics can be easily described. This is the idea of cavity quantum electrodynamics (CQED). Here in this section, the Jaynes Cummings model is briefly reviewed and how it models the dynamics of atom-cavity field system.

To begin, consider a two-level atom with ground and excited states $|g\rangle$ and $|e\rangle$ respectively; interacting with a single cavity field with an electric field component given as

$$\mathbf{E} = \mathbf{e}\left(\frac{\hbar\omega}{\varepsilon_0 V}\right)^{1/2}(a + a^\dagger)\sin(kx). \tag{3.120}$$

Before interaction, the atom-field free Hamiltonian can be written as

$$H_0 = \hbar\omega a^\dagger a + \hbar\Omega\sigma_z \tag{3.121}$$

#### *Interaction Hamiltonian*

The interaction Hamiltonian is given as

$$H_{\text{int}} = -\hat{\mathbf{d}}\cdot\hat{\mathbf{E}} = \hat{d}\lambda(a + a^\dagger) \tag{3.122}$$

where $\lambda = -\sin(kx)\left(\frac{\hbar\omega}{\varepsilon_0 V}\right)^{1/2}$ is the interaction strength (coupling constant), and $\hat{d} = \hat{\mathbf{d}}\cdot\mathbf{e}$ is the electric dipole operator. Since the operators

$$|g\rangle\langle g|, |g\rangle\langle e|, |e\rangle\langle g|, |e\rangle\langle e| \tag{3.123}$$

form a complete basis, we can expand the dipole operator $\hat{d}$ in this basis.

$$\hat{d} = \langle g|\, d|g\rangle |g\rangle\, \langle g| + \langle g|\, d|e\rangle |g\rangle\, \langle e| + \langle e|\, d|g\rangle |e\rangle\, \langle g| + \langle e|\, d|e\rangle |e\rangle\, \langle e|$$

therefore

$$\hat{d} = d_+\sigma^+ + d_-\sigma^-, \qquad d_+ = \langle e|\, d|g\rangle, d_- = \langle g|\, d|e\rangle \tag{3.124}$$

We note that an atom exhibits electric dipole moment because we have assumed it is in a superposition of $|e\rangle$ and $|g\rangle$ states respectively. In the case where we consider an atom either in the ground or excited state, then a monopole is described [97]. Thus combining terms, the interaction Hamiltonian (3.122) becomes

$$H_{\text{int}} = \hbar\,\lambda\,(\sigma^+ a + \sigma^- a^\dagger + \sigma^- a + \sigma^+ a^\dagger) \tag{3.125}$$

We see that $H_{\text{int}}$ contains four terms

- $\sigma^+ a \longleftrightarrow$ absorption of photons while the atom transit from state $|g\rangle \to |e\rangle$.
- $\sigma^- a^\dagger \longleftrightarrow$ emission of photons while the atom transit from state $|e\rangle \to |g\rangle$
- $\sigma^+ a^\dagger \longleftrightarrow$ emission of photons and transition of atoms from state $|g\rangle \to |e\rangle$
- $\sigma^- a \longleftrightarrow$ absorption of photons and transition of atoms from state $|e\rangle \to |g\rangle$

To simplify the Jaynes-Cummings interaction Hamiltonian (3.125), the rotating wave approximation can be employed. First moving from Schrödinger picture to the interaction picture with respect to $H_0$, through the unitary operator $U = e^{\frac{\mathrm{i}}{\hbar}H_0 t}$, the atom and field operators transform according to the relation

$$\begin{aligned} Ua^\dagger U^\dagger \to a^\dagger e^{\mathrm{i}\omega t}, \quad UaU^\dagger \to a e^{-\mathrm{i}\omega t}, \\ U\sigma^+ U^\dagger \to \sigma^+ e^{\mathrm{i}\Omega t}, \quad U\sigma^- U^\dagger \to \sigma^- e^{-\mathrm{i}\Omega t} \end{aligned}$$

Thus Jaynes Cummings Hamiltonian in the interaction picture becomes

$$H_{\text{int}}(t) = \hbar\lambda\Big(\sigma^+ a e^{-\mathrm{i}(\omega-\Omega)t} + \sigma^- a^\dagger e^{\mathrm{i}(\omega-\Omega)t} + \sigma^- a e^{-\mathrm{i}(\omega+\Omega)t} + \sigma^+ a^\dagger e^{\mathrm{i}(\omega+\Omega)t}\Big) \tag{3.126}$$

The first two terms $\sigma^+ a$ and $\sigma^- a^\dagger$ are multiplied by exponentials that are slowly oscillating while the last two terms $\sigma^- a$ and $\sigma^+ a^\dagger$ are multiplied by exponentials that are rapidly oscillating. Now usually one is interested in the near resonant case $\omega \approx \Omega$, at which

$$|\omega - \Omega| \ll \omega + \Omega. \tag{3.127}$$

which implies the rapidly oscillating terms will average to zero during the time evolution. Again, one requires situation where the atom-cavity interaction time is long enough compared to cavity decay and spontaneous emission rates respectively. This is the strong coupling regime ($\frac{\lambda}{\omega} \approx 10^{-6} - 10^{-7}$). Now when we integrate in time over the Hamiltonian (3.126), the energy conserving terms are related to the ratio $\frac{\lambda}{\omega-\Omega}$ that are very dominant compared to the energy non-conserving terms which are related to $\frac{\lambda}{\omega+\Omega}$. Hence by considering a resonant interaction of an atom-field system in CQED, we can disregard contributions from the counter rotating wave terms $\sigma^+ a^\dagger$ and $\sigma^- a$ and the effective Jaynes Cummings interaction Hamiltonian in the interaction picture is given as

$$\hat{H}_{\text{int}} = \hbar\lambda(\sigma^+ a\, e^{-\mathrm{i}(\omega-\Omega)t} + \sigma^- a^\dagger\, e^{\mathrm{i}(\omega-\Omega)t}) \tag{3.128}$$

Transforming back to the Schrödinger's picture, we obtain

$$\hat{H}_{\text{int}} = \hbar\lambda(\sigma^+ a + \sigma^- a^\dagger) \tag{3.129}$$

The Jaynes-Cummings Hamiltonian is then

$$\hat{H}_{jc} = \frac{1}{2}\hbar\Omega\sigma_z + \hbar\omega a^\dagger a + \hbar\lambda(\sigma^+ a + \sigma^- a^\dagger) \tag{3.130}$$

Although eliminating the counter rotating wave terms enabled us to find a simplification for the Jaynes Cummings Hamiltonian, it is important to know that such terms can be a limiting factor to some problems in physics. We will show later in the chapter how keeping the rotating (slowly oscillating) terms can jeopardize our ability of reading information about the cavity field system.

### *Understanding the atom-field dynamics*

Here we want to understand how the Jaynes-Cummings model describes effectively the coupling of a single atom to a cavity mode, and we also discuss some basic phenomena associated with such interactions. To begin, consider an initially excited two level atom interacting with a field trapped in a cavity mode and containing $n$ photons. We will first solve the Schrödinger's equation of motion for the system's interaction Hamiltonian (3.129). In the interaction picture, the Schrödinger's equation is given as

$$\mathrm{i}\hbar\frac{d|\psi(t)\rangle}{dt} = H_{\text{int}}|\psi(t)\rangle \tag{3.131}$$

Now let the initial atom-field state vector be written as a superposition state

$$|\psi(0)\rangle = C_i|i\rangle + C_f|f\rangle. \tag{3.132}$$

As an initial condition, assume all the population to be in the ground state:

$$C_i(0) = 1, \qquad C_f(0) = 0 \tag{3.133}$$

Our task is to find the solution to the Schrödinger's equation. To proceed, the initial atom-field state is $|i\rangle = |e, n\rangle$ and at a later time, the only possible transition is to the final state $|f\rangle = |g, n+1\rangle$. The states $|e, n\rangle$ and $|g, n+1\rangle$ are known as the bare states of the Jaynes-Cummings model. Substituting the interaction Hamiltonian (3.129) and the state (3.132) in (3.131), we obtain

$$\Big(\dot{C}_i|n, e\rangle + \dot{C}_f|n+1, g\rangle\Big) = -\mathrm{i}\lambda\Big(C_i\sqrt{n+1}|n+1, g\rangle + C_f\sqrt{n+1}|n, e\rangle\Big)$$

We arrive at the following system of uncoupled equations

$$\dot{C}_i + \mathrm{i}\lambda C_f\sqrt{n+1} = 0, \qquad \dot{C}_f + \mathrm{i}\lambda C_i\sqrt{n+1} = 0.$$

Differentiating the uncoupled equations, we obtain the corresponding second order differential equations

$$\ddot{C}_i + \lambda^2 C_i(n+1) = 0, \qquad \ddot{C}_f + \lambda^2 C_f(n+1) = 0.$$

Imposing the initial conditions (3.133), the solutions to the second order equations can be written as

$$C_i(t) = \cos\Big(\lambda t\sqrt{n+1}\Big), \qquad C_f(t) = -\mathrm{i}\sin\Big(\lambda t\sqrt{n+1}\Big) \tag{3.134}$$

And we have final atom-field state vector at later time $t$ is given as

$$|\psi(t)\rangle = \cos\Big(\lambda t\sqrt{n+1}\Big)|e, n\rangle - \mathrm{i}\sin\Big(\lambda t\sqrt{n+1}\Big)|g, n+1\rangle \tag{3.135}$$

***Vacuum Rabi oscillations***

The probability that the system makes a transition to the final state is

$$P_f \;=\; |C_f(t)|^2 = \sin^2\Big(\lambda t\sqrt{n+1}\Big), \tag{3.136}$$

while the probability that the system remains in the initial state is

$$P_i = |C_i(t)|^2 = \cos^2\left(\lambda t\sqrt{n+1}\right) \tag{3.137}$$

It is interesting to consider the atomic inversion ($W(t)$), defined as the difference between in the excited state and ground state populations:

$$W(t) = P_i - P_f \tag{3.138}$$

$$= \cos(2\lambda t\sqrt{n+1}) \tag{3.139}$$

where we have used the trigonometric identity $\cos^2 x - \sin^2 x = \cos 2x$. We see that the atomic population oscillates with frequency $\omega_R = 2\lambda\sqrt{n+1}$ back and forth between the ground and excited states. We notice that even in the absent of the radiation field, that is in the case of no photons $n = 0$, we have $W(t) = \cos(2\lambda t)$, that is the oscillation is not absent. This is in contrast to the Rabi oscillation of the atoms induced by classical external field [5], the vacuum Rabi oscillation is purely a quantum mechanical phenomena.

### *The dressed states*

One of the most striking manifestations of the quantum nature of atom-field interaction is the collapse and revival of the vacuum Rabi oscillations and the splitting in the spontaneous-emission spectra of atoms in cavity. In this section we will discuss this collapse and revival of the Rabi oscillations.

To begin, we will solve the Schrödinger's equation for the full Jaynes-Cummings Hamiltonian (3.130). Assuming the field initially in a number state $|n\rangle$ with $n$ number of photons. First note that in the Jaynes-Cummings model, the total number of excitation $\hat{N} = \sigma_+\sigma_- + a^\dagger a$ is a constant of motion, that is $[\hat{N}, \hat{H}] = 0$. We can solve the dynamics of the system for the subspace spanned by the bare states $\{|n, e\rangle, |n+1, g\rangle\}$.

Eigenstates and Eigenenergies

By fixing $n$, let us now write the full Jaynes-Cummings Hamiltonian (3.130) in the basis state $\{|n, e\rangle, |n+1, g\rangle\}$.

$$\hat{H}_n = \sum_{ij} \langle i| H_{jc}|j\rangle|i\rangle \langle j| = \sum_{ij} \langle i| \left(\hbar\omega a^\dagger a + \frac{1}{2}\hbar\Omega\sigma_z + \hbar\lambda(\sigma^+ a + \sigma^- a^\dagger)\right)|j\rangle|i\rangle \langle j|$$

Here $\{i,j\} \in \{(n,e),(n+1,g)\}$. This gives

$$\begin{aligned}
H_n &= \langle n,e|\left(\hbar\omega a^\dagger a + \frac{1}{2}\hbar\Omega\sigma_z + \hbar\lambda(\sigma^+ a + \sigma^- a^\dagger)\right)|n,e\rangle|n,e\rangle\langle n,e| \\
&+ \langle n,e|\left(\hbar\omega a^\dagger a + \frac{1}{2}\hbar\Omega\sigma_z + \hbar\lambda(\sigma^+ a + \sigma^- a^\dagger)\right)|n+1,g\rangle|n,e\rangle\langle n+1,g| \\
&+ \langle n+1,g|\left(\hbar\omega a^\dagger a + \frac{1}{2}\hbar\Omega\sigma_z + \hbar\lambda(\sigma^+ a + \sigma^- a^\dagger)\right)|n,e\rangle|n+1,g\rangle\langle n,e| \\
&+ \langle n+1,g|\left(\hbar\omega a^\dagger a + \frac{1}{2}\hbar\Omega\sigma_z + \hbar\lambda(\sigma^+ a + \sigma^- a^\dagger)\right)|n+1,g\rangle|n+1,g\rangle\langle n+1,g|
\end{aligned}$$

Evaluating each term yields

$$\begin{aligned}
H_n &= \left(\hbar\omega n + \frac{1}{2}\hbar\Omega\right)|n,e\rangle\langle n,e| + \left(\hbar\,\lambda\sqrt{n+1}\right)|n,e\rangle\langle n+1,g| \\
&+ \left(\hbar\,\lambda\sqrt{n+1}\right)|n+1,g\rangle\langle n,e| + \left(\hbar\omega(n+1) - \frac{1}{2}\hbar\Omega\right)|n+1,g\rangle\langle n+1,g|
\end{aligned}$$

In matrix form, the Hamiltonian can be written as

$$\hat{H}_n = \frac{\hbar}{2}\begin{pmatrix} 2n\omega+\Omega & 2\lambda\sqrt{n+1} \\ 2\,\lambda\sqrt{n+1} & 2\omega(n+1)-\Omega \end{pmatrix} = \frac{\hbar}{2}\begin{pmatrix} (2n+1)\omega-\delta & \Omega_n \\ \Omega_n & (2n+1)\omega+\delta \end{pmatrix} \tag{3.140}$$

$\Omega_n = 2\,\lambda\sqrt{n+1}$, while $\delta = \omega - \Omega$ is the frequency detuning between the field and atomic transition. The energy eigenvalues are

$$E_\pm = \left(n+\frac{1}{2}\right)\hbar\omega \pm \frac{\hbar}{2}\Delta_n, \quad \Delta_n = \sqrt{\delta^2+\Omega_n^2} \tag{3.141}$$

The corresponding eigenstates $|\pm,n\rangle$ associated with the energy eigenvalues are given as [90]

$$|+,n\rangle = \sin\theta_n|e,n\rangle + \cos\theta_n|g,n+1\rangle, \tag{3.142a}$$
$$|-.n\rangle = \cos\theta_n|e,n\rangle - \sin\theta_n|g,n+1\rangle \tag{3.142b}$$

where

$$\sin\theta_n = \frac{\Omega_n}{\sqrt{(\Delta_n-\delta)^2+\Omega_n^2}}, \quad \cos\theta_n = \frac{\Delta_n-\delta}{\sqrt{(\Delta_n-\delta)^2+\Omega_n^2}}$$

The states $|n, \pm\rangle$ are called the dressed states. We define the Stark shift as the splitting of the bare states into dressed states. Here $\Delta_n$ is the Rabi frequency. We see that at exact resonance when $\delta = 0$, we obtain $\Delta_n = \Omega_n$. and the energy eigenvalues are given by

$$E_{\pm} = \Big(n + \frac{1}{2}\Big)\hbar\omega \pm \frac{\hbar}{2}\Omega_n \tag{3.143}$$

The corresponding eigenstates become

$$|+, n\rangle = \frac{1}{\sqrt{2}}(|e, n\rangle + |g, n+1\rangle), \tag{3.144a}$$

$$|-.n\rangle = \frac{1}{\sqrt{2}}(|e, n\rangle - |g, n+1\rangle) \tag{3.144b}$$

and the bare states are degenerate and separated by the frequency

$$\Omega_n(0) = 2\lambda \tag{3.145}$$

Experiments to show the vacuum Rabi frequency have been performed recently [25, 129]

***The dispersive interaction***

In our previous discussion, we have mostly assumed a zero frequency detuning between the field and two-level atom. That is atomic transition frequency is resonant with the cavity field frequency. An interesting version of the Jaynes-Cummings model is seen in which this detuning is large enough such that direct atomic transition is suppressed, however a dispersive interaction between the atom and cavity field do occur. This dispersive interaction regime is important in a number of applications for fundamental tests of quantum mechanical theories.

In this section, we will discuss the dispersive interaction. Within this dispersive limit, the effective Hamiltonian for the Jaynes-Cummings model can be written as [120, 107, 100, 51]

$$H_{\text{eff}} = \frac{\hbar\Omega}{2}\sigma_z + \frac{\hbar\lambda^2}{\delta}\sigma^+\sigma^- + \Big(\hbar\omega + \frac{\hbar\lambda^2}{\delta}\sigma_z\Big)a^\dagger a \tag{3.146}$$

In addition to the free field and free atom Hamiltonian, this effective Hamiltonian constitutes the dispersive coupling

$$H'_{\text{eff}} = \frac{\hbar\lambda^2}{\delta}\Big(\sigma^+\sigma^- + \sigma_z a^\dagger a\Big) \tag{3.147}$$

We can draw some physical implications from the effective Hamiltonian. When we compare (3.146) and (3.129), we see that during the atom-field interaction in the dispersive Hamiltonian, the oscillator frequency is shifted by an amount $\omega = \omega \pm \lambda^2/\delta$, that depends on the state of the qubit. To see how this works, let us consider the initial atom-field state $|\psi(0)\rangle = |g, \alpha\rangle$, then at a later time under the effective interaction Hamiltonian, we get

$$|\psi(t)\rangle = e^{-\mathrm{i}H'_{\mathrm{eff}}t/\hbar}|\psi(0)\rangle = |g\rangle|\alpha e^{-\mathrm{i}\lambda^2 t/\delta}\rangle \tag{3.148}$$

and for initial atom-field state $|\psi(0)\rangle = |e, \alpha\rangle$, we get

$$|\psi(t)\rangle = e^{-\mathrm{i}H'_{\mathrm{eff}}t/\hbar}|\psi(0)\rangle = e^{-\mathrm{i}\lambda^2 t/\delta}|g\rangle|\alpha e^{-\mathrm{i}\lambda^2 t/\delta}\rangle \tag{3.149}$$

So the field amplitude is unchanged when the qubit is in the ground state but it is rotated in phase space by the angle $\lambda^2 t/\delta$ when the qubit is in the excited state. If now we consider the atom initial in the state $|\psi_{\mathrm{atom}}\rangle = |g\rangle + e^{\mathrm{i}\phi}|e\rangle$ where $\phi$ is some local phase. Thus with the atom-field in the initial state $|\psi(0)\rangle = |\psi_{\mathrm{atom}}\rangle|\alpha\rangle$, we get at a later time

$$|\psi(t)\rangle = e^{-\mathrm{i}H'_{\mathrm{eff}}t/\hbar}|\psi(0)\rangle = \frac{1}{\sqrt{2}}\Big(|g\rangle|\alpha e^{-\mathrm{i}\lambda^2 t/\delta}\rangle + e^{-\mathrm{i}(\lambda^2/\delta-\phi)t}|g\rangle|\alpha e^{-\mathrm{i}\lambda^2 t/\delta}\rangle\Big) \tag{3.150}$$

Depending on the choice of $\lambda^2 t/\delta$, Eqn. (3.150) is an entangled state analogous to the state in the Schrödinger's gedanken experiment [118],

$$|\psi_{\text{atom-cat}}\rangle = \frac{1}{\sqrt{2}}\Big[|\text{undecayed atom}\rangle|\text{cat alive}\rangle + |\text{decayed atom}\rangle|\text{cat dead}\rangle\Big] \tag{3.151}$$

where the state of the two-level atom play the role of the radioactive atom, and the phase-separated cavity field states play the role of the cat.

### 3.4.2 The Unruh deWitt model

Another model that describes well the atom-field interaction is the Unruh deWitt (UdW) model [49]. describes the interaction between a monopole detector coupled to a massless scalar field. It has been used to study the response of detectors experiencing acceleration, to provide a proof for the Unruh effect and to probe the dynamics of quantum entanglement in the context of the recent fields of relativistic quantum information.

The detector described here is usually a two-level system. The UdW interaction Hamiltonian in the Schrödinger picture is given by

$$H_{\mathrm{UdW}} = \lambda\, \mu_s\, \hat{\phi}\,[\mathbf{x}_d(t)] \tag{3.152}$$

where $\mathbf{x}_d$ is the atom's position, assuming the detector's monopole moment $\mu_s$ is coupled through the coupling constant $\lambda$ to the field amplitude $\phi$ along the detector's trajectory. The monopole moment $\mu_s$ and the field operator $\phi_s$ in the Schrödinger picture are given respectively as

$$\mu_s = \sigma^+ + \sigma^-, \tag{3.153}$$

$$\phi(x(t)) = \sum_j [a_j + a_j^\dagger] \frac{\sin[k_j x(t)]}{\sqrt{\omega_j L}}. \tag{3.154}$$

Again, moving to the interaction picture, the UdW interaction Hamiltonian is given by ($\hbar$)

$$H_{\text{int}} = \lambda \sum_j (\sigma^+ e^{\mathrm{i}\Omega t} + \sigma^- e^{-\mathrm{i}\Omega t})(a_j e^{-\mathrm{i}\omega_j t} + a_j^\dagger e^{\mathrm{i}\omega_j t}) \frac{\sin[k_j x(t)]}{\sqrt{\omega_j L}}. \tag{3.155}$$

We comment that using a scalar field instead of an electromagnetic field does not introduce a fundamental difference in the model [88, 119]. The UdW has been applied in many experimental proposals including [87, 86]. The main caveat is that it models the light-matter interaction only in the absence of orbital angular momentum.

The similarity between the Unruh-DeWitt type monopole detector and the Jaynes Cummings (JC) model (3.125) is obvious. The main difference is that the monopole moment is here an extra degree of freedom, whereas the dipole moment in the JC model is directly related to the position of the electron. Hence the trajectory of the monopole detector can be arbitrary in our model.

### 3.4.3 Evolution operator - Perturbative analysis

We have noted that the atom-field interaction system is governed by a free Hamiltonian $H_0$ with known spectrum and an interaction Hamiltonian $H_{\text{int}}$ - a perturbation that causes transition between the eigenstates of $H_0$. To study the transitions, let us define the evolution operator $U(T, 0)$ that is capable of causing transitions governed by the interaction Hamiltonian $H_{\text{int}}$.

We work perturbatively in the coupling constant $\lambda$

$$U(T, 0) = \mathcal{T}\Big\{ \exp[-\mathrm{i} \int_0^T d\tau H_{\text{int}}(\tau)] \Big\} \tag{3.156}$$

where $\mathcal{T}$ is a time ordering. Expanding the terms in the exponential,

$$U(T,0) = \mathbb{1} + U^{(1)} + U^{(2)} + \cdots + U^{(n)} \tag{3.157}$$

where

$$U^{(1)} = -\,\mathrm{i}\int_0^T d\tau H_{\mathrm{int}}(\tau) \tag{3.158}$$

$$U^{(2)} = (-\mathrm{i})^2 \int_0^T d\tau \int_0^\tau dt\, H_{\mathrm{int}}(\tau)\, H_{\mathrm{int}}(t) \tag{3.159}$$

$$U^{(n)} = (-\mathrm{i})^n \int_0^T d\tau \cdots \int_0^{\tau^{(n-1)}} d\tau^{(n)} H_{\mathrm{int}}(\tau) \cdots H_{\mathrm{int}}(\tau^{(n)}) \tag{3.160}$$

Now substituting Eqn. (3.155), the corresponding terms give

$$\begin{aligned} U^{(1)} &= \frac{\lambda}{\mathrm{i}} \sum_j (\sigma^+ a_j^\dagger I_{+,j} + \sigma^+ a_j I^*_{-,j}) \\ U^{(2)} &= -\,\lambda^2 \sum_{lj} \big(\sigma^-\sigma^+ a_j^\dagger a_l^\dagger I_{-,j} \circ I_{+,l} + \sigma^-\sigma^+ a_j^\dagger a_l I_{-,j} \circ I^*_{-,l} + \sigma^-\sigma^+ a_j a_l I^*_{+,j} \circ I^*_{-,l} \\ &\quad + \sigma^-\sigma^+ a_j a_l^\dagger I^*_{+,j} \circ I_{+,l}\big) \end{aligned}$$

where for notational convenience we have defined

$$I_{\pm,j} = \frac{1}{\sqrt{k_j L}} \int_0^T \mathrm{dt}\; e^{\mathrm{i}(\omega_j \pm \Omega)t} \sin[k_j x(t)], \tag{3.161}$$

and the double integral

$$I_{\pm,j} \circ I_{\pm,l} = \frac{1}{\sqrt{(k_j L)(k_l L)}} \int_0^T \mathrm{dt} \int_0^t \mathrm{d}\tau\; e^{\mathrm{i}(\omega_j \pm \Omega)t} e^{\mathrm{i}(\omega_l \pm \Omega)\tau} \sin[k_j x(t)] \sin[k_l x(\tau)] \tag{3.162}$$

with the latter relation defining the $\circ$ operation. In writing the respective unitary terms $U^{(1)}$ and $U^{(2)}$ we note that our probe is prepared in its ground state $|g\rangle$, and so terms with $\sigma^-$ in front can be neglected since $\sigma^-|g\rangle = 0$.

We are usually interested in evaluating the state of the detector (two-level atom) after the evolution which can be calculated by tracing out the field from the combined atom-field system. Now let $\rho_0 = \rho_0^{(A)} \otimes \rho_0^{(F)}$ be the initial density state of the combined atom-field system, then at time $T$ the system would evolve according to equation $\rho_T = U(T,0)\rho_0 U(T,0)^\dagger$ which according to (3.156), we write as

$$\rho_T = [\mathbb{1} + U^{(1)} + U^{(2)} + \mathcal{O}(\lambda^3)]\rho_0[\mathbb{1} + U^{(1)} + U^{(2)} + \mathcal{O}(\lambda^3)]^\dagger \tag{3.163}$$

From this we can identify the order correction to the density matrix evolution

$$\rho_T = \rho_0 + \underbrace{U^{(1)}\rho_0 + \rho_0 U^{(1)\dagger}}_{\rho^{(1)}} + \underbrace{U^{(1)}\rho_0 U^{(1)\dagger} + U^{(2)}\rho_0 + \rho_0 U^{(2)\dagger}}_{\rho^{(2)}} + \mathcal{O}(\lambda^3) \tag{3.164}$$

Therefore the reduced state of the detector will be given by

$$\rho_T^{(A)} = \mathrm{Tr}_F[\rho_T] \tag{3.165}$$

In other scenario, we might be interested in evaluating the evolution of the combined atom-field system given in vector form. That is suppose $|\Psi\rangle_0 = |\psi\rangle_\mathrm{A}|\psi\rangle_\mathrm{F}$ is the initial combined atom-field state in vector form, then at a later time $T$, the state evolves according to substituting (3.156), we obtain

$$|\Psi\rangle_T = |\Psi\rangle_0 + |\Psi^{(1)}\rangle + |\Psi^{(2)}\rangle + \mathcal{O}(\lambda^3)$$

where $|\Psi^n\rangle = U^{(n)}|\Psi^{(n)}\rangle$ are the different contributions.

## 3.5 Decoherence in cavity quantum electrodynamics

We have seen in Sec 3.3.2 that quantum superposition of two coherent states exhibit different nonclassical (quantum) properties. However at the classical limit where the amplitude of the coherent states is apparently large, such state superposition loses its quantum nature (interference) and decohere to a statistical mixture of coherent states. Quantum decoherence [140] is the evolution of a quantum superposition state into a classical mixture due to interactions with the environment.

Since quantum physics is assumed to describe our world, one would expect that the existence of quantum interference (a quantum property) at the microscopic level should be equally applicable to macroscopic states. The non existence of quantum superpositions at the macroscopic level has been a long standing problem in quantum mechanics. Proposals to solve this problem stress the role of decoherence [59, 34, 51, 138, 137, 27]. Due to interactions with the environment (a dissipative process), quantum coherence between quantum state superpositions tend to decay faster than the physical observables of the system. This implies that during a measurement scheme, since the decoherence time is very short, we lose the quantum coherence that displays the quantum nature of superposition, even before detecting the state superposition. It is important therefore to imagine an experiment that accounts for interference effects between macroscopically distinct states [34].

In cavity quantum electrodynamics (CQED), superpositions of coherent states and entangled superposition of coherent states have been generated [134, 59]. Here the fields are generated and trapped in superconducting cavities while Rydberg atoms [68] are used as detectors for these fields. Microwave cavities or optical cavities with high Q factor are used and are well suited for trapping fields for a long time. Likewise Rydberg atoms are required because they are strongly coupled to microwaves and they have very long radiative decay times, making them suited for preparing and detecting strong correlations between atom and field states [59, 34].

Dissipative effects due to cavity losses and atomic decay are inevitable in these experiments, and they result in decoherence phenomena in the system. We will now discuss decoherence phenomena in CQED.

## Dissipative interactions and decoherence

Dissipation is modelled as a linear coupling between the field mode and an environment (usually a thermal bath of oscillators at zero temperature). Consider an initial state of a superposition of coherent state and a quantum state of the environment $|E\rangle$ . The problem is treated with the density operator formalism and demands that we solve a master equation for the reduced field density state.

$$\frac{d\rho_F}{dt} = \frac{\kappa}{2}[2\hat{a}\hat{\rho}_F\hat{a}^\dagger - \hat{a}^\dagger\hat{a}\hat{\rho}_F - \hat{\rho}_F\hat{a}^\dagger\hat{a}]. \tag{3.166}$$

where $\rho_F$ is the density matrix of the cat state given by

$$\rho_F = \frac{1}{N_1^2}\Big(|\alpha\rangle\langle\alpha| + e^{-\mathrm{i}\Psi_1}|\alpha\rangle\langle-\alpha| + e^{\mathrm{i}\Psi_1}|-\alpha\rangle\langle\alpha| + |-\alpha\rangle\langle-\alpha|\Big). \tag{3.167}$$

$\kappa = \omega_f/Q = 1/t_c$ is the cavity-damping rate which describes the strength of the coupling, $t_c$ is the damping time, $\omega_f$ is the cavity field frequency and $Q$ the cavity quality factor. The solution to the master equation (3.166) for $\rho_F$ is given as [34]

$$\rho_F(t) = \frac{1}{\mathcal{N}_1^2}\Big(|\alpha(t)\rangle\langle\alpha(t)| + |-\alpha(t)\rangle\langle-\alpha(t)| + e^{\mathrm{i}\psi}f(t)|-\alpha(t)\rangle\langle\alpha(t)| + e^{-\mathrm{i}\psi}f^*(t)|\alpha(t)\rangle\langle-\alpha(t)|\Big),$$

where $f(t)$

$$f(t) = \exp\Big[-2|\alpha|^2(1-e^{-\kappa t})\Big], \tag{3.168}$$

multiplying the coherence terms $|\pm\alpha(t)\rangle\langle\mp\alpha(t)|$, is a decay function that quantifies the state coherence, and $\alpha(t) = \alpha e^{-\kappa t/2}$. In the transient regime $\kappa t \ll 1$ where almost no damping or motion has occurred, then $f(t) \approx e^{-2|\alpha|^2\kappa t}$ where $t_{\text{decoh}} = 1/2|\alpha|^2\kappa = t_c/2|\alpha|^2$ is the decoherence time, that is the characteristic time over which the coherence terms vanish. Thus whenever the distance $|\alpha|^2$ between the superposed coherent states $\{|\alpha\rangle, |-\alpha\rangle\}$ is large, that is $|\alpha|^2 \gg 1$ or in the steady state regime when $\kappa t \to \infty$, their mutual coherence vanishes since $f(t) \to 0$. Thus quantum superposition reduces to a statistical mixture:

$$\rho_F(t)^m = \frac{1}{2}\Big[|\alpha(t)\rangle\langle\alpha(t)| + |-\alpha(t)\rangle\langle-\alpha(t)|\Big] \tag{3.169}$$

To summarize, the decoherence time $t_{\text{decoh}}$ is shorter than the energy dissipation time in the cavity $t_c$ by $2|\alpha|^2$, a factor precisely equal to the size of the field measured by its photon number $|\alpha|^2$. Therefore for large fields, the decoherence time becomes short. To monitor this decoherence, an atom is used and sent into an interaction with $\rho_F(T)$ [34].

We have seen that decoherence limits our ability to observe the superposition of coherent states as the field state is often destroyed before observation. One of the goals in this part of the thesis is to characterize a superposition of coherent states stored in a cavity in a nondestructive way. Due to the problem of decoherence, the quantum non-demolition (QND) measurement scheme was introduced as a way to eliminate perturbation inherent in quantum measurement. We will review the QND scheme in the next section.

## 3.6 Quantum non-demolition measurement: A review

In the standard approach to quantum measurement [62], consider a pair of non-commuting physical quantities, represented as operators A and B. Non-commuting observables implies the commutation relation $[\hat{A}, \hat{B}] = \hat{A}\hat{B} - \hat{B}\hat{A} \neq 0$. Now Heisenberg's uncertainty relation predicts that there exist a lower bound in the measurement of $A$ and $B$. That is

$$\Delta A \Delta B \geq \frac{1}{2}\langle[A, B]\rangle. \tag{3.170}$$

$\Delta A$ and $\Delta B$ are standard deviations which quantify the precison in the measurement of $A$ and $B$ respectively.

$$\Delta A = \sqrt{\langle A^2\rangle - \langle A\rangle^2}, \quad \Delta B = \sqrt{\langle B^2\rangle - \langle B\rangle^2} \tag{3.171}$$

Intuitively from the relation (3.172), a precision in a single measurement of A will result in smaller value of $\Delta A$ and hence a larger value of $\Delta B$. Large fluctuations induced in B when measuring A may eventually couple back to A, which will then also be perturbed, making it difficult to perform repeated or continuous measurements.

If we consider the position and momentum quadrature operators (3.81), the Heisenberg uncertainty relation as derived in unit 5 yields the relation

$$\Delta x \Delta p \geq \frac{1}{2}\langle [x, p] \rangle = \frac{\hbar}{2}, \tag{3.172}$$

where $\hbar$ is the reduced Planck's constant. To evade the problem of such measurement back action, the concept of quantum non-demolition (QND) measurement [16] was introduced, in which a strategy is chosen that kept the back-action noise entirely within unwanted observables.

We remark here that the key features of a QND measurement include its ability to preserve useful information for subsequent processing and its repeatability, in which quantum-state evolution into a different state is prohibited and successive measurement yields the same result as the first measurement. In a general measurement scheme, the system to be measured is coupled to a probe system (which reads out the number of photons without perturbing the signal), and the interaction of the two systems correlates the states of the probe and measured system. A destructive measurement allows for a subsequent measurement of the relevant state. The relevant observable remains unperturbed by the measurement process, allowing repeated measurements to be performed with high accuracy.

For the measurement to be a QND measurement, the measurement scheme should satisfy a set of conditions [16, 29, 120] that we recapitulate below

1. There should be some information about the measured observable that is encoded in the probe system after the interaction.
2. The measurement should not affect the measured observable after the measurement.
3. The measurement should be repeatable: Identical repeated measurements of the system should consistently provide the same outcome.

## Quantum non demolition measurement of photon number

Detecting photons is usually a destructive process, in that detectors annihilate photons and convert them into electrical signals, making it impossible to see a single photon twice. The idea of quantum non-demolition measurement is to eliminate this destructive process.

Suppose we want to monitor the number of photons in a radiation field. The relevant Heisenberg relation is the number - phase inequality

$$\Delta N \Delta \Phi \geq \frac{1}{2} \tag{3.173}$$

where $\Delta N$ and $\Delta\Phi$ are the dispersions in the number of photons $N$ and phase of the light wave $\Phi$ respectively. Quantum non-demolition measurements of light intensity have been demonstrated [56, 49]. Ideally, according to the basic requirement for QND measurements, there should be no exchange of energy between the signal and meter. This can be obtained through a non-resonant atom field interaction, where the frequency of light is detuned from that of the atomic transition. In this non-resonant situation the exchange of information is purely dispersive, that is, the atomic wavefunction only picks up a phase shift, which is proportional to the number of photons in the cavity. Implementing this scheme is difficult because the fact that the atom-field interaction is non-resonant makes it very weak. An alternative scheme is to consider a fully resonant atom-field interaction where the field frequency is set equal to the atomic transition frequency. Together with the extremely large number of photons in an optical resonator, the atom-field coupling rate is also very large compared to dissipative couplings to the environment. Although an energy exchange does occur, the parameters are chosen so that a single photon in the cavity is coherently absorbed and re-emitted by the atom before it leaves the cavity, hence reversing the energy exchange. However a phase shift occurs in the atomic wavefunction. caused by a cycle of photon absorption and emission, which is measured using atomic interferometry. The phase information is extracted from the meter atom using an interference effect, which transforms the phase shift into a detectable change in the atomic energy level. A demerit in this scheme is that to generalize to higher photon numbers would require using a non-resonant interaction.

A measurement scheme that considers a resonant atom-field interaction and consequently a weak coupling between the atom and field has been described [97]. In this scheme, which is called the mode-invisibility (MI) scheme, it was observed that one could take advantage of the geometry of the cavity and let the field be trapped in only 'even' cavity modes. In this way, the absorption/emission processes during the first half of an atom's motion in the cavity are canceled during the second half, before it leaves the cavity. A phase shift occurs in the atom's wavefunction, which is further extracted using an interference effect through an atomic interferometer. This method was proposed for implementing a QND measurement of Fock states of light [97] and later general states of light such as coherent states and squeezed coherent states [98]. It could distinguish Fock states from each other.

The MI scheme is indeed a QND measurement for the following reasons:

1. The interferometric phase encodes information about the number of photons and it is resolvable to a precision that tells apart few-photon states satisfying the QND criterion 1.

2. The probability that the measurement takes the system to a different state is approximately zero ($P \sim 10^{-22}$ for physical parameters), showing that the system does not get perturbed after the measurement.

3. Given this probability for physical parameters, for our measurement outcome to be significantly altered, the measurement would have to be repeated on the order of more than $10^{15}$ times.

We will generalize the mode-invisibility technique to measure the Bell cat states and a squeezed superposition of coherent states.

# Chapter 4

# Characterizing entanglement and quantum state superposition

In the preceding chapter 3, we reviewed the generation of superposition of two coherent states of equal amplitude and $\pi$- out of phase.

$$|\Psi_{\text{cat}}\rangle = \frac{1}{\mathcal{N}}\Big(|\alpha\rangle + e^{\mathrm{i}\psi}|-\alpha\rangle\Big), \tag{4.1}$$

where the normalization factor is given by

$$\mathcal{N} = \Big[2(1+\exp(-2|\alpha|^2\cos\psi)\Big]^{-1/2}$$

With $\psi = 0, \pi$ and $\pi/2$, we have the even coherent state, odd coherent state and Yuker-Stoler states respectively. Quantum superpositions of the form (4.1) are referred to as Schrodinger cat states at the limit when the component states $|\alpha\rangle$ and $|-\alpha\rangle$ are macroscopically distinguishable, that is for large amplitude $|\alpha|$. At this limit, decoherence sets in and the Schrodinger's cat state changes to a classical mixture of coherent states [59] of the form

$$\rho = \frac{1}{2}\Big(|\beta\rangle\langle\beta| + |-\beta\rangle\langle-\beta|\Big) \tag{4.2}$$

where $\beta = \alpha e^{-\gamma t/2}$, with $\gamma$ related to the rate of dissipation. The decoherence increases with increasing $|\alpha|$. During observation, one must be able to distinguish between the statistical mixture and between the the different the cat states, which are superpositions of coherent

states $|\alpha\rangle$ and $|-\alpha\rangle$. That is, as the corresponding density operator for a cat state is

$$\rho = \frac{1}{2}|\alpha\rangle\langle\alpha| + |-\alpha\rangle\langle-\alpha| + e^{-i\psi}|\alpha\rangle\langle-\alpha| + e^{-i\psi}|-\alpha\rangle\langle\alpha| \tag{4.3}$$

we need to detect the coherence terms $|\alpha\rangle\langle-\alpha|$ and $|-\alpha\rangle\langle\alpha|$.

Superposition states [117] play a major role in the area of quantum information [108, 139] due to their ability to encode information in a way that is impossible to achieve by a classical system having the same amount of resources. For practical applications in quantum computation, superposition states such as (4.1) have the powerful property of executing large parallel processing. It has been proposed to encode qubits in superposition states because they are naturally generated in any cavity QED systems [23, 24, 34, 80, 107, 120, 129] compared to multi-qubit states that require a large amount of control. In terms of quantum resources, architecture with superposition of coherent states provide a simpler and cheaper error correcting scheme [11].

Another important class of states we discussed at the end of Chapter 3 is an entangled state of a qubit and a superposition of coherent states (also known as Bell cat state [134])

$$|\Psi_{\text{Bell-cat}}\rangle = \frac{1}{\sqrt{2}}(|g,\alpha\rangle + |e,\beta\rangle) \tag{4.4}$$

The two atomic states $|e\rangle$ and $|g\rangle$ are here correlated to the two field states $|\alpha\rangle$ and $|\beta\rangle$. Just like the correlated two-qubit states in the Einstein-Podolsky-Rosen (EPR) paradox [7] that highlights the concept of quantum entanglement [64] in qubits, the Bell cat state also highlights the concept of quantum entanglement in macroscopically distinguishable systems. Quantum information necessitates entanglement between multi-qubit states, but for these states, decoherence sets in and preserving entanglement becomes a difficult task. An alternative encoding with coherent states would take advantage of the much larger Hilbert space of the cavity resonator. In this way a redundant qubit encoding is attainable that simplifies the operations needed to initialize, manipulate and measure the encoded information. For such a system to be viable as a quantum computing platform, efficient measurement of such encoded qubit observables must be possible.

Different methods have been proposed for detecting entanglement [64, 107, 134, 132, 91]. The most popular approach to the problem of detecting the presence of entanglement in "Bell-cat states" is based on violation of Bell-type inequalities [134]. One can also perform complete quantum-state tomography [62]. However these methods are not only destructive processes, they also pose both fundamental and technical challenges. Another method entails measuring entanglement witnesses. This is efficient, but not universal and requires information about the state prior to its measurement [82, 128].

In this chapter, we demonstrate efficient measurement of such encoded qubit observables as well as measurement of Schrödinger's cat states using the mode invisibility (MI) measurement scheme.

## 4.1 Model and method: A review

To begin this section, we first review the mode invisibility measurement scheme [97]. Then we apply the scheme to characterize the Bell cat state and superposition of coherent states.

### 4.1.1 Atom interferometry with single atom

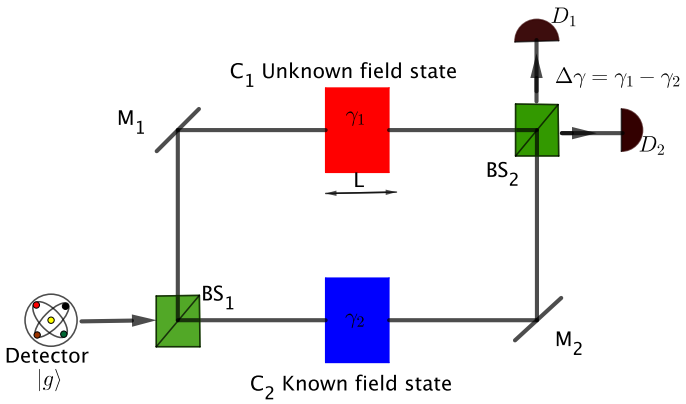


Figure 4.1: A schematic representation of an atom interferometer with a single atom input; a form of Mach Zehnder interferometer. The atom beam is split into two parts by $BS_1$, one of which is coupled to the signal in the cavity $C_1$, the other being used as reference is coupled to the signal in $C_2$. The two parts are recombined at $BS_2$ before reading the atom output intensity. $M_1$ and $M_2$ are mirrors, and the two cavities labeled $C_1$ and $C_2$ store an unknown and known field state respectively. Each partial atom acquires a phase $\gamma_i$ ( where $i = 1, 2$ labels the different atomic trajectory) due to an interaction with the cavity field on its path. The atomic states and probabilities are detected by two ionized detectors $D_1$ and $D_2$.

The setup of the MI measurement scheme is depicted in FIG. 4.1. It is an atom interferometer ( a type of Mach Zehnder interferometer) which is analogous to two-slit experiment.

In the atom interferometer (FIG. 4.1), an incoming atom beam initially in its ground state is split into two partial components at the first beam splitter $\mathrm{BS}_1$

$$|\psi\rangle \xrightarrow{\mathrm{BS}_1} \frac{1}{\sqrt{2}}\begin{pmatrix}1 & 1\\ 1 & -1\end{pmatrix}\begin{pmatrix}g\\ 0\end{pmatrix} = \frac{1}{\sqrt{2}}\begin{pmatrix}g\\ g\end{pmatrix} \tag{4.5}$$

where $\frac{1}{\sqrt{2}}\begin{pmatrix}1 & 1\\ 1 & -1\end{pmatrix}$ is the 50-50% Beam splitter operator. The component states

$$|g_1\rangle = \frac{1}{\sqrt{2}}\begin{pmatrix}g\\ 0\end{pmatrix} = \frac{1}{\sqrt{2}}|g\rangle, \quad |g_2\rangle = \frac{1}{\sqrt{2}}\begin{pmatrix}0\\ g\end{pmatrix} = \frac{1}{\sqrt{2}}|g\rangle, \tag{4.6}$$

travel along the different interferometric paths, bounce off the two mirrors and recombine at the second beam splitter $\mathrm{BS}_2$. Then two output beams from $BS_2$ are incident on the two detectors $D_1$ and $D_2$. The intensity yield the interferometric phase difference.

***Equal interferometric path length***

If we define the different path length $\Delta L$ and a phase $\phi$, then the state inside the atom interferometer setup just before recombination at $\mathrm{BS}_2$ can be written as

$$|\Psi\rangle \longrightarrow \begin{pmatrix}1 & 0\\ 0 & e^{\mathrm{i}\phi}\end{pmatrix}\frac{g}{\sqrt{2}}\begin{pmatrix}1\\ 1\end{pmatrix} = \frac{g}{\sqrt{2}}\begin{pmatrix}1\\ e^{\mathrm{i}\phi}\end{pmatrix} \tag{4.7}$$

At the second beam splitter, the state undergoes another transformation given as

$$|\Psi\rangle' \longrightarrow \frac{1}{\sqrt{2}}\begin{pmatrix}1 & 1\\ 1 & -1\end{pmatrix}\frac{g}{\sqrt{2}}\begin{pmatrix}1\\ e^{\mathrm{i}\phi}\end{pmatrix} = \frac{g}{2}\begin{pmatrix}1+e^{\mathrm{i}\phi}\\ 1-e^{\mathrm{i}\phi}\end{pmatrix} \tag{4.8}$$

So the atom can be registered on one of the two detectors $D_1, D_2$ with probabilities

$$P_1 = |D_1|^2 = \frac{1}{4}(1+e^{\mathrm{i}\phi})(1+e^{-\mathrm{i}\phi}) = \frac{1}{2}\Big(1+\cos\phi\Big) \tag{4.9}$$

$$P_2 = |D_2|^2 = \frac{1}{4}(1-e^{\mathrm{i}\phi})(1-e^{-\mathrm{i}\phi}) = \frac{1}{2}\Big(1-\cos\phi\Big). \tag{4.10}$$

In the setup 4.1, the upper and lower path lengths are set to be exactly equal so that $\phi = 0$. Under these conditions, there is complete destructive interference at the detection zone $D_2$ and constructive interference at the detection zone $D_1$. Intuitively, there is zero probability for an incident atom to reach detector $D_2$ while the probability to reach detector $D_1$ is 1. Thus any experiment where $D_2$ clicks will yield information about an obstacle on the upper arm of the interferometer. We will now look at how this works in the succeeding section.

### 4.1.2 Atom interferometer with atom-field interaction

Now let us look at the atom interferometer Fig. 4.1. First note that the detector enters the atom interferometer at constant velocity $v = L/t$ , where $t$ is the interaction time and $L$ the cavity length. We assume the field state to be measured is produced and trapped within a single mode of the upper cavity $C_1$ (with other modes being empty), while the lower cavity $C_2$ is empty (we model this as the vacuum state $|0\rangle$ of an EM field). Before $BS_2$, the atomic states $|g_1\rangle$ and $|g_2\rangle$ from (4.6) travel along paths 1 and 2 thus interacting with fields in cavities $C_1$ and $C_2$ respectively. Due to this interaction, the wavefunction of the partial atoms will change by a global phase factor $\gamma_1$ and $\gamma_2$ respectively. In the proposed experimental setup, the states of quantum cavities $C_1$ and $C_2$ are initially prepared to be separable with the field state in the upper and lower cavities given as $|\psi_1\rangle$ and $|\psi_2\rangle$ respectively.

The atom-field state in the upper arm that enters the port of the second beam splitter $BS_2$ is obtained as:

$$|\Phi_1\rangle = e^{i\gamma_1}|g_1\rangle|\psi_1\rangle \tag{4.11}$$

and in the lower arm, the atom-field state that enters the next port of beam splitter is obtained as

$$|\Phi_2\rangle = e^{i\gamma_2}|g_2\rangle|\psi_2\rangle \tag{4.12}$$

So the atom-field state entering $BS_2$ is

$$|\Phi\rangle = \Big(e^{i\gamma_1}|g_1\rangle|\psi_1\rangle + e^{i\gamma_2}|g_2\rangle|\psi_2\rangle\Big). \tag{4.13}$$

The two states (4.11) and (4.12) are recombined by $BS_2$ with transformation given as

$$|\Phi\rangle' \longrightarrow \frac{g}{2}\begin{pmatrix}1 & 1\\ 1 & -1\end{pmatrix}\begin{pmatrix}e^{i\gamma_1}|\psi_1\rangle\\ e^{i\gamma_2}|\psi_2\rangle\end{pmatrix} = \begin{pmatrix}e^{i\gamma_1}|\psi_1\rangle + e^{i\gamma_2}|\psi_2\rangle\\ e^{i\gamma_1}|\psi_1\rangle - e^{i\gamma_2}|\psi_2\rangle\end{pmatrix} \tag{4.14}$$

The detectors $D_1$ and $D_2$ measure the state of outgoing atomic states with probabilities

$$P_1 = |D_1|^2 = \frac{1}{2}\Big(1 + \mathrm{Re}\left[\,\langle\psi_1|\,\psi_2\rangle e^{-i(\gamma_1-\gamma_2)}\right]\Big) \tag{4.15a}$$

$$P_2 = |D_2|^2 = \frac{1}{2}\Big(1 - \mathrm{Re}\left[\,\langle\psi_1|\,\psi_2\rangle e^{-i(\gamma_1-\gamma_2)}\right]\Big). \tag{4.15b}$$

We see that the interferometric output depends on the phase difference $\Delta\gamma = \gamma_1 - \gamma_2$, acquired by the partial atoms in the cavities $C_1$ and $C_2$ respectively. Thus measurement of $\Delta\gamma$

allows us to determine $\gamma_1$ which subsequently yields information about the unknown field state in $C_1$. The phase value has to be significant for a precise and accurate measurement of $\gamma_1$

We propose a QND measurement scheme to measure this phase factor for an atom interacting with an unknown Bell cat state and squeezed superposition of coherent states respectively. As we shall demonstrate, the phase difference can be significant and thus measured. If the state of the field is not significantly altered, then repeated measurement can be used to estimate the phase, thereby revealing information about the unknown field state [49, 123] such as entanglement in the Bell cat state [134].

## Evolution dynamics of the atom-field system

In this section, we will discuss the evolution of the atom-field states (4.11) and (4.12) respectively.

First consider the state (4.11) in $C_1$ with initial joint atom-quantum field state $|\psi(0)\rangle = |g\rangle \otimes |\Phi_\alpha\rangle$. We have dropped the subscripts here and assumed the field state to be trapped in the cavity mode $\alpha = 1, 2, \cdots \infty$ of frequency $\omega_\alpha = \alpha\pi/L$. We assume that single atoms enter the cavity in their ground state $|g\rangle$. During interactions, the joint system therefore undergoes oscillations at angular frequencies $(\omega_\alpha \pm \Omega)$ between various possible states.

The heart of our work lies in our ability to "manipulate" the interaction between these single atoms and field modes trapped in the optical cavity without perturbing the combined quantum system very much. These systems are assumed to be coupled via the Unruh de-Witt interaction Hamiltonian (3.152) for a short time $T$, by a unitary evolution operator $U(0,T)$ (3.156), so that the joint atom-field state after the interaction is $|\psi(T)\rangle = U(0,T)|\psi(0)\rangle$.

### *Measurement conditions*

Recalling that our aim to is implement a QND measurement of the relevant state of light perturbing the field states as low as possible. To this end we require that the coupling to the cavity modes is taken to be weak enough so that the effect of the atom-field interaction when the atom flies through the cavity for short times does not alter the probability distribution of the joint quantum state. Specifically, the field-atom system starts from an initial state $|\psi(0)\rangle$ and traverses the cavity during a time $T$. Requiring the probability

that the whole system remains in the same state to be approximately unity, i.e,

$$\left|\langle\psi(0)|U(0,T)|\psi(0)\rangle\right|^2 \approx 1, \tag{4.16}$$

ensures the minimal possible alteration to the field state. In other words, with the atom state initially in the ground state, we require that the probability of an atomic transition into an excited state while crossing the cavity

$$P_{|e\rangle} = \langle e|\,\mathrm{Tr}_F[U^{(1)}\rho(0)U^{(1)\dagger}]|e\rangle \simeq 0 \tag{4.17}$$

where $\mathrm{Tr}_F$ is a trace over the cavity field components and $\rho(0) = |\Psi(0)\rangle\langle\Psi(0)|$ is the initial density state of the joint atom-cavity field. In writing (4.17), we have considered a perturbative expansion of the evolution operator $U(0,T)$ and the leading order in $\lambda$ (see Sec 3.4.3).

Under this assumption the final state of the system would be very approximately equal to the initial state except for a global dynamical phase, and some state orthogonal to the initial state. Mathematically this is expressed as

$$|\psi(T)\rangle = U(0,T)|\psi(0)\rangle \simeq e^{i\gamma_1}|\psi(0)\rangle + |\psi_\perp(T)\rangle \tag{4.18}$$

where $\langle\psi(0)|\psi_\perp(T)\rangle = 0$. Hence the global phase factor $\gamma_1$ can be obtained from above as

$$\gamma_1 = -\mathrm{i}\ln\Big[\langle\psi(0)|U(0,T)|\psi(0)\rangle\Big] \tag{4.19}$$

which is the phase we wish to calculate. Expanding the unitary operator $U(0,T)$ gives the different contributions to the phase as

$$\gamma_1^{(0)} = \mathbb{1} \tag{4.20a}$$
$$\gamma_1^{(1)} = \langle\psi(0)|U^{(1)}|\psi(0)\rangle \tag{4.20b}$$
$$\gamma_1^{(2)} = \langle\psi(0)|U^{(2)}|\psi(0)\rangle \tag{4.20c}$$

In general $\gamma_1$ has both real and imaginary parts, $\gamma_1 = \Re(\gamma_1) + i\Im(\gamma_1)$. Normalization implies that

$$1 = \langle\psi(T)|\psi(T)\rangle = e^{-2\Im(\gamma_1)(T)} + \langle\psi_\perp(T)|\psi_\perp(T)\rangle \tag{4.21}$$

As time increases eventually the final state becomes $|\psi_\perp(T)\rangle$. Thus $\Im(\gamma_1(T))$ translates into a loss of visibility in the interference pattern. However in realistic terms, $\Im(\gamma(T)) << 1$

for the time the probe is in the cavity so that $|\Psi_\perp(T)\rangle$ is negligible. Therefore the phase factor $\gamma$ to be determined is given by

$$\gamma_1 = \mathrm{Re}(\gamma_1) \tag{4.22}$$

To summarize, the state of the measuring device (the single atom) remains the same before and after it exits the cavity except for a dynamical phase. Even in regimes where the interaction between a single atom and the quantum field is so weak such that the field state to be measured is unperturbed, we expect that the measured phase value will hold information about this field state.

For this scheme to work we have to make sure that (a) the hypothesis (4.16) holds and (b) the phase is significantly measurable in the regimes where this is so. Even with these conditions satisfied, we note that the information that can be extracted from the joint system is limited: the only way to measure a global phase is by means of an interferometry experiment. To this end we have to compare the state of the field with another known state. The second cavity $C_2$ in FIG 4.1 will serve this purpose. For simplicity, we assume it is empty (vacuum) with no EM-field although vacuum fluctuations are not negligible. Thus the interferometric phase difference is given by the relation

$$\Delta\gamma = \mathrm{Re}[\gamma_1] - \mathrm{Re}[\gamma_2] \tag{4.23}$$

where $\gamma_2$ is the phase in cavity $C_2$.

### 4.1.3 Review of the mode invisibility measurement scheme

We recall that our aim is to implement a QND measurement of the Bell cat states and superposition of coherent states using the proposed experiment in the preceding section. For the experiment to be feasible the phase (4.22) acquired by the atom flying through the cavity must be maximized. This can be achieved if cavity field frequency is on resonance with atomic transition frequency [94, 119]. When a detector interacts on resonance with the cavity mode, it does so strongly, in general altering the field state. Such an interaction enables one to gain significant information about the field (in a case where the atom is used as a detector to probe a field trapped in a cavity). On the other hand, a strong interaction leads to alteration of the cavity mode thereby jeopardizing the QND measurement criteria 3.6. One needs therefore a scenario where the alteration in the cavity mode is minimized whilst permitting acquisition of information.

The mode invisibility (MI) measurement scheme was introduced to minimize the effect of the resonant mode on the transition probability and still have a strong contribution

to the phase. The key point is to eliminate the largest contribution to the transition probability which comes from the resonant modes, while keeping the leading contribution to the interferometric phase difference.

The idea of the MI scheme is to take advantage of the spatial symmetry of cavity field modes (as shown in FIG. 3.2) so that the atoms interact with light in a non-destructive way [114, 21, 116]. Specifically, when the atom interacts (on resonance) with an even mode of the cavity, we are able to eliminate the resonant mode terms. To see how this works, in evaluating the atom's transition probability using the evolution operator (3.156), one comes across integrals such as (3.161), which are given explicitly as

$$I_{\pm\kappa} = \frac{\left[e^{\mathrm{i}\frac{L}{v}(\omega_\kappa \pm \Omega)}(-1)^\kappa - 1\right] Lv\sqrt{\kappa\,\pi}}{(\kappa\,\pi v)^2 - L^2(\omega_\kappa \pm \Omega)^2}. \tag{4.24}$$

For a resonant interaction ($\omega_\kappa = \Omega$), and $\kappa = 2n, (n = 1, 2, \cdots)$, the rotating wave term $I_{-,\kappa}$ vanishes while the counter-rotating wave term $I_{+,\kappa}$ does not. The mode invisibility technique is robust against a slight detuning from resonance and can be improved by carefully selecting the detector's speed, eliminating any dependence it has on the probed mode. This makes the mode completely 'invisible' to the detector [97].

Intuitively, when the atom interacts (on resonance) with an even mode of the cavity most of the changes that it will introduce in the field state while flying half the way through the cavity $x \in [0, L/2]$ will be undone when the atom flies through the second half $x \in [L/2, L]$ before it exits the cavity. As a first approximate description of the phenomenon, whatever the atom absorbs while flying through the first half of the cavity will be identically re-emitted while flying through the second half so that the state of field and atom are the same modulo a phase. This is possible because the effective sign of the coupling to the cavity ($\lambda$ times the spatial distribution of the mode) reverses half way through the flight path of the atom.

In the setting this will only be true for the first order terms of the perturbative expansion, since the even orders in the coupling strength $\lambda$ will not see this effective sign change. This will have the advantage that we can cancel out the leading order contribution to the transition amplitude for the field and the detector while keeping constant the leading order in the phase effects. Hence provided the highly excited state we wish to probe is prepared in one of those even modes, the mode is invisible to the atom (at leading order in perturbation theory) and therefore will not perturb it.

## 4.2 Mode invisibility as a nondestructive probe of Bell cat states

Here we characterize the Bell cat state

$$|\psi\rangle = A|g,\alpha\rangle + B|e,\beta\rangle \tag{4.25}$$

using the MI measurement technique. $A$ and $B$ are constants satisfying the condition $A^2 + B^2 = 1$. The coherent states $|\alpha\rangle$ and $|\beta\rangle$ have amplitudes $|\alpha|, |\beta|$ and phase $\theta, \phi$ respectively.

### 4.2.1 Quantum evolution of the Bell-cat state

Let us assume that an unknown Bell cat state is prepared in an even mode $\kappa$ of frequency $\omega_\kappa = \kappa\pi/L$ in the upper cavity $C_1$. All the rest of the modes $\varsigma$ are prepared in the vacuum (or in very low-populated states). Given that our detector is prepared in the ground state $|g_p\rangle$, the initial atom-field state is

$$|\psi(0)\rangle = |g_p\rangle\Big(A|g_q\rangle|\alpha_\kappa\rangle + B|e_q\rangle|\beta_\kappa\rangle\Big)\bigotimes_{\kappa\neq\varsigma}|0_\varsigma\rangle. \tag{4.26}$$

The subscript $q$ denotes the qubit that is entangled with the field state; we refer to this as the cavity-qubit so as to distinguish it from the state of our probe, which will be given the subscript $p$. The lower cavity $C_2$, which serves as a reference, sustains a vacuum state.

In the interaction time $t = T$, the state (4.26) evolves to a final state given by

$$|\Psi(T)\rangle = U(T,0)|\Psi(0)\rangle \tag{4.27}$$

where the unitary operator $U(T,0)$ is governed by the total interaction Hamiltonian

$$\hat{H}_I = \lambda_p\hat{\mu}_p(t)\hat{\phi}[x_p(t)] + \lambda_q\hat{\mu}_q(t)\hat{\phi}[x_q]. \tag{4.28}$$

The terms on the right hand side of (4.45) correspond to the probe-field and qubit-field interactions, with respective coupling strengths $\lambda_p$ and $\lambda_q$. $\mu_p(t)$ and $\mu_q(t)$ are the monopole moments of the probe and qubit respectively. We model our field system as a massless scalar field $\phi[x(t)]$, where $x(t) = vt$ describes the atomic trajectory through the cavity. For

simplicity, we assume that the qubit entangled to a field state is at a fixed position $x_0$ in the cavity. So in the interaction picture

$$\phi[x_p(t)] = \sum_{\delta=1}^{\infty}(a_\delta^\dagger e^{\mathrm{i}\omega_\delta t} + a_\delta e^{-\mathrm{i}\omega_\delta t})\frac{\sin[k_\delta x_p(t)]}{\sqrt{k_\delta L}}$$

for the probe moving on a trajectory $x_p(t)$, whereas

$$\phi[x_q(t)] = \sum_{\delta=1}^{\infty}(a_\delta^\dagger e^{\mathrm{i}\omega_\delta t} + a_\delta e^{-\mathrm{i}\omega_\delta t})\frac{\sin[k_\delta x_0]}{\sqrt{k_\delta L}}$$

for the cavity qubit at a fixed position $x_0$ in a cavity mode. The mode invisibility technique assumes a resonant interaction between probe and cavity field, so that $\Omega_p = \omega_\kappa$. We further assume that the qubit's transition frequency is set off-resonance relative to the cavity mode frequency; in other words $\Omega_q \neq \omega_\kappa$ with detuning $\delta = \omega_\kappa - \Omega_q$.

We work perturbatively in the coupling strengths $(\lambda_p, \lambda_q)$ and extend our calculation of the evolution operator $U(0,T)$ to second order. The phase factor $\eta$ in equation (4.22) has information about the entangled state (4.25). Our task therefore is to find a way to evaluate this phase value provided that the criteria (4.16) and (4.18) are satisfied.

### *Transition Probability*

We consider now the effect of the interaction between the probe and the entangled state. The probe is initially in the state $|g_p\rangle$ with constant speed $v$. We calculate the probability that it gets excited after the interaction time $T = L/v$. If the entangled state is not perturbed, we expect that this excitation transition probability is approximately zero.

To compute this probability, we note that the evolution of the system is, to second order in the coupling constant, given by (3.164)

$$\rho(T) = \rho + U^{(1)}\rho + \rho U^{(1)\dagger} + U^{(2)}\rho + \rho U^{(2)\dagger} + U^{(1)}\rho U^{(1)\dagger} \tag{4.29}$$

where $\rho(0)$ is the initial density operator for the combined state (4.26) and $U^{(1)}$, $U^{(2)}$ are the first and second order contributions in $(\lambda_p, \lambda_q)$ to the unitary operator. By tracing over the entangled state (ES), the only term contributing to the excitation probability is $U^{(1)}\rho(0)U^{(1)\dagger}$ so that after the interaction time $t > 0$, the transition probability of exciting this detector is

$$P_{|e_p\rangle} = \langle e_p|\,\mathrm{Tr}_{\mathrm{ES}}\left[U^{(1)}\rho(0)U^{(1)\dagger}\right]|e_p\rangle. \tag{4.30}$$

There are three contributions to this probability; we have the contribution from the excitation probability due to the detector absorbing a photon from the field mode $\kappa$. This is the rotating-wave term corresponding to the integral term $X_{-,\kappa}$ (see below). The second term corresponds to the atom getting excited and emitting a photon to the mode $\kappa$. This is the typical counter-rotating contribution corresponding to $X_{+,\kappa}$. The third term corresponds to the vacuum fluctuations due to the rest of the modes (see for instance [119, 71]). Assuming the detector is tuned to be resonant with the mode of the field we want to probe, the largest contribution would come from the rotating wave term. This is the principal contribution that can jeopardize the hypothesis (see equation (4.16)). We can cancel this contribution from the rotating wave term if the unknown field state (Fig. 4.1) is prepared in an even mode of the cavity (see discussion 4.1.3 ) so that

$$P_{|e_p\rangle} = \lambda_p^2 \left[ (|A|^2|\alpha|^2 + |B|^2|\beta|^2)|X_{+,\kappa}|^2 + \sum_{\gamma} |X_{+,\gamma}|^2 \right] \tag{4.31}$$

We note here that as defined in (3.161) the integral

$$X_{\pm,j} = \frac{1}{\sqrt{k_j L}} \int_0^T \mathrm{dt}\ e^{\mathrm{i}(\omega_j \pm \Omega_p)t} \sin[k_j x(t)],$$

is associated with the probe-qubit while the integral

$$I_{\pm,j} = \frac{1}{\sqrt{k_j L}} \int_0^T \mathrm{dt}\ e^{\mathrm{i}(\omega_j \pm \Omega_q)t} \sin[k_j x_0],$$

which we refer later in the text, is associated with the cavity-qubit. Before proceeding, we note that the information gained from this approach is information about the initial state of the system. Indeed, the qubit-cavity system evolves with time. Provided $P_{|e_p\rangle} \ll 1$ in (4.17), the evolution of the system is not disturbed by the probe. Given the Hamiltonian for the system, the information gained from mode invisibility about the initial state is sufficient to reconstruct the evolution of the system at any subsequent time.

Furthermore, although we shall ensure that $P_{|e_p\rangle} \ll 1$ for all of our parameter choices, we shall find that the phase $\gamma_1$ in (4.22) is not small. We proceed to compute $\gamma_1$ in the next subsection.

### *Estimating the phase imprint of the probe*

We now compute the phase (4.22) acquired by the atom after its interaction time $T$ with the Bell cat state trapped in the cavity mode in $C_1$. To leading order in coupling constants

$\lambda_p$ and $\lambda_q$, we obtain from (4.20b)

$$\gamma_1^{(1)} = -\frac{2\mathrm{i}\lambda_q}{\sqrt{k_\kappa L}}\,\mathrm{Re}\left\{\left(I^*_{+\kappa}\beta + I_{-\kappa}\alpha^*\right)\langle\alpha|\beta\rangle A^* B\right\} \tag{4.32}$$

only dependent on $\lambda_q$ with

$$I_{\pm,\kappa} \equiv \int_0^T \mathrm{d}t\, e^{\mathrm{i}(\pm\Omega_q+\omega_\kappa)t}\frac{\sin[k_\kappa x_0]}{\sqrt{\kappa\pi}} \tag{4.33}$$

In general $\gamma_1 \neq 0$. It is purely imaginary and so must remain small to ensure that the contribution of $|\psi_\perp(T)\rangle$ in (4.21) remains negligible. There are several ways of doing this. One is to ensure that the qubit sits at a node so that $\sin[k_\kappa x_0] = 0$. This will cause all $I_{\pm,\kappa}$ integrals to vanish, and the results will be the same as those obtained for $B = 0$ [98]. Another is to fine-tune the speed of the probe (i.e. $v/c$) relative to the qubit phase so that $I_{\pm,\kappa}$ vanishes but $I_{\pm,\kappa} \circ I^*_{\pm,\kappa}$ will not. A third approach is to choose the relative phase of the coherent states so that $\langle\beta|\alpha\rangle = e^{-\frac{1}{2}(|\beta|^2+|\alpha|^2-2\beta^*\alpha)} = e^{-\frac{1}{2}(|\beta|+|\alpha|)^2}$. Our choice of phase ensures this relation. The maximal value of this quantity is less than unity, and over the range of parameters we choose we find that $\Im(\gamma_1) \leq 10^{-5}$ for all $|\beta|$ and $|\alpha|$; for most of this range it is many orders of magnitude smaller than this.

Since $\gamma_1$ does not depend on any parameters of the probe, we must compute the $\gamma_1^{(2)}$ term in (4.20c) in order for the probe to be a useful diagnostic of the generalized CAT state. To this end, we obtain

$$\begin{aligned}\gamma_1^{(2)} = -\lambda_q^2\Big\{&I^*_{-\kappa}\circ I_{-,\kappa}B^2|\beta|^2 + I_{-,\kappa}\circ I^*_{-,\kappa}A^2|\alpha|^2 + I_{+\kappa}\circ I^*_{+,\kappa}B^2|\beta|^2 + I^*_{+,\kappa}\circ I_{+,\kappa}A^2|\alpha|^2\\ &+ I_{-,\kappa}\circ I_{+,\kappa}(\alpha^*)^2A^2 + I^*_{-,\kappa}\circ I^*_{+,\kappa}B^2\beta^2 + I_{+,\kappa}\circ I_{-,\kappa}B^2(\beta^*)^2 + I^*_{+,\kappa}\circ I^*_{-,\kappa}A^2\alpha^2\\ &+ \sum_\delta A^2 I^*_{+,\delta}\circ I_{+,\delta} + \sum_\delta B^2 I^*_{-,\delta}\circ I_{-,\delta}\Big\} - \lambda_p^2\Big\{X^*_{+\kappa}\circ X_{+,\kappa}\left[A^2|\alpha|^2 + B^2|\beta|^2\right]\\ &+ X_{-,\kappa}\circ X_{+,\kappa}\left[(\alpha^*)^2A^2 + (\beta^*)^2B^2\right] + X^*_{+,\kappa}\circ X^*_{-,\kappa}\left[\alpha^2A^2 + \beta^2B^2\right] + \sum_\delta X^*_{+,\delta}\circ X_{+,\delta}\Big\}\end{aligned}$$

Again here the double integral

$$I_{\pm,\kappa}\circ I_{\pm,\delta} \equiv \int_0^T \mathrm{d}t_2\, e^{\mathrm{i}(\pm\Omega_q+\omega_\kappa)t_2}\int_0^{t_2}\mathrm{d}t_1\, e^{\mathrm{i}(\pm\Omega_q+\omega_\delta)t_1}\frac{\sin[k_\kappa x_0]\sin[k_\delta x_0]}{\sqrt{\kappa\pi}\sqrt{\delta\pi}} \tag{4.34}$$

is associated with the qubit while

$$X_{\pm,\kappa}\circ X_{\pm,\delta} \equiv \int_0^T \mathrm{d}t_2\, e^{\mathrm{i}(\pm\Omega_p+\omega_\kappa)t_2}\frac{\sin[k_\kappa v t_2]}{\sqrt{\delta\pi}}\int_0^{t_2}\mathrm{d}t_1\, e^{\mathrm{i}(\pm\Omega_p+\omega_\delta)t_1}\frac{\sin[k_\delta v t_1]}{\sqrt{\delta\pi}}. \tag{4.35}$$

is associated with the probe. Thus the phase acquired by the detector in cavity $C_1$ is given as

$$\gamma_1 = -\mathrm{i}\ln[1-\gamma_1^1-\gamma_1^2] \tag{4.36}$$

The phase acquired in the cavity $C_2$ that sustains the vacuum state is given by

$$\gamma_2 = -\mathrm{i}\ln[1-\lambda_p^2\sum_{\delta} X_{+,\delta}\circ X_{+,\delta}^*] \tag{4.37}$$

which depends only on the vacuum terms. Thus we can evaluate the interferometric phase difference using Eq.(4.23) .

We note that the relevant contribution to the interferometric phase difference (4.23) is not cancelled out by the 'mode invisibility' technique unlike the case for the atomic transition probability.

***Analysis***

In the next section, we will characterize the Bell cat state assuming we are able to measure the interferometric phase difference (4.23). Specifically we will investigate the behaviour of the Bell cat state by carefully studying the interferometric phase difference within the coupling range $10^{-2} \leq \lambda_q/\lambda_p \leq 5$. The coupling strength $\lambda$ for the microwave to the optical regime lies in the range $(10^{-6}-10^{-4})\Omega$ as is typical in quantum optical settings [59]. To consider a particular case, we present results for an optical microcavity of length $L \sim 1$ $\mu$m. We will consider the detector's (atomic) gap $\Omega$ to be resonant with a lower even harmonic of the cavity $\kappa = 2$. In the relevant cavity mode, there is an unknown Bell cat state whose entanglement as well as the physical properties of the component states (cat state and qubit) we want to determine.

We consider additionally another cavity prepared with a reference field state (for simplicity we assume the vacuum state) and set up an atomic interferometer as shown in FIG. 4.1. We need first to make sure that, as claimed, the approximation (4.17) holds when we send the atom with a given constant speed $v = 1013$ m/s through the cavity due to the mode invisibility effect. We find that the transition probability – even for a relatively strong coupling $\lambda_p = 10^{-4}\Omega_p$ – remains below $10^{-20}$ for the detection parameters $\theta = \frac{\pi}{2} = -\phi$, $|\beta| = |\alpha| = 0.1$, and $x_0 = \frac{L}{4}$. This is consistent with our perturbative approach and the assumption (4.17). Hence for realistic values of the parameters the 'mode invisibility' technique is rather effective: the atom will not significantly modify the state of the field while flying through it.

To realistically obtain the atomic interference pattern (4.15) (from which the experimental value of probe-qubit phase is determined), a sequence of repeated measurements must be made by sending $N$ probe qubits into the cavity one by one [94]. In a QND experiment, dissipation due to cavity losses and atom decay must be negligible during such repeated measurements. Suppose the time it takes to perform a single experiment is $T = L/v$. Then the time $NT$ it takes to carry out the repeated measurement must be shorter than both the cavity photon loss-time $T_{\text{loss}}$ and entangled-state decay time $T_{\text{ent}}$. That is $NT < T_{\text{loss}}$ where $T_{\text{loss}} = Q/\omega_c$ is the ratio of cavity quality factor $Q$ to the resonant cavity frequency $\omega_c$. So we require $NT\omega_c < Q$. With the parameters we are considering, $T \sim 10^{-5}$ s and $\omega_c \sim 10^{11}\text{s}^{-1}$, we obtain $NT\omega_c \sim N10^6$. We notice that for $N \sim 10^2$ (which should be sufficient to obtain an interference pattern) we need cavities with $Q \sim 10^9$, which can be achieved with current optical systems [59].

Similarly computation of $T_{\text{ent}}$ (which our analysis has neglected), is sensitive to the relative magnitudes of the cavity photon loss time and the cavity qubit-field coupling. The latter dominates in the strong coupling regime in which we are working, in which case the entanglement decay time $T_{\text{ent}}$ is the same as the photon loss time $T_{\text{loss}}$, and so the preceding bound on $N$ remains valid. A more detailed investigation of the various loss terms is an interesting subject for future study.

### 4.2.2 Characterizing the Bell cat state

Our goal in this section is to be able to compare the different dynamical phases acquired by different states through an atomic interferometry experiment. For that we need to know that the global phase acquired depends on the parameters of the relevant states studied.

From (4.22) we see that the global phase acquired by the atom crossing a cavity where a Bell cat state is prepared, is sensitive to (1) the size of the cat state $|\alpha - \beta|$, (2) the position of the qubit entangled to the cat state, and (3) the velocity of the probe flying through the cavity. If we were able to measure it we could use it to characterize entanglement in the Bell cat state, of even the component states (the cat state and qubit).

To characterize the entangled state, we consider two scenarios

1. First, we assume we have knowledge of $A$ and $B$, the degree of qubit-field entanglement. We then go ahead to evaluate the physical features of the composite of the entangled state.

2. Second, we assume we have knowledge of the features of the entangled state. We then want to measure the entanglement between the field and the qubit after the interaction.

**Case 1:** ***Characterizing the physical features of the Bell cat state***

Cavity cat size:

Here we characterize the size $|\alpha - \beta|$ of the cat state entangled to the qubit assuming the component states are maximally entangled with $A = 1/\sqrt{2} = B$. In figure 4.2, we plot $\Delta\gamma$ from Eq. (4.23) as a function of $|\alpha|$ while varying $|\beta|$. We see that $\Delta\gamma$ monotonically increases from $-\pi/2$ to $+\pi/2$ as $|\alpha|$ increases (see Fig 4.2), with the asymptotic value of $\pi/2$ effectively reached once $|\alpha|$ becomes sufficiently large.

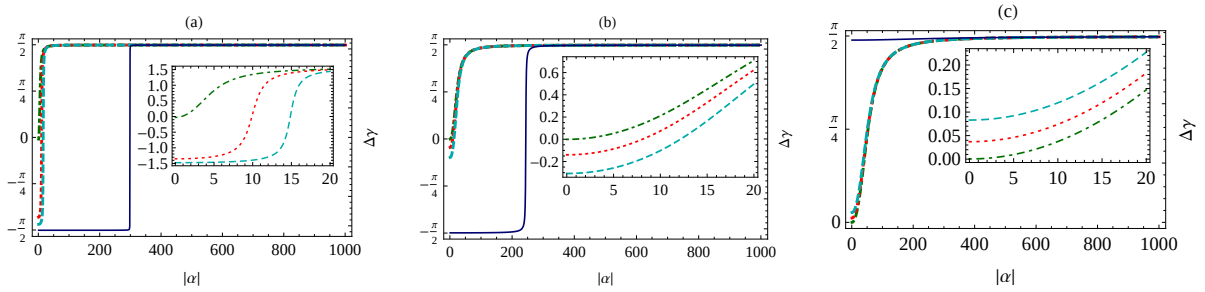


Figure 4.2: The phase factor $\Delta\gamma$ (defined in (4.23)) as a function of $|\alpha|$. Here, the qubit-field system is maximally entangled with $A = B = 1/\sqrt{2}$. Different lines show different values of $|\beta|$: $|\beta| = 1$(green dotdashed Line), $|\beta| = 10$ (red dotted line), $|\beta| = 15$ (Cyan dashed line), $|\beta| = 300$(blue solid line). Inset shows this relation for a small range of $|\alpha|$ parameter. We compared different ratios of $\lambda_q = r\lambda_p$: (a) $r = 5$, (b) $r = 1$, and (c) $r = 10^{-2}$.

For the special case $\lambda_q \ll \lambda_p$, one would expect that the probe-field interaction dominates and the entangled state behaves as if it were a coherent state in the cavity. We indeed find this to be the case when we compare FIG. 4.2(c) with the behaviour of a coherent state in a cavity probed by a qubit as considered in [98]. Note that $\Delta\gamma$ is most efficacious as a diagnostic for the value of $|\alpha|$ when $\lambda_q \geq \lambda_p$, as FIG. 4.2(a) and 4.2(b) demonstrate: for a broad range of values of $|\beta|$ a measurement of $\Delta\gamma$ yields information about the value of $|\alpha|$. However this becomes increasingly less so once $|\beta|$ becomes sufficiently large; as shown in Fig 4.11(a), we see that $\Delta\gamma$ is insensitive to the value of $\alpha$ except near $|\beta| = |\alpha| = 300$. In a narrow region near $|\beta| = |\alpha| = 300$, we observe the sudden rise of $\Delta\gamma$ to $\pi/2$, after which we lose information about the state amplitude $|\alpha|$. This sudden response deviates

slightly to the left as $\lambda_q = \lambda_p$ (see FIG. 4.2(b)) until we have a zero response to $|\alpha|$ (Fig 4.2(c)).

Qubit's position in the cavity:

Here we demonstrate that the mode invisibility technique can be used to obtain information about the qubit's position in a cavity. Recall that we assumed that the transition frequency of the qubit is detuned from the cavity field frequency. The probe's interaction with the entangled qubit-field system imparts a phase shift $\Delta\gamma$ to the entangled state. The magnitude of this phase shift depends also on the qubit's position $x_0$ relative to the nodes and antinodes of the cavity modes.

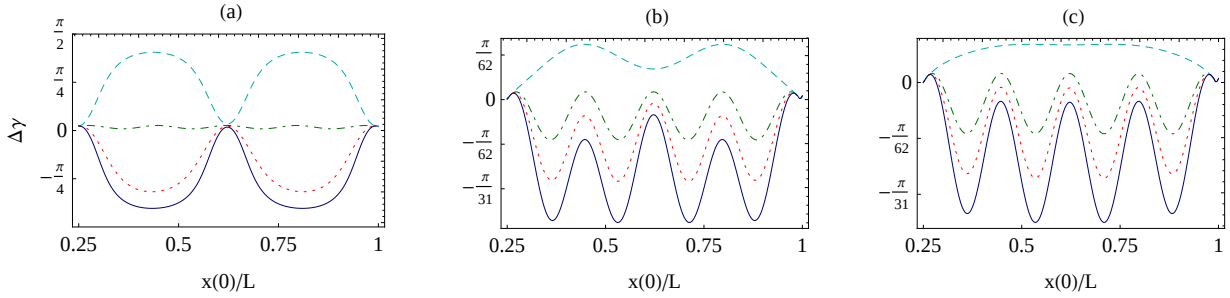


Figure 4.3: The phase factor $\Delta\gamma$ (defined in (4.23)) as a function of $x_0$– the qubit's position in the cavity. Each graph plots different values of $|\alpha| = |\beta|$ : (a) $|\alpha| = |\beta| = 10$, (b) $|\alpha| = |\beta| = 1$ and (c) $|\alpha| = |\beta| = 0.3$. The different lines within each graph illustrate different values of $A, B$ : $A = 1/2, B = \sqrt{3}/2$ (red Line), $A = 1/\sqrt{2}, B = 1/\sqrt{2}$ (green line), $A = 1, B = 0$ (cyan line), $A = 0, B = 1$(blue line). Here we considered $\lambda_q = 3\lambda_p$.

We illustrate the relationship between the interferometric phase difference as a function of qubit's position $x_0$ in Fig 4.3. The phase $\Delta\gamma$ oscillates between maximal and minimal values that depend on the relative magnitude of $|\alpha|/|\beta|$. The amplitude of oscillation varies as the quantum state (4.25) goes from being one of maximal entanglement to a product state. In the latter situation, for large $|\alpha| = |\beta|$ (Fig 4.3(a)) the qubit's position for $A = 0, B = 1$ is completely out of phase relative to the case $A = 1, B = 0$; with equal but opposite amplitudes they cancel each other. The maximally entangled case $A = B = \frac{1}{\sqrt{2}}$ has near-zero amplitude.

The qubit's position (up to a wavelength) can therefore be determined from the phase, providing some advantage for preparing the qubit in an entangled state. As $|\alpha| = |\beta|$ decreases in value the distinctions between the two possible product states become increasingly pronounced. This asymmetry is due to the distinction between the less rapidly oscillating counter-rotating ($A$-coefficient) and more rapidly oscillating rotating ($B$-coefficient)

vacuum contributions to $\eta_2$, which dominate for small $|\alpha|, |\beta|$. The increase in phase oscillation frequency makes it somewhat more difficult to determine the location of the qubit. The phase symmetry for large $|\alpha|, |\beta|$ becomes increasingly less valid, with large changes in the phase occuring for $A = 0, B = 1$ corresponding to small changes for $A = 1, B = 0$ and vice-versa, as shown in Fig 4.3(c).

Detector's speed:

We now consider the sensitivity of the relative phase (4.23) to the velocity of the probe. For our choice of probe velocity $v = 1013$ m/s, we have seen (figure 4.4) how the relative phase varies with respect to the parameters $(|\alpha|, |\beta|)$. In figure 4.4 we illustrate the dependence of the relative phase on $v$ for various values of these parameters and on the coefficients $A$ and $B$.

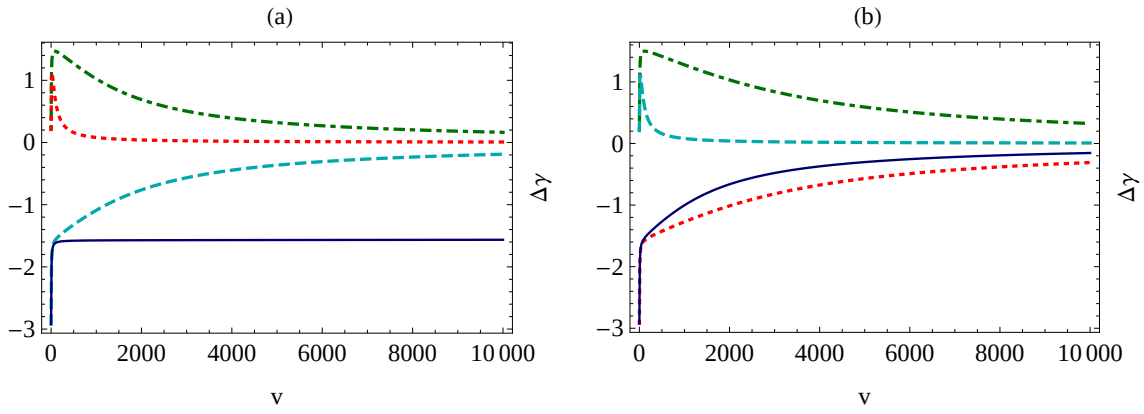


Figure 4.4: The phase factor $\Delta\gamma$ (defined in (4.23)) as a function of probe velocity $v$ $(m/s)$. Left: $A = B = 1/\sqrt{2}$; the different lines within each graph illustrate different values of $|\beta|$ for fixed $|\alpha| = 10$ : $|\beta| = 1$ (green dot dashed Line), $|\beta| = 10$ (red dotted line), $|\beta| = 15$ (cyan dashed line), $|\beta| = 300$(blue solid line). Right: $|\alpha| = |\beta| = 10$; different lines within each graph illustrate different values of $A, B$ : $A = 1/2, B = \sqrt{3}/2$ (blue solid line), $A = 1/\sqrt{2}, B = 1/\sqrt{2}$ (cyan dahsed line), $A = 1, B = 0$ (green dot dashed line), $A = 0, B = 1$(red dotted line), and we considered the ratio $\lambda_q = 3\lambda_p$

We see that for large $v$ that $\Delta\gamma$ is small and so the sensitivity is low. However for values of $v$ ranging from 100 m/s to 1200 m/s (an appropriate range for experimental realization [120, 34], there is sufficient sensitivity to yield information about about the cavity field. Furthermore, the dependence on probe velocity is smooth, a desirable feature for experimental realization.

Understanding the qubit's dynamics :

We close this section by exploring what properties of the state of the cavity qubit can be obtained using the mode invisibility technique. The reduced density operator for the qubit is given by tracing over the detector and cat field variables:

$$\rho_q(t) = \mathrm{Tr}_{\mathrm{FP}}\Big[\rho(t)\Big] = \rho_{gg}|g\rangle\langle g| + \rho_{ge}|g\rangle\langle e| + \rho_{eg}|e\rangle\langle g| + \rho_{ee}|e\rangle\langle e| \tag{4.38}$$

where $\rho_{gg}, \rho_{ge}, \rho_{eg}$ and $\rho_{ee}$ are respectively defined as

$$\begin{aligned}
\rho_{gg} &= A^2\Big[1 - \lambda_q^2\Big(\{I^*_{+,\kappa}, I_{+,\kappa}\}|\alpha|^2 + \{I^*_{-,\kappa}, I_{-,\kappa}\}|\alpha|^2 + \{I_{-,\kappa}, I_{+,\kappa}\}(\alpha^*)^2 + \{I^*_{+,\kappa}, I^*_{-,\kappa}\}(\alpha)^2 + \sum_\gamma \{I^*_{+,\gamma}, I_{+,\gamma}\}\Big) \\
&- \lambda_p^2\Big(\{X^*_{+,\kappa}, X_{+,\kappa}\}|\alpha|^2 + \{X^*_{-,\kappa}, X_{-,\kappa}\}|\alpha|^2 + \{X_{-,\kappa}, X_{+,\kappa}\}(\alpha^*)^2 + \{X^*_{+,\kappa}, X^*_{-,\kappa}\}(\alpha)^2 + \sum_\gamma \{X^*_{+,\gamma}, X_{+,\gamma}\}\Big)\Big] \\
&+ \lambda_q^2 B^2\Big[|I_{+,\kappa}|^2|\beta|^2 + 2\,\mathrm{Re}[I_{-,\kappa}I_{+,\kappa}(\beta^*)^2] + \sum_\gamma |I_{-,\gamma}|^2 + |I_{-,\kappa}|^2|\beta|^2\Big] + \lambda_p^2 B^2\Big[\sum_\delta |X_{+,\delta}|^2 + |X_{+,\kappa}|^2|\alpha|^2\Big] \\
&- \mathrm{i}\lambda_q AB\Big(I^*_{+,\kappa}\beta + I_{-,\kappa}\alpha^*\Big)\langle\alpha_\kappa|\beta_\kappa\rangle + \mathrm{i}\lambda_q AB\Big(I_{+,\kappa}\beta^* + I^*_{-,\kappa}\alpha\Big)\langle\beta_\kappa|\alpha_\kappa\rangle
\end{aligned}$$

$$\begin{aligned}
\rho_{ee} &= B^2\Big[1 - \lambda_q^2\Big(\{I^*_{+,\kappa}, I_{+,\kappa}\}|\beta|^2 + \{I^*_{-,\kappa}, I_{-,\kappa}\}|\beta|^2 + \{I_{-,\kappa}, I_{+,\kappa}\}(\beta^*)^2 + \{I^*_{+,\kappa}, I^*_{-,\kappa}\}(\beta)^2 + \sum_\gamma \{I^*_{-,\gamma}, I_{-,\gamma}\}\Big) \\
&\quad - \lambda_p^2\Big(\{X^*_{+,\kappa}, X_{+,\kappa}\}|\beta|^2 + \{X^*_{-,\kappa}, X_{-,\kappa}\}|\beta|^2 + \{X_{-,\kappa}, X_{+,\kappa}\}(\beta^*)^2 + \{X^*_{+,\kappa}, X^*_{-,\kappa}\}(\beta)^2 + \sum_\gamma \{X^*_{+,\gamma}, X_{+,\gamma}\}\Big)\Big] \\
&\quad + \lambda_q^2 A^2\Big[|I_{+,\kappa}|^2|\alpha|^2 + 2\,\mathrm{Re}[I_{-,\kappa}I_{+,\kappa}(\alpha^*)^2] + \sum_\gamma |I_{-,\gamma}|^2 + |I_{-,\kappa}|^2|\alpha|^2\Big] + \lambda_p^2 B^2\Big[\sum_\delta |X_{+,\delta}|^2 + |X_{+,\kappa}|^2|\alpha|^2\Big] \\
&\quad - \mathrm{i}\lambda_q AB\Big(I_{+,\kappa}\beta^* + I^*_{-,\kappa}\alpha\Big)\langle\beta_\kappa|\alpha_\kappa\rangle + \mathrm{i}\lambda_q AB\Big(I^*_{+,\kappa}\beta + I_{-,\kappa}\alpha^*\Big)\langle\alpha_\kappa|\beta_\kappa\rangle.
\end{aligned}$$

$$\begin{aligned}
\rho_{ge} &= AB\langle\beta|\alpha\rangle\Big[1 - \lambda q^2\Big(\{I^*_{+,\kappa}, I_{+,\kappa}\}\alpha\beta^* + \{I^*_{-,\kappa}, I_{-,\kappa}\}\alpha\beta^* + \{I_{+,\kappa}, I_{-,\kappa}\}(\beta^*)^2 + \{I^*_{+,\kappa}, I^*_{-,\kappa}\}\alpha^2\Big) \\
&\quad - \lambda_p^2\Big(\{X^*_{+,\kappa}, X_{+,\kappa}\}\beta^*\alpha + \sum_\delta \{X^*_{+,\delta}, X_{+,\delta}\} + \{X^*_{+,\kappa}, X^*_{-,\kappa}\}\alpha^2 + \{X_{-,\kappa}, X^*_{-,\kappa}\}\beta^*\alpha + \{X_{-,\kappa}, X_{+,\kappa}\}(\beta^*)^2\Big)\Big] \\
&\quad + \Big[I^*_{+,\kappa}I^*_{-,\kappa}\beta\alpha^* + (I^*_{+,\kappa})^2\beta^2 + \sum_\gamma I_{-,\gamma}I^*_{+,\gamma} + I_{-,\kappa}I^*_{+,\kappa}\alpha^*\beta + (I_{-,\kappa})^2(\alpha^*)^2\Big]AB\langle\alpha_\kappa|\beta_\kappa\rangle \\
&\quad + \lambda_p^2 AB\langle\beta_\kappa|\alpha_\kappa\rangle\Big(|X_{+,\kappa}|^2\beta^*\alpha + \sum_\delta |X_{+,\delta}|^2\Big) - \mathrm{i}B^2\lambda_q\Big[I^*_{+\kappa}\beta + I_{-,\kappa}\beta^*\Big] + \mathrm{i}A^2\Big[I^*_{+\kappa}\alpha + I_{-,\kappa}\alpha^*\Big]
\end{aligned}$$

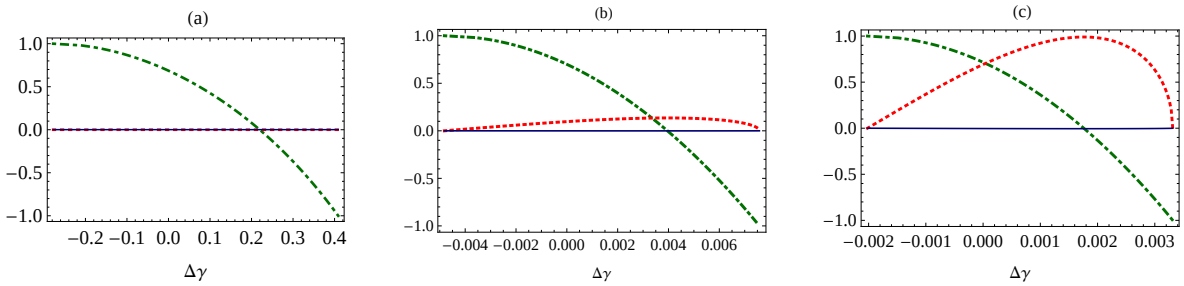


Figure 4.5: Population inversion (Green dotdashed line), dipole current (blue solid line) and dipole moment (red dotted line) as a function of interferometric phase difference $\Delta\gamma$ for different field amplitudes: (a) $|\alpha| = |\beta| = 10$, (b) $|\alpha| = |\beta| = 1$ (c) $|\alpha| = |\beta| = 0.1$ respectively. Here we considered the ratio $\lambda_q = \lambda_p$. With the normalization condition in mind $A^2 + B^2 = 1$, we start with $A = 0, B = 1$ and gradually increase $A$ up to 1.

$$\begin{aligned}\rho_{eg} =& AB\langle\alpha|\beta\rangle\Big[1 - \lambda q^2\Big(\{I^*_{+,\kappa}, I_{+,\kappa}\}\alpha^*\beta + \{I^*_{-,\kappa}, I_{-,\kappa}\}\alpha^*\beta + \{I_{+,\kappa}, I_{-,\kappa}\}(\alpha^*)^2 + \{I^*_{+,\kappa}, I^*_{-,\kappa}\}\beta^2\Big) \\ &- \Big(\{X^*_{+,\kappa}, X_{+,\kappa}\}\beta\alpha^* + \sum_\delta\{X^*_{+,\delta}, X_{+,\delta}\} + \{X^*_{+,\kappa}, X^*_{-,\kappa}\}\beta^2 + \{X_{-,\kappa}, X^*_{-,\kappa}\}\beta\alpha^* + \{X_{-,\kappa}, X_{+,\kappa}\}(\alpha^*)^2\Big)\Big] \\ &+ \Big[I^*_{+,\kappa}I^*_{-,\kappa}\beta^*\alpha + (I_{+,\kappa})^2(\beta^*)^2 + \sum_\gamma I^*_{-,\gamma}I_{+,\gamma} + I^*_{-,\kappa}I_{+,\kappa}\alpha\beta^* + (I^*_{-,\kappa})^2(\alpha)^2\Big]AB\langle\beta_\kappa|\alpha_\kappa\rangle + \\ &\lambda_p^2 AB\langle\alpha_\kappa|\beta_\kappa\rangle\Big(|X_{+,\kappa}|^2\beta\alpha^* + \sum_\delta|X_{+,\delta}|^2\Big) - \mathrm{i}A^2\lambda_q\Big[I_{+\kappa}\alpha^* + I^*_{-,\kappa}\alpha\Big] + \mathrm{i}B^2\lambda_q\Big[I_{+\kappa}\beta^* + I^*_{-,\kappa}\beta\Big]\end{aligned}$$

with the diagonal elements satisfying $\rho_{ee} + \rho_{gg} = 1$ and the off-diagonal elements are in general complex and satisfy $\rho_{eg} = \rho^*_{ge}$. Eq. (4.38) enables us to study some properties of the qubit. By definition, $\{I_{+,\kappa}, I^*_{-,\kappa}\} = I_{+,\kappa} \circ I^*_{-,\kappa} + I^*_{-,\kappa} \circ I_{+,\kappa}$ and similarly for other circle products (defined in (4.34)). From these expressions, we can evaluate the properties (including population inversion, dipole current, dipole moment) of the qubit entangled to the cat state.

We plot in Fig. 4.5 these functions against the interferometric phase difference $\Delta\gamma$. Starting with $B = 1$ and $A = 0$, as we increase $A$ gradually we see that the interferometric phase difference increases as the population inversion decreases, this relationship is seen for different range of $|\alpha|, |\beta|$. In figure 4.5(a), we see that for large values of $|\alpha|, |\beta|$, there is no dependence on the dipole moment and dipole current. The dipole moment $(f)$ is proportional $\mathrm{Re}[\langle\alpha|\beta\rangle]$ which is vanishing for large values of $|\alpha||\beta|$, while the dipole current is proportional to $\mathrm{Im}[\langle\alpha|\beta\rangle]$, which is vanishing for all values of $|\alpha|, |\beta|$ since the argument of the imaginary operator is real. However while we decrease the values of $|\alpha|, |\beta|$, although a response of the dipole current is never seen, we see a dipole moment response attaining

a maximum at some intermediate positive value of $\Delta\gamma$. Within this limitation the phase difference provides a diagnostic of the cavity qubit's state.

### Case 2: *Characterizing entanglement in the Bell cat state*

In this section, we consider another possibility for probing states of the form in Eq. (4.25): we assume we have knowledge of the features of the entangled state and we want to measure the entanglement between the field and the qubit after the interaction.

Although several entanglement measures exist [9, 10, 11, 64, 132], we choose the von Neumann entropy [93] of the reduced state $S(\rho_q)$ which is given as

$$S(\pi_i) = \begin{cases} -\sum_i \pi_i \operatorname{Log} \pi_i & \text{if } \pi_i > 0 \\ 0 & \text{if } \pi_i = 0 \end{cases} \tag{4.39}$$

where $\rho_q = \rho_q(t) = \mathrm{Tr}_{\mathrm{FP}}[\rho(t)] = \sum_i \pi_i |i\rangle\langle i|$ is the qubit's reduced density operator given in (4.38), with eigenvalues $\pi_j$ given as

$$\pi_{\pm j} = \frac{1}{2}\Big(\rho_{gg} + \rho_{ee} \pm \sqrt{4\rho_{ge}\rho_{eg} + (\rho_{ee} - \rho_{gg})^2}\Big). \tag{4.40}$$

Fixing the qubit at $x_0 = L/4$, we consider the values $\theta = \pi/2 = -\phi$. We plot the resultant von Neumann entropy $S(\rho_q)$ as a function of $\Delta\gamma$ for three distinct ratios of the couplings: $\lambda_q = r\lambda_p$ with $r = 10^{-2}, 5$, and 1 in FIG 4.6, 4.7 and 4.8 respectively. We find that $\Delta\gamma$ provides an excellent measure of the entropy over a broad range of $|\alpha|$ and $|\beta|$ for all coupling ratios $\frac{\lambda_q}{\lambda_p}$ explored. However for small $\lambda_q/\lambda_p$, the range of $\Delta\gamma$ becomes increasingly narrow as $|\alpha|/|\beta| \to 1$, becoming very sharply peaked in this limit.

We find that the maxima of $S(\rho_q)$ are less than unity for small values of $|\alpha|, |\beta| \leq 1$. Setting $|\alpha| = |\beta|$, we find that these maxima approach unity as $|\alpha| \to 1$ (see the green curves in FIG 4.6(c), 4.7(c) and 4.8(c)), with little change for larger values of $|\alpha|$. Alternatively if we fix $|\alpha|$, the maxima increase with increasing $|\beta|$ until attaining $S(\rho_q) = 1$ (within our limits of numerical precision) after which they gradually decrease.

In summary, the von Neumann entropy for the reduced qubit state (which is equal to the von Neumann entropy for the cavity cat state) increases with an increase in the cavity cat amplitudes $|\alpha|$ and $|\beta|$. This provides us with a tool for measuring the entropy of a quantum system after interaction, a question of common interest [93]. Since the mode invisibility process does not significantly affect the entanglement between the cavity qubit

and the field, we infer that $\Delta\gamma$ is providing a measure of the constant entropy between them.

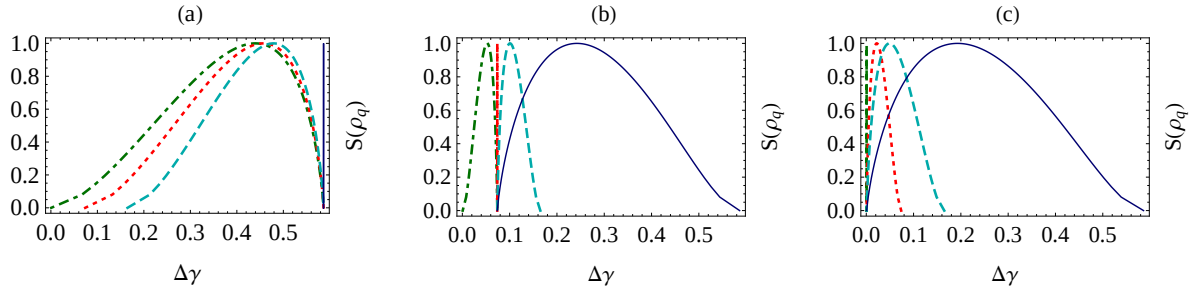


Figure 4.6: von Neumann entropy as a function of $\Delta\gamma$ for different $|\alpha|$; (a) $|\alpha| = 30$ (b) $|\alpha| = 10$ (c) $|\alpha| = 1$. Here $\lambda_q = 10^{-2}\lambda_p$. Different curves show different values of $|\beta|$: $|\beta| = 1$ (green dotdashed line), $|\beta| = 10$ (red dotted line), $|\beta| = 15$ (cyan dashed line), $|\beta| = 30$ (blue solid line).

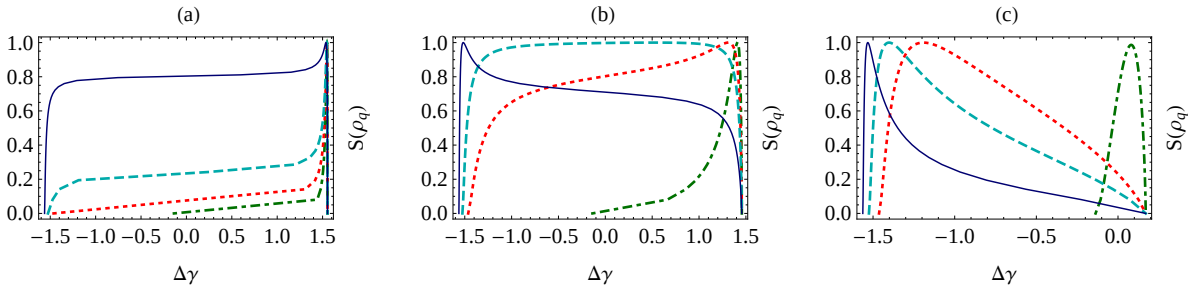


Figure 4.7: von Neumann entropy as a function of $\Delta\gamma$ for different $|\alpha|$; (a) $|\alpha| = 30$ (b) $|\alpha| = 10$ (c) $|\alpha| = 1$. Here $\lambda_q = 5\lambda_p$. Different curves reveal different values of $|\beta|$: $|\beta| = 1$ (green dotdashed line), $|\beta| = 10$ (red dotted line), $|\beta| = 15$ (cyan dashed line), $|\beta| = 30$ (blue solid line).

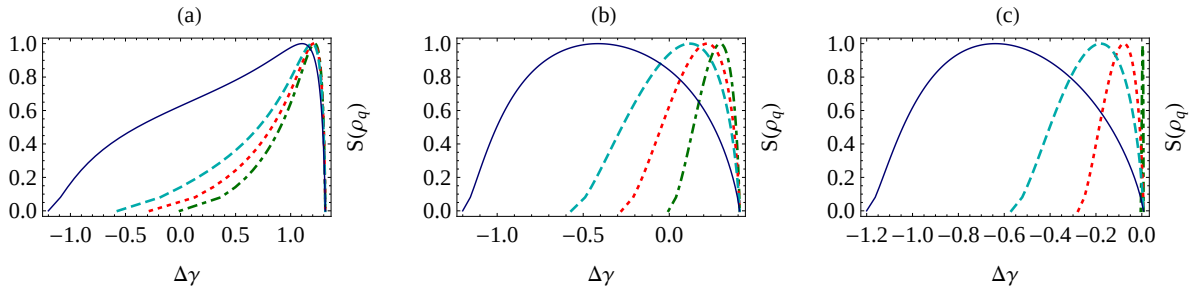


Figure 4.8: von Neumann entropy as a function of $\Delta\gamma$ for different $|\alpha|$; (a) $|\alpha| = 30$ (b) $|\alpha| = 10$ (c) $|\alpha| = 1$. Here $\lambda_q = \lambda_p$. Different curves reveal different values of $|\beta|$: $|\beta| = 1$ (green dotdashed line), $|\beta| = 10$ (red dotted line), $|\beta| = 15$ (cyan dashed line), $|\beta| = 30$ (blue solid line).

### 4.2.3 Phase resolution and visibility

#### *Phase Resolution*

For any given setting, the atom interferometer can resolve the values of the parameters only to a certain level of precision. The magnitude of the resolution of the interferometric experiment conditions our ability to distinguish the phase acquired by the state having amplitude $|\alpha + \delta\alpha|$ from another of amplitude $|\alpha|$. Knowing that typical resolutions in atomic interferometry are of the order of fractions of milliradians [59]. The phase resolution of the interferometric setting is

$$R_{\delta\alpha}(\alpha) = |\gamma_{\alpha+\delta\alpha} - \gamma_{\alpha}| \tag{4.41}$$

and by fixing a value for $|\beta|$, Eq. (4.41) defines our ability to distinguish the phase acquired by the state having amplitude $|\alpha + \delta\alpha|$ from another of amplitude $|\alpha|$.

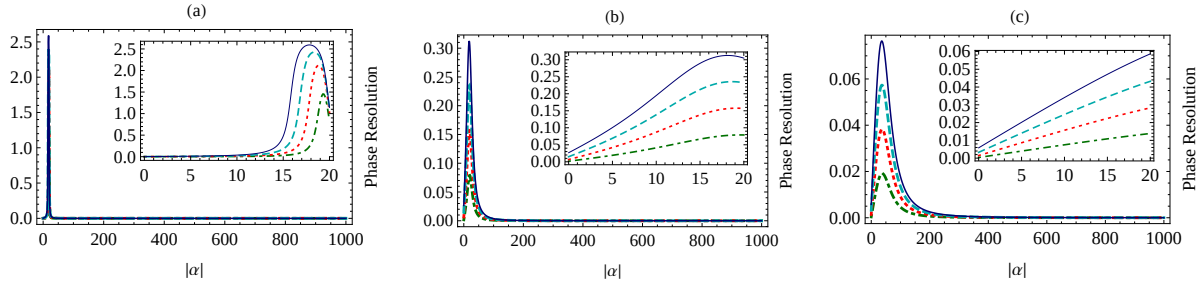


Figure 4.9: The phase resolution $R_{\delta\alpha}(\alpha)$ as a function of $|\alpha|$ for different ratios $\lambda_q = r\lambda_p$, (a) $r = 5$, (b) $r = 1$ and (c) $r = 10^{-2}$. In this case, the qubit is fixed at $x_0 = L/4$ and we use the values $\theta = \pi/2$, $\phi = -\pi/2$, $|\beta| = 20$ and different values of $\delta\alpha$: $\delta\alpha = 1$ (green dotdashed line), $\delta\alpha = 2$ (red dotted line), $\delta\alpha = 3$ (cyan dashed line), $\delta\alpha = 4$ (blue solid line).

We illustrate in figure 4.9 the phase resolution for a fixed value of $|\beta| = 20$. We see that we have enough resolution for an interferometric experiment, provided $|\alpha|$ is not too large, with the best discrimination over the broadest range of $|\alpha|$ occurring for $\lambda_q = \lambda_p$.

#### *Interferometric visibility*

The last point we need to analyze is how good the visibility of the interferometric pattern will be, taking into account that we would have second order effects taking us out of the ground state. They are guaranteed to be small due to their second order nature, but they

would impact the visibility of the fringes. As discussed in section 4.1.2, $\gamma_1$ is a complex number due to contributions from terms orthogonal to our initial chosen quantum state. This yields an observable loss in the visibility, where

$$|\langle\Psi(T)|\Psi(0)\rangle|^2 = \exp[-2\Im[\gamma_1]] \tag{4.42}$$

defines the visibility, with $|\Psi(T)\rangle$ the final quantum state at time $T$. This provides a measure of how non-destructive the probe is. We present in figure 4.10 the visibility factor as a function of $|\alpha|$ for different regimes of $\lambda_q$ and $\lambda_p$.

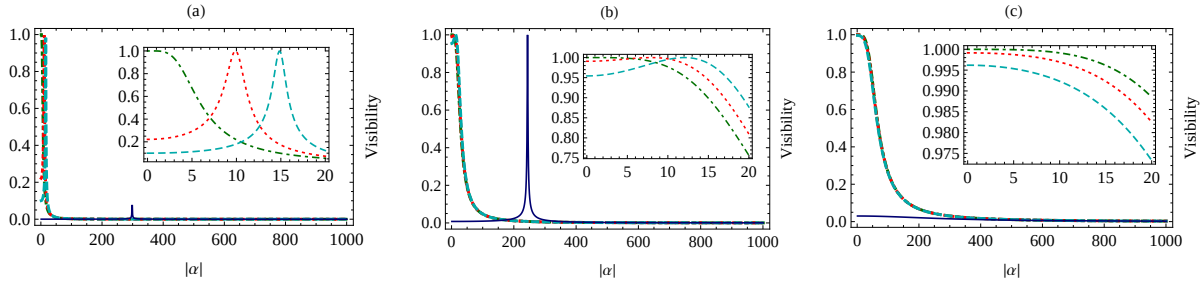


Figure 4.10: Visibility Exp[$\Im[\eta]$] as a function of $|\alpha|$ . The qubit is fixed at $x_0 = L/4$ and we use the values $\theta = \pi/2$, $\phi = -\pi/2$ and different values of $|\beta|$: $|\beta| = 1$ (green dotdashed line),$|\beta| = 10$ (red dotted line), $|\beta| = 15$ (cyan dashed line),$|\beta| = 300$ (blue solid line). We see a peak for the case $\lambda_q = 5\lambda_p$. This occurs at point $|\alpha| = |\beta|$. This peak gradually shifts from this position as $\lambda_q$ becomes smaller compared to $\lambda_p$ until it dies out.

For small values of $|\beta|$ visibility remains largest over the broadest range of $|\alpha|$ for $\lambda_q = \lambda_p$; $|\alpha| < 100$ yields non-destructive measurement capacity for the probe at better than 99%. There is not much decline in visibility over the same range of $|\alpha|$ as $\lambda_q$ decreases. However as $\lambda_q$ increases, visibility gets notably weaker over increasingly small ranges of $|\alpha|$. However we also see an interesting trend as $|\beta|$ increases: for a given value of $|\beta|$ visibility peaks, with the location of the peak occurring approximately at $|\alpha| = |\beta|$. At this point, we say the two coherent states $|\alpha\rangle, |\beta\rangle$ coincide.

### 4.2.4 Conclusion

We have demonstrated the utility of the mode-invisibility measurement technique [97] for probiing an entangled generalized qubit/cat state in a cavity mode in a non-destruct way. For realistic physical parameters, and provided that the amplitude of the cavity field is not too large, the technique provides a good measure for the state, especially in the regime

where $\lambda_q \approx \lambda_p$. However it breaks down once $|\alpha|$ is sufficiently large, which is where $\Delta\gamma$ reaches its asymptotic value of $\pi/2$. This is confirmed by means of the visibility, where we get up to 99% non-demolition probe of the state for values of $|\alpha|$ close to $|\beta|$. In regimes where the mode-invisibility technique works, the interferometric phase resolution is sufficient to perform the experiment.

## 4.3 Taming an Optical Schrödinger's cat– quantum non-demolition approach

In this section, we consider the effect of a squeeze operator on the superposition of coherent states. Specifically, we study the squeezed superposition of coherent states (SSCS) written as

$$|\Psi_\psi\rangle = S(\zeta)|\text{cat}\rangle = \frac{1}{\mathcal{N}_\psi} S(\zeta)\big[|\alpha\rangle + e^{\mathrm{i}\psi}|-\alpha\rangle\big]. \tag{4.43}$$

Here $S_\kappa(\zeta) = e^{1/2(\zeta^* a^2 - \zeta a^{\dagger 2})}$ is a squeeze operator with squeeze parameter $\zeta = re^{\mathrm{i}\delta}$, squeezing amplitude $r$ and phase $\delta$. We are interested in the squeezed even, odd and Yuker-Stoler cat states respectively which is given according to the phase factor $\psi$; with $\psi = 0, \pi$ and $\pi/2$ respectively.

As with the setup 4.1, in cavity $C_1$ the relevant field is the SSCS. An atom initially in the ground state is used as a probe for this field. Thus the the combined atom-field state before interaction can be written as

$$|\Phi_\psi\rangle = |g\rangle \otimes |\Psi_\psi\rangle \bigotimes_{\kappa\neq\gamma} |0_\gamma\rangle \tag{4.44}$$

where we have assumed that the SSCS is confined in the cavity mode $\kappa$ and the rest of the modes $\gamma$ are empty (approximately the vacuum field mode). During interaction, the joint system undergoes an evolution governed by the Unruh-De-Witt interaction Hamiltonian Eq. (3.155)

$$\hat{H}_I = \lambda_p \hat{\mu}_p(t)\hat{\phi}[x_p(t)] \tag{4.45}$$

so that the state of the combined atom-field system after interaction time $T$ is given as $|\Phi_\psi(T)\rangle = U(T,0)|\Phi_\psi(0)\rangle$.

Following the same analysis as in 4.2, we hope to measure the SSCS in a nondestructive way. To see how this works, we calculated the detector's excitation transition probability and the interferometric phase difference in the setup 4.1 with a reference vacuum state.

### 4.3.1 Results

***Transition probability***

According to (4.17), we obtained the probe's excitation transition probability to first order in the atom-field coupling constant $\lambda$ as [89]

$$P_{|e\rangle} = \lambda^2 \Big\{ \big|I_{+,\kappa}\big|^2 \overline{n}_{\psi}(r) + \sum_{\beta} |I_{+,\beta}|^2 \Big\} \tag{4.46}$$

where

$$\overline{n}_{\psi}(r) = \sinh^2 r + \overline{n}_{\psi}(0)(\cosh^2 r + \sinh^2 r) - 2|\alpha|^2 \cos(\delta - 2\theta) \cosh r \sinh r \tag{4.47}$$

is the average number of photons in the squeezed cat state and

$$\overline{n}_{\psi}(0) = |\alpha|^2 \left( \frac{1 - e^{-2|\alpha|^2} \cos\psi}{1 + e^{-2|\alpha|^2} \cos\psi} \right) \tag{4.48}$$

is the mean photon number in a cat state (with no squeezing). Again, we have applied the mode invisibility scheme to eliminate the resonant terms ($|I_{-,j}|$), which is the highest contribution to this transition probability.

***Interferometric phase difference***

The interferometric phase difference was evaluated according to equation (4.23). In cavity $C_1$ with the superposition of coherent states, we have the phase [89]

$$\gamma_1(\psi, r) = -\mathrm{i} \ln \left\{ 1 - \lambda^2 \Big( \sum_{\beta} I^*_{+,\beta} \circ I_{+,\beta} + \overline{n}_{\psi}(r)\, I^*_{+,\kappa} \circ I_{+,\kappa} \Big) \right\}, \tag{4.49}$$

where $I_{-,\kappa} \circ I_{-,\kappa}$ is given as in (3.162). Similarly in cavity $C_2$ with the EM vacuum field, the phase acquired is

$$\gamma_2(\psi) = -\mathrm{i} \ln \Big\{ 1 - \lambda^2 \sum_{\gamma} I^*_{+,\gamma} \circ I_{+,\gamma} \Big\} \tag{4.50}$$

Therefore, we can evaluate the interferometric phase difference (4.23) in the atom interferometer after the detector-cavity field interaction.

### 4.3.2 Characterizing the squeezed superposition of coherent states

From (4.49) we see that the global phase acquired by the atom crossing a cavity where a SSCS is prepared, is sensitive to (1) the parameter $|\alpha|$, (2) the squeezing parameter r, and (3) the angles $\theta$ and $\delta$. This means that If we were able to measure (4.23), we could use it to characterize a superposition of coherent state or a squeezed superposition of coherent state. We now see how this works.

***Analysis***

In addition to the parameters discussed in 4.2.1, we consider the field parameters ($|\alpha| = 0.5, r = 0.5, \delta = \pi, \theta = \frac{\pi}{2}$) for our analysis and we set the detector's speed $v = 1000\text{m/s}$ through the cavity. Using these parameters, we find the detector's transition probability to be $\approx 10^{-21}$, a value which is approximately zero. Our ability to manipulate and control the detector's motion through the cavity such that its transition probability is approximately zero again indicates that we have a measurement scheme where the atom-field interaction does not significantly perturb the cavity field. Our next goal is to see how the parameters can be obtained assuming a measurement of the interferometric phase difference.

Amplitude of the cat state

The amplitude of the cat states is defined by the parameter $|\alpha|$.

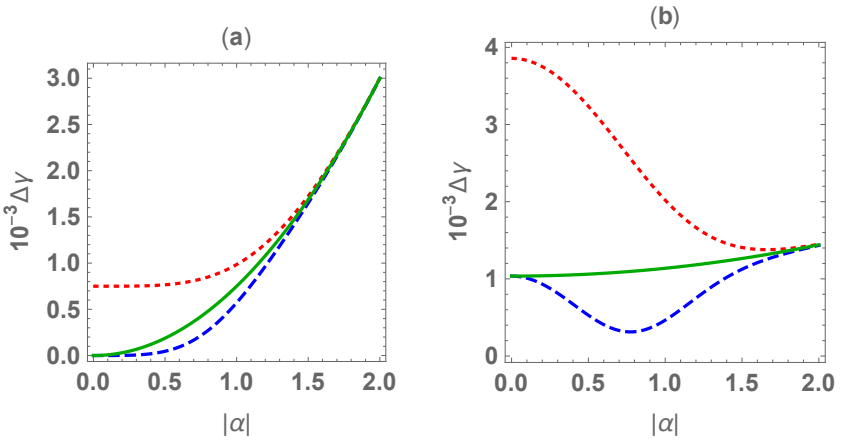


Figure 4.11: Plot of the relative phase difference $\Delta\gamma$ vs $|\alpha|$ in the absence of squeezing (a) and modest squeezing $\zeta = |1|$ (b) for the various cat states: even (blue dashed line), odd (red dot line), and Yuker-Stoler (green solid line) cat states respectively with $\theta = \pi/2$.

In Fig. 4.11 we plot the interferometric phase difference $\Delta\gamma$ as a function of $|\alpha|$. Squeezing enhances our ability to distinguish between the three cat states, as the curves are well separated from one another (see Fig 4.11(a)). In the range of $|\alpha| = [1, 1.8]$, $\Delta\gamma$ is a strictly decreasing function for the odd cat state (red dotted line), and a strictly increasing function for even cat state (blue dashed line). This at least distinguishes between the odd and even cat states. For the Yuker-Stoller cat state, $\Delta\gamma$ is a linear function in $|\alpha|$. Hence an experimentalist can verify through the mode-invisibility technique that the state has macroscopically distinguishable components without significantly destroying the states.

Phase of complex amplitude

We see from (4.49) that the interferometric phase difference $\Delta\gamma$ is a sensitive function of $\theta$–the phase of the coherent states, only in the presence of squeezing.

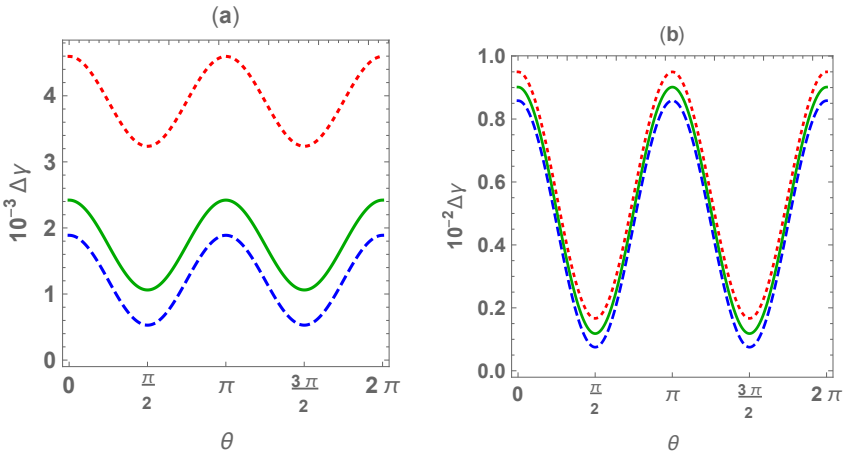


Figure 4.12: Plot of the relative phase difference $\Delta\gamma$ vs the parameter $\theta$ against $|\alpha| = 0.5$ (a) and $|\alpha| = 1.5$ (b) for the different cat states: even (blue dashed line), odd (red dotted line), and Yuker-Stoler (green solid line) cat states respectively with $\zeta = |1|$.

We illustrate in. Fig. 4.12 the relationship between $\Delta\gamma$ and $\theta$. For $0.5 \leq |\alpha| \leq 2$, we see distinct oscillatory behaviour for each of the three cat states. However this behaviour is damped by the second term in (4.47) resulting from the mean photon number in the cat states. Choosing $\theta = \frac{\pi}{n}$ where $n$ is an integer, yields the best result. This offers a possibility of distinguishing between a squeezed cat state and a cat state.

Squeeze parameter detection

We also show in fig. 4.13 the interferometric phase differences $\Delta\gamma$ as a function of $r$ and $\delta$, the amplitude and phase of the squeeze operator respectively. The three different cat states are distinguishable only from $r \approx 1$ corresponding to $10\text{Log}_{10}(e^{2r}) \gtrsim 9\text{dB}$; a value which is reachable with present technology [131]. This distinction is also dependent on the coherent state amplitude $|\alpha|$ and phase $\theta$. We require that $|\alpha| < 2$ and $\theta = \frac{\pi}{n}$ with $n$ being an integer to achieve a good distinguishability of the cat states. We comment here

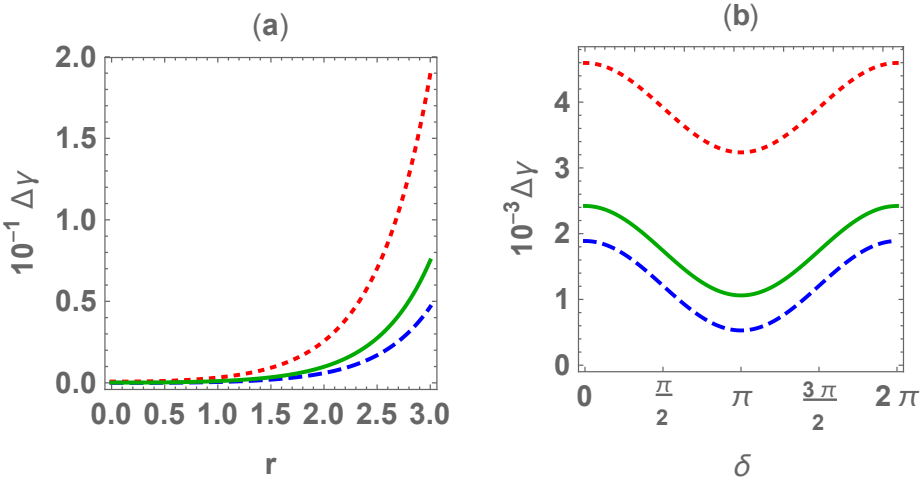


Figure 4.13: Plot of the relative phase difference $\Delta\gamma$ vs $|\alpha|^2$ in the absence of squeezing (a) and modest squeezing $\zeta = |1|$ (b) for the various cat states: even (blue dashed line), odd (red dot line), and Yuker-Stoler (green solid line) cat states respectively with $\theta = \pi/2$.

that the maximum effect of squeezing is felt when $\delta = \pi$, where the three cat states have a minimum.To conclude, we have shown that distinguishing the even, odd and Yuker-Stoller cat states is best achieved with small amplitudes of the constituent coherent states in the presence of squeezing resulting from the term $2\mathsf{C}_r\mathsf{S}_r|\alpha|^2\cos(\delta - 2\theta)$.

We will now discuss a detection of some non-classical properties of the cat states that can be used to distinguish the three states.

### 4.3.3 Measuring the photon statistics

The resultant relative phase shift $\Delta\gamma$ obtainable from each cat state dependent on the intensities of light in the state marks an important signature that experimentalists can

measure and use to describe the characteristic features of these cat states. Here we discuss the dependence of the interferometric phase and show that the measurement does not alter the quantum properties of the cat states.

***Photon number distribution***

Superpositions of coherent states can be distinguished from a statistical mixture of coherent states by looking at the photon number distribution as discussed in 3.3.2. Fig. 4.14 shows the relationship between the photon number distribution and the interferometric phase difference when we vary the amplitude of the three cat states. In Fig 4.14(a), the photon number is constant at $n = 4$, we see here that the photon number distribution for the odd cat state is vanishing (for an even photon number) as expected.

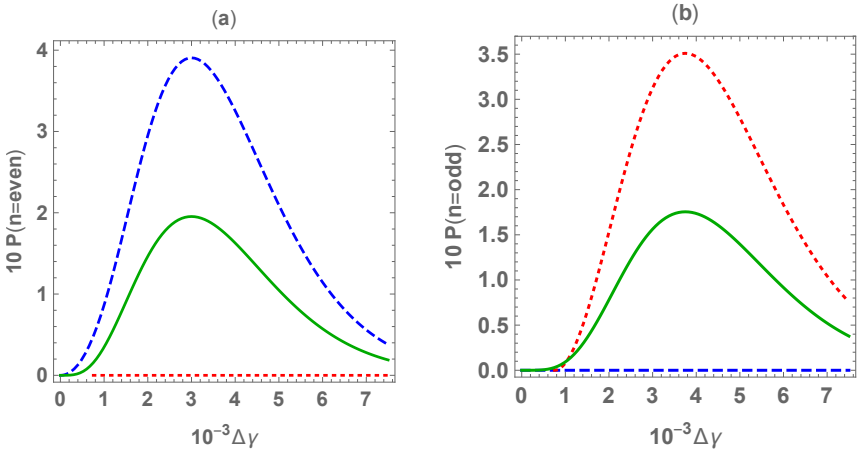


Figure 4.14: With the coherent amplitude varied, this is the photon number distribution function plotted as a function of the relative phase difference $\Delta\gamma$ for our cat states a) when $n = 4$ and (b) $n = 5$. The red dotted line, blue dashed line and green solid lies represent the odd, even and Yuker-Stoller cat states respectively.

In Fig. 4.14(b), the photon number is fixed at $n = 5$ and we see the distribution vanishing for the even cat state. Summarizing, we find that our measurement scheme yields useful information about the photon number probability distribution for the cat states, thereby offering a possibility for distinguishing between them.

### *Mandel Q parameter*

Another nonclassical effect that describes a superposition of coherent states is the Mandel Q parameter 3.3.2. We illustrate the relationship between the Q-parameter and the interferometric phase difference for the different cat states in Fig. 4.15. Indeed the figure reveals the Mandel Q properties for the different cat states. We observe that $\Delta\gamma$ is strictly decreasing, increasing, and constant for the even, odd and Yuker-Stoler cat states respectively.

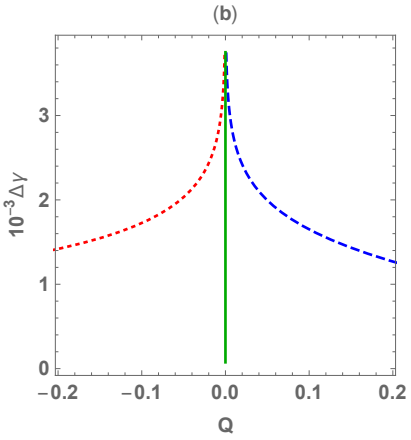


Figure 4.15: Plot of the relative phase difference $\Delta\gamma$ vs the Mandel Q parameter with varying coherent amplitude for the different cat states: odd (red dotted line), even (blue dashed line) and Yuker Stoler (green solid line) cat states respectively.

### *Quadrature Amplitude*

The last nonclassical property we will consider is quadrature squeezing 3.3.2

Figure 4.16 shows the relationship between the interferometric phase difference and the quadrature amplitudes. We observe the deep in the $X$ amplitude relation for the even and Yuker-Stoler cat states corresponding to the X-squeezing in such states. We note that for $|\alpha| \geq 2$, the three cat states have effectively indistinguishable quadrature amplitudes.

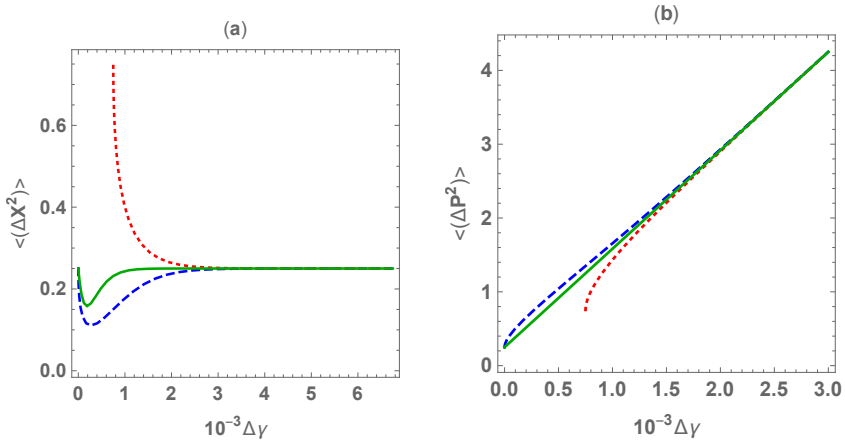


Figure 4.16: Plot of the relative phase difference $\Delta\gamma$ vs $\langle(\Delta X^2)\rangle$ (a) and $\langle(\Delta P^2)\rangle$ (b) with varying coherent amplitude for the different cat states: odd (red dotted line), even (blue dashed line) and Yuker Stoler (green solid line) cat states respectively.

### 4.3.4 Conclusion

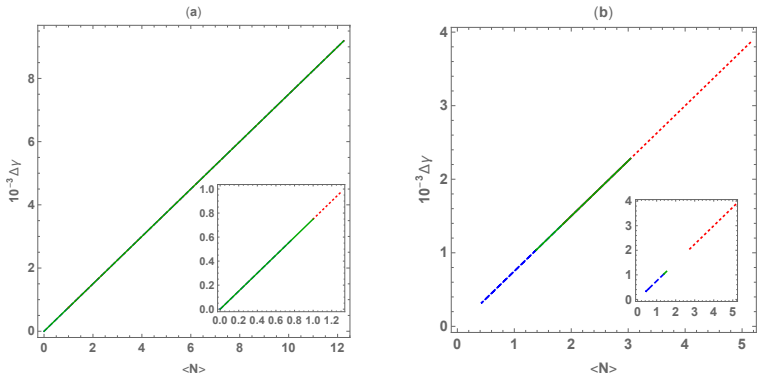


Figure 4.17: Plot of the relative phase difference $\Delta\gamma$ vs the mean photon number for the different cat states: odd (red dotted line), even (blue dashed line) and Yuker Stoller (green solid line) respectively. Each figure shows the different cases for no squeezing (left figure (a)) and with $\zeta = 1\%$ squeeing present (right figure (b)). Inset shows the variation or smaller range of $|\alpha|$.

We have shown that the mode-invisibility technique provides (at least in principle) a good measurement scheme for observing the quantum nature of a superposition of coherent

states. We demonstrated this explicitly for the even, odd, and Yuker-Stoller cat states respectively. For small values of the magnitude $|\alpha|$ of the coherent state parameter, we find it straightforward to distinguish these states. The distinguishability of the three cat states is enhanced by squeezing. Interestingly is the fact that oscillations are present in the interferometric phase difference only when squeezing is introduced and absent without squeezing. Therefore our method also offers a scheme to distinguish between cat states and squeezed cat states.

To summarize, in contrast to the several ways in which the nonclassical properties of coherent states have been investigated, our method provides a measure for studying the behaviour of a superposed cat state, most importantly distinguishing between them in a non-destructive way. We comment that there are limitations to our ability to distinguish the three states. One of which is visible when $|\alpha| \geq 2$. Exploring ways to better distinguish the three states using the mode invisibility technique are for future studies. Of course the natural question is how to realize this mode-invisibility technique in the laboratory and use it to study the decoherence properties of these cat states. We leave this project for future study.

# Part II

# Quantum thermodynamics for fermions

# Chapter 5

# Introduction

The subject of this part of the thesis is quantum thermodynamics for fermionic systems. Generally, it is known that fermions are restricted by their property that no two particles of the same type can be in the same state. This property owing to the Pauli exclusion principle restricts the $N$ fermionic system to $2^N$ dimensional Hilbert space unlike bosons with iniinite dimensional Hilbert space. As a result, this properties has many consequences in the use of fermions and bosons for quantum information processing and quantum thermodynamics. We investigate the problem of work extraction from non-interacting fermionic systems and the dynamics of open fermionic systems. Where we note that the case for bosonic systems have been explored [22, 58].

One of the task in quantum thermodynamics that have attracted the interest of researchers in the field of quantum information processing is the task of work extraction from quantum systems. Here we ask if a process that performs work on a quantum system can be thought of as a useful resource [17, 127]. Ideally, work is said to be done if the average energy of a system is lowered by reversible cyclic processes acting on the system. From the so called passive states [106] no work can be extracted if only a single copy of the system is available. That is, given a system $S$ that is described by a density operator $\rho$ and Hamiltonian $H$. The state $\rho$ is called passive if [126, 76, 106, 101]

$$\mathrm{Tr}[\rho H] \leq \mathrm{Tr}[\sigma H] \tag{5.1}$$

Intuitively, given only a single copy, the average energy $\mathrm{Tr}[\rho H]$ of the passive state cannot be reduced via general unitary transformation $U$ acting on the system; $\sigma = U\rho U^\dagger$ is the transformed density state. However most passive states may have extractable work that can only be accessed given multiple copies of the system and a global (entangling

) unitary operation. Quantum States from which no work can be extracted unitarily, irrespective of the number of available copies are called completely passive, an example is the thermal Gibb's state [106]. Since thermal states are the only completely passive states, any resource state for a unitary work extraction (cyclic engine) must be out of thermal equilibrium. In the bosonic setting, constructing a heat engine (which is arguably the simplest out-of-equilibrium resource) requires access to two thermal baths at different temperatures. However, in the fermionic setting, we will show later that constructing a heat engine requires access to at least three thermal baths at different temperatures.

On the other hand, while work can be extracted from non-passive states using general unitary transformations, realizing these unitary transformations may be difficult in practice. For example, the global unitaries required to extract work from passive but not completely passive states are not feasible. This motivates the notion of Gaussian passivity [22] where we concern our selves to work extraction via Gaussian transformations that are practically realizable. Just like the definition of passive states, Gaussian passive states are states from which no work can be extracted via Gaussian operations acting on the system. The characteristics of Gaussian passive state are discussed using the tools of Gaussian quantum mechanics (GQM) [135, 41].

The theoretical concepts of GQM includes gaussian states and Gaussian transformations (those that take Gaussian states to Gaussian states). Gaussian states and transformations have simple mathematical structure and can be easily produced in the laboratory compared to any general unitary transformation. As a result, GQM has been applied in areas including quantum information processing [135, 46, 57, 77], quantum computing [41, 20, 18, 19, 69, 61], quantum entanglement [14, 15, 45, 110], thermodynamics [54, 99, 133, 38] and quantum thermodynamics [22, 96, 28].

Again, GQM provides us with a powerful tool in simplifying the description of open quantum systems. In this regard, we will also employ the tools of fermionic GQM to investigate the dynamics of an open fermionic system. By open quantum system, we mean a system that is in constant interaction with its environment. Such interaction influences the dynamics of the relevant system. Because it is almost impossible to isolate a system of interest from its surrounding, hence it is important to consider the influence of the environment when we study the dynamical evolution of a physical system [103, 102, 30, 67, 111]. However tracking the dynamical evolution of the full system+environment either theoretically or experimentally, becomes almost impossible. Several approaches have been presented to study the dynamics of an open quantum system each depending on the specific quantum system in question and the demand thereof.

By applying the tools from fermionic GQM, a classification scheme for the generators

of open fermionic Gaussian dynamics was introduced [95] and the corresponding dynamics were simultaneously partitioned along the following four lines: 1) unitary vs. non-unitary, 2) active vs. passive, 3) state-dependent vs. state-independent, and 4) single-mode vs. multi-mode. It was observed that only nine of these sixteen types of dynamics are possible. This is in contrast to the bosonic case [58] where eleven dynamics are possible. This difference is attributed to the structure of fermionic systems which is generally more restricted due to Pauli exclusion principle as compared to bosonic systems with infinite dimensions.

Using the partitions, the consequences of imposing complete positivity on fermionic Gaussian dynamics was discussed. In particular, I show that completely positive dynamics must be either unitary (and so can be implemented without a quantized environment) or active (and so must involve particle exchange with an environment). The discussion employs Gaussian quantum mechanics (GQM) and the covariance-matrix (CM) formalism, which allows to characterize the generators of the dynamics in terms of their action on the CM by two matrices. These are then decomposed into parts corresponding to the different dichotomies.

## 5.1 The fermionic system

In this section we describe the structure of the fermionic system and the corresponding properties. To begin, the fermionic modes by $N$ canonical modes $\kappa$.

### 5.1.1 Hilbert space

The Hilbert space $\mathcal{H} = \bigotimes_{\kappa=1}^{N} \mathcal{H}_\kappa$ (with dimension $2^N$) of a fermionic system is spanned by the basis $|n_\kappa = 0\rangle$ and $|n_\kappa = 1\rangle$ known as the Fock or number state basis.

Since fermions have half-integer spin and obey the Pauli exclusion principle, it follows that fermionic excitations behave nontrivially when rotated by $2\pi$ (denoted $R_{2\pi}$) around any axis. For example a single fermionic system in Fock basis,

$$|1\rangle \xrightarrow{R_{2\pi}} -|1\rangle, \qquad |0\rangle \xrightarrow{R_{2\pi}} |0\rangle,$$

and for two fermionic systems in Fock basis,

$$|01\rangle \xrightarrow{R_{2\pi}} -|01\rangle, \qquad |11\rangle \xrightarrow{R_{2\pi}} (-1)^2|11\rangle,$$

Specifically the fermionic excited state picks up a sign change under $R_{2\pi}$ relative to its unexcited state. Note that the effect that $\hat{R}_{2\pi}$ has on elements of the Fock basis is to flip their sign if the total number of excitations is odd. We may therefore refer to $\hat{R}_{2\pi}$ here as just the parity operator, $\hat{P}$.

### 5.1.2 Physical states of a fermionic system

Since a rotation by $2\pi$ should not change the state of a quantum system, we can identify physical states as those whose state vector only changes by a global phase when acted on by $\hat{R}_{2\pi} = \hat{P}$, that is

$$\hat{P}|\psi\rangle = e^{\mathrm{i}\theta}|\psi\rangle. \tag{5.2}$$

The fermionic algebra (to be discussed later) together with the Pauli exclusion principle set limits on permissible quantum states in the fermionic settings. In this regard, all admissible quantum states are referred to as physical states. It is our aim in this section to describe what conditions a quantum state must satisfy for it to be regarded as a the fermionic physical states

To begin, we recall in quantum mechanics that a state $|\psi\rangle$ of a quantum system is described mathematically by a complex valued probability amplitude known as wave function. The probability amplitude $\alpha$ is a complex number characterized by phase and an amplitude. Now If $|\psi\rangle$ is a state vector of the system, we consider two quantum states $|\psi\rangle$ and $|\phi\rangle = e^{\mathrm{i}\theta}|\psi\rangle$, by definition $|\phi\rangle$ is also a state vector of the system, where $e^{\mathrm{i}\theta}$ is a global phase factor which shows up in interference experiments. Equivalently, the two states

$$|\Psi\rangle = \alpha|\psi\rangle + \beta|\phi\rangle, \quad \text{and} \tag{5.3}$$

$$|\Phi\rangle = e^{\mathrm{i}\theta}(\alpha|\psi\rangle + \beta|\phi\rangle) \tag{5.4}$$

would also describe the same state where $e^{\mathrm{i}\theta}$ is a global phase factor. However with

$$|\chi\rangle = |\psi\rangle + e^{\mathrm{i}\theta}|\phi\rangle, \tag{5.5}$$

we may say $|\Psi\rangle$ and $|\chi\rangle$ do not correspond to the same quantum state. As such, certain superpositions of fermionic excitations are unphysical [3]. For instance the state, $|0\rangle + |1\rangle$, is unphysical because

$$\hat{P}(|0\rangle + |1\rangle) = |0\rangle - |1\rangle \neq e^{\mathrm{i}\theta}(|0\rangle + |1\rangle), \tag{5.6}$$

whereas $|00\rangle + |11\rangle$ and $|01\rangle + |10\rangle$ are physical states. Generally, pure states are physical if they are either superpositions of states with an odd number of excitations, or of states with an even number of excitations.

### 5.1.3 The fermionic algebra

#### *Creation and annihilation operators*

The fermionic system is characterized by the creation $\hat{a}^\dagger$ and annihilation $\hat{a}$ operators which satisfy the Fermi-Dirac canonical anti-commutation relations (CAR):

$$\{\hat{a}_i, \hat{a}_j^\dagger\} = \delta_{ij}\mathbb{1} \tag{5.7}$$

$$\{a_i, a_j\} = \{a_i^\dagger, a_j^\dagger\} = 0. \tag{5.8}$$

where $i$ and $j$ are mode indices indicating different fermionic modes. Here, $\mathbb{1}$ is the identity operator, $\delta_{ij}$ is Kronecker delta and $\{X, Y\} = XY + YX$ is the anti-commutation symbol respectively.

Eq. (5.8) implies that $aa = a^\dagger a^\dagger = 0$, that is each mode may have at most one excitation (a manifestation of Pauli exclusion principle).

#### *Fermionic Fock space*

We can create and annihilate particles in the fermionic Fock space using the operators $\hat{a}_j^\dagger$ and $\hat{a}_j$ respectively. We define the fermionic Fock space as

$$|n_1, n_2, \cdots\rangle = (a_1^\dagger)^{n_1}(a_2^\dagger)^{n_2}\cdots(a_N^\dagger)^{n_N}|0\rangle. \tag{5.9}$$

For single fermion modes, the action of the $a$ and $a^\dagger$ operators on the fermionic Fock basis is given by

$$\hat{a}|0\rangle = 0, \quad a^\dagger|0\rangle = |1\rangle \tag{5.10}$$

$$a|1\rangle = |0\rangle, \quad a^\dagger|1\rangle = 0. \tag{5.11}$$

Now consider the case for $N$ fermionic system. The total occupation number is given as $N = \sum_j n_j$ and counts the number of excitations in all modes. In this case, the fermionic Hilbert space

$$\mathcal{F} = \bigotimes_{N=0}^{\infty} \mathcal{H}_N = \mathcal{H}_0 \oplus \mathcal{H}_1 \oplus \mathcal{H}_2 \oplus \mathcal{H}_3 \oplus \cdots \tag{5.12}$$

The $\mathcal{H}_0$ block here spans a the vacuum state $|0\rangle$ while the $\mathcal{H}_1$ block spans the single particle state $|1\rangle$. Following the convention in Eq. (5.9), we may represent $|1\rangle = a^\dagger|0\rangle$. Similarly, the $\mathcal{H}_2$ block of $\mathcal{F}$ spans states

$$|1_j 1_k\rangle = a_j^\dagger a_k^\dagger|0\rangle \tag{5.13}$$

with $j \neq k$, where states such as $|2,0\rangle$ with doubly occupied modes are not allowed. Note that in Eq. (5.13) exchanging $j$ and $k$ results in the same physical state but with an opposite sign (because $a_j^\dagger$ and $a_k^\dagger$ anti-commute). To be precise

$$|1_j 1_k\rangle = a_j^\dagger a_k^\dagger |0\rangle = -a_k^\dagger a_j^\dagger |0\rangle = -|1_k 1_j\rangle \tag{5.14}$$

similarly for three different modes, the $\mathcal{H}_3$ block spans states

$$|1_j, 1_k, 1_l\rangle = a_l^\dagger a_k^\dagger a_j^\dagger |0\rangle \tag{5.15}$$

etc. In all cases, the order of the modes $j, k, l, \cdots$ does not matter physically but affects the overall sign of the state. Therefore together with the superselection rule that superposition of fermionic state with odd fermion number is unphysical, it is important to also consider the issue of the antisymmetric wave function of fermionic system and always adopt the convention (5.9) when writing product state of fermionic modes.

### *Free Hamiltonian*

The free Hamiltonian for these modes is

$$\hat{H}_0 = \sum_{j=1}^{N} E_j \, \hat{n}_j \tag{5.16}$$

where $E_j$ is the $j^{th}$ mode's excitation energy and $\hat{n}_j = \hat{a}_j^\dagger \hat{a}_j$ is the number operator for the $j^{th}$ mode.

### *Majorana operators*

The fermionic creation and annihilation operators defined above are non-hermitian, that is $a_j^\dagger \neq a_j$, however from these operators, we can construct a set of $2^N$ dimensional Hermitian operators for their real and imaginary parts.

$$c_{2j-1} = \frac{1}{\sqrt{2}}(a_j + a_j^\dagger) \qquad \text{and} \qquad c_{2j} = \frac{\mathrm{i}}{\sqrt{2}}(a_j - a_j^\dagger) \tag{5.17}$$

These are the Majorana operators, they are analogous to the canonical momentum and position operators for bosonic modes. They have the following properties

- they are Hermitian $c_j^\dagger = c_j$,

- from the CAR algebra (5.8), it follows that they satisfy the anticommutation relation

$$\{c_k, c_l\} = \delta_{kl}\mathbb{1} \tag{5.18}$$

  This relation is known as the Clifford algebra (C-algebra)

- the square of the Majorana operator is $\mathbb{1}/2$, a consequence of the C-algebra

$$\{c_j, c_j\} = c_j c_j + c_j c_j = 2c_j c_j = \mathbb{1} \Rightarrow c_j c_j = \frac{\mathbb{1}}{2} \tag{5.19}$$

***Even and odd fermionic operators***

Let us denote the Clifford algebra generated by the set $\{c_m\}$ as $\mathcal{C}_{2N}$. An arbitrary operator $\mathcal{A} \in \mathcal{C}_{2N}$ can be written as a polynomial in the Majorana operators. $A \in \mathcal{C}_{2N}$ is said to be even (odd) if it contains only even (odd) powers of the generator $\hat{c}$ [15].

To conclude this section, we write the Majorana operators in compact form by defining a vector

$$\begin{aligned} \mathbf{x}^T &:= \begin{pmatrix} c_1 & c_3 & \cdots & c_{2N-1}; c_2, c_4, \cdots, c_{2N} \end{pmatrix} = (c_{2j-1}, c_{2j}) \\ \mathbf{x} &:= \begin{pmatrix} c_1 & c_3 & \cdots & c_{2N-1}; c_2, c_4, \cdots, c_{2N} \end{pmatrix}^T = (c_{2j-1}, c_{2j})^T \end{aligned} \tag{5.20}$$

So that the CAR reduces to

$$\{x_i, x_j\} = \delta_{ij}\hat{\mathbb{1}} \tag{5.21}$$

### 5.1.4 The fermionic quadratic Hamiltonians

The general form of a quadratic Hamiltonian in the creation and annihilation operators is given by

$$H = \sum_{j,k=1}^{N} \left[ A_{jk} a_j^\dagger a_k + \frac{1}{2} B_{j,k} a_j^\dagger a_k^\dagger - \frac{1}{2} B_{j,k}^* a_j a_k \right] \tag{5.22}$$

where $j$ and $k$ label the field modes. The Hermicity and canonical anticommutation relations of $H$ requires that $A$ is Hermitian and $B$ is antisymmetric. Our goal is to discuss the physical processes that may arise from such a quadratic Hamiltonian. To go about this, we have grouped the Hamiltonian into two parts: the number conserving case and the number non conserving case, respectively. This grouping will be particularly important when we want to discuss the quantum evolutions generated by quadratic Hamiltonian.

***Number-conserving quadratic Hamiltonians***

The total number operator is defined as $\hat{N} = \sum_l a_l^\dagger a_l$. Now we say a Hamiltonian operator is number conserving if it commutes with the total number operator, that is $[\hat{N}, \hat{H}] = \hat{N}\hat{H} - \hat{H}\hat{N} = 0$. Hence a number-conserving Hamiltonian can be written in the form

$$H_{\rm nc} = \sum_{jk} A_{jk} a_j^\dagger a_k \tag{5.23}$$

We can deduce two cases from the Hamiltonian. First with $j = k$, we have $H_{\rm nc} = \sum_j A_{jj} a_j^\dagger a_j$. Physically, the Hamiltonian generates the free evolution of the field modes, thus we can can describe $A_{jj}$ as the energy of individual modes. In terms of the Majorana operators, we have

$$a_j^\dagger = \frac{1}{\sqrt{2}}(c_{2j-1} + {\rm i}c_{2j}), \qquad a_j = \frac{1}{\sqrt{2}}(c_{2j-1} - {\rm i}c_{2j}), \tag{5.24}$$

this Hamiltonian reads

$$H_{\rm nc}^{(1)} = \frac{1}{2}\sum_{j=1}^{2N} A_{jj}\Big(c_{2j-1}c_{2j-1} - {\rm i}\, c_{2j-1}\, c_{2j} + {\rm i}c_{2j}c_{2j-1} + c_{2j}c_{2j}\Big)$$

Which considering the Majorana basis $\mathbf{x} = (c_{2j-1}, c_j)^T$, can be written in matrix form as

$$H_{\rm nc}^{(1)} = \frac{1}{2}{\rm Tr}[\mathbf{A}]\mathbb{1} + \frac{1}{2}\sum_j A_{jj}\begin{pmatrix} c_{2j-1} & c_{2j}\end{pmatrix}\begin{pmatrix} 0 & -{\rm i} \\ {\rm i} & 0\end{pmatrix}\begin{pmatrix} c_{2j-1} \\ c_{2j}\end{pmatrix} \tag{5.25}$$

$$= \frac{1}{2}{\rm Tr}[\mathbf{A}]\mathbb{1} + \frac{1}{2}\sum_j A_{jj}\begin{pmatrix} c_{2j-1} & c_{2j}\end{pmatrix}\sigma_2\begin{pmatrix} c_{2j-1} \\ c_{2j}\end{pmatrix} \tag{5.26}$$

where we note that $c_j^2 = \mathbb{1}/2$, and $\sigma_2$ is the Pauli matrix. Note that the term proportional to $\mathbb{1}$ can be removed by adding an energy offset (that is -$\sum_j A_{jj}$) to the general Hamiltonian (5.22).

Also, a second class of the number conserving quadratic Hamiltonian can be generated by considering $j \neq k$ so that the Hamiltonian is of the form

$$H_{\rm nc}^{(2)} = A_{jk} a_j^\dagger a_k + A_{kj} a_k^\dagger a_j \tag{5.27}$$

Such a Hamiltonian, which also preserves the total fermionic number, is associated with processes that describe the linear interaction between two field modes. An example is a beam splitter. In terms of the Majorana operators, we obtain

$$H_{\rm nc}^{(2)} = A_a(c_{2j-1}c_{2k-1} + c_{2j}c_{2k}) - {\rm i}A_s(c_{2j-1}c_{2k} - c_{2j}c_{2k-1})$$

Here $A_{s/a} = \frac{1}{2}(A \pm A^T)$ denotes the symmetric/antisymmetric part of the matrix $A$, and for $A = A_{jk}$ we have $A^T = A_{kj}$. In terms of the Majorana basis $\mathbf{x}$,

$$H_{\rm nc}^{(2)} = \begin{pmatrix} c_{2j-1} & c_{2j} \end{pmatrix} \begin{pmatrix} A_a & -\mathrm{i}A_s \\ \mathrm{i}A_s & A_a \end{pmatrix} \begin{pmatrix} c_{2k-1} \\ c_{2k} \end{pmatrix} = \begin{pmatrix} c_{2j-1} & c_{2j} \end{pmatrix} \Big( A_a \otimes \mathbb{1} + A_s \otimes \sigma_2 \Big) \begin{pmatrix} c_{2k-1} \\ c_{2k} \end{pmatrix}$$

Here the term proportional to $\mathbb{1}$ can also be removed by assuming $A$ to be symmetric so that

$$H_{\rm nc}^{(2)} = \begin{pmatrix} c_{2j-1} & c_{2j} \end{pmatrix} \begin{pmatrix} 0 & -\mathrm{i}A \\ \mathrm{i}A & 0 \end{pmatrix} \begin{pmatrix} c_{2k-1} \\ c_{2k} \end{pmatrix} = \begin{pmatrix} c_{2j-1} & c_{2j} \end{pmatrix} \Big( A \otimes \sigma_2 \Big) \begin{pmatrix} c_{2k-1} \\ c_{2k} \end{pmatrix}$$

Thus we have a general form of the number conserving quadratic Hamiltonian

$$H_{\rm nc} = \mathbf{x}^T \mathcal{H}_{\rm nc} \mathbf{x} \tag{5.28}$$

where $\mathcal{H}_{\rm nc} = A \otimes \sigma_2$ is a Hermitian matrix with real entries.

***Number nonconserving quadratic Hamiltonians***

As the name implies, a number nonconserving Hamiltonian does not preserve the total number of particles in the field mode. It corresponds to

$$H_{\rm nnc} = \frac{1}{2} \sum_{jk} \left( B_{jk} a_j^\dagger a_k^\dagger - B_{jk}^* a_j a_k \right) = \frac{1}{2}(B_{jk} - B_{kj}) a_j^\dagger a_k^\dagger - \frac{1}{2}(B_{jk}^* - B_{kj}^*) a_j a_k$$

In the last equality, we applied the anticommutation relation (5.18). This Hamiltonian is applicable to "pairing" theory in fermionic systems where we observe conservation of parity but violation of the number operator conservation. We note in writing out the Hamiltonian explicitly, we neglect terms with $j = k$, since $a^{\dagger 2} = a^2 = 0$ for fermionic modes. The Hamiltonian describes physical processes in Fermi systems such as superconductivity, superfluids, and anti-ferromagnetism, (two-mode) squeezing. In terms of the Majorana operators

$$\begin{aligned} H_{\rm nnc} = &\frac{1}{4}(B_{jk} - B_{kj}) \Big[ c_{2j-1} c_{2k-1} + \mathrm{i} c_{2j-1} c_{2k} + i c_{2j} c_{2k-1} - c_{2j} c_{2k} \Big] \\ &- \frac{1}{4}(B_{jk}^* - B_{kj}^*) \Big[ c_{2j-1} c_{2k-1} - \mathrm{i} c_{2j-1} c_{2k} - \mathrm{i} c_{2j} c_{2k-1} - c_{2j} c_{2k} \Big] \end{aligned}$$

and using the fact that $B$ is antisymmetric ($B_{kj} = -B_{jk}$), we collect like terms in the Majorana operators and obtain

$$H_{\rm nnc} = \frac{1}{2}\begin{pmatrix} c_{2j-1} & c_{2j} \end{pmatrix}\begin{pmatrix} B - B^* & \mathrm{i}(B + B^*) \\ -\mathrm{i}(B + B^*) & -(B - B^*) \end{pmatrix}\begin{pmatrix} c_{2k-1} \\ c_{2k} \end{pmatrix} \tag{5.29}$$

Without loss of generality we can also assume $B$ is real so that

$$H_{\rm nnc} = \begin{pmatrix} c_{2j-1} & c_{2j} \end{pmatrix}\begin{pmatrix} 0 & \mathrm{i}B \\ -\mathrm{i}B & 0 \end{pmatrix}\begin{pmatrix} c_{2k-1} \\ c_{2k} \end{pmatrix} \tag{5.30}$$

the off–diagonal terms vanish and we have a general form of the antisymmetric part of the quadratic Hamiltonian given as

$$H_{\rm nnc} = \mathbf{x}^T \mathcal{H}_{\rm nnc}\, \mathbf{x} \tag{5.31}$$

where $\mathcal{H}_{\rm nnc} = \begin{pmatrix} 0 & \mathrm{i}B \\ -\mathrm{i}B & 0 \end{pmatrix}$

To summarize this section, we have a general form of the quadratic Hamiltonian in the Majorana basis given as $H = H_{\rm nc} + H_{\rm nnc}$:

$$H = \frac{\mathrm{i}}{2}\sum_{j,k=1}^{2N} \mathcal{H}_{jk} c_j c_k = \frac{\mathrm{i}}{2}\,\mathbf{x}^T \mathcal{H}\, \mathbf{x} \tag{5.32}$$

where

$$\mathcal{H} = \begin{pmatrix} 0 & B - A \\ -(B - A) & 0 \end{pmatrix} \tag{5.33}$$

is a real antisymmetric matrix.

### 5.1.5 Standard form of the quadratic Hamiltonian

We turn to the theory that any real antisymmetric matrix such as $\mathcal{H}$ in the quadratic Hamiltonian (5.32) can be brought to a standard form by an orthogonal transformation,

$$\tilde{\mathcal{H}} = O\mathcal{H}O^T = \bigoplus_{j=1}^{N}\begin{pmatrix} 0 & \beta_j \\ -\beta_j & 0 \end{pmatrix}$$

with $\beta_j \geq 0$ and $\pm\lambda_j$ are the Williamson eigenvalues [15] of the Hermitian matrix $\mathrm{i}\mathcal{H}$.

We can use this representation to express the quadratic Hamiltonian in the standard form. To see how this works, consider the inverse transformation $\mathcal{H} = O^T\tilde{\mathcal{H}}O$ and define a new set of transformed Majorana operators $\tilde{\mathbf{x}} = O\mathbf{x}$. Recall Eqn. (5.20), thus the transformed set of Majorana vectors would be given as $\tilde{\mathbf{x}} = \begin{pmatrix}\tilde{c}_{2j-1} & \tilde{c}_{2j}\end{pmatrix}^T$. Hence we obtain

$$\begin{aligned} H &= \frac{\mathrm{i}}{2}\mathbf{x}^T\mathcal{H}\mathbf{x} = \frac{\mathrm{i}}{2}\mathbf{x}^T\Big(O^T\tilde{\mathcal{H}}O\Big)\mathbf{x} = \frac{\mathrm{i}}{2}\tilde{\mathbf{x}}^T\tilde{\mathcal{H}}\tilde{\mathbf{x}} \\ &= \frac{\mathrm{i}}{2}\begin{pmatrix}\tilde{c}_{2j-1} & \tilde{c}_{2j}\end{pmatrix}\bigoplus_{j=1}^{N}\begin{pmatrix}0 & \beta_j \\ -\beta_j & 0\end{pmatrix}\begin{pmatrix}\tilde{c}_{2j-1} \\ \tilde{c}_{2j}\end{pmatrix} \\ &= \frac{\mathrm{i}}{2}\sum_{j=1}^{N}\beta_j\big(\tilde{c}_{2j}\tilde{c}_{2j-1} - \tilde{c}_{2j-1}\tilde{c}_{2j}\big) \end{aligned}$$

The relation $\tilde{c}_{2j-1}\tilde{c}_{2j} = -\tilde{c}_{2j}\tilde{c}_{2j-1}$ between the Majorana operators holds so that

$$H_{\mathrm{sf}} = -\mathrm{i}\sum_{j}^{N}\beta_j\tilde{c}_{2j-1}\tilde{c}_{2j} \tag{5.34}$$

where $\tilde{c}_k = \sum_l O_{kl}c_l$ are new Majorana operators.

In the next section, we will discuss an important subclass of states known as fermionic Gaussian states. These states, which can be written as an exponential in quadratic form in the fermion Majorana operators, appear as ground and thermal states of the quadratic Hamiltonian.

## 5.2 Fermionic Gaussian states

Now that we have reviewed the basic structure and algebra of the fermionic system, we will discuss the Fermionic Gaussian state (FGS). This is a very important quantum state that is at the heart of quantum information processing.

Gaussian states have trivial mathematical structure, and it is common with current technology to produce Gaussian states in the laboratory. We present the general properties of the FGS and their corresponding mathematical algebra. Despite their simplicity, Gaussian states are useful for quantum information processing tasks such as entanglement

distillation, or metrology, probabilistic teleportation. Later in this thesis, we will focus on the application of Gaussian states to quantum information linked to quantum thermodynamics.

### 5.2.1 Basic notation and definition

Consider the system of $n$ fermions in the canonical ensemble. The density matrix of the system is given as

$$\rho = \frac{1}{\mathcal{Z}} e^{-\beta H} \tag{5.35}$$

where $\mathcal{Z} = \mathrm{Tr}(e^{-\beta H})$ is the normalization factor also known as the partition function which can be obtained by ensuring the condition $\mathrm{tr}(\rho) = 1$ [93]. $H$ is the system's Hamiltonian and $\beta$ the inverse temperature. For systems described by Hamiltonians that are quadratic in the Majorana terms (that is the quadratic Hamiltonian (5.32)), the density matrix is written as

$$\rho = \frac{1}{\mathcal{Z}} \exp\Big[ -\frac{\mathrm{i}}{2} \mathbf{x}^T \mathcal{H} \mathbf{x} \Big], \tag{5.36}$$

where we have enclosed the inverse temperature $\beta$ in the definition of the real antisymmetric matrix $\mathcal{H}$. A fermionic system of $j = 1, \cdots, N$ fermionic modes and whose quantum state is described by the density matrix $\rho$ in (5.36) is called a Fermionic Gaussian system.

#### *Standard form of the fermionic Gaussian state*

We recall as discussed in 5.1.5 that the real antisymmetric matrix $\mathcal{H}$ that characterizes the quadratic Hamiltonian (5.36) can be brought to a diagonal form $\tilde{\mathcal{H}} = O\mathcal{H}O^T$ by an orthogonal transformation $O$. This allowed us to write the quadratic Hamiltonian in standard form (5.34). We can equally write the fermionic Gaussian state in the standard form by substituting (5.34) in (5.35).

$$\rho_{sf} = \frac{1}{\mathcal{Z}} \exp\Big[\mathrm{i} \sum_{j=1}^{N} \beta_j \tilde{c}_{2j-1} \tilde{c}_{2j}\Big] = \frac{1}{\mathcal{Z}} \prod_{j=1}^{N} \exp\Big[\mathrm{i}\beta_j \tilde{c}_{2j-1} \tilde{c}_{2j}\Big] = \frac{1}{\mathcal{Z}} \prod_{j=1}^{N} \sum_{n=0}^{\infty} \frac{\Big(\mathrm{i}\beta_j \tilde{c}_{2j-1} \tilde{c}_{2j}\Big)^n}{n!}.$$

In the last term, we used the relation $e^x = \sum_n \frac{x^n}{n}$. Note that

$$(\mathrm{i}\tilde{c}_{2j-1}\tilde{c}_{2j})^2 = \frac{\mathbb{1}}{4}.$$

For example consider the case $j=1$. We have $(\tilde{c}_{2j-1}\tilde{c}_{2j}) = \tilde{c}_1\tilde{c}_2 = \mathrm{i}(\tilde{a}+\tilde{a}^\dagger)(\tilde{a}-\tilde{a}^\dagger)/2 = \mathrm{i}(2\tilde{a}^\dagger\tilde{a}-1)/2$. Consequently

$$\begin{aligned}(\mathrm{i}\tilde{c}_{2j-1}\tilde{c}_{2j})^2 = -(\tilde{c}_1\tilde{c}_2)(\tilde{c}_1\tilde{c}_2) &= \frac{1}{4}(2\tilde{a}^\dagger\tilde{a}-1)(2\tilde{a}^\dagger\tilde{a}-1)\\ &= \frac{1}{4}\Big(4\tilde{a}^\dagger \underbrace{\tilde{a}\tilde{a}^\dagger}_{1-\tilde{a}^\dagger\tilde{a}}\tilde{a} - 2\tilde{a}^\dagger\tilde{a} - 2\tilde{a}^\dagger\tilde{a} + 1\Big)\\ &= \frac{1}{4}\Big(-4\tilde{a}^\dagger\tilde{a}^\dagger\tilde{a}\tilde{a} + 4\tilde{a}^\dagger\tilde{a} - 4\tilde{a}^\dagger\tilde{a} + 1\Big) = \frac{1}{4}\end{aligned}$$

where we have recalled that for fermionic operators $\tilde{a}\tilde{a} = 0 = \tilde{a}^\dagger\tilde{a}^\dagger$. Thus expanding the term in the exponential, we obtain

$$\rho_{sf} = \frac{1}{\mathcal{Z}}\prod_{j=1}^{N}\Big(\cosh\Big(\frac{\beta_j}{2}\Big)\mathbb{1}_N + \mathrm{i}\sinh\Big(\frac{\beta_j}{2}\Big)\tilde{c}_{2j-1}\tilde{c}_{2j}\Big) \tag{5.37}$$

To find the constant $\mathcal{Z}$, normalization entails that $\mathrm{tr}\rho = 1$ so that

$$\mathcal{Z} = \mathrm{Tr}\Big[\prod_{j=1}^{N}\Big(\cosh\Big(\frac{\beta_j}{2}\Big)\mathbb{1}_N + \mathrm{i}\sinh\Big(\frac{\beta_j}{2}\Big)\tilde{c}_{2j-1}\tilde{c}_{2j}\Big)\Big] \tag{5.38}$$

computing the trace in the Fock basis, the first term yields $\prod_{j=1}^{N} 2^N\cosh\left(\frac{\beta_j}{2}\right)$. The second term vanishes for all values of $N$. To see this, let us consider the case for single mode $N=1$,

$$\begin{aligned}\mathrm{Tr}\Big[\mathrm{i}\sinh\Big(\frac{\beta_1}{2}\Big)\tilde{c}_1\tilde{c}_2\Big] &= \mathrm{i}\sinh\Big(\frac{\beta_1}{2}\Big)\sum_{n=0}^{1}\langle n|\,(2\tilde{a}^\dagger\tilde{a}-1)|n\rangle\\ &= \mathrm{i}\sinh\Big(\frac{\beta_1}{2}\Big)\Big(2\,\langle 0|\,\tilde{a}^\dagger\tilde{a}|0\rangle + 2\,\langle 1|\,\tilde{a}^\dagger\tilde{a}|1\rangle - \langle 0|\,0\rangle - \langle 1|\,1\rangle\Big) = 0\end{aligned}$$

We have taken note from (5.18) that $\tilde{c}_{2j-1}\tilde{c}_{2j} = 2\tilde{a}_j^\dagger\tilde{a}_j - 1$. Therefore normalization constant becomes

$$\mathcal{Z} = \prod_{j=1}^{N} 2^N\cosh\Big(\frac{\beta_j}{2}\Big) \tag{5.39}$$

Substituting (5.39) in (5.37) gives the fermionic Gaussian state in standard form

$$\rho_{sf} = \frac{1}{2^N}\prod_{j=1}^{N}\Big(\mathbb{1} + \mathrm{i}\tanh\Big(\frac{\beta_j}{2}\Big)\tilde{c}_{2j-1}\tilde{c}_{2j}\Big) \tag{5.40}$$

where we have taken note that $\tanh(A) = \sinh(A)/\cosh(A)$.

### 5.2.2 Statistical properties

The statistical properties including the first and second moments of a quantum state give information about the state. In this section, we give the definition of the statistical properties of FGS and see how they interpret the properties of the state.

***First moment***

The first moment of a FGS $\rho$ known as the displacement vector is defined by:

$$\langle c_j \rangle = \mathrm{Tr}(c_j \rho), \tag{5.41}$$

which vanishes for physical fermionic states (that is the even FGS (5.40) ) but not for odd FGS. By odd FGS, we mean FGS that are characterized by terms linear in Majorana operators. Our focus is on even FGS, so we consider that the first moment is vanishing.

***Second moment***

The second moment is referred to as the covariance matrix (CM). The CM for FGS which we denote as $\mathbf{\Gamma}$, is a real and anti-symmetric $2N \times 2N$ matrix whose elements in terms of the Majorana operators are defined by

$$\Gamma_{kl} := \frac{\mathrm{i}}{2}\mathrm{Tr}[\rho(c_k c_l - c_l c_k)] = \begin{cases} \mathrm{i}\mathrm{Tr}[\rho(c_k c_l)], & \text{for } k \neq l \\ 0, & \text{for } k = l \end{cases} \tag{5.42}$$

that they are completely characterized by only the second moment $\Gamma_{kl}$ [20, 15].

***Complete positivity condition***

The Pauli exclusion principle together with the anticommutation relation among the fermionic operators impose a constraint on the CM of fermionic systems. A covariance matrix $\Gamma$ corresponds to that of a physical state if and only if it obeys the positivity condition

$$\mathrm{i}\Gamma \leq \mathbb{1}_{2N} \quad \text{or equivalently} \quad \Gamma\Gamma^{\intercal} \leq \mathbb{1}_{2N}, \tag{5.43}$$

where $\mathbb{1}_{2N}$ is the $2N$ dimensional identity matrix. This condition translates to $\Gamma^2 = -\mathbb{1}$ for pure states. We now comment that the state of an even FGS is completely described by its CM [19, 20].

### 5.2.3 Characterizing the fermionic Gaussian states

In the previous section, we stated that an FGS is completely characterized by its CM so that all our analysis about a quantum state is based on CM formalism. In this section, by considering a one-mode system and two-mode systems respectively, we want to look at some of these characteristics we can describe.

#### *Single mode Gaussian states*

The single mode Gaussian state in standard form can be obtained from (5.40)

$$\rho_{sf} = \frac{1}{2}(1 + \mathrm{i}\lambda\tilde{c}_1\tilde{c}_2), \qquad \lambda = \tanh\left(\frac{\beta}{2}\right) \tag{5.44}$$

The covariance matrix of a single mode FGS is a $2 \times 2$ matrix given as,

$$\Gamma^{\mathrm{sm}} = \begin{pmatrix} \Gamma_{11} & \Gamma_{12} \\ \Gamma_{21} & \Gamma_{22} \end{pmatrix} \tag{5.45}$$

Since $\Gamma^{\mathrm{sm}}$ is real-valued and antisymmetric by definition its elements are given as $\Gamma_{11} = 0 = \Gamma_{22}$ and $\Gamma_{12} = -\Gamma_{21} = \nu$ for some real parameter $\nu$. Thus

$$\Gamma^{\mathrm{sm}} = \nu\,\Omega; \qquad \Omega = \begin{pmatrix} 0 & -1 \\ 1 & 0 \end{pmatrix} \tag{5.46}$$

and the positivity condition (5.43) on $\Gamma^{\mathrm{sm}}$ implies the inequality relation

$$\mathbb{1}_2 - \mathrm{i}\nu\Omega \geq 0. \tag{5.47}$$

that is, $\mathbb{1}_2 - \mathrm{i}\nu\Omega$ has nonnegative eigenvalues which restricts $\nu$ to the range of values

$$-1 \leq \nu \leq 1\ . \tag{5.48}$$

Let us now describe some properties of the single-mode FGS in terms of the CM

1. *Expectation value of the number operator:* The number operator $\hat{n} = \hat{a}^\dagger\hat{a}$ for the single mode counts the number of quanta in the mode. Its expectation value in terms of the CM can be calculated

$$\langle a_1^\dagger a_1\rangle = \mathrm{Tr}\left[\rho a_1^\dagger a_1\right] = \mathrm{Tr}[\frac{\rho}{2}(c_1 + \mathrm{i}c_2)(c_1 - \mathrm{i}c_2)] = \frac{1}{2} - \frac{1}{2}\langle \mathrm{i}[\hat{c}_1, \hat{c}_2]\rangle = \frac{1}{2} - \frac{1}{2}\Gamma_{12} \tag{5.49}$$

Again from (5.46), $\Gamma_{12} = \nu$ and

$$\langle \hat{n}_1 \rangle = \frac{1}{2} - \frac{\nu}{2}. \tag{5.50}$$

Since (5.48) holds for $\nu$, thus the allowed values for number of quanta in the single mode of a fermionic state is in the range $0 \leq \langle \hat{n}_1 \rangle \leq 1$, a consequence of the Pauli exclusion principle.

2. *Average energy of single mode:* The average energy of a system in state $\rho$ with Hamiltonian $H$ is given by the expectation value of the systems' Hamiltonian, $E = \langle H \rangle = \mathrm{Tr}[\rho H]$. Now for a single fermionic mode with the quadratic Hamiltonian (5.32) the average energy is

$$E(\rho) = \frac{\mathrm{i}}{2} \mathrm{Tr}\Big[\sum_{ij}^{2} \mathcal{H}_{ij} c_i c_j \rho\Big] = \frac{\mathrm{i}}{2} \sum_{ij} \mathcal{H}_{ij} \mathrm{Tr}[\mathrm{i} c_i c_j \rho] = \frac{1}{2} \sum_{ij} \mathcal{H}_{ij} \Gamma_{ij} = \frac{1}{2} \mathrm{Tr}(\mathcal{H}\Gamma) \tag{5.51}$$

Using the $2 \times 2$ symplectic matrix $\Omega$ in (5.46)

$$\Omega = \begin{pmatrix} 0 & -1 \\ 1 & 0 \end{pmatrix}, \qquad \Omega\Gamma = \begin{pmatrix} \Gamma_{12} & 0 \\ 0 & \Gamma_{12} \end{pmatrix}$$

we find

$$\mathrm{Tr}\Big(\Omega\Gamma\Big) = \mathrm{i}\langle \big[c_1, c_2\big] \rangle = \mathrm{Tr}(\mathrm{i}[c_1, c_2]\rho) \tag{5.52}$$

The average energy

$$\begin{aligned} E(\rho) =& \omega \,\mathrm{Tr}[\rho a^\dagger a] \\ =& \frac{\omega}{2} \mathrm{Tr}\Big[\rho\big(c_1^2 - \mathrm{i}[c_1, c_2] + c_2^2\big)\Big] \end{aligned} \tag{5.53}$$

Substituting (5.52) in (5.53) and taking note that $c_1^2 = 1/2 = c_2^2$, we obtain

$$E(\Gamma) = \frac{\omega}{2}\Big(1 - \mathrm{Tr}(\Omega\Gamma)\Big) \tag{5.54}$$

as expected. This is the average energy for a single mode of the state with frequency $\omega$. for some real symplectic matrix $\Omega$. As we consider non-interacting fermionic

modes, the average energy of an $n$-mode state is defined as the sum of the average energy of each of the individual modes. In terms of covariance matrix this is given as

$$E(\Gamma_n) = \frac{\omega_1}{2}\Big(1 - \mathrm{Tr}(\Omega_1\Gamma_1)\Big) + \cdots + \frac{\omega_n}{2}\Big(1 - \mathrm{Tr}(\Omega_n\Gamma_n)\Big) \tag{5.55}$$

where the symplectic matrix for the entire system is $\Omega = \bigoplus_{j=1}^{n} \Omega_j$.

3. *Temperature and frequency of the single mode:* Another characteristic of the single mode we would like to discuss is its temperature and frequency. We note that for single $N = 1$ modes, all physical states with respect to their free Hamiltonian $H = \omega a^\dagger a$ are thermal states. To see this clearly, the thermal state $\tau(\beta)$ of a fermionic mode is given by

$$\tau(\beta) = \frac{1}{\mathcal{Z}} e^{-\beta H},$$

with inverse temperature $\beta = 1/T$ and partition function $\mathcal{Z} = \mathrm{Tr}(e^{-\beta H})$ . Here $H = \omega a^\dagger a$ is the free Hamiltonian of the mode with frequency $\omega$ and $a$ and $a^\dagger$ are the mode annihilation and creation operators respectively. We can expand the thermal state in the Fock basis $|n; n = 0, 1\rangle$

$$\tau(\beta) = \sum_{nm} P_{nm} |n\rangle \langle m| \tag{5.56}$$

where

$$P_{nm} = \langle n| \tau(\beta) |m\rangle = \frac{1}{\mathcal{Z}} \langle n| e^{-\beta H} |m\rangle = \frac{1}{\mathcal{Z}} \langle n| e^{-\beta\omega a^\dagger a} |m\rangle$$

From the CAR algebra $\{a, a^\dagger\} = 1$, we find that $(a^\dagger a)^n = a^\dagger a$ for $n > 0$. Therefore

$$P_{nm} = \frac{1}{\mathcal{Z}} e^{-m\beta\omega} \delta_{mn} \tag{5.57}$$

and the partition function

$$\mathcal{Z} = \mathrm{Tr}[e^{-\beta H}] = \mathrm{Tr}[e^{-\beta\omega a^\dagger a}] = \sum_{n=0}^{1} \langle n| e^{-\beta\omega a^\dagger a} |n\rangle = 1 + e^{-\beta\omega} \tag{5.58}$$

Substituting in (5.56), we obtain

$$\tau(\beta) = \frac{1}{(1 + e^{-\beta\omega})} \sum_{n=0}^{1} e^{-n\beta\omega} |n\rangle\langle n|$$

The covariance matrix of a thermal state can be computed using Eqn. (5.42) with

$$\begin{aligned}\nu = \Gamma_{12} =& 2\,\mathrm{i}\,\mathrm{Tr}\left[\rho c_1 c_2\right] = -\,\mathrm{Tr}\left[\rho(2a^\dagger a - 1)\right] \\ =& 1 - \frac{2e^{-\beta\omega}}{1+e^{-\beta\omega}} = \frac{1-e^{-\beta\omega}}{1+e^{-\beta\omega}} \equiv \tanh\left(\frac{\beta\omega}{2}\right)\end{aligned} \tag{5.59}$$

Therefore the covariance matrix for a single fermionic mode in a thermal state is given by

$$\Gamma_{\mathrm{th}} = \begin{pmatrix} 0 & \nu \\ -\nu & 0 \end{pmatrix}, \quad \Gamma^2 < -\mathbb{1}$$

as given in Eq. (5.46). So we see that we can characterize the state of the system from our knowledge of the covariance matrix. For example, rearranging the equation, we can determine the state's inverse temperature, $\beta$ as

$$e^{-\beta\,\omega} = \frac{1-\nu}{1+\nu}, \tag{5.60}$$

where $\omega$ is the mode's frequency.

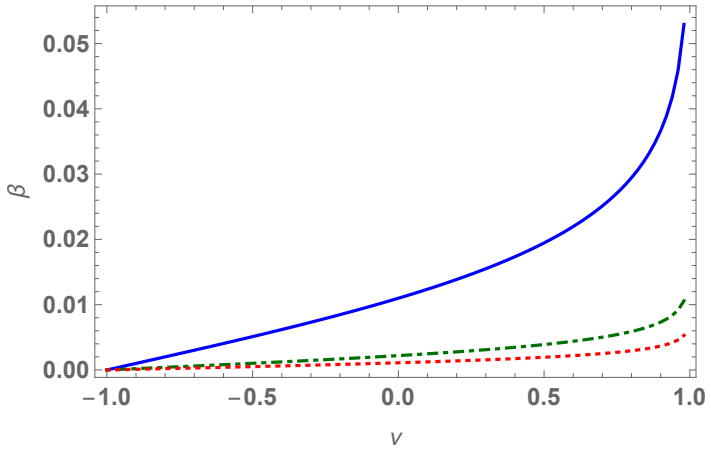


Figure 5.1: Plot of the inverse temperature $\beta$ of the thermal state vs the real parameter $\nu$ for the different frequency values $\omega$: 100 (blue solid line), 500 (green dotdashed line) and 1000 (red dotted line) respectively.

We show in FIG. 5.1 a plot of the inverse temperature $\beta$ versus the real-parameter $\nu$. Note that $\nu = 1$ corresponds to the ground state with $\langle \hat{n}_1 \rangle = 0$ and $T = 0$. Decreasing $\nu$ increases the temperature until at $\nu = 0$ the mode is at $T = \infty$. For $\nu < 0$ the population is inverted.

***Two-mode fermionic Gaussian states***

The two-mode FGS is the simplest scenario to investigate the fundamental issue of entanglement in quantum information. Consider a bipartite fermionic system, AB, where system A is composed of $N$ fermionic modes and system B is composed of $M$ fermionic modes, assume $\omega_A = \omega_B = \omega$. Suppose the joint system is in a Gaussian state. Thus a generic covariance matrix for $N = 2$ modes can be written as,

$$\Gamma_{\text{tm}} = \begin{pmatrix} 0 & \nu_1 & g_1 & g_2 \\ -\nu_1 & 0 & g_3 & g_4 \\ -g_1 & -g_3 & 0 & \nu_2 \\ -g_2 & -g_4 & -\nu_2 & 0 \end{pmatrix} \tag{5.61}$$

for some local temperature monotones $\nu_1$ and $\nu_2$ and four correlation numbers: $g_1$, $g_2$, $g_3$, and $g_4$. The bipartite covariance matrix can be divided into blocks as

$$\Gamma = \begin{pmatrix} \Gamma_A & \Gamma_{AB} \\ -\Gamma_{AB}^{\intercal} & \Gamma_B \end{pmatrix}, \tag{5.62}$$

and where each element of $\Gamma_{\text{tm}}$ is a $2 \times 2$ matrix

$$\Gamma_A = \begin{pmatrix} 0 & \nu_1 \\ -\nu_1 & 0 \end{pmatrix}, \quad \Gamma_B = \begin{pmatrix} 0 & \nu_2 \\ -\nu_2 & 0 \end{pmatrix}, \quad \Gamma_{AB} = \begin{pmatrix} g_1 & g_2 \\ g_3 & g_4 \end{pmatrix}.$$

$\Gamma_A$ and $\Gamma_B$ are $2N$ by $2N$ and $2M$ by $2M$ matrices respectively representing the reduced state of the individual systems and where $\Gamma_{AB}$ is a $2(N+M)$ by $2(N+M)$ matrix recording the correlations between the two systems.

***Standard form of CM of two-mode FGS***

The CM (5.61) can be brought to the standard form

$$\Gamma_{sf} = \begin{pmatrix} 0 & a & 0 & -e_1 \\ -a & 0 & -e_2 & 0 \\ 0 & e_2 & 0 & b \\ e_1 & 0 & -b & 0 \end{pmatrix} \tag{5.63}$$

by a local orthogonal operation (LOO) $O_{\text{loc}} = O_{\text{loc,a}} \oplus O_{\text{loc,b}}$, that is $\Gamma_{sf} = O_{\text{loc}} \Gamma_{\text{tm}} O_{\text{loc}}^T$ [45]. The average energy of the bipartite system according to equation (5.55) is given in terms of the CM as

$$E(\Gamma_{sf}) = \frac{\omega_a}{2}(1-2a) + \frac{\omega_b}{2}(1-2b) \tag{5.64}$$

where $\omega_a$ and $\omega_b$ are the frequencies of the modes. For two-mode fermionic pure Gaussian state, the CM in standard form is given by

$$\Gamma_{sf}^{p} = \begin{pmatrix} 0 & a & 0 & -e \\ -a & 0 & -e & 0 \\ 0 & e & 0 & a \\ e & 0 & -a & 0 \end{pmatrix} \tag{5.65}$$

with $e = (1-a^2)^{1/2}$ [15, 45] so that the fermionic system depends only on one parameter $a$.

## 5.3 Evolution of fermionic Gaussian states

In order to apply the Gaussian formalism to some dynamic scenario, one must ensure that the relevant states not only are initially Gaussian but remain Gaussian throughout their evolution. Thus the dynamics of the system must also be Gaussian, that is it must take Gaussian states to Gaussian states. Here we define Gaussian operations as those operations that preserve the Gaussian properties of a quantum state. Such an operation can be generated through Gaussian means.

We consider two cases of transformations which map Gaussian states to Gaussian states. The first is an evolution induced by the unitary operator $U = \exp(-\mathrm{i}Ht)$, with H a

quadratic Hamiltonian (5.32) of the system. The unitary evolution is described by the von Neumann equation of motion

$$\frac{\mathrm{d}}{\mathrm{d}t}\rho = -\mathrm{i}[\hat{H}, \rho], \tag{5.66}$$

and yields a suitable transformation on the field operators (example the Majorana operators for fermionic systems) that preserve the anti-commutation relation. These transformations as we will later show are called orthogonal transformations, which correspond to unitary transformations on the system's Hilbert space. Another class of transformations that map Gaussian states to Gaussian states are dissipative dynamics described by the Lindblad master equation

$$\frac{\mathrm{d}\rho}{\mathrm{d}t} = \mathcal{L}\rho = -\mathrm{i}[\hat{H}, \rho] + \sum_{\alpha} \Big( 2\hat{L}_\alpha \rho \hat{L}_\alpha^\dagger - \{\hat{L}_\alpha^\dagger \hat{L}_\alpha, \rho\} \Big), \tag{5.67}$$

where $L_\alpha$ are Lindblad operators linear in the system's operators (Majorana operators for our case) [65, 105, 19]. Therefore for our study, we focus on time evolutions of the fermionic systems generated by quadratic Hamiltonians and Lindblad operators linear in the fermionic operators.

### 5.3.1 Gaussian unitary transformations

In this subsection, we discuss how fermionic operators transform under a quadratic Hamiltonian $H = H(\mathcal{H})$. Precisely we focus on closed fermionic systems described by the density operator $\rho$ and evolving unitarily according to the von Neumann equation

$$\frac{\mathrm{d}}{\mathrm{d}t}\rho = -\mathrm{i}[\hat{H}, \rho], \tag{5.68}$$

where $[A, B] = AB - BA$ is the commutation operation. A set of unitary transformations under the quadratic Hamiltonian gives rise to a class of unitary Gaussian operations, that is unitaries that map Gaussian states to Gaussian states. Before we discuss such classes, we will see how the fermionic operators including the Majorana operators and covariance matrix transform under such dynamics. This knowledge will be particularly instructive for later discussions in this chapter.

We will generalize this to the dissipative case later in the chapter. We note that an operator generated by quadratic Hamiltonians are invariant under any canonical transformation. It turns out that a unitary transformation on a system's Hilbert space under a quadratic Hamiltonian corresponds to a (special-)orthogonal rotation $O(2N)$ in phase space [19].

***Unitary evolution of the Majorana operators***

First starting from the Heisenberg equation of motion for the set of Majorana vectors $\mathbf{x}$

$$\frac{\mathrm{d}}{\mathrm{dt}}\hat{\mathbf{x}} = -\mathrm{i}[\hat{H}, \hat{\mathbf{x}}], \tag{5.69}$$

The standard solution to this equation is given as [19]

$$\hat{\mathbf{x}}(t) = e^{\mathrm{i}\,\hat{H}\,t}\hat{\mathbf{x}}(0)e^{-\mathrm{i}\,\hat{H}\,t}.$$

which is a unitary transformation of $\mathbf{x}$ on the system's Hilbert space. We will show below that this transformation corresponds to an orthogonal transformation of $\mathbf{x}$ in phase space, that is

$$\hat{\mathbf{x}}(t) = e^{\mathrm{i}\hat{H}t}\,\hat{\mathbf{x}}\,e^{-\mathrm{i}\hat{H}t} = O\,\hat{\mathbf{x}}, \tag{5.70}$$

where $O = e^{\mathcal{H}t}$. First we can convert Eq. (5.69) into a linear differential equation on $\mathbf{x}$. In the case where $H$ is a quadratic Hamiltonian in the Majorana operators (5.32), we find

$$\frac{\mathrm{d}}{\mathrm{dt}}\hat{x}_k = -\mathrm{i}[\hat{H}, \hat{x}_k] = -\frac{1}{2}[\sum_{n,m=1}^{2N} \mathcal{H}_{nm}\hat{x}_n\hat{x}_m, \hat{x}_k] = -\frac{1}{2}\sum_{n,m=1}^{2N} \mathcal{H}_{nm}[\hat{x}_n\hat{x}_m, \hat{x}_k].$$

We can use the identity $[\hat{A}\hat{B}, \hat{C}] = \hat{A}\{\hat{B}, \hat{C}\} - \{\hat{A}, \hat{C}\}\hat{B}$ and the relation (5.21) to find

$$\begin{aligned}
\frac{\mathrm{d}}{\mathrm{dt}}\hat{x}_k &= -\frac{1}{2}\sum_{n,m=1}^{2N} \mathcal{H}_{nm}\Big(\hat{x}_n\{\hat{x}_m, \hat{x}_k\} - \{\hat{x}_n, \hat{x}_k\}\hat{x}_m\Big) \\
&= -\frac{1}{2}\sum_{n,m=1}^{2N} \mathcal{H}_{nm}\Big(\hat{x}_n\delta_{mk} - \hat{x}_m\delta_{nk}\Big) \\
&= -\frac{1}{2}\Big(\sum_{n=1}^{2N} \mathcal{H}_{nk}\hat{x}_n - \sum_{m=1}^{2N} \mathcal{H}_{km}\hat{x}_m\Big)
\end{aligned}$$

Relabelling indices in the second term, and since $\mathcal{H}$ is antisymmetric we have

$$\frac{\mathrm{d}}{\mathrm{dt}}\hat{x}_k = -\frac{1}{2}\sum_{n=1}^{2N}(\mathcal{H}_{nk} - \mathcal{H}_{kn})\hat{x}_n = \sum_{n=1}^{2N} \mathcal{H}_{kn}\hat{x}_n = (\mathcal{H}\hat{x})_k$$

From here we see that we have the linear differential equation on $\mathbf{x}$

$$\frac{\mathrm{d}}{\mathrm{dt}}\hat{\mathbf{x}} = \mathcal{H}\,\hat{\mathbf{x}}. \tag{5.71}$$

and we can write a solution of this equation as

$$\hat{\mathbf{x}}(t) = \mathbf{O}\hat{\mathbf{x}}(0). \tag{5.72}$$

where $O = e^{\mathcal{H}t} \in SO(2N)$ with $\mathcal{H}$ as the generator of the special orthogonal group $O$ [19].

***Unitary evolution of covariance matrix***

Fermionic Gaussian states are completely characterized by their CM such that in order to track the evolution of a FGS Gaussian state, we need only track the evolution of its covariance matrix. Thus starting from a Gaussian initial state $\rho$, at some time $t$, we can derive an equation for the CM $\Gamma$ of the time evolved state. We note that we follow similar derivation as in [19]. Starting from the equation of motion (5.68)

$$\frac{\mathrm{d}}{\mathrm{dt}}\rho = -\mathrm{i}[H, \rho]$$

multiply both sides by $\mathrm{i}c_ic_j$ and take the trace of both sides, we obtain

$$\frac{\mathrm{d}}{\mathrm{dt}}\mathrm{Tr}(\mathrm{i}\rho c_ic_j) = \mathrm{Tr}([H,\rho]c_ic_j) = \mathrm{Tr}\Big(H\rho c_ic_j - \rho H c_ic_j\Big) = -\mathrm{Tr}\Big(\rho[H, c_ic_j]\Big)$$

where we have used the cyclicity of the trace $\mathrm{Tr}[ABC] = \mathrm{Tr}[BCA]$. For the quadratic Hamiltonian $H(\mathcal{H})$ as given in (5.32),

$$\frac{\mathrm{d}}{\mathrm{dt}}\mathrm{Tr}(\mathrm{i}\rho c_ic_j) = -\frac{\mathrm{i}}{2}\mathrm{Tr}\Big(\rho\sum_{m,n}\mathcal{H}_{mn}[c_mc_n, c_ic_j]\Big)$$

Using the identity $[AB, CD] = [AB, C]D + C[AB, D]$ we have $[c_m c_n, c_i c_j] = [c_m c_n, c_i]c_j + c_i[c_m c_n, c_j]$ so that

$$\begin{aligned}
\frac{\mathrm{d}}{\mathrm{dt}}\mathrm{Tr}(\mathrm{i}\rho c_i c_j) &= -\frac{\mathrm{i}}{2}\mathrm{Tr}\Big(\rho \sum_{m,n} \mathcal{H}_{mn}[c_m c_n, c_i c_j]\Big) \\
&= -\frac{\mathrm{i}}{2}\mathrm{Tr}\Big(\rho \underbrace{\sum_{m,n} \mathcal{H}_{mn}[c_m c_n, c_i]}_{=-2\sum_k \mathcal{H}_{ik}c_k} c_j\Big) - \mathrm{Tr}\Big(\rho c_i \underbrace{\sum_{m,n} \mathcal{H}_{mn}[c_m c_n, c_j]}_{=-2\sum_k \mathcal{H}_{jk}c_k}\Big) \\
&= \sum_k \mathcal{H}_{ik}\mathrm{Tr}[\mathrm{i}c_k c_j \rho] + \mathrm{Tr}[\mathrm{i}c_i c_k \rho]\sum_k \mathcal{H}_{jk} \\
&= -\sum_k \mathcal{H}_{ki}\mathrm{Tr}[\mathrm{i}c_k c_j \rho] + \mathrm{Tr}[\mathrm{i}c_i c_k \rho]\sum_k \mathcal{H}_{jk} = -\mathcal{H}\Gamma + \Gamma\mathcal{H}^T
\end{aligned}$$

To summarize, we have shown that the covariance matrix of a system with density operator $\rho$ obeys the relation

$$\frac{\mathrm{d}}{\mathrm{dt}}\Gamma(t) = [\Gamma(t), \mathcal{H}] \tag{5.73}$$

which has the solution [19]

$$\Gamma(t) = O(t)\Gamma(0)O^{\mathrm{T}}(t), \qquad O = e^{-\mathcal{H}t} \in SO(2N, \mathcal{R}) \tag{5.74}$$

We have shown how Majorana operators and the covariance matrix of a fermionic mode transform under quadratic Hamiltonians. We will now go ahead to look at some classes of unitary transformations that can be generated under quadratic Hamiltonian.

### 5.3.2 Classes of Gaussian unitary transformations

Gaussian unitary transformations can be implemented by means of optical elements such as phase shifters, beam splitters and squeezers together with Homodyne measurement–these transformations are experimentally accessible with present technology [124]. Such optical elements are either capable of changing the number of particles (in our case fermions) in a quantum system, or they may preserve them. Our goal in this section is to classify a unitary transformation according to its ability to change/preserve the total number of fermions.

***Passive Gaussian transformations***

Passive Gaussian transformations are transformations that preserve the total number of fermions $N = \sum_k a_k^\dagger a_k$ in in the Gaussian system. Mathematically, this means that the quadratic Hamiltonian (5.22) can only have terms of the form $a_k^\dagger a_l$. We can identify two physical processes; the phase rotation and beam splitting operations.

1. *Phase rotation operation:* here we have the quadratic Hamiltonian proportional to $Aa^\dagger a$. This term describes the free evolution of the modes and adds just an overall phase shift on the fermionic operators. The transformation is described by the operator

$$R(\theta) = \exp(\mathrm{i}\theta a^\dagger a) \tag{5.75}$$

and acts as a phase rotation on the fermionic creation and annihilation operators according to the relation

$$a \to e^{\mathrm{i}\theta a^\dagger a} a e^{-\mathrm{i}a^\dagger a} = e^{\mathrm{i}\theta} a, \qquad a^\dagger \to e^{\mathrm{i}\theta a^\dagger a} a^\dagger e^{-\mathrm{i}a^\dagger a} = e^{-\mathrm{i}\theta} a^\dagger \tag{5.76}$$

where $\theta$ is a phase angle. In obtaining the above relation (5.76), we applied the Baker-Campbell-Hausdorff (BCH) formula [115] for two operators $X$ and $Y$

$$e^{-X} Y e^X = Y + [X, Y] + \frac{1}{2!}[X, [X, Y]] + \frac{1}{3!}[X, [X, [X, Y]]] + \cdots \tag{5.77}$$

and the anticommutation relation (5.18) for the fermionic operators. Subsequently, the action of the phase operator on the Majorana basis $x = (c_{2j-1}, c_{2j})^T$, is given as

$$\begin{pmatrix} \tilde{c}_1 \\ \tilde{c}_2 \end{pmatrix} = U \begin{pmatrix} c_1 \\ c_2 \end{pmatrix} U^\dagger = \frac{1}{\sqrt{2}} U \begin{pmatrix} a + a^\dagger \\ a - \mathrm{i}a^\dagger \end{pmatrix} U^\dagger = \begin{pmatrix} e^{\mathrm{i}\theta} a + e^{-\mathrm{i}\theta} a^\dagger \\ e^{\mathrm{i}\theta} a - e^{-\mathrm{i}\theta} a^\dagger \end{pmatrix}$$

By expanding $e^{\mathrm{i}\theta} = \cos\theta + \mathrm{i}\sin\theta$, we obtain the relation

$$\begin{pmatrix} \tilde{c}_1 \\ \tilde{c}_2 \end{pmatrix} = \begin{pmatrix} \cos\theta & \sin\theta \\ -\sin\theta & \cos\theta \end{pmatrix} \begin{pmatrix} c_1 \\ c_2 \end{pmatrix} \tag{5.78}$$

which shows that a phase rotation operation on Hilbert space of the Majorana operators corresponds to an orthogonal transformation on phase space. This can be extended to $N$ modes, so that the orthogonal matrix is

$$O(\theta) = \bigoplus_{j=1}^{2N} \begin{pmatrix} \cos(\theta_j) & \sin(\theta_j) \\ -\sin(\theta_j) & \cos(\theta_j) \end{pmatrix} \tag{5.79}$$

2. *Beam splitting operation:* the second process that arises from the Hamiltonian with terms $ga_k^\dagger a_l$ describes linear mixing of two modes which in quantum optics corresponds to a Hamiltonian of the form $H \propto ab^\dagger + a^\dagger b$. This Hamiltonian describes the action of a beamsplitter operation. The evolution operator is defined by

$$B(\phi) = \exp\left[\phi(ab^\dagger + a^\dagger b)\right] \tag{5.80}$$

where $a(a^\dagger)$ and $b(b^\dagger)$ define the annihilation (creation) operators of the two modes and $\phi$ is the transmissivity of the beam splitter. In the case of two fermionic modes specified by the operators $a$ and $b$ and satisfying the CAR $\{a, a^\dagger\} = \{b, b^\dagger\} = 1$, with all the other anti commutation relations being zero, in the Heisenberg picture, the annihilation operators are transformed via the Bogoliubov transformation

$$\begin{pmatrix} a \\ b \end{pmatrix} = \begin{pmatrix} \cos(\phi) & -\sin(\phi) \\ \\ \sin(\phi) & \cos(\phi) \end{pmatrix} \begin{pmatrix} a \\ b \end{pmatrix} \tag{5.81}$$

Correspondingly, the Majorana operators in the basis $\mathbf{x} = (c_1, c_2, c_3, c_4)^\intercal$ are transformed via the map

$$\hat{\mathbf{x}} \to B(\phi)\hat{\mathbf{x}}, \quad B(\phi) = \begin{pmatrix} \cos(\phi)\mathbb{1} & -\sin(\phi)\mathbb{1} \\ \\ \sin(\phi)\mathbb{1} & \cos(\phi)\mathbb{1} \end{pmatrix} \tag{5.82}$$

where $\mathbb{1}$ is the identity matrix.

### *Active Gaussian transformations*

Active transformations are transformations that do not preserve the total fermion number in a fermionic system. Such transformations arise from Hamiltonians with terms of the form $H \propto a^2 + a^{\dagger 2}$ for single modes and $H \propto ab + a^\dagger b^\dagger$ for double modes. This describes the squeezing process. A consequence of the Pauli exclusion principle is that single-mode squeezing is not possible for fermionic systems but two-mode is possible. The two-mode evolution operator is given by [72]

$$S(r) = \exp\left[r(ab - b^\dagger a^\dagger)\right]$$

where $r$ quantifies the two-mode squeezing. In the Heisenberg picture, the field operators under this transformation according to the relation

$$\tilde{a} = S(r)aS^{\dagger}(r) = \cos(r)a - \sin(r)b^{\dagger}$$
$$\tilde{b} = S(r)bS^{\dagger}(r) = \cos(r)b + \sin(r)a^{\dagger}$$

Similarly, the Majorana operators in the basis $\hat{x} = (c_1, c_2, c_3, c_4)^{\intercal}$ are transformed according to the relation

$$\hat{\mathbf{x}} \to S(r)\hat{\mathbf{x}}, \quad S(r) = \begin{pmatrix} \cos(r)\mathbb{1} & -\sin(r)\sigma_z \\ \sin(r)\sigma_z & \cos(r)\mathbb{1} \end{pmatrix} \tag{5.83}$$

where $\sigma_z = \mathrm{diag}(1, -1)$ is the usual Pauli matrix and $\mathbb{1}$ is the identity matrix.

It is instructive to check that the passive and active transformations discussed preserve the anticommutation relation

### 5.3.3 Gaussian dissipative transformations

In general, real (open) systems would interact with their environment and exhibit some quantum properties such as decoherence. So instead of the unitary transformation (5.68), we need to account for the noise/decoherence process by including a dissipative term. Precisely, we need an equation that governs the dynamics of the composite system+environment.

### 5.3.4 Covariance matrix formalism

An open fermionic system as we have described would consist of a system of interest we call $A$ and an environment (a bath) say $B$ both described by the joint density operator $\rho_{AB}$. Assume systems $A$ and $B$ are composed of $N$ fermionic modes and $M$ fermionic modes respectively and suppose the joint system is in a Gaussian state. The corresponding CM $\Gamma_{AB}$ of this joint state can be written as

$$\Gamma_{AB} = \begin{pmatrix} \Gamma_A & \gamma_{AB} \\ -\gamma_{AB}^{\intercal} & \Gamma_B \end{pmatrix}, \tag{5.84}$$

where $\Gamma_A$ and $\Gamma_B$ are $2N \times 2N$ and $2M \times 2M$ covariance matrices respectively representing the reduced state of the individual systems and $\gamma_{AB}$ is an $2N \times 2M$ matrix recording the

correlations between the two systems. In other words, tracing out systems $A$ or $B$ from the joint state $\rho_{AB}$ yields a reduced density matrix $\mathrm{Tr}_B(\rho_{AB})$ or $\mathrm{Tr}_A(\rho_{AB})$ with covariance matrices $\Gamma_A$ and $\Gamma_B$ respectively.

To describe the evolution of subsystem $A$, we note that a quantum channel (trace-preserving completely positive map) that preserves the Gaussian nature of system $A$ can be fully characterized by how they transform the covariance matrix (CM) of the input states. Given that Gaussian states and their corresponding Gaussian transformations are easily attainable in the laboratory, the Gaussian formalism therefore offers a powerful tool for treating the dynamics of open quantum systems.

### *Deriving the general form of fermionic Gaussian master equation in terms of the CM*

*Fermionic Gaussian channel*

We assume that subsystems $A$ and $B$ are initially uncorrelated, that is $\gamma_{AB} = 0$, so that the joint CM (5.84) at an initial time of the evolution process reduces to a direct sum of the individual CM

$$\Gamma_{AB}(0) = \begin{pmatrix} \Gamma_A & \\ & \Gamma_B \end{pmatrix} = (\Gamma_A \oplus \mathbf{0}) + (\mathbf{0} \oplus \Gamma_B) \tag{5.85}$$

where $\mathbf{0}$ denotes all zero matrices. To find the CM of the reduced system $A$ from an initial time $t = 0$ to a later time $t$, it is sufficient to compute the evolution of the joint CM and tracing over the subsystem $B$. The remaining task is to find an update rule for the covariance matrix. Recall that the CM of a fermionic Gaussian system undergoes an orthogonal transformation which can be written for the joint system as $\tilde{\Gamma}_{AB} = O\Gamma_{AB}O^T$. With

$$O = \begin{pmatrix} O_A & O_{AB} \\ O_{BA} & O_B \end{pmatrix}, \qquad O^T = \begin{pmatrix} O_A & O_{BA} \\ O_{AB} & O_B \end{pmatrix}, \tag{5.86}$$

We obtain

$$\tilde{\Gamma}_{AB} = \begin{pmatrix} \tilde{\Gamma}_A & \tilde{\Gamma}_{AB} \\ \tilde{\Gamma}_{BA} & \tilde{\Gamma}_B \end{pmatrix}$$

where

$$\tilde{\Gamma}_A = O_{\mathrm{A}}(\Gamma_{\mathrm{A}} \oplus \mathbf{0})O_{\mathrm{A}}^{\intercal} + O_{\mathrm{AB}}(\mathbf{0} \oplus \Gamma_B)O_{\mathrm{AB}}^{\intercal} \qquad \tilde{\Gamma}_{AB} = O_{\mathrm{A}}(\Gamma_{\mathrm{A}} \oplus \mathbf{0})O_{\mathrm{BA}}^{\intercal} + O_{\mathrm{AB}}(\mathbf{0} \oplus \Gamma_B)O_{\mathrm{B}}^{\intercal}$$
$$\tilde{\Gamma}_B = O_{\mathrm{BA}}(\Gamma_{\mathrm{A}} \oplus \mathbf{0})O_{\mathrm{BA}}^{\intercal} + O_{\mathrm{B}}(\mathbf{0} \oplus \Gamma_B)O_{\mathrm{B}}^{\intercal} \qquad \tilde{\Gamma}_{BA} = O_{\mathrm{BA}}(\Gamma_{\mathrm{A}} \oplus \mathbf{0})O_{\mathrm{A}}^{\intercal} + O_{\mathrm{B}}(\mathbf{0} \oplus \Gamma_B)O_{\mathrm{AB}}^{\intercal}$$

Note that $O_A$, $O_B$, $O_{AB}$ are not necessarily orthogonal themselves. We can see that the reduced state of system $A$ is updated as [28]

$$\Gamma_{\mathrm{A}}(0) \to \Gamma_{\mathrm{A}} = O_{\mathrm{A}}(\Gamma_{\mathrm{A}} \oplus \mathbf{0})O_{\mathrm{A}}^{\intercal} + O_{\mathrm{AB}}(\mathbf{0} \oplus \Gamma_B)O_{\mathrm{AB}}^{\intercal} \tag{5.87}$$

Eqn. (5.87) defines a fermionic Gaussian quantum map $\Phi_G$ that takes the initial state with CM $\Gamma_A(0)$ to a state with CM $\Gamma_A(t)$ at a later time $t$. We see in general that a fermionic Gaussian channel $\Phi_G$ is defined by a $2N$ by $2M$ matrix $O$ and an antisymmetric $2N$ by $2N$ matrix $R$ as

$$\Phi_G : \Gamma \to O\Gamma O^{\intercal} + R. \tag{5.88}$$

*Positivity condition*

As we have earlier discussed, $\Gamma$ is a valid covariance matrix of a physical fermionic system if it satisfies the positivity condition

$$\mathrm{i}\Gamma \leq \mathbb{1} \quad \text{or} \quad \Gamma\Gamma^T \leq \mathbb{1} \tag{5.89}$$

Now in order for such a Gaussian map to be physical it must map physical states to physical states. That is if $\Gamma$ satisfies (5.89) then $\Phi_G[\Gamma]$ should too. To see how this works, substitute the transformed CM in (5.88) in (5.89)

$$\mathbb{1} \leq \mathrm{i}(O\Gamma O^{\intercal} + R) = \mathrm{i}R + O\mathrm{i}\Gamma O^{\intercal}$$

$\Gamma(0)$ in turn is a valid CM satisfying (5.89), thus

$$\mathrm{i}R \leq \mathbb{1}_{2N} - O\,O^{\intercal}. \tag{5.90}$$

*The master equation*

Now we can find the general form of a fermionic Gaussian master equation by taking the above Gaussian channel to be differential as

$$O = \mathbb{1}_{2N} + A\,\mathrm{d}t, \quad R = C\,\mathrm{d}t, \tag{5.91}$$

for some $2N$ by $2N$ real-valued matrices $A$ and $C$, with $C$ antisymmetric. We can write the complete positivity condition (5.90) in terms of the generators $A$ and $C$. Upon substitution, we obtain

$$\begin{aligned} \mathrm{i}C\mathrm{d}t &\leq \mathbb{1}_{2N} - (\mathbb{1}_{2N} + A\,\mathrm{d}t)(\mathbb{1}_{2N} + A\,\mathrm{d}t,)^T && (5.92)\\ &\leq -A^T\,\mathrm{d}t - A\,\mathrm{d}t && (5.93) \end{aligned}$$

so that

$$A + A^{\intercal} + \mathrm{i}C \leq 0. \tag{5.94}$$

Now to derive a general form of master equation, substituting Eqn. (5.91) in (5.88) yields

$$\begin{aligned}\Gamma(t) &= (\mathbb{1}_{2N} + A\,\mathrm{d}t,)\Gamma(\mathbb{1}_{2N} + A\,\mathrm{d}t)^T + C\mathrm{d}t \\ &= \Gamma + \Gamma\, A^T \mathrm{d}t + A\,\Gamma\,\mathrm{d}t + C dt + \mathcal{O}(dt^2)\end{aligned}$$

So that

$$\frac{\mathrm{d}}{\mathrm{d}t}\Gamma(t) = A\Gamma(t) + \Gamma(t)A^T + C. \tag{5.95}$$

In the next chapter, we give a classification of the different dynamics this master equation (5.95) can produce.

***Comparison with Lindblad Master equation***

Here we will show that any dynamics for the covariance matrix of the form (5.95) satisfying (5.94) can be equivalently written as a differential equation for the state's density matrix, $\rho$ in Lindblad form. First recall that the master equation governing the evolution of the density matrix $\rho(t)$ of a dissipative system is given in Lindblad form as

$$\frac{\mathrm{d}\rho}{\mathrm{d}t} = \mathcal{L}\rho = \underbrace{-\mathrm{i}[\hat{H}, \rho]}_{\mathcal{L}_0(\rho)} + \sum_{\alpha} \underbrace{\left(2\hat{L}_\alpha \rho \hat{L}_\alpha^\dagger - \{\hat{L}_\alpha^\dagger \hat{L}_\alpha, \rho\}\right)}_{\mathcal{L}_D(\rho)}, \tag{5.96}$$

This equation gives an accurate description of the time evolution of a system coupled to an environment. The first term, which we labeled $\mathcal{L}_0$, describes the unitary part of the dynamics generated by the effective Hamiltonian $H$ of the system. The second term, labeled $\mathcal{L}_D$, describes the dissipative process resulting from interaction of the system with the environment. $\mathcal{L}, \mathcal{L}_0$ and $\mathcal{L}_D$ are superoperators, that is linear operators acting on the density operator $\rho$ of the system. $L_\alpha$ are Liouville operators which describe the coupling of the system to the environment. We note that this coupling can be taken to be quadratic or linear in the system's operators [65, 105, 19]. However for a transformation that map Gaussian states to Gaussian states, we require Lindblad operators that are linear in the Majorana operators [19].

***Lindblad master equation in terms of Majorana operator***

We wish to construct a Liouville map $\mathcal{L} = \mathcal{L}_0 + \mathcal{L}_D$ that maps a Gaussian operator $\rho(0)$ at time $t = 0$ to another Gaussian operator $\rho(t)$ at time $t$. This corresponds to finding the superoperators $\mathcal{L}_0$ and $\mathcal{L}_D$ respectively. To begin, let us consider the Liouville operators given as linear terms in the Majorana operators and recall the quadratic Hamiltonian (5.32)

$$H = \frac{\mathrm{i}}{2}\sum_{jk}\mathcal{H}_{jk}c_j c_k, \qquad L_\alpha = \sum_j \ell_{\alpha,j}c_j, \quad L_\alpha^\dagger = \sum_k \ell^*_{\alpha,k}c_k \tag{5.97}$$

So from the unitary part of the dynamics $\mathcal{L}_0\rho = -\mathrm{i}[H,\rho]$, one has the superoperator $\mathcal{L}_0$ given as [105]

$$\mathcal{L}_0 = -\mathrm{i}\sum_{jk=1}^{2N}\mathcal{H}_{jk}c_j c_k \tag{5.98}$$

where $\mathcal{H}_{jk}$ describes the unitary (orthogonal) dynamics that is the coupling between two modes. We note that for an arbitrary matrix $\mathcal{H}_{jk}$, the operator $\mathcal{L}_0$ preserves the total fermionic number $N = \sum_j c^\dagger c_j$ in a system, that is $[\mathcal{L}_0, N] = 0$. Next for the dissipative part

$$\mathcal{L}_\alpha\rho = 2\hat{L}_\alpha\rho\hat{L}_\alpha^\dagger - \{\hat{L}_\alpha^\dagger\hat{L}_\alpha,\rho\} = 2\sum_{jk}\gamma_\alpha\,\ell_{\alpha,j}\,\ell^*_{\alpha,k}\Big(c_j\rho c_k - c_k c_l\rho - \rho c_k c_l\Big) = \sum_{jk}M_{jk}\mathcal{L}_{jk}$$

where for physical observables, the map $\mathcal{L}_{jk} = (c_j\rho c_k - c_k c_l\rho - \rho c_k c_l)$ can be evaluated on even parity subspace [105] and we have defined

$$M_{jk} = \sum_\alpha \gamma_\alpha \ell_{\alpha,j}\ell^*_{\alpha,k} \tag{5.99}$$

is a matrix parameterizing the Lindblad operators, that is the dissipative part of the dynamics.

*Lindblad master equation for the system's covariance matrix*

To write a master equation for a system's covariance matrix, we will follow the derivation method in [19]. To begin, recall the definition of the covariance matrix $\Gamma_{jk}(t) = \mathrm{i}\mathrm{Tr}[\rho c_j c_k]$. Taking its time derivative

$$\frac{\mathrm{d}}{\mathrm{d}t}\Gamma(t) = \mathrm{i}\mathrm{Tr}[c_j c_k\frac{\mathrm{d}\rho}{\mathrm{d}t}] = \mathrm{i}\mathrm{Tr}[c_j c_k\mathcal{L}(\rho(t))] = \mathrm{i}\mathrm{Tr}[\mathcal{L}^\dagger(c_j c_k)\rho] \tag{5.100}$$

where $\frac{\mathrm{d}\rho}{\mathrm{d}t} = \mathcal{L}(\rho(t))$. We have also taken note of the Hilbert Schmidt inner product $\mathrm{Tr}[\rho A(\sigma)] = \mathrm{Tr}[A^\dagger(\rho)\sigma]$. The action of the adjoint Liouvillian $\mathcal{L}^\dagger$ on an observable $O$ is give according to the relation [19] $\mathcal{L}^\dagger(O) = \mathrm{i}[H, O] + \sum_\alpha L_\alpha^\dagger[O, L_\alpha] + [L_\alpha^\dagger, O]L_\alpha$, so that taking $O = c_j c_k$ we have the expression

$$\frac{\mathrm{d}}{\mathrm{d}t}\Gamma(t) = \mathrm{i}\mathrm{Tr}\Big[(\mathrm{i}[H, c_j c_k] + \sum_\alpha L_\alpha^\dagger[c_j c_k, L_\alpha] + [L_\alpha^\dagger, c_j c_k]L_\alpha)\rho\Big]$$

Evaluating this expression gives [105]

$$\frac{\mathrm{d}}{\mathrm{d}t}\Gamma(t) = \mathbf{X}\Gamma(t) + \Gamma(t)\mathbf{X}^T + \mathbf{Y} \tag{5.101}$$

where

$$\mathbf{X} = -\mathcal{H} - 2(\mathbf{M} + \mathbf{M}^*), \quad \text{and} \quad \mathbf{Y} = 4\mathrm{i}(\mathbf{M} - \mathbf{M}^*) \tag{5.102}$$

$\mathcal{H}$ is a real antisymmetric matrix that characterizes the quadratic Hamiltonian (5.32) while $M$ as defined in (5.99) is a complex Hermitian matrix parameterizing the Lindblad operators $L_\alpha$. $\mathbf{X}$ and $\mathbf{Y}$ are real valued $2N \times 2N$ matrices with $\mathbf{Y}$ being antisymmetric (that is $\mathbf{Y} = -\mathbf{Y}^T$). We see that unitary evolution of the CM given by unitary equation (5.73) can be obtained from (5.101) when $\mathbf{M} = 0$, that is $\mathbf{Y} = 0$ and $\mathbf{X} = -\mathcal{H}$.

### 5.3.5 General application

What we have presented so far is a description of the structure of fermionic systems, Gaussian fermionic states and their possible characterization in the covariance matrix formalism. We then briefly talked about the evolution of the Fermionic Gaussian states. We can apply this knowledge to some physical problems in quantum information and quantum thermodynamics. One of the main reasons for these applications is because Gaussian states and their corresponding Gaussian unitaries can be effectively generated in the laboratory. Secondly the unitary and dissipative dynamics can be efficiently simulated in a classical computer [19] and master equation is solvable [105]. .

To proceed, our first application, which is discussed in Chapter 6, focus on the problem of extracting work from quantum (fermionic) systems. Passive state are states from which work cannot be extracted unitarily if only a single copy of the system is available. It follows that given several ($n$) copies of passive states, there may exist extractable energy in the system via global unitary transformations [73]. Complete passive states are states

for which no work can be extracted no matter the number of copies of the system that are available – the only example is the thermal state [106, 125]. Can we identify passive but not completely passive fermionic states from which work can be extracted? On the other hand, a problem arises when realizing the global unitary transformation is far-fetched from current technology. This naturally leads us to consider work extraction via Gaussian unitary transformations [22], that are practically realizable. Just like passive states, Gaussian passive states are states from which no work can be extracted via Gaussian unitary transformations. Two important questions which we answer in the chapter include 1) What are the characteristics of Gaussian passive states? 2) What energy is sacrificed using Gaussian unitaries to extract work rather than arbitrary unitary transformation?

The second application, which is presented in Chapter 7, characterizes the dynamics of a fermionic open system by taking advantage of the properties of Gaussian states and Gaussian operations. In the covariance matrix formalism, the Markov master equation that governs an open system was derived and characterized according to the following dichotomies: active and passive dynamics depending on the system's ability to change and preserve its energy respectively, and orthogonal and non orthogonal dynamics, depending on the ability that the dynamics preserves information in the system or exchanges information with an external environment. We also consider the multimode vs single mode case, and lastly state dependent vs state independent dynamics respectively. The classification reveals that only nine out of the expected sixteen dynamics are possible.We go ahead to give the physical interpretation of the different classifications and how they relate in physical quantum processes.

# Chapter 6

# Work Extraction from non-interacting fermionic systems

## 6.1 Introduction

Energy is a quantitative property that is transferred to a system in order to perform work on a system. Obviously energy is of fundamental and practical importance, and it follows that the process of storing energy and subsequently extracting it is one of the most important applications of quantum thermodynamics. In this line, a major task in quantum thermodynamics is to understand which quantum states allow for work extraction from quantum systems. Such states are called non-passive, while states from which no work can be extracted are called passive states. Interestingly, passive states can be activated in a way that they become non-passive. This property, known as activation, is seen when several copies of passive states are processed as a whole by a global (entangling) unitary transformation. Thermal (or completely passive) states are those that lack the property of activation irrespective of the number of available copies. This implies that any device for unitary work extraction must be out-of equilibrium. In the bosonic setting [22], the simplest out-of-equilibrium cycle engine for unitary work extraction is a heat engine which requires minimum access to two thermal baths at different temperatures. We will show that this is not the case for two fermionic modes. Instead the minimum number of baths required to construct a heat engine in the fermionic setting is three [96].

On the other hand, while work can be extracted from non-passive and passive (but not completely passive) states, the relevant cyclic unitary transformation may be difficult to realize. For feasible technological applications, we require unitary transformations that are

cost efficient and readily available. Gaussian unitary transformations offer such advantages, which motivates the notion of Gaussian passivity [22]: a state property requiring that work may be extracted via Gaussian operations.

The main goal of this current chapter is to characterize those states in fermionic systems that allow or do not allow for work extraction via 1) cyclic unitary process and 2) Gaussian unitary process respectively. As a first task, we will find the minimum number of copies of passive states that achieve activation in non-interacting fermionic systems. This number will give the minimum number of thermal baths required for constructing a heat engine in the fermionic setting.

## 6.2 Cyclic unitary process and work extraction

### 6.2.1 Cyclic unitary process

Consider an isolated system $S$ in initial state $\rho(0)$, that is driven by the Hamiltonian $H(t) = V(t) + H$ where $H$ given as

$$H = \sum_j \varepsilon_j |j\rangle \langle j| , \quad \varepsilon_j \leq \varepsilon_{j+1} \tag{6.1}$$

is the system's free Hamiltonian and $V(t)$ is any time-dependent interaction applied to the system for a time $T$, and accounts for work transfer. A cyclic process is defined as one in which $S$ is coupled at the time $t = 0$ to external sources of work, and decouples from them at the time $t = \tau$. Thus, the potential $V(t)$ vanishes before the process at t = 0 and after the process at $t = \tau$. That is $V(0) = V(\tau) = 0$.

The corresponding driving gives rise to a unitary evolution operator

$$U(T) = \mathcal{T}\Big( \exp -\mathrm{i} \int_0^T dt(H + V(t))\Big) \tag{6.2}$$

with the resulting final state given as

$$\rho(T) = U(T)\rho U^\dagger(T) \tag{6.3}$$

Within the framework of cyclic unitary processes, work extracted from a system is given by the change in average energy of the system

$$W = \mathrm{Tr}[H\rho] - \mathrm{Tr}[H\rho(T)] = E_i - E_f \tag{6.4}$$

Intuitively, if such $U$ exists, then work is generated from the system when $W > 0$; that is

$$E_f = \mathrm{Tr}[H\rho(T)] < \mathrm{Tr}[H\rho] = E_i. \tag{6.5}$$

It follows that some quantum states do not allow the reduction of its average energy by a cyclic unitary process. These are called passive states, while those for which the average energy can be reduced via cyclic unitary process are called non-passive. We will come back to the notion of passive and non-passive states.

### 6.2.2 Work extraction from quantum systems

The process of work extraction from a system starts with an initial non-passive state $\rho(0)$ of the system. Under the action of a unitary operation, we reach a possible final state $\rho(T)$. The work extracted from $\rho(0)$ is maximized if

$$\mathcal{W}_{\max} = \mathrm{Tr}[H\rho] - \mathrm{Tr}[H\sigma_p] \tag{6.6}$$

This suggests that the maximum work extractable from a system is achieved once the final state is passive. This is called ergotropy [4] - the average work extractable from the state $\rho$ of a system by means of unitary operations. The task is to identify what form the potential would take in order to extract maximum work from the quantum system. The unitary operator minimizing $E_f$ (hence maximizing $\mathcal{W}$) is the one that results in a permutation of the elements of $\rho$ so that the largest element of $\rho$ is matched with the smallest one of $H$. Thus all passive states are diagonal in the eigenbasis of $H$ with probability of occupation decreasing as the energy associated with the eigenstates of $H$ increases. That is, passive states $\sigma_p$ with Hamiltonian (6.1), are given as

$$\sigma_p := \sum p_j |j\rangle\langle j|, \quad \text{with} \quad p_j \geq p_{j+1} \; \forall \, j$$

where $0 \leq p_j \leq 1$ and $\sum_j p_j = 1$.

We will come back to the notion of passive state later in the chapter. We will now discuss work extraction by considering the case for single and composite quantum systems respectively.

#### *The case of a single quantum system*

Consider a d-dimensional single quantum system with Hamiltonian

$$h = \sum_{j}^{d-1} \varepsilon_j |j\rangle \langle j| , \qquad \text{with} \quad \varepsilon_j \leq \varepsilon_{j+1} \tag{6.7}$$

and density state

$$\rho = \sum_{i=1}^{d} p_j |j\rangle \langle j| \tag{6.8}$$

We have assumed that $H$ is diagonal in its eigenbasis $\{|j\rangle\}$. Here the maximal work extracted from a single quantum system is given as in (6.6)

***The case of composite quantum systems***

Now consider that $S$ is made of $n$ identical $d$-dimensional noninteracting subsystems. Assume each subsystem has the same local Hamiltonian (6.7) and density state (6.8). The total Hamiltonian $H$ of the system is the sum of the individual local Hamiltonians $H = \sum_k h_k$ and can be written as [66]

$$H_0 = H \otimes \mathbb{1}^{\otimes(n-1)} + \mathbb{1} \otimes H \otimes \mathbb{1}^{\otimes(n-2)} + \cdots + \mathbb{1}^{\otimes(n-1)} \otimes H \tag{6.9}$$

The system is driven by the time-dependent cyclic Hamiltonian

$$H(t) = H + V(t) \tag{6.10}$$

where $V(t)$ is a potential that will act on the whole system at time $t \in (0, T)$. The task is to identify what form the potential would take in order to extract maximum work from the global system. A classical work strategy would act locally on each ensemble. So assume if for a single system starting from an active state $\rho_A$, the maximum work is $\mathcal{W}_{\max}$, then such a classical strategy can extract at most $n\mathcal{W}_{\max}$ from the system.

As we have discussed, a permutation operation is required to achieve maximal work extraction. Now note that after maximal work extraction the final state of the ensemble is a passive state which is separable because it is diagonal in the eigenbasis of the noninteracting hamiltonian $H$, as the initial state. However, permutation operators are not local and can have maximal entangling power [101, 48]. A consequence of this is that some passive states may be activated for work extraction, when many copies of them are processed by global (thus entangling) unitary operations. This leads us to the notion of passivity, complete passivity and activation, discussed in the next section.

### 6.2.3 Passivity, complete passivity and activation

Given the state $\rho$ of a finite dimensional quantum system associated with the Hilbert space $\mathcal{H} \equiv \mathbb{C}^d$, and Hamiltonian $H = \sum_{j=0}^{d-1} \varepsilon_j |j\rangle \langle j|$, with energy eigenstates $|i\rangle$ and eigenvalues

$\varepsilon_i$. We ask whether the average energy of the system can be lowered by a cyclic unitary transformation $U$ acting on the system. This question naturally leads us to the notions of passivity, complete passivity and activation, which we will now describe explicitly.

### *Passive states*

Passive states are states from which no work can be extracted unitarily if only a single copy of the system is available. Passivity of a quantum state is often expressed as a property of the state and its Hamiltonian. Consider a state $\rho$ and a reference Hamiltonian $H$, both written in their respective eigenbasis,

$$H := \sum E_n |n\rangle\langle n|, \quad \text{with} \quad E_{n+1} \geq E_n \ \forall n, \tag{6.11}$$

$$\rho := \sum p_n |\rho_n\rangle\langle\rho_n|, \quad \text{with} \quad p_{n+1} \leq p_n \ \forall n \tag{6.12}$$

where $0 \leq p_n \leq 1$ and $\sum_n p_n = 1$. $\rho$ is passive if and only if

1. it is diagonal in the same basis as the Hamiltonian $H$ of the system, that is $[\rho, H] = 0$. This can be interpreted as $\{|\rho_n\rangle\}$ coinciding with $\{|n\rangle\}$,
2. it has no population inversion, that is populations $p_j$ are strictly decreasing as energy $\varepsilon_j$ increases.

Otherwise we say $\rho$ is non-passive.

### *Complete passivity and activation*

Passive states have the property of activation where it becomes possible to extract work from many copies of passive states; this leads to a more restricted notion of passivity. Suppose we have $n$ copies of our system with a total Hamiltonian (6.9) and described by the state $\rho^{\otimes n}$. It follows that through some global unitary operations, some passive states can be activated to yield work, provided we have more than one copy of the system. A state $\rho^{\otimes n}$ is completely passive if and only if the state is passive for all $n$. A result in quantum thermodynamics shows that the thermal states

$$\tau(\beta_j) = \frac{1}{Z} \exp(-\beta_j H_j), \tag{6.13}$$

with inverse temperature $\beta_j$ are the only completely passive states [106, 81], where $Z = \mathrm{Tr}(e^{-\beta H_j})$ is the partition function and $\beta = \frac{1}{T}$ is the inverse temperature. If the state $\rho^{\otimes n}$ becomes activable for some $n \geq k$ then it is said to be k-activable [126].

It was shown in [125] that the notion of passivity and complete passivity of a quantum system can be equivalently described in terms of virtual temperatures. There by associating virtual temperatures to the transition between populations of different energy transitions that passive states are those at which every transition is at positive temperature while complete passivity are those at which every transition is at the same positive temperature.

We will now go ahead to describe examples of passive states but not completely passive states and show how work can be extracted from such state.

### 6.2.4 Thermal states

Many copies of passive states may have extractable energy when processed by global unitary transformations, while from the so-called completely passive states no work can be extracted no matter the number of available copies of the system. Thermal states are the only completely passive states.

Thermal states have been defined in (6.13) as

$$\tau(\beta) = \frac{1}{Z}\exp(-\beta H), \tag{6.14}$$

where $\mathcal{Z} = \mathrm{Tr}[e^{-\beta H}]$ is the partition function. We can represent thermal states in the single fermionic Fock basis $\{|n\rangle\}$ as

$$\begin{aligned}\tau(\beta) &= (1+e^{-\beta\omega})^{-1}\sum_{n=0}^{1} e^{-n\beta\omega}|n\rangle\langle n| \qquad n \in \{0,1\} \\ &= (1+e^{-\beta\omega})^{-1}\Big[|0\rangle\langle 0| + e^{-\beta\omega}|1\rangle\langle 1|\Big]\end{aligned} \tag{6.15}$$

Suppose we have a number of fermionic modes initially in a thermal state (6.13). The Hamiltonian $H$ of the system can be written

$$H = \sum_j \omega_j a_j^\dagger a_j \tag{6.16}$$

with $\omega_j$ the mode frequencies and the field operators $a_j, a_j^\dagger$ satisfy the CAR relation (5.18) $[a_j, a_k^\dagger] = \delta_{jk}$. For such a free Hamiltonian describing non-interaction of the modes (see 5.1.4 for discussion), the initial state of the system is a product state

$$\tau(\beta) = \bigotimes_i \tau(\beta_i) \tag{6.17}$$

## 6.3 Unitary work extraction

So far we have discussed that work can be extracted from non-passive states through unitary operations. Work can also be extracted by processing several copies of passive but not completely passive states through global (entangling) unitary operations. Then we defined thermal (completely passive) states as those from which no work can be extracted cyclically no matter the number of available copies [126, 125, 106], this implies any resource state for unitary work extraction (cyclic engine) must be out of thermal equilibrium.

Let us now consider a technical observation of the heat engines. It was shown in [22] that for two bosonic modes at the same frequency, the product state of two thermal states with different temperatures is not passive. This implies that in the bosonic setting, constructing a quantum heat engine (the simplest out-of-equilibrium resource) requires access to two thermal baths at different temperatures. We will show that this is not the case for two fermionic modes. However for three fermionic modes at the same frequency, the product state of three thermal states with different temperatures can be non passive. Thus suggesting that the minimum number of thermal baths which is required to construct a quantum heat engine in fermionic setting is three [96]. We will now present a proof for the case of fermionic systems.

### 6.3.1 The case for two-mode fermionic system

Consider a non-interacting two-mode fermionic system of equal frequency $\omega$ each with local Hamiltonian $h_i = \omega a_i^\dagger a_i$. The total Hamiltonian $H$ of the system is simply the sum of the individual local Hamiltonians: $H_s = \omega(a_1^\dagger a_1 + a_2^\dagger a_2)$. The fermionic two-mode thermal state in the Fock basis may then be expressed as [32]

$$\tau(\beta_1, \beta_2) = \frac{1}{\mathcal{Z}_1 \mathcal{Z}_2} \sum_{m,n=0}^{1} e^{-\omega(n\beta_1 + m\beta_2)} |n\rangle\langle n|_1 \otimes |m\rangle\langle m|_2, \qquad n, m \in \{0, 1\} \tag{6.18}$$

where $\mathcal{Z}_1\mathcal{Z}_2 = (1+e^{-\beta_1\omega})(1+e^{-\beta_2\omega})$ and up to a common factor, the matrix elements are

$$\epsilon = e^{-\omega(\beta_1 n+\beta_2 m)} = e^{-\frac{\omega}{T_1T_2}(mT_1+nT_2)}.$$

We see that $H_s$ commutes with the product state $\tau(\beta_1,\beta_2)$. The sum of the occupational numbers in the state is $N_i = m+n$. From (6.12), the state $\tau(\beta_1,\beta_2)$ is non passive if there exist pairs of non-negative integers $(m,n),(m',n')$ such that

$$\epsilon' > \epsilon, \quad \text{while} \quad m'+n' > m+n \tag{6.19}$$

where $\epsilon' = e^{-\omega(\beta_1 n'+\beta_2 m')} = e^{-\frac{\omega}{T_1T_2}(m'T_1+n'T_2)}$ is the population, from which up to a common factor yields the condition

$$mT_1+nT_2 > m'T_1+n'T_2, \quad \text{while} \quad m'+n' > m+n \tag{6.20}$$

by making use of the fact that $e^{-AX} > e^{-AY} \Rightarrow X < Y$. Given that $m,n,m',n' \in \{0,1\}$, equation (6.20) cannot be satisfied for any combination of the $m,n,m',n'$. We then conclude that for two-mode fermionic states, regardless of frequencies of the modes and its temperature, the product of two thermal states is always passive, in contrast to the bosonic case [22].

### 6.3.2 The case for three-mode fermionic system

We will now extend the analysis above to a three-mode fermionic system in thermal states at equal frequencies and different temperatures. The state can be written as

$$\tau(\beta_1,\beta_2,\beta_3) = \frac{1}{Z_1Z_2Z_3}\sum_{m,n,l=0}^{1} e^{-\omega(n\beta_1+m\beta_2+l\beta_3)}|m\rangle\langle m|\otimes|n\rangle\langle n|\otimes|l\rangle\langle l| \tag{6.21}$$

and the total Hamiltonian of the system is $H = \omega(a_1^\dagger a_1 + a_2^\dagger a_2 + a_3^\dagger a_3)$. The non-passivity condition becomes

$$n\beta_1+m\beta_2+l\beta_3 > n'\beta_1'+m'\beta_2'+l'\beta_3' \quad \text{while} \quad m'+n'+l' > m+n+l \tag{6.22}$$

The matrix element is now proportional to $e^{-\omega(n\beta_1+m\beta_2+l\beta_3)}$ and $m,n,l \in \{0,1\}$. One can now find a three-dimensional subspace in which a unitary can reduce the average energy, proving that the state $\tau(\beta_1,\beta_2,\beta_3)$ is not always passive. For example, let $m'=n'=1, l'=0$ and $m=n=0, l=1$, it is obvious that $m'+n'+l' > m+n+l$. Also,

$$\beta_3 > \beta_1+\beta_2 \tag{6.23}$$

which can hold for sufficiently large $\beta_3$. In general the condition (6.22) can be satisfied provided $\beta_i \ll \beta_j, \beta_k$ for distinct $i, j, k$. Hence a product of thermal states $\rho = \prod_j^n \tau(\beta_j) = \tau(\beta_1) \otimes \cdots \otimes \tau(\beta_n)$ for fermionic modes can be activated to become non-passive for $n \geq 3$. In other words, the state is 3-activable [126].

### 6.3.3 Practical implementation

According to our discussion above we see that a system of fermionic modes in a thermal state, with equal frequencies and at different temperatures, is 3-activable. We will now present a protocol that extracts work from three mode non-interacting fermionic system in a thermal state.

***Protocol:***

Consider the three-mode fermionic system described by the state (6.21). From the non-passivity condition (6.22), we note that for the above transformation to be possible, the action of the unitary operation must be such that

- The initial state with a composition of the three modes should consist at least of an unpopulated mode and a populated mode. That is, initial states of the system of the form $|111\rangle$ and $|000\rangle$ are not allowed.
- The action of the unitary should take the initially populated (unpopulated) mode to an unpopulated (populated) mode of the final state.
- One can always guess the temperature relationship of the different modes: The sum of the inverse temperature of the initially unpopulated modes must be less than the inverse temperature of the populated mode.
- If a transformation leaves a mode unaffected, then the temperature of such a mode does not matter during the transformation process.

We now turn to a practical example of such a transformation. The three mode state can be explicitly written as

$$\begin{aligned}\rho_{nml} =& \frac{1}{Z_1 Z_2 Z_3}\Big[e^{-\omega\beta_1}|100\rangle\langle 001| + e^{-\omega\beta_3}|001\rangle\langle 100| + e^{-\omega\beta_2}|010\rangle\langle 010| + e^{-\omega(\beta_1+\beta_3)}|101\rangle\langle 101| \\ &+ e^{-\omega(\beta_1+\beta_2)}|110\rangle\langle 011| + e^{-\omega(\beta_2+\beta_3)}|011\rangle\langle 110| + |000\rangle\langle 000|\Big]\end{aligned}$$

where we have ignored the term in $|111\rangle\langle 111|$. Upon expanding the sum in (6.21). Consider a unitary of the form

$$U = |101\rangle\langle 010| + |010\rangle\langle 101| - |101\rangle\langle 101| - |010\rangle\langle 010| + \mathbb{1} \tag{6.24}$$

where $U$ induces a transition between the two degenerate states

$$|010\rangle \leftrightarrow |101\rangle \tag{6.25}$$

We note that $U = U^\dagger$. This type of unitary has been applied to generate a mixed state of the Werner- type thermal state [1] necessary for quantum information processing. The amount of work extracted from the system (the change in its average energy) is given by [125]

$$\begin{aligned} W &= \mathrm{Tr}[H(\rho_{nml} - U\rho_{nml}U^\dagger)] \\ &= \omega e^{-\omega\beta_2}\left(1 - e^{-\omega((\beta_1+\beta_3)-\beta_2)}\right) \end{aligned}$$

which must be positive for the state to be non-passive. Clearly this will hold whenever $(\beta_1 + \beta_3) - \beta_2 < 0$ or in other words

$$\beta_2 > \beta_1 + \beta_3 \tag{6.26}$$

which agrees with the non-passivity condition in (6.22). Alternatively one could employ a unitary that interchanges the $|001\rangle$ and $|110\rangle$ states and one would obtain (6.23).

The problem of generating a unitary analogous to (6.24) for more copies of fermion states is rather challenging. In the next section, I will discuss a more restricted class of unitary transformations.

## 6.4 Work extraction and Gaussian unitary operations

We have seen in Sec 6.3.1, that a product of two non-interacting thermal states at different temperatures is passive unlike its bosonic counterpart [22]. Now given that constructing a quantum heat engine requires access to two thermal baths at different temperatures, does this suggest that we cannot construct a heat engine out of a product of two thermal states in fermionic modes? It follows that to extract work, instead of the arbitrary cyclic unitary transformation, we could consider a set of restricted quantum operations known as Gaussian unitary transformations. This leads us to the notion of Gaussian passivity, a

characteristic of a quantum system for which work can be extracted via Gaussian unitary transformation.

Just like in the definition of passive states, a state (not necessarily Gaussian) is said to be Gaussian passive if no work can be extracted from it through Gaussian unitary operations. In terms of work extraction, our aim in this section is to see what is achievable using Gaussian unitary transformations. We work in the covariance formalism that is, given a Gaussian unitary transformation, we are interested in the effect of the Gaussian transformation induced by this unitary on an arbitrary state via its effect on the corresponding covariance matrix. We ask for which (not necessarily Gaussian) states of two non-interacting fermionic modes with frequencies $\omega_a$ and $\omega_b$ ($\omega_a \leq \omega_b$) can energy be extracted using only Gaussian operations. States from which energy cannot be extracted using Gaussian operations are called Gaussian passive [22].

### 6.4.1 Gaussian passive states

We are now ready to characterize a quantum state with covariance matrix $\Gamma$ for which the average energy (5.55) can be minimized by a Gaussian unitary transformation.

To begin, consider a fermionic system made up of two non-interacting fermionic modes $a$ and $b$ respectively. Let $\rho$ and $\Gamma$ be the density state and covariance matrix of the system respectively, according to (5.63) $\Gamma$ is given in the standard form as

$$\Gamma_{sf} = \begin{pmatrix} 0 & a & 0 & -e_1 \\ -a & 0 & -e_2 & 0 \\ 0 & e_2 & 0 & b \\ e_1 & 0 & -b & 0 \end{pmatrix} \tag{6.27}$$

In terms of $2 \times 2$ blocks, we have

$$\Gamma_{sf} = \begin{pmatrix} \Gamma_{\text{A}} & \Gamma_{\text{AB}} \\ -\Gamma_{\text{AB}}^T & \Gamma_{\text{B}} \end{pmatrix}, \quad \text{with} \quad \Gamma_{\text{A}} = \begin{pmatrix} 0 & a \\ -a & 0 \end{pmatrix}, \quad \Gamma_{\text{B}} = \begin{pmatrix} 0 & b \\ -b & 0 \end{pmatrix}, \quad \Gamma_{\text{AB}} = \begin{pmatrix} 0 & e_1 \\ e_2 & 0 \end{pmatrix}.$$

In the case of pure fermionic systems, the two-mode covariance matrix in the standard form is written as

$$\Gamma_{sf}^{p} = \begin{pmatrix} 0 & a & 0 & -e \\ -a & 0 & -e & 0 \\ 0 & e & 0 & a \\ e & 0 & -a & 0 \end{pmatrix} \tag{6.28}$$

with $e = (1 - a^2)^{1/2}$ [15, 45] so that the fermionic system depends only on one parameter $a$.

***Average energy in terms of state covariance matrix***

Recall the average energy of a system with Hamiltonian $H$ and described by the density operator $\rho$ is given according to Eqn. (5.55) as

$$E(\Gamma_n) = \frac{\omega_1}{2}\Big(1 - \mathrm{Tr}(\Omega_1\Gamma_1)\Big) + \cdots + \frac{\omega_n}{2}\Big(1 - \mathrm{Tr}(\Omega_n\Gamma_n)\Big) \tag{6.29}$$

for a real symplectic matrix $\Omega = \bigoplus_{j=1}^{n}\Omega_j$, with $\Omega_1 = \begin{pmatrix} 0 & -1 \\ 1 & 0 \end{pmatrix}$. For a two mode system, the average energy is given as

$$E(\Gamma_n) = \frac{\omega_a}{2}\Big(1 - \mathrm{Tr}(\Omega_{\mathrm{A}}\Gamma_{\mathrm{A}})\Big) + \frac{\omega_b}{2}\Big(1 - \mathrm{Tr}(\Omega_{\mathrm{B}}\Gamma_{\mathrm{B}})\Big)$$

Evaluating $\Omega_j\Gamma_j$ for each mode $j$, we obtain the average energy of a state with CM given in (6.27)

$$E(\Gamma_{sf}) = \frac{\omega_a}{2}(1 - 2a) + \frac{\omega_b}{2}(1 - 2b) \tag{6.30}$$

where $\omega_a$ and $\omega_b \geq \omega_a$ are the frequencies of the modes. We will now go ahead to see if a state with CM (6.27) is Gaussian passive or Gaussian (active) non-passive. From there we give the general characteristics that describes Gaussian passivity of a system.

We consider the three Gaussian unitaries – local orthogonal transformation, beam splitting, two-mode squeezing – and the following steps of operation. Let the initial state of the system have the covariance matrix $\Gamma_{\mathrm{I}}$ and an average energy $E$. The Gaussian unitary that acts on $\Gamma$ will take it to a new CM given as $\Gamma_{\mathrm{F}}$ with average energy $E'$. By comparison:

1. If $E' < E$, then work has been extracted from the system and we say the state is Gaussian non-passive. Next we check if there is more extractable work from the system. If yes, we then apply another Gaussian unitary on $\Gamma_{\mathrm{F}}$ to further reduce $E'$ until the system's average energy is minimal. At this point we say there is no more extractable work from the system and the system is Gaussian passive.

2. If however $E' \geq E$, then the system is Gaussian passive and work cannot be extracted from the system via the Gaussian unitary operation that yields $\Gamma'$. We can try other Gaussian unitaries to extract work from the system until we arrive at a Gaussian passive state from which no more work can be extracted via Gaussian unitary operation.

The question now is, what is the nature of the CM of the system whose state is Gaussian passive. Answering this question results in stating the characteristics of Gaussian passivity of a system as we will now discuss.

### 6.4.2 Characteristics of Gaussian passive states.

At this point, we characterize Gaussian passive states:

**Theorem 1.** *Any (not necessarily Gaussian) state of two noninteracting fermionic modes with frequencies $\omega_b \geq \omega_a$ is Gaussian-passive if and only if its covariance matrix $\Gamma$ is*

*(i) in Williamson standard form [15]*

$$\Gamma = \begin{pmatrix} 0 & a & 0 & 0 \\ -a & 0 & 0 & 0 \\ 0 & 0 & 0 & b \\ 0 & 0 & -b & 0 \end{pmatrix} \tag{6.31}$$

*with $a > b$ for $\omega_b \neq \omega_a$, or*

*(ii) in the normal form*

$$\Gamma = \begin{pmatrix} 0 & a & 0 & -e \\ -a & 0 & e & 0 \\ 0 & -e & 0 & b \\ e & 0 & -b & 0 \end{pmatrix} \tag{6.32}$$

*for equal frequencies $\omega_b = \omega_a$.*

*Proof.* Let us now prove the theorem 1

#### *Local Orthogonal Transformations*

Let our initial two-mode non-interacting fermionic system be described by the density state $\rho$ and a corresponding CM $\Gamma$. The first Gaussian unitary operation we consider is the local orthogonal transformation which is applied on each system's mode.

It is a theorem that the covariance matrix $\Gamma$ of a two-mode fermionic system can be brought to its standard form through a local orthogonal transformation $O_{\text{loc}} = O_{\text{loc}_a} \oplus O_{\text{loc}_b}$, that is

$$\Gamma_{sf} = O_{\text{loc}} \Gamma O_{\text{loc}}^T, \qquad O_{\text{loc}_j} = \begin{pmatrix} \cos(\phi_j) & \sin(\phi_j) \\ -\sin(\phi_j) & \cos(\phi_j \end{pmatrix} \tag{6.33}$$

By inverting equation (6.33), we can write the local covariance matrix of a two-mode system as

$$\Gamma = O_{\text{loc}}^T \Gamma_{sf} O_{\text{loc}} \tag{6.34}$$

and we note that the inverse operations are also local orthogonal transformations. Computing $\Gamma$, we obtain

$$\Gamma = \begin{pmatrix} O_{\text{loc}_a}^T \Gamma_{\text{A}} O_{\text{loc}_a} & O_{\text{loc}_a}^T E O_{\text{loc}_b} \\ -O_{\text{loc}b}^T E^T O_{\text{loc}_a} & O_{\text{loc}_b}^T \Gamma_{\text{B}} O_{\text{B}} \end{pmatrix} = \begin{pmatrix} \Gamma'_{\text{A}} & \Gamma'_{\text{AB}} \\ \Gamma'_{\text{BA}} & \Gamma'_{\text{B}} \end{pmatrix} \tag{6.35}$$

Evaluating the average energy, we find $E(\Gamma) = E(\Gamma_{\text{sf}})$. So it becomes clear that applying a local orthogonal transformation to bring the CM of a system to standard form (6.27) does not lower the energy of the system. Thus a state with $\Gamma = \Gamma_{\text{sf}}$ is Gaussian passive with no extractable work via local orthogonal transformations. However, the energy of such a system may be lowered via global transformations that act on many copies of the system.

### *Two mode Squeezing*

Now suppose a state has a covariance matrix in the standard form (6.33). We have seen in the previous subsection that such a state is Gaussian passive under a local orthogonal transformation. In this section, we will apply the global orthogonal transformation (5.83) to the system and see if its average energy can be reduced. Computing the corresponding two-mode squeezed covariance matrix $\hat{\Gamma}_{TM} = S(r)\Gamma_{sf}S(r)^T$, we find

$$\hat{\Gamma}_{TM} = \begin{pmatrix} 0 & a' & 0 & -e'_1 \\ -a' & 0 & -e'_2 & 0 \\ 0 & e'_2 & 0 & b' \\ e'_1 & 0 & -b' & 0 \end{pmatrix} \tag{6.36}$$

where

$$a' = ac_r^2 - bs_r^2 - \frac{1}{2}(e_1 + e_2)s_{2r}, \quad b' = -as_r^2 + bc_r^2 - \frac{1}{2}(e_1 + e_2)s_{2r} \tag{6.37a}$$

$$e'_1 = \frac{1}{2}(a+b)s_{2r} + e_1 c_r^2 - e_2 s_r^2, \quad e'_2 = \frac{1}{2}(a+b)s_{2r} + e_2 c_r^2 - e_1 s_r^2 \tag{6.37b}$$

with $c_r = \cos(r)$ and $s_r = \sin(r)$ respectively. To see if this transformation can reduce the average energy, we compute $E(\hat{\Gamma}_{TM})$ using (5.54), obtaining

$$E(\hat{\Gamma}_{TM}) = \frac{\omega_a}{2}(1 - 2a') + \frac{\omega_b}{2}(1 - 2b') \tag{6.38}$$

and substituting equations (6.37) into (6.38), we get

$$E(\hat{\Gamma}_{TM}) = \omega_a\Big[b\sin^2(r) - a\cos^2(r)\Big] + \omega_b\Big[a\sin^2(r) - b\cos^2(r)\Big] + \frac{(\omega_a+\omega_b)}{2}\Big[1 + (e_1+e_2)\sin(2r)\Big] \tag{6.39}$$

Minimizing this with respect to the squeezing parameter $r$ we find the condition

$$\frac{\partial}{\partial r}E(\hat{\Gamma}_{TM}) = 0 \Rightarrow (a+b)\sin(2r) + (e_1+e_2)\cos(2r) = 0 \tag{6.40}$$

whose solution is

$$r = -\frac{1}{2}\tan^{-1}\left[\frac{e_1+e_2}{(a+b)}\right] = -\frac{1}{2}\tan^{-1}(\lambda) \tag{6.41}$$

where $\lambda = (e_1+e_2)/(a+b)$. The minimized energy is

$$E_{\min}(\hat{\Gamma}_{TM}) = \frac{(\omega_a+\omega_b)}{2}\Big(1 - (a+b)\sqrt{1+\lambda^2}\Big) + \frac{1}{2}(\omega_b-\omega_a)(a-b). \tag{6.42}$$

Defining $e = (e_1-e_2)/2$, the elements of the covariance matrix (6.37) are now

$$\tilde{a}' = \frac{(a+b)}{2}\sqrt{1+\lambda^2} + \frac{(a-b)}{2} \tag{6.43a}$$

$$\tilde{b}' = \frac{(a+b)}{2}\sqrt{1+\lambda^2} - \frac{(a-b)}{2} \tag{6.43b}$$

$$\tilde{e}_1' = e, \quad \tilde{e}_2' = -e \tag{6.43c}$$

We pause to comment on the interpretation of these matrix elements. In addition to minimizing the system's average energy, the squeezing parameter (6.41) reduces the off-diagonal elements in (6.36) to a single parameter $e$ so that the resulting covariance matrix is of the form

$$\Gamma_{GP} = \begin{pmatrix} 0 & \tilde{a}' & 0 & -e \\ -\tilde{a}' & 0 & e & 0 \\ 0 & -e & 0 & \tilde{b}' \\ e & 0 & -\tilde{b}' & 0 \end{pmatrix} \tag{6.44}$$

If the state is a two-mode pure fermionic Gaussian state whose covariance matrix is of the form (6.28), the two-mode squeezing operation takes the state's covariance matrix to the form

$$\Gamma^{p}_{GP} = \begin{pmatrix} 0 & 1 & 0 & 0 \\ -1 & 0 & 0 & 0 \\ 0 & 0 & 0 & 1 \\ 0 & 0 & -1 & 0 \end{pmatrix} \tag{6.45}$$

with property $(\Gamma^{p}_{GP})^2 = -\mathbb{1}$. This corresponds to the covariance matrix of a pure fermionic Gaussian state in the Williamson normal form [15]. To achieve a Williamson normal form covariance matrix for the general two-mode fermionic system, we consider further Gaussian unitary transformations on the system.

### *Beam Splitting*

The last Gaussian operation we have to consider is the beam splitting operation. This transformation on fermionic phase space is represented by the transformation matrix (5.82). We find

$$\Gamma_{BS} = B(\theta)\hat{\Gamma}_{GP}B^{\dagger}(\theta) = \begin{pmatrix} 0 & A & 0 & D \\ -A & 0 & -D & 0 \\ 0 & D & 0 & B \\ -D & 0 & -B & 0 \end{pmatrix} \tag{6.46}$$

where

$$A = \tilde{a}' \cos^2\theta + \tilde{b}' \sin^2(\theta) + e\sin(2\theta) \tag{6.47a}$$

$$B = \tilde{b}' \cos^2\theta + \tilde{a}' \sin^2(\theta) - e\sin(2\theta) \tag{6.47b}$$

$$D = \frac{1}{2}(\tilde{a}' - \tilde{b}')\sin 2\theta - e\cos(2\theta) \tag{6.47c}$$

The average energy corresponding to $\Gamma_{BS}$ is

$$E(\Gamma_{BS}) = -\omega_a\Big[\tilde{b}' \sin^2(\theta) + \tilde{a}' \cos^2(\theta)\Big] - \omega_b\Big[\tilde{a}' \sin^2(\theta) + \tilde{b}' \cos^2(\theta)\Big] \tag{6.48}$$

$$+ \frac{(\omega_a + \omega_b)}{2} + (\omega_b - \omega_a)e\sin(2\theta) \tag{6.49}$$

Again energy is minimized for the value of $\theta$ satisfying the equation

$$(\omega_b - \omega_a)\Big[(\tilde{b}' - \tilde{a}')\sin(2\theta) + 2e\cos(2\theta)\Big] = 0 \tag{6.50}$$

implying

$$\theta = -\frac{1}{2}\tan^{-1}\left(\frac{2e}{\tilde{b}' - \tilde{a}'}\right) = -\frac{1}{2}\tan^{-1}\mu$$

where $\mu = 2e/(\tilde{b}' - \tilde{a}')$. The minimized energy under the beam splitting operation is then

$$E_{\min}(\hat{\Gamma}_{BS}) = \frac{(\omega_b - \omega_a)}{2}\Big((\tilde{a}' - \tilde{b}')\sqrt{1+\mu^2}\Big) + \frac{1}{2}(\omega_b + \omega_a)\Big(1 - (\tilde{a}' + \tilde{b}')\Big), \tag{6.51}$$

and the corresponding minimized matrix elements are

$$A = \frac{(\tilde{a}' + \tilde{b}')}{2} + \frac{(\tilde{a}' - \tilde{b}')}{2}\sqrt{1+\mu^2} \tag{6.52a}$$

$$B = \frac{(\tilde{a}' + \tilde{b}')}{2} - \frac{(\tilde{a}' - \tilde{b}')}{2}\sqrt{1+\mu^2} \tag{6.52b}$$

$$D = 0 \tag{6.52c}$$

For equal frequencies $\omega_a = \omega_b$, the average energy is unchanged, that is $E_{\min}(\hat{\Gamma}_{TM}) = E_{\min}(\hat{\Gamma}_{BS})$ and we conclude that the state with covariance matrix (6.44) is Gaussian passive. However for different frequencies, assuming w.l.o.g. that $\omega_b > \omega_a$, the covariance matrix for the minimized state under the beam splitting operation is in the Williamson normal form [15]

$$\Gamma^1_{GP} = \begin{pmatrix} 0 & A & 0 & 0 \\ -A & 0 & 0 & 0 \\ 0 & 0 & 0 & B \\ 0 & 0 & -B & 0 \end{pmatrix}, \tag{6.53}$$

with eigenvalues given as $\lambda_a = \pm \mathrm{i}A$ and $\lambda_b = \pm \mathrm{i}B$. If $a > b$, we find that $\lambda_a > \lambda_b$ and so the lower frequency mode has the higher population. □

We see that the effect of the orthogonal transformation on the fermionic two-mode covariance matrix is to decompose the modes and bring them into a product of single-mode locally thermal states diagonal in the Fock basis. An example of a Gaussian passive state

of two modes with different frequencies is that of a product of single mode thermal states, in which each mode has different temperature. In this case, the Williamson eigenvalues are $\lambda_i = \tanh\left(\frac{\omega_i}{2T_i}\right)$. For $T_b \neq 0$ the condition $\lambda_a > \lambda_b$ for Gaussian passivity can be expressed as

$$\frac{\omega_a}{\omega_b} > \frac{T_a}{T_b} \tag{6.54}$$

As shown in section 6.3.1, within the framework of general operations, the product of two thermal states at different temperature is passive, regardless of the frequencies of the modes involved. And from above, we see that such a state is also Gaussian passive showing that all passive states are obviously Gaussian passive. However the converse may not be true [22] as we will show in the next section.

## 6.5 Passivity vs Gaussian passivity

So far we have focused on characterizing a general fermionic state according to whether work can be extracted or not using Gaussian unitary transformations. We started with the covariance matrix of a general two-mode non-interacting fermionic system, applied Gaussian unitary operations to extract energy from the system and then we arrived at the Gaussian passive state (6.53), where no further energy could be extracted by an additional Gaussian unitary transformation. A reasonable question then arises: in the process of characterizing a (not necessarily Gaussian) state, how much extractable work is sacrificed by using Gaussian unitary transformations instead of general unitary transformations? To address this question we will follow a procedure similar to that in the bosonic case [22].

The answer to the above question depends on the particular state. We see that in the characterization process we fixed the second moment of the fermionic state, which only uniquely identifies states if they are Gaussian. Two steps therefore lead us to answering the above question. 1) First we must find a (non-Gaussian) pure state that is compatible with a given Gaussian passive state, or in other words we must find a non-Gaussian state with the same second moment as that of the Gaussian passive state. 2) We must show that a general unitary transformation on the resulting (non-Gaussian) pure state can lower its energy to the minimal value. These observations can be recast in the following lemma

**Lemma 1.** *The second moments of any Gaussian passive state are compatible with a (non Gaussian) pure state for which the entire energy is extractable by unitary transformation.*

*Proof.* To proceed, we first note that the covariance matrix of a Gaussian-passive state (6.53) of an arbitrary number of modes with different frequencies is identical to the covariance matrix of a product of locally thermal states with different effective temperature for each mode. One could then consider a single fermionic mode in a thermal state with arbitrary temperature and then find a pure state whose second moment is that of this single mode thermal state. Then one could certainly find pairs of states of this kind whose tensor product is compatible with a Gaussian-passive locally thermal two-mode state. For example, in the Fock basis, the fermionic state

$$|\psi\rangle = \sqrt{1-p}|0\rangle + \sqrt{p}|1\rangle, \qquad 0 \leq p \leq 1 \tag{6.55}$$

has a covariance matrix of the form

$$\begin{pmatrix} 0 & 2p-1 \\ 1-2p & 0 \end{pmatrix} \tag{6.56}$$

and so by carefully choosing the continuous parameter $p$, we can bring the covariance matrix to look like that of a single-mode fermionic thermal state with inverse temperature $\beta$

$$\Gamma_{th} = \begin{pmatrix} 0 & \tanh\left(\frac{\beta\omega}{2}\right) \\ -\tanh\left(\frac{\beta\omega}{2}\right) & 0, \end{pmatrix} \tag{6.57}$$

where $\omega$ is the mode frequency. Unfortunately, the state (6.55) is prohibited by a superselection rule [3] and so does not exist.

However, another example would be the fermionic vacuum state $|0\rangle$ and a single fermion state $|1\rangle$ each having covariance matrices

$$\Gamma_{\rho_0} = \begin{pmatrix} 0 & 1 \\ -1 & 0 \end{pmatrix}, \quad \Gamma_{\rho_1} = \begin{pmatrix} 0 & -1 \\ 1 & 0 \end{pmatrix},$$

respectively. Given that the $(|1\rangle, |0\rangle)$ states are pure, their covariance matrices satisfy the condition $\Gamma^2_{|i\rangle} = -\mathbb{1}$. We define the free energy of these states as

$$F(\rho) = E(\rho) - TS(\rho), \tag{6.58}$$

where $S(\rho) = -\mathrm{Tr}[\rho \ln(\rho)]$ is the von Neumann entropy which is vanishing for pure states, and $E(\rho)$ is the average (internal) energy.

Now to achieve our first task, consider pairs of the single fermionic systems encoded into a bipartite Hilbert space $\mathcal{H}_{ab} = \mathcal{H}_a \otimes \mathcal{H}_b$ of subsystems $a$ and $b$ respectively. The state is defined by a density operator $\rho^1_{ab} = |00\rangle_{ab}\langle 00|$ and $\rho^2_{ab} = |11\rangle_{ab}\langle 11|$ respectively, the resulting states correspond to direct sum of locally pure fermionic Gaussian states. Their covariance matrices are respectively

$$\Gamma_{\rho^1_{ab}} = \Gamma^a_{\rho_1} \oplus \Gamma^b_{\rho_1}, \quad \Gamma_{\rho^2_{ab}} = \Gamma^a_{\rho_2} \oplus \Gamma^b_{\rho_2},$$

which is the same as the CM of pure fermionic Gaussian passive state (6.45). For our second task, given that the constructed states are pure, their free energy is thus identical to the average energy. Interestingly there is no way to lower the average energy of the constructed state $\rho^1_{ab}$. However the energy of the state $\rho^2_{ab}$ can be lowered by applying a (non Gaussian) unitary transformation that takes the pure state to the vacuum state. This shows that $\rho^2_{ab}$ is Gaussian passive but not passive while $\rho^1_{ab}$ is both passive and Gaussian passive, as expected.

□

## 6.6 Discussion

We have investigated the problem of work extraction from fermionic systems, finding a number of similarities and differences with their bosonic counterparts.

Thermal states at positive temperatures are the only completely passive states from which work cannot be extracted no matter the number of available copies [126, 125, 106]. Any quantum state out-of-equilibrium is a potential resource for work extraction. However for fermions the situation is somewhat subtle. We have shown that under arbitrary unitary transformations there is no way to process a product of two fermionic modes in different thermal states to extract work, independent of mode temperatures and frequency. This is quite unlike the situation for the bosonic counterpart [22], and suggests that fermionic systems are not as useful for quantum thermodynamic applications such as construction of quantum heat engines [73]. However we found that a product of more than two fermionic modes in different thermal states was non-passive (under a certain temperature constraint), implying work extraction is possible in this system. The challenge of generating the necessary unitary operation for this work extraction could be a limitation.

We extended the notion of Gaussian passivity to fermionic systems and presented criteria for identifying fermionic states according to their Gaussian (non-Gaussian) passivity;

that is, according to our ability (inability) to extract work from them using Gaussian unitary transformations. This characterization is based on the second statistical moment of the two-mode fermionic system, which is known to have complete information about the system. This implies that our characterization provides information about the Gaussian ergotropy of the system (that is the maximum extractable energy in a Gaussian unitary process). Our result showed that under non-Gaussian (general) unitaries, we showed that work can be extracted from a general two-mode fermionic system.

There is still much that can be done with Fermionic Gaussian systems. A classification of their dynamics for open systems (analogous to the bosonic case [58]) remains to be carried out, along with their time evolution under rapid bombardment. This is the subject of the next chapter.

# Chapter 7

# Classification of Markovian fermionic Gaussian master equation

## 7.1 Introduction

The general Gaussian master equation (GGME) that governs the dynamics of open fermionic systems was derived in section 5.3.4 and is written as

$$\frac{\mathrm{d}}{\mathrm{d}t}\Gamma(t) = A\Gamma(t) + \Gamma(t)A^T + C. \tag{7.1}$$

Equation (7.1) is an affine transformation with linear terms $A\Gamma(t) + \Gamma(t)A^T$ and an affine term $C$. $A$ satisfies the complete positivity condition

$$A + A^T + \mathrm{i}C \leq 0 \tag{7.2}$$

Any dynamics for the covariance matrix of the form (7.1) satisfying (7.2) can be equivalently written as a differential equation for the covariance matrix of a state in Lindblad form [105, 19].

$$\frac{\mathrm{d}}{\mathrm{dt}}\Gamma(t) = \mathbf{X}\Gamma(t) + \Gamma(t)\mathbf{X}^T + \mathbf{Y} \tag{7.3}$$

We present in this section a classification of dynamics that this master equation can produce. Our classification of the master equation will be channeled based on the following dichotomies

1. *Orthogonal vs non-orthogonal:* we can identify an orthogonal (non orthogonal) dynamics with the dynamics of systems that require (do not require) an external system in order that particle exchange would occur.

2. *Passive vs active:* The dynamic could be passive (active) if it preserves (changes) the total number of particles in the system.

3. *State dependent vs state independent:* as the name implies, we define state dependent (independent) dynamics as those that depend (do not depend) on the physical properties of the system.

4. *Single mode vs multimode:* here, the dynamics may involve single modes of the system or multimode necessary to study correlations and entanglement.

## 7.2 Dichotomies of classification

### 7.2.1 Orthogonal vs non-orthogonal dynamics

We showed in 5.3.1 that a unitary transformation on a system's Hilbert space corresponds to an orthogonal transformation on the system's phase space. It follows that we can define an orthogonal (non orthogonal) transformation in the same way a unitary (non unitary) transformation is defined. By definition, a unitary time evolution would give rise to conservation of probability which consequently results in conservation of quantum information in a system, while a non unitary time evolution results in the loss of quantum information to an external system. Therefore we define non-orthogonal dynamics as those that require an external system for an exchange of information whereas orthogonal dynamics are defined as those that preserve quantum information in the system.

To relate this definition to the GGME, recall the unitary and dissipative evolution equation for a system's covariance matrix $\Gamma$

$$\frac{\mathrm{d}}{\mathrm{d}t}\Gamma(t) = -\mathcal{H}\Gamma(t) + \Gamma(t)\mathcal{H}^T \qquad \text{unitary dynamics} \tag{7.4}$$

$$\frac{\mathrm{d}}{\mathrm{d}t}\Gamma(t) = \mathbf{X}\Gamma(t) + \Gamma(t)\mathbf{X}^T + \mathbf{Y} \qquad \text{dissipative dynamics} \tag{7.5}$$

where $\mathbf{X} = -\mathcal{H} - 2(\mathbf{M} + \mathbf{M}^*)$ and $\mathbf{Y} = 4\mathrm{i}(\mathbf{M} - \mathbf{M}^*)$. From these equations, we see that the dissipative case reduces to a unitary case when $\mathbf{M} = 0$, that is $\mathbf{Y} = 0$ so that $\mathbf{X} = -\mathcal{H}$.

Likewise we see that our derived GGME (7.1) for dissipative systems will reduce to the case for unitary evolution (7.4), when the affine term $C = 0$ and the generator of the linear term $A$ is antisymmetric (that is $A_o = A - A^T$), where we have denoted the orthogonal part of the matrix $A$ as $A_o$. Obviously we can associate

$$\mathcal{H}_{\text{eff}} = A_0, \qquad \mathcal{H}_{\text{eff}} = \frac{\mathrm{i}}{2}\mathbf{x}^T\, A_0\, \mathbf{x} \tag{7.6}$$

. In the same way, the non-orthogonal part of the dynamics corresponds to all $C \neq 0$ and the symmetric part of $A$ (that is $A = A^T$). Again comparing with the Lindblad master equation (7.4), we can associate the non-orthogonal dynamics $A_{\text{N}} + C_{\text{N}} = M_{jk}$. To summarize

$$A_{\text{O}} = A - A^T, \quad C_{\text{O}} = 0 \tag{7.7}$$

$$A_{\text{N}} = A + A^T, \quad C_{\text{N}} = C \tag{7.8}$$

### 7.2.2 Passive vs active dynamics

A quantum evolution that is number preserving (non preserving) is called passive (active). As we already discussed in section 5.3.1, number conserving (non conserving) transformations would commute (non commute) with the excitation number. Thus we can equivalently define passive (active) dynamics as those that preserve (changes) the expected excitation number respectively, so that active dynamics would require an environment for particle exchange. We will now demonstrate how the GGME (7.1) generates a passive and an active dynamics.

Define the total number operator $\sum_j^N a_j^\dagger a_j$. This counts the average number of particles in a system of $N$ fermions. In terms of the Majorana operators and system's covariance matrix we have

$$\sum_{j=1}^{N}\langle a_j^\dagger a_j\rangle = \mathrm{Tr}[\rho a_j^\dagger a_j] = \frac{1}{2}\,\mathrm{Tr}[\rho(c_{2j-1} + \mathrm{i}c_{2j})(c_{2j-1} - \mathrm{i}c_{2j})] = \frac{1}{2}N - \mathrm{i}\langle[c_{2j-1}, c_{2j}]\rangle. \tag{7.9}$$

Now define a symplectic matrix $\Omega$

$$\Omega = \bigoplus_{j=1}^{N} J = \mathbb{1}_N \otimes J; \quad J = \begin{pmatrix} 0 & 1 \\ -1 & 0 \end{pmatrix}. \tag{7.10}$$

and recall that the single mode covariance matrix is given as $\Gamma = \begin{pmatrix} 0 & a \\ -a & 0 \end{pmatrix}$ where $a = \frac{\mathrm{i}}{2}\langle [c_{2j-1}, c_{2j}] \rangle$. It is easy to show that $\mathrm{Tr}[\Omega\Gamma] = -2a$. To summarize

$$\langle a_j^\dagger a_j \rangle = \frac{1}{2}N + \mathrm{Tr}[\Omega\Gamma] \tag{7.11}$$

We will now see how the GGME (7.1) produces a passive (active) dynamics. We compute the rate of change of the expected excitation number,

$$\begin{aligned} \frac{\mathrm{d}}{\mathrm{d}t}\langle a^\dagger a \rangle = \mathrm{Tr}(\Omega \frac{\mathrm{d}\Gamma}{\mathrm{d}t}) =& \mathrm{Tr}\Big(\Omega\big(A\Gamma + \Gamma A^\intercal + C\big)\Big) \\ =& \mathrm{Tr}\Big(\Omega A\Gamma + A^\intercal\Omega\Gamma + \Omega C\Big) \\ =& \mathrm{Tr}\Big(\big(\Omega A - (\Omega A)^\intercal\big)\Gamma + \Omega C\Big), \end{aligned} \tag{7.12}$$

where we have used the cyclic property of trace and that $\Omega$ is antisymmetric. By our above definition, the dynamics is passive if $\frac{\mathrm{d}}{\mathrm{d}t}\langle \hat{n} \rangle = 0$ for all $\Gamma$. This is only the case if $\Omega A$ is symmetric and $\Omega C$ is traceless.

Thus we can identify the part of $A$ which is passive, $A_{\mathrm{P}}$ (active $A_{\mathrm{A}}$), as that part which becomes symmetric (antisymmetric) when multiplied by $\Omega$. Specifically

$$\Omega A_{\mathrm{P}} = \frac{1}{2}(\Omega A + (\Omega A)^\intercal), \quad \Omega A_{\mathrm{A}} = \frac{1}{2}(\Omega A - (\Omega A)^\intercal). \tag{7.13}$$

so that $A_{\mathrm{P}} + A_{\mathrm{A}} = A$. Using the symplectic identities $\Omega^{-1} = \Omega^T = -\Omega$ we have

$$A_{\mathrm{P}} = \frac{1}{2}\big(A + \Omega A^\intercal \Omega\big), \quad A_{\mathrm{A}} = \frac{1}{2}\big(A - \Omega A^\intercal \Omega\big). \tag{7.14}$$

In order to identify the active and passive parts of $C$ we must split it into parts that do and do not contribute to the trace of $\Omega C$. This is not trivial and will be discussed in greater detail once we introduce the other dichotomies in Sec. 7.3.1.

### 7.2.3 Single mode vs multimode dynamics

Consider a dynamical system composed of many fermionic modes. State evolution may be established within the same mode, for example, motion of electrons with the nucleus. On the other hand, interactions between two or more modes are possible leading to physical phenomena such as correlations and entanglement. To understand how

dissipative fermionic system describes such dynamics, first suppose we have a composite fermionic Gaussian system described by $N$ Majorana modes in the basis $(c_{j-1}, c_{2j})$, with $j = 1, 2, \cdots, N$ labelling the modes. In section 5, we were able to construct the Hamiltonian matrix (5.32), covariance matrix (5.42) and the $A$ and $C$ matrices in (7.1) by considering the Majorana basis so that adjacent pairs of rows and columns making up the matrices would correspond to individual modes. Thus in this mode basis, a general $2N \times 2N$ covariance matrix $\Gamma_\nu$ of a fermionic system is written as

$$\Gamma_\nu^{ab} = \begin{pmatrix} \Gamma_1 & \delta_{12} & \dots & \delta_{1N} \\ -\delta_{12}^T & \Gamma_2 & \dots & \delta_{2N} \\ \vdots & \vdots & \ddots & \vdots \\ -\delta_{1N}^T & -\delta_{2N}^T & \dots & \Gamma_N \end{pmatrix}, \tag{7.15}$$

where the $2 \times 2$ block diagonal terms $\Gamma_j$, describe the correlations within each mode, and the off diagonal terms $\delta_{jk}$ describe the correlations between the $j$ and $k$ modes. Relating this to the GGME (7.1), we can describe the block diagonal (block off diagonal) terms in $A$ and $C$ as those generating the single (multimode) dynamics respectively. So by definition, a multimode dynamic is one that directly or indirectly couple different modes of the system through an environment.

### 7.2.4 State dependent vs state independent dynamics

A state dependent dynamic may be defined as one where update rules are not fixed with time, but rather changes as a function of the current state of the system.

Now consider again Eq. (7.1). We see that the linear terms generated by the matrix $A$, would correspond to state dependent part of the dynamics as its effect on the states's covariance matrix depends on the current state of the system. Conversely the affine term would be the state independent part of the dynamics.

## 7.3 Partitioning the different dynamics

To understand the distinction between different types of dynamics we discussed above, it is helpful we introduce a basis for a real $2 \times 2$ matrix,

$$\mathbb{1}_2 = \begin{pmatrix} 1 & 0 \\ 0 & 1 \end{pmatrix}, J = \begin{pmatrix} 0 & 1 \\ -1 & 0 \end{pmatrix}, X = \begin{pmatrix} 0 & 1 \\ 1 & 0 \end{pmatrix}, Z = \begin{pmatrix} 1 & 0 \\ 0 & -1 \end{pmatrix} \tag{7.16}$$

From equation (5.95), we expand $A$ over this basis in the second tensor factor as,

$$A = A_I \otimes \mathbb{1}_2 + A_j \otimes J + A_x \otimes X + A_z \otimes Z \tag{7.17}$$

We can write $\Omega = \mathbb{1} \otimes J$. In the previous section, we partitioned $A$ into its orthogonal and non-orthogonal parts, $A_{\text{O}}$ and $A_{\text{N}}$ by isolating its symmetric and antisymmetric parts. Likewise we partitioned $A$ into its active and passive parts. In this section, we will use the expansion in (7.17), we will isolate each part of $A$ that we have just described.

The following identities will be useful for our study

$$\text{anti}(A_\mu \otimes Y). = \begin{cases} \text{anti}(A_\mu) \otimes Y & \text{if} \quad Y \quad \text{is symmetric} \\ \\ \text{sym}(A_\mu) \otimes Y & \text{if} \quad Y \quad \text{is antisymmetric} \end{cases} \tag{7.18}$$

where we have defined the linear functions

$$\text{anti}(X) = X - X^T, \qquad \text{sym}(X) = X + X^T \tag{7.19}$$

Similarly

$$\text{sym}(A_\mu \otimes Y). = \begin{cases} \text{sym}(A_\mu) \otimes Y & \text{if} \quad Y \quad \text{is symmetric} \\ \\ \text{anti}(A_\mu) \otimes Y & \text{if} \quad Y \quad \text{is antisymmetric} \end{cases} \tag{7.20}$$

### 7.3.1 The case for state dependent dynamics

We have discussed in 7.2.4 that $A$ generates the state dependent part of the dissipative dynamics. In this section, we are going to partition $A$ following two steps. The first step involves partitioning $A$ into its orthogonal active $A_{\text{OA}}$, nonorthogonal active $A_{\text{NA}}$, orthogonal passive $A_{\text{OP}}$ and nonorthogonal passive $A_{\text{NP}}$ parts respectively. In the next step, we further partition the results above into single mode and mulitimode parts of $A$ dynamics.

#### *First step of partition*

The first thing we do is to find $A_{\text{OA}}$, the orthogonal active part of $A$. We note that the computation is tedious but straightforward, and the procedure can be applied to find

the other parts $A_{\text{OA}}, A_{\text{OA}}, A_{\text{OA}}$. To begin, we first compute $A_O$ which is given in (7.7) as $\text{anti}(A) = A - A^T$. Using the expansion of $A$ in (7.17),

$$\begin{aligned} A_{\text{O}} =& \text{anti}(A) = \text{anti}(A_I \otimes \mathbb{1}_2 + A_j \otimes J + A_x \otimes X + A_z \otimes Z) \\ =& \text{anti}(A_I \otimes \mathbb{1}_2) + \text{anti}(A_j \otimes J) + \text{anti}(A_x \otimes X) + \text{anti}(A_z \otimes Z) \end{aligned}$$

From the identity relation (7.18), we have

$$A_{\text{O}} \;=\; \text{anti}(A_I) \otimes \mathbb{1}_2 + \text{sym}(A_j) \otimes J + \text{anti}(A_x) \otimes X + \text{anti}(A_z) \otimes Z \tag{7.21}$$

Next we find the active part of $A_{\text{O}}$ which is given in (7.13) as

$$A_{\text{O}} = \Omega^{-1}\text{anti}(\Omega A_{\text{O}}) \tag{7.22}$$

Recall that $\Omega$ can be written as $\Omega = \mathbb{1}_N \otimes J$, so we first compute $\Omega A_{\text{O}}$. Making use of the identity $(A \otimes B)(C \otimes D) = (A \otimes C)(B \otimes D)$ and taking note that

$$J \otimes J = -\mathbb{1}_2, \;\; J \otimes X = Z, \;\; J \otimes Z = -X, \tag{7.23}$$

we obtain

$$\begin{aligned} \Omega A_{\text{O}} \;=& (\mathbb{1}_2 \otimes \omega)\Big(\text{anti}(A_I) \otimes \mathbb{1}_2 + \text{sym}(A_j) \otimes J + \text{anti}(A_x) \otimes X + \text{anti}(A_z) \otimes Z\Big) \\ =& \,\text{anti}(A_I) \otimes J - \text{sym}(A_j) \otimes \mathbb{1}_2 + \text{anti}(A_x) \otimes Z - \text{anti}(A_z) \otimes X \end{aligned}$$

and

$$\begin{aligned} &\text{anti}(\Omega A_{\text{O}}) \\ &=\text{anti}\Big(\text{anti}(A_I) \otimes J - \text{sym}(A_j) \otimes \mathbb{1}_2 + \text{anti}(A_x) \otimes Z - \text{anti}(A_z) \otimes X\Big) \\ &=\text{sym}(\text{anti}(A_I)) \otimes J - \text{anti}(\text{sym}(A_j)) \otimes \mathbb{1}_2 + \text{anti}(\text{anti}(A_x)) \otimes Z - \text{anti}(\text{anti}(A_z)) \otimes X \\ &=\text{anti}(\text{anti}(A_x)) \otimes Z - \text{anti}(\text{anti}(A_z)) \otimes X \end{aligned} \tag{7.24}$$

where we have used that sym and anti are orthogonal projectors, that is for any matrix $Y$,

$$\begin{aligned} \text{sym}(\text{anti}(Y)) &= \text{sym}(Y - Y^T) = (Y - Y^T) + (Y - Y^T)^T = 0 \\ \text{anti}(\text{sym}(Y)) &= \text{anti}(Y + Y^T) = (Y + Y^T) - (Y + Y^T)^T = 0 \end{aligned}$$

Finally multiplying the resulting $\text{anti}(A_{\text{OA}})$ (7.24) by $\Omega^{-1}$ on the left,

$$\begin{aligned} A_{\text{OA}} =& \Omega^{-1}\text{anti}(\Omega A_{\text{O}}) \\ =& -(\mathbb{1}_2 \otimes J)(\text{anti}(\text{anti}(A_x)) \otimes Z - \text{anti}(\text{anti}(A_z)) \otimes X) \\ =& \,\text{anti}(A_x) \otimes X + \text{anti}(A_z) \otimes Z. \end{aligned} \tag{7.25}$$

In obtaining the last line, we again used the relation (7.23). Thus the orthogonal active part of $A$ given by $A_{\text{OA}}$ is the sum of two $N$ by $N$ antisymmetric matrices tensored with $X$ and $Z$. We can perform similar analysis on the other parts of $A$ yielding

$$A_{\text{OA}} = A_{x,\text{anti}} \otimes X + A_{z,\text{anti}} \otimes Z, \tag{7.26a}$$
$$A_{\text{OP}} = A_{1,\text{anti}} \otimes \mathbb{1}_2 + A_{w,\text{sym}} \otimes J, \tag{7.26b}$$
$$A_{\text{NA}} = A_{1,\text{sym}} \otimes \mathbb{1}_2 + A_{w,\text{anti}} \otimes J, \tag{7.26c}$$
$$A_{\text{NP}} = A_{x,\text{sym}} \otimes X + A_{z,\text{sym}} \otimes Z, \tag{7.26d}$$

where $A_{\mu,\text{sym}}$ and $A_{\mu,\text{anti}}$ are some symmetric and antisymmetric $N$ by $N$ matrices for $\mu \in \{1, j, x, z\}$.

***Second step of partition***

Finally each of these can be further subdivided into its single and multi-mode parts by isolating their block diagonal elements. Note that in the expansion given by (7.17) the block diagonal elements of, for instance, the $A_x \otimes X$ term correspond to the diagonal elements of $A_x$. Defining $A^D_\mu$ to be the diagonal elements of $A_\mu$ we find the single mode parts of each term to be,

$$A^{\text{S}}_{\text{OA}} = A^D_{x,anti} \otimes X + A^D_{z,anti} \otimes Z = 0 \tag{7.27a}$$
$$A^{\text{S}}_{\text{OP}} = A^D_{1,anti} \otimes \mathbb{1}_2 + A^D_{j,sym} \otimes J = A^D_{j,sym} \otimes J, \tag{7.27b}$$
$$A^{\text{S}}_{\text{NA}} = A^D_{1,sym} \otimes \mathbb{1}_2 + A^D_{j,anti} \otimes J = A^D_{1,sym} \otimes \mathbb{1}_2, \tag{7.27c}$$
$$A^{\text{S}}_{\text{NP}} = A^D_{x,sym} \otimes X + A^D_{z,sym} \otimes Z. \tag{7.27d}$$

Note that the single-mode orthogonal active state-dependent part of the dynamics ($A^{\text{S}}_{\text{OA}}$) vanishes since the diagonals of an antisymmetric matrices are zero. The multi-mode parts of each term are given by the difference between the terms and their single mode parts, $A^{\text{M}} = A - A^{\text{S}}$. From the classification above, we see that one cannot have dynamics which is single-mode, orthogonal and active, that is $A_{OA}$ is always multi-mode, while every other combination is possible.

### 7.3.2 The case for state independent dynamics

We turn our attention to partitioning the state-independent part of our dissipative dynamics. As discussed already this is given by the antisymmetric matrix $C$ which was shown

in 7.2.1 to be entirely non-orthogonal $C_{\mathrm{N}} = C$ and $C_{\mathrm{O}} = 0$. So what we need to do is to compute the single-mode and multi-mode parts of $C$ followed by the active and passive parts.

To begin, we can expand $C$ over the $2 \times 2$ basis (7.16) as we did for $A$.

$$C = C_{\mathrm{N}} = C_1 \otimes \mathbb{1}_2 + C_j \otimes J + C_x \otimes X + C_z \otimes Z, \tag{7.28}$$

where $C_\mu$ are $N$ by $N$ matrices for $\mu \in \{1, j, x, z\}$. Since $C$ must be an antisymmetric matrix, it follows that its coefficient matrices in the expansion (7.28) must be either symmetric or antisymmetric depending on their accompanying tensor factor. Specifically, since $\mathbb{1}_2$, $X$, and $Z$ are symmetric $C_1$, $C_x$, and $C_z$ must be antisymmetric. Similarly since $J$ is antisymmetric $C_j$ must be symmetric.

### *First step of partition*

We want to compute the single and multimode parts of $C_{\mathrm{N}}$. As before this means splitting $C_{\mathrm{N}}$ into its block-diagonal and block-off-diagonal elements. This again corresponds to isolating the diagonal elements of $C$'s coefficient matrices

$$\begin{aligned} C_{\mathrm{N}}^{\mathrm{S}} &= C_1^D \otimes \mathbb{1}_2 + C_J^D \otimes J + C_x^D \otimes X + C_z^D \otimes Z \\ &= C_J^D \otimes J, \end{aligned} \tag{7.29}$$

and

$$C_{\mathrm{N}}^{\mathrm{M}} = C_{\mathrm{N}} - C_{\mathrm{N}}^{\mathrm{S}} \tag{7.30}$$

where we have again exploited the fact that the diagonals of antisymmetric matrices vanish.

### *Second step of partition*

Next we will divide the resulting $C_{\mathrm{N}}^{\mathrm{M}}$ and $C_{\mathrm{N}}^{\mathrm{S}}$ into their active and passive parts respectively, according to how it affects a system's average excitation number. Recalling equation (7.12) we can see that $C$ contributes to the average excitation number through the trace of $\Omega C$. To see how this works, we will compute $C$'s contribution to the change of particle number; that implies computing $\mathrm{Tr}[\Omega C] = \mathrm{Tr}(\Omega C_{\mathrm{N}}^{\mathrm{S}}) + \mathrm{Tr}(\Omega C_{\mathrm{N}}^{\mathrm{M}})$. Starting with the multimode

| | Active | | Passive | |
|---|---|---|---|---|
| **Orthogonal** | $A_{\rm OA}^{(\ /{\rm M})}$ | | $A_{\rm OP}^{({\rm S}/{\rm M})}$ | |
| **Non-orthogonal** | $A_{\rm NA}^{({\rm S}/{\rm M})}$ | $C_{\rm NA}^{({\rm S}/\ )}$ | $A_{\rm NP}^{({\rm S}/{\rm M})}$ | $C_{\rm NP}^{(\ /{\rm M})}$ |
| | **S.D.** | **S.I.** | **S.D.** | **S.I.** |

Table 7.1: The results of the partition performed in Sec. 7.3.1. Note each cell is divided horizontally into a state-dependent (S.D.) and state-independent (S.I.) part. The superscripts on each term indicate whether or not such terms can be single-mode (S) or multi-mode (M) or both. An empty cell indicates the dynamics is not possible. Note that the partition has revealed that only 9 of the potential 16 types of dynamics are realized.

component of $C$,

$$\begin{aligned}\mathrm{Tr}(\Omega C_{\rm N}^{\rm M}) &= \mathrm{Tr}\Big((\mathbb{1}_2\otimes J)(C_1^{oD}\otimes\mathbb{1}_2 + C_j^{oD}\otimes J + C_x^{oD}\otimes X + C_z^{oD}\otimes Z)\Big)\\ &= \mathrm{Tr}\Bigg((\mathbb{1}_2\otimes C_{\rm N}^{oD})(J\otimes\mathbb{1}_2) + (\mathbb{1}_2\otimes C_{\rm N}^{oD})(J\otimes J)\\ &\qquad + (\mathbb{1}_2\otimes C_{\rm N}^{oD})(J\otimes X) + (\mathbb{1}_2\otimes C_{\rm N}^{oD})(J\otimes Z)\Bigg) \;=\; 0\end{aligned}$$

where "$C_{\rm N}^{oD}$" denotes off diagonal element of the matrix $C$. The trace is vanishing because its element is off-diagonal. So we conclude following 7.2.2 that the multimode component of $C$ is passive. Next we look at the single mode component of $C_{\rm N}$

$$\begin{aligned}\mathrm{Tr}(\Omega C_{\rm N}^{\rm S}) &= \mathrm{Tr}\Big((\mathbb{1}_N\otimes J)(C_1^{D}\otimes\mathbb{1}_2 + C_j^{D}\otimes J + C_x^{D}\otimes X + C_z^{D}\otimes Z)\Big)\\ &= \mathrm{Tr}\Bigg((\mathbb{1}_2\otimes C_{\rm N}^{D})(J\otimes\mathbb{1}_2) + (\mathbb{1}_2\otimes C_{\rm N}^{D})(J\otimes\omega)\\ &\qquad + (\mathbb{1}_2\otimes C_{\rm N}^{D})(J\otimes X) + (\mathbb{1}_2\otimes C_{\rm N}^{D})(J\otimes Z)\Bigg)\\ &= \mathrm{Tr}\Big((\mathbb{1}_2\otimes C_{\rm N}^{D})(J\otimes J)\Big) = -\mathrm{Tr}\Big(C_j^{D}\otimes\mathbb{1}_2\Big)\end{aligned}$$

So the diagonal elements of $C_\omega$ determine if $C$ is active or not. Thus we are led to identify the active and passive parts of $C$ as,

$$C_{\mathrm{NA}} = C_\omega^D \otimes \omega, \tag{7.31}$$
$$C_{\mathrm{NP}} = C - C_{\mathrm{NA}}, \tag{7.32}$$

respectively. Coincidentally these are the same terms we found when dividing $C$ into its single and multi-mode parts, $C_{\mathrm{N}}^{\mathrm{S}} = C_{\mathrm{NA}} = C_{\mathrm{NA}}^{\mathrm{S}}$ and $C_{\mathrm{N}}^{\mathrm{M}} = C_{\mathrm{NP}} = C_{\mathrm{NP}}^{\mathrm{M}}$.

The results of this partition are summarized in Table 7.1. Note that the partition has revealed that only 9 of the potential 16 types of dynamics are realized.

### 7.3.3 Complete positivity

Table 7.1 shows that an open system in the fermionic setting is capable of producing nine distinct types of dynamics. It follows that not all of these dynamics are completely positive in isolation. As we stated earlier, dynamics in the fermionic setting is said to be a valid dynamics if it satisfies the positivity condition (7.2)

$$A + A^T + \mathrm{i}C \leq 0. \tag{7.33}$$

We will show that any non-orthogonal dynamics (either $C \neq 0$ or $A_{\mathrm{N}} \neq 0$) must be accompanied by a non-zero amount of noise. We prove this by showing that for completely positive dynamics $C \neq 0$ implies $A_{\mathrm{N}} \neq 0$ which itself implies $\mathrm{Tr}(\mathrm{A_N}) < 0$. Following this we will show that $A_{\mathrm{NA}}^{\mathrm{S}}$ is the only part of the dynamics which contributes to this trace. Later, in the chapter we will show why it is appropriate to interpret $A_{\mathrm{NA}}^{\mathrm{S}}$ as generating noise.

*Proof.* To begin our proof, we note that according to (7.8), we can rewrite (7.33) as

$$2A_{\mathrm{N}} + \mathrm{i}C \leq 0, \tag{7.34}$$

Taking the complex conjugate of (7.34) gives

$$2A_{\mathrm{N}} - \mathrm{i}C \leq 0 \tag{7.35}$$

We see from (7.34) and (7.35) that if $A_{\mathrm{N}} = 0$, then $\mathrm{i}C \leq 0$ and $-\mathrm{i}C \leq 0$ (or equivalently $\mathrm{i}C \geq 0$) respectively. The only way that both of these inequalities in $C$ can be true is if we have $C = 0$. Taking the contrapositive of this result gives $C \neq 0$ implies $A_{\mathrm{N}} \neq 0$.

***Properties of a non-positive matrix***

By adding (7.34) to its complex conjugate we see that completely positive dynamics has $A_{\text{N}} \leq 0$. Now the following properties follow for the non-positive matrix $A_{\text{N}}$

1. The eigenvalues of $A_{\text{N}}$ are all real and non-positive, which implies the sum of all eigenvalues are non-positive.

2. Since it is a theorem that the sum of all eigenvalues of a matrix is equal to its trace, it follows that

$$\text{Tr}(A_{\text{N}}) \leq 0 \tag{7.36}$$

Given that the eigenvalues of $A_{\text{N}}$ are non-positive, their sum can only vanish if they are themselves zero that is if $\text{Tr}(A_{\text{N}}) = 0$, which implies $A_{\text{N}} = 0$. Thus since we cannot have $A_{\text{N}}$ vanishing, then neither can $\text{Tr}(A_{\text{N}})$. So the inequality (7.36) reduces to

$$\text{Tr}(A_{\text{N}}) < 0, \tag{7.37}$$

which shows that for completely positive dynamics, the presence of any non-orthogonal dynamics implies that $\text{Tr}(A_{\text{N}}) < 0$.

Let us now go ahead to identify which part of the partitions in Table 7.1 contributes to this trace (7.37). Note that $A_N$ has both single mode and multimode passive (active) parts $A_{\text{NP}}^{s/m}(A_{\text{NA}}^{s/m})$ respectively. We start with the contribution from the passive part of the dynamics $A_{\text{NP}}$ given in (7.27a). So

$$\begin{aligned} \text{Tr}(A_{\text{NP}}) &= \text{Tr}(A_{x,\text{sym}} \otimes X + A_{z,\text{sym}} \otimes Z) \\ &= \text{Tr}(A_{x,\text{sym}})\ \text{Tr}(X) + \text{Tr}(A_{z,\text{sym}})\ \text{Tr}(Z) = 0 \end{aligned} \tag{7.38}$$

where we have it that $\text{Tr}(X) = \text{Tr}(Z) = 0$. With vanishing contribution from the passive part of the dynamics, this implies that the dynamics that contribute to $\text{Tr}(A_{\text{N}})$ must be active. Next we can argue that since the multi-mode parts of $A$ are block-off-diagonal they cannot contribute to this trace either. Thus the dynamics contributing to $\text{Tr}(A_{\text{N}})$ must be single-mode. Thus the only part of the dynamics contributing to $\text{Tr}(A_{\text{N}})$ is $A_{\text{NA}}^{\text{S}}$. □

Hence, completely positive non-orthogonal dynamics must have $A_{\text{NA}}^{\text{S}} \neq 0$. As we will see in the next section, this type of dynamics can be interpreted as generating noise. The fact that non-orthogonal (and more generally non-unitary) dynamics must be noisy is well

known and holds outside of the Gaussian context we are discussing here. The novel connection here is that for Gaussian fermionic systems this noise must be active. That is particle-number non-conserving and requiring an environment for its particle exchange. Though some active dynamics do not necessarily require an environment to exchange particles with, we also comment that such dynamics are not Gaussian, that is they do not map Gaussian states to Gaussian states and thus cannot be regarded as fermionic Gaussian maps.

Any non-trivial interaction with an environment must involve particle/excitation exchange with that environment, for at least some initial states. In other words, any completely positive interaction with an environment having no particle/excitation exchange is orthogonal and thus can be implemented/explained/modelled without that environment.

Moreover, since any state-independent dynamics is necessarily non-orthogonal it must also be noisy ($A^{\mathrm{S}}_{\mathrm{NA}} \neq 0$) in order to be completely positive. Since this noise term is state dependent, all completely positive fermionic Gaussian dynamics must include a state-dependent part.

Lastly, it is worth noting that complete positivity can be violated if the dynamics is non-Markovian [112]. In such cases non-orthogonal dynamics could in principle appear without an additional noise term.

## 7.4 Physical interpretation of the different partitions

Having completed the classification and partition of the dynamics, we now study the different types of dynamics that are possible for fermionic systems and how they relate to the partition we performed above. Note that it is sufficient to consider systems composed of one or two modes ($N = 1, 2$) in order to build illustrative examples of every type of dynamics

### 7.4.1 Single mode dynamics

The single mode simplifies the state space available to a fermionic system. Specifically, all physical single-mode states are thermal states with respect to their free Hamiltonian (5.16). The dynamics of a single mode are equally trivial. Since $N = 1$ the coefficient matrices of $A$ and $C$ in (7.17) and (7.28) are just scalars.

Let us see how our partitions apply to the single mode dynamics. From (7.27), the single mode dynamics summarizes to

$$A_{N=1} = a_{\text{OP}}\ \omega + a_{\text{NA}}\ \mathbb{1}_2 + a_{\text{NP,X}}\ X + a_{\text{NP,Z}}\ Z,$$

for some real parameters $a_{\text{OP}}$, $a_{\text{NA}}$, $a_{\text{NP,X}}$, and $a_{\text{NP,Z}}$. Likewise,

$$C_{N=1} = c_{\text{NA}}\omega,$$

for some real parameter $c_{\text{NA}}$. The complete positivity condition (5.90) here reduces to

$$-a_{\text{NA}}\ \mathbb{1}_2 \leq a_{\text{NP,X}}\ X + a_{\text{NP,Z}}\ Z - \frac{\mathrm{i}}{2}\, c_{\text{NA}}\omega$$

or equivalently,

$$-a_{\text{NA}}\ \mathbb{1}_2 \leq -(-a_{\text{NP,X}}\ X - a_{\text{NP,Z}}\ Z + \frac{\mathrm{i}}{2}\, c_{\text{NA}}\omega) \tag{7.39}$$

Taking the square of (7.39), we obtain

$$\begin{aligned} a_{\text{NA}}^2 &\geq (a_{\text{NP,X}}\ X + a_{\text{NP,Z}}\ Z - \frac{\mathrm{i}}{2}\, c_{\text{NA}}\omega)(a_{\text{NP,X}}\ X + a_{\text{NP,Z}}\ Z - \frac{\mathrm{i}}{2}\, c_{\text{NA}}\omega) \\ &\geq a_{\text{NP,X}}^2 + a_{\text{NP,Z}}^2 + \frac{1}{4}c_{\text{NA}}^2 \end{aligned}$$

so

$$a_{\text{NA}}\ \geq\ \sqrt{a_{\text{NP,X}}^2 + a_{\text{NP,Z}}^2 + c_{\text{NA}}^2/4}\ \geq\ 0. \tag{7.40}$$

Note that, as discussed above, the presence of any non-orthogonal dynamics necessitates the presence of $a_{\text{NA}} \neq 0$.

Recall that the covariance matrix for a single mode fermionic system is given by (5.46),

$$\Gamma = \nu\,\omega; \qquad \omega = \begin{pmatrix} 0 & 1 \\ -1 & 0 \end{pmatrix}, \tag{7.41}$$

where $\nu = \tanh(\beta E/2)$ is a temperature monotone and $E$ is the mode's excitation energy. Recall the parameter $\nu$ is related to the expected excitation number of the mode as $\langle \hat{n} \rangle = \frac{1}{2} - \frac{\nu}{2}$. In order for a state with covariance matrix (7.41) to be a physically valid state we must have $-1 \leq \nu \leq 1$ such that $0 \leq \langle \hat{n} \rangle \leq 1$. We will now go ahead to interpret the different single mode dynamics.

### *Orthogonal single mode dynamics*

Table 7.1 shows that our orthogonal single mode dynamics is passive and state dependent. Such dynamics is generated by $A^{\mathrm{S}}_{\mathrm{OP}}$ as shown in (7.6) and given in the form

$$A^{\mathrm{S}}_{\mathrm{OP}} = -E\,\omega, \qquad C = 0 \tag{7.42}$$

for a single $N = 1$ mode, where $E$ is some real parameter. To interpret this type of dynamics, we compute its effective Hamiltonian. From (7.6) we find

$$\hat{H}_{\mathrm{eff}} = \frac{-\mathrm{i}}{2} E(\hat{x}_1\hat{p}_1 - \hat{p}_1\hat{x}_1) = E(\hat{n}_1 - \frac{1}{2}). \tag{7.43}$$

Thus we can interpret this dynamics as the free evolution of the mode, where $E$ is its excitation energy. Similarly, the effect of this dynamics on the system's covariance matrix can be computed from (5.3.4)

$$\Gamma'(t) = A^{\mathrm{S}}_{\mathrm{OP}}\,\Gamma(t) + \Gamma(t)\,(A^{\mathrm{S}}_{\mathrm{OP}})^T \tag{7.44}$$

$$= -E\,\nu(t)\,(\omega\omega + \omega\omega^T) \;=\; 0 \tag{7.45}$$

that is, the dynamics that does not change the state of the system. One may have anticipated this by recalling that for one mode ($N = 1$) all physical states are thermal and therefore stationary under free evolution. This could also have been anticipated by noting that this dynamics is passive, and so cannot change $\langle\hat{n}\rangle$ (and therefore cannot change $\nu$ or $\Gamma$).

### *Non-orthogonal single-mode dynamics*

The partition described above identifies three types of non-orthogonal single-mode dynamics ($A^{\mathrm{S}}_{\mathrm{NA}}$, $C^{\mathrm{S}}_{\mathrm{NA}}$, and $A^{\mathrm{S}}_{\mathrm{NP}}$) and which we will now discuss in turn.

1. As discussed above, complete positivity requires that any non-orthogonal dynamics is accompanied by some $A^{\mathrm{S}}_{\mathrm{NA}} \neq 0$. For one mode ($N = 1$) the generator of this dynamics is of the form

   $$A^{\mathrm{S}}_{\mathrm{NA}} = -r\,\mathbb{1}_2 \tag{7.46}$$

   for some real parameter $r$. Complete positivity requires $r \geq 0$. Using equation (5.97) we can associate this dynamics with Lindblad operators that are linear in the Majorana operators.

   $$\hat{L}_1 = \sqrt{2\,r}\;\hat{x}_1, \qquad \hat{L}_2 = \sqrt{2\,r}\;\hat{p}_1. \tag{7.47}$$

Next we compute the effect of this dynamics on the system's covariance matrix, finding

$$\frac{\mathrm{d}}{\mathrm{d}t}\nu(t) = -2r\,\nu(t). \tag{7.48}$$

which can be rearranged to

$$\frac{\mathrm{d}\nu(t)}{\nu} = -2r\,\mathrm{d}t.$$

Integrating both sides then gives

$$\ln\left(\frac{\nu}{\nu_0}\right) = -2rt$$

and taking the exponential of both sides gives

$$\nu(t) = \nu_0 e^{-2rt} \tag{7.49}$$

which is a law that governs the exponential decay of $\nu$ at time $t$. Thus this dynamics causes $\nu$ to decay exponentially to zero at a rate $2\,r$. Once $\nu = 0$ the state is maximally mixed. Thus we can identify $A^{\mathrm{S}}_{\mathrm{NA}}$ as adding noise to the system.

2. Next let us now look at state-independent active non-orthogonal single-mode dynamics, that is $C^{\mathrm{S}}_{\mathrm{NA}}$. This type of dynamics is generated by

$$C^{\mathrm{S}}_{\mathrm{NA}} = c\,\omega \tag{7.50}$$

for some real parameter $c$. In order to be completely positive this dynamics must be accompanied by a minimum level of noise. Specifically, $A^{\mathrm{S}}_{\mathrm{NA}} = -r\,\mathbb{1}_2$ with $r \geq |c/2|$. Using equation (5.97) we can associate this dynamics with Lindblad operators that are linear in the Majorana operators.

$$\hat{L}_1 = \sqrt{r - c/2}\;\hat{a}_1, \qquad \hat{L}_2 = \sqrt{r + c/2}\;\hat{a}_1^\dagger. \tag{7.51}$$

Computing the effect of this dynamics on the system's covariance matrix, we find

$$\nu'(t) = -2r\;\nu(t) + c. \tag{7.52}$$

This results in $\nu$ being exponentially attracted towards $\nu(\infty) = c/2r$ at a rate $2\,r$. Note that the complete positivity of the dynamics implies that this final state of the system is physical, i.e. $-1 \leq \nu(\infty) \leq 1$. In the limiting case where $c = \pm 2r$ the system's final state has $\nu(\infty) = \pm 1$. These are the system's two pure states, $|0\rangle$ and $|1\rangle$. Hence we identify $C^{\mathrm{S}}_{\mathrm{NA}}$ dynamics as purifying the state.

3. Finally, let us look at state-dependent passive non-orthogonal single-mode dynamics, that is $A^{\text{S}}_{\text{NP}}$. This type of dynamics is generated by

$$A^{\text{S}}_{\text{NP}} = b_x\, X + b_z\, Z \tag{7.53}$$

for some real parameters $b_x$ and $b_z$. In order to be completely positive this dynamics must be accompanied by a minimum level of noise. Specifically, $A^{\text{S}}_{\text{NA}} = -r\, \mathbb{1}_2$ with $r \geq \sqrt{b_x^2 + b_z^2}$.

Note that as we discussed in Section 7.2 our classification scheme is invariant under a change of local basis. Thus without loss of generality, it is sufficient to only investigate the $b_x$ term. Using equation (5.97) we can associate this term with Lindblad operators that are linear in the Majorana operators.

$$\hat{L}_1 = \sqrt{r - b_x}\ (\hat{x}_1 + \hat{p}_1), \qquad \hat{L}_2 = \sqrt{r + b_x}\ (\hat{x}_1 - \hat{p}_1). \tag{7.54}$$

As we saw with free evolution, this dynamics cannot affect $\nu$ since it is passive. However, this does not mean that this dynamics is completely trivial. As we will see in the next section, this dynamics affects the evolution of the mode's correlations with other uncoupled systems.

### 7.4.2 Multimode dynamics

We recall from (5.61), a generic covariance matrix for $N = 2$ modes can be written as

$$\Gamma = \begin{pmatrix} 0 & \nu_1 & g_1 & g_2 \\ -\nu_1 & 0 & g_3 & g_4 \\ -g_1 & -g_3 & 0 & \nu_2 \\ -g_2 & -g_4 & -\nu_2 & 0 \end{pmatrix}$$

for some local temperature monotones $\nu_1$ and $\nu_2$ and four correlation numbers: $g_1$, $g_2$, $g_3$, and $g_4$. Multi-mode dynamics couples these parameters together via the master equation (5.95). Specifically, the six parameters of the covariance matrix, $\boldsymbol{g} = \{\nu_1, \nu_2, g_1, g_2, g_3, g_4\}^\intercal$, will evolve under a system of first order differential equations as,

$$\boldsymbol{g}'(t) = \mathcal{A}\, \boldsymbol{g}(t) + \mathcal{C} \tag{7.55}$$

for some 6 by 6 real-valued matrix, $\mathcal{A}$, and 6 dimensional real-valued vector, $\mathcal{C}$.

In order to examine the effect of multi-mode dynamics we will convert the dynamics into the above form and then perform an eigen-decomposition of $\mathcal{A}$.

***Revisiting Single-Mode Dynamics***

Before we look at multi-mode dynamics let us look at how single-mode dynamics affect existing correlations.

First we will look at the effect of free rotation on the system's correlations. Taking each mode to have excitation energies, $E_1$ and $E_2$, their free evolution is generated by

$$A = -E_1\,\omega \oplus -E_2\omega. \tag{7.56}$$

Computing from (5.95) the rate of change of the covariance matrix using (7.56) and (5.61) we find

$$\frac{\mathrm{d}\Gamma}{\mathrm{d}t} = \begin{pmatrix} 0 & 0 & -E_2\,g_2 - E_1\,g_3 & E_2\,g_1 - E_1\,g_4 \\ & 0 & E_1\,g_1 - E_2\,g_4 & E_1\,g_2 + E_2\,g_3 \\ & & 0 & 0 \\ & & & 0 \end{pmatrix} \tag{7.57}$$

where the lower left triangle is the negation of the upper right one. Note that as expected the free rotation does not affect the reduced state of either system; $\nu_1$ and $\nu_2$ are constant. From this we can read off $\mathcal{A}$ as

$$\mathcal{A} = \begin{pmatrix} 0 & 0 & 0 & 0 & 0 & 0 \\ 0 & 0 & 0 & 0 & 0 & 0 \\ 0 & 0 & 0 & -E_2 & -E_1 & 0 \\ 0 & 0 & E_2 & 0 & 0 & -E_1 \\ 0 & 0 & E_1 & 0 & 0 & -E_2 \\ 0 & 0 & 0 & E_1 & E_2 & 0 \end{pmatrix}. \tag{7.58}$$

To analyze how the correlations effect each other we can diagonalize $\mathcal{A}$. However in this case it is more convenient to diagonalize $\mathcal{A}^2$, which is related to the second order differential equations $\boldsymbol{g}''(t) = \mathcal{A}^2\boldsymbol{g}(t)$ (note $\mathcal{C} = 0$). The result is

$$\frac{\mathrm{d}^2}{\mathrm{d}t^2}\begin{pmatrix} \nu_1 \\ \nu_2 \\ g_1 + g_4 \\ g_1 - g_4 \\ g_2 + g_3 \\ g_2 - g_3 \end{pmatrix} = \mathrm{diag}\begin{pmatrix} 0 \\ 0 \\ -(E_1 - E_2)^2 \\ -(E_1 + E_2)^2 \\ -(E_1 + E_2)^2 \\ -(E_1 - E_2)^2 \end{pmatrix}\begin{pmatrix} \nu_1 \\ \nu_2 \\ g_1 + g_4 \\ g_1 - g_4 \\ g_2 + g_3 \\ g_2 - g_3 \end{pmatrix} \tag{7.59}$$

where diag is the usual notation for a diagonal matrix with its non-zero elements given by the argument. Thus the correlations do rotate among themselves. In particular the $g_1 + g_4$

and $g_2 - g_3$ correlations oscillate at a rate $E_1 - E_2$ and the $g_1 - g_4$ and $g_2 + g_3$ correlations oscillate at a rate $E_1 + E_2$.

Next, let us examine the effect of $A^{\mathrm{s}}_{\mathrm{NP}}$ on multi-mode correlations. Since this dynamics is non-orthogonal we must introduce a certain amount of noise to make it completely positive. Restricting our attention to the $b_x$ term in (7.53) we can take

$$A = (-r\,\mathbb{1}_2 + b_x\,X) \oplus 0_2,$$

where $0_2$ is the 2 by 2 zero matrix and $r \geq |b_x|$ is required for complete positivity.

Computing $\mathcal{A}$ and diagonalizing it we find

$$\frac{\mathrm{d}}{\mathrm{d}t}\begin{pmatrix} \nu_1 \\ \nu_2 \\ g_1 + g_3 \\ g_1 - g_3 \\ g_2 + g_4 \\ g_2 - g_4 \end{pmatrix} = \mathrm{diag}\begin{pmatrix} -2\,r \\ 0 \\ -(r - b_x) \\ -(r + b_x) \\ -(r - b_x) \\ -(r + b_x) \end{pmatrix}\begin{pmatrix} \nu_1 \\ \nu_2 \\ g_1 + g_3 \\ g_1 - g_3 \\ g_2 + g_4 \\ g_2 - g_4 \end{pmatrix} \tag{7.60}$$

such that unless $b_x = \pm r$, all of the parameters of the covariance matrix (except $\nu_2$) are driven to zero. That is, eventually the first mode becomes maximally mixed and all of its correlations with the second mode are broken. The effect of $A^{\mathrm{s}}_{\mathrm{NP}}$ is to modify the rates at which the parameters decay. In the limiting case where $b_x = \pm r$ then the $g_1 \pm g_3$ and $g_2 \pm g_4$ correlations are completely shielded from this decay. For the purpose of our classification we will call this dynamics 'correlation shielding'.

Repeating this analysis on the $b_z$ term we find,

$$\frac{\mathrm{d}}{\mathrm{d}t}\begin{pmatrix} \nu_1 \\ \nu_2 \\ g_1 \\ g_2 \\ g_3 \\ g_4 \end{pmatrix} = \mathrm{diag}\begin{pmatrix} -2\,r \\ 0 \\ -(r - b_z) \\ -(r - b_z) \\ -(r + b_z) \\ -(r + b_z) \end{pmatrix}\begin{pmatrix} \nu_1 \\ \nu_2 \\ g_1 \\ g_2 \\ g_3 \\ g_4 \end{pmatrix} \tag{7.61}$$

where $r \geq |b_z|$ is required for complete positivity. Note that as before all of the parameters of the covariance matrix (except $\nu_2$) are again driven to zero unless $b_z = \pm r$. If $b_z = r$ then the $g_1$ and $g_2$ correlations are shielded from decay, and if $b_z = -r$ the $g_3$ and $g_4$ correlations are shielded.

***Orthogonal, passive and state-dependent dynamics***

For $N = 2$ the multi-mode orthogonal passive state-dependent dynamics are given by

$$A_{\text{OP}} = \begin{pmatrix} 0_2 & a_1 \mathbb{1}_2 + A_j \omega \\ -a_1 \mathbb{1}_2 + A_j \omega & 0_2 \end{pmatrix}. \tag{7.62}$$

Since this dynamics is orthogonal we can compute its effective Hamiltonian from Eq. (7.6) obtaining

$$\hat{H}_{\text{eff}} = \frac{\mathrm{i}}{2} b_1 (\hat{x}_1 \hat{x}_2 + \hat{p}_1 \hat{p}_2) + \frac{\mathrm{i}}{2} b_w (\hat{x}_1 \hat{p}_2 - \hat{p}_1 \hat{x}_2) + \text{h.c.} \tag{7.63}$$

Written in terms of the modes' creation and annihilation operators this is

$$\hat{H}_{\text{eff}} = (b_w + \mathrm{i} b_1) \hat{a}_1 \hat{a}_2^\dagger - (b_w - \mathrm{i} b_1) \hat{a}_1^\dagger \hat{a}_2. \tag{7.64}$$

Note that every term in this effective Hamiltonian has an equal number of creation and annihilation operators, such that it is manifestly number conserving/passive. We should also note that these are the type of terms that would arise from a "rotating wave"-like approximation.

To analyze the effect of this dynamics let us restrict our attention to the $b_w$ term. Computing and diagonalizing $\mathcal{A}^2$ we find,

$$\frac{\mathrm{d}^2}{\mathrm{d}t^2} \begin{pmatrix} \nu_1 - \nu_2 \\ \nu_1 + \nu_2 \\ g_1 + g_4 \\ g_1 - g_4 \\ g_2 + g_3 \\ g_2 - g_3 \end{pmatrix} = \text{diag} \begin{pmatrix} -4\, b_w^2 \\ 0 \\ -4\, b_w^2 \\ 0 \\ 0 \\ 0 \end{pmatrix} \begin{pmatrix} \nu_1 - \nu_2 \\ \nu_1 + \nu_2 \\ g_1 + g_4 \\ g_1 - g_4 \\ g_2 + g_3 \\ g_2 - g_3 \end{pmatrix}. \tag{7.65}$$

Thus we can see that this dynamics causes the difference in the modes' excitation level, $\nu_1 - \nu_2$, and the $g_4 + g_1$ correlations to oscillate at a rate $2\, b_w$.

Note that the remaining variables do not grow linearly with time but are constant. This can be shown by considering $\mathcal{A}$ (instead of $\mathcal{A}^2$), for which the equations reduce to

$$\frac{\mathrm{d}}{\mathrm{d}t} \begin{pmatrix} \nu_1 - \nu_2 \\ g_1 + g_4 \end{pmatrix} = \begin{pmatrix} 0 & 2\, b_w \\ -2\, b_w & 0 \end{pmatrix} \begin{pmatrix} \nu_1 - \nu_2 \\ g_1 + g_4 \end{pmatrix} \tag{7.66}$$

with all other first derivatives vanishing.

Repeating our analysis on the $b_1$ term we find the same result as above but the $g_2 - g_3$ correlation oscillates instead.

***Orthogonal active and state-dependent dynamics***

For $N = 2$ the multi-mode orthogonal active state-dependent dynamics are given by

$$A_{\text{OA}} = \begin{pmatrix} 0_2 & b_x X + b_z Z \\ -b_x X - b_z Z & 0_2 \end{pmatrix}. \tag{7.67}$$

Since this dynamics is orthogonal we can again from equation compute its effective Hamiltonian, obtaining

$$\hat{H}_{\text{eff}} = \frac{\mathrm{i}}{2} b_x (\hat{x}_1 \hat{p}_2 + \hat{p}_1 \hat{x}_2) + \frac{\mathrm{i}}{2} b_z (\hat{x}_1 \hat{x}_2 - \hat{p}_1 \hat{p}_2) + \text{h.c.} \tag{7.68}$$

Written in terms of creation and annihilation operators this is

$$\hat{H}_{\text{eff}} = (b_x + \mathrm{i} b_z) \hat{a}_1^\dagger \hat{a}_2^\dagger - (b_x - \mathrm{i} b_z) \hat{a}_1 \hat{a}_2. \tag{7.69}$$

Note that every term in this effective Hamiltonian has an unequal number of creation and annihilation operators, such that it is manifestly number non-conserving/active. We should also note that these are the terms which would be dropped when taking the "rotating wave"-like approximation.

To analyze the effect of this dynamics, let us restrict our attention to the $b_x$ term. Computing and diagonalizing $\mathcal{A}^2$ we find

$$\frac{\mathrm{d}^2}{\mathrm{d}t^2} \begin{pmatrix} \nu_1 + \nu_2 \\ \nu_1 - \nu_2 \\ g_1 + g_4 \\ g_1 - g_4 \\ g_2 + g_3 \\ g_2 - g_3 \end{pmatrix} = \text{diag} \begin{pmatrix} -4b_x^2 \\ 0 \\ 0 \\ -4b_x^2 \\ 0 \\ 0 \end{pmatrix} \begin{pmatrix} \nu_1 + \nu_2 \\ \nu_1 - \nu_2 \\ g_1 + g_4 \\ g_1 - g_4 \\ g_2 + g_3 \\ g_2 - g_3 \end{pmatrix}. \tag{7.70}$$

Thus we can see this dynamics causes the total excitation level, $\nu_1 + \nu_2$, and the $g_1 - g_4$ correlations to oscillate at a rate $2b_x$. One can imagine the modes both becoming more excited and unexcited in unison while correlations between them rise and fall. As before, the remaining variables do not grow linearly with time but are constant.

Repeating our analysis on the $b_z$ term we find the same result as above but the $g_2 + g_3$ correlations oscillate instead.

***Non-orthogonal active and state-dependent dynamics***

For $N = 2$ the multi-mode non-orthogonal active state-dependent dynamics are given by

$$A_{\text{NA}} = \begin{pmatrix} 0_2 & b_1 \mathbb{1}_2 + b_w \omega \\ b_1 \mathbb{1}_2 - b_w \omega & 0_2 \end{pmatrix}. \tag{7.71}$$

Since this dynamics is non-orthogonal we must introduce a certain amount of noise to make it completely positive. Restricting our attention to the $b_w$ term we first examine

$$A = \begin{pmatrix} -r\,\mathbb{1}_2 & b_w\,\omega \\ -b_w\,\omega & -r\,\mathbb{1}_2 \end{pmatrix}, \tag{7.72}$$

where $r \geq |b_w|$ is required for complete positivity.

Using equation (5.97) we can associate this term with Lindblad operators that are linear in the Majorana operators.

$$\hat{L}_1 = \sqrt{r - b_w}\ (\hat{x}_1 + \hat{p}_2), \quad \hat{L}_2 = \sqrt{r - b_w}\ (\hat{p}_1 - \hat{x}_2), \tag{7.73}$$

$$\hat{L}_3 = \sqrt{r + b_w}\ (\hat{x}_1 - \hat{p}_2), \quad \hat{L}_4 = \sqrt{r + b_w}\ (\hat{p}_1 + \hat{x}_2). \tag{7.74}$$

Computing and diagonalizing $\mathcal{A}$ we find,

$$\frac{\mathrm{d}}{\mathrm{d}t} \begin{pmatrix} \nu_1 + \nu_2 + g_1 + g_4 \\ \nu_1 + \nu_2 - g_1 - g_4 \\ \nu_1 - \nu_2 \\ g_1 - g_4 \\ g_2 + g_3 \\ g_2 - g_3 \end{pmatrix} = \text{diag} \begin{pmatrix} -2(r + b_w) \\ -2(r - b_w) \\ -2r \\ -2r \\ -2r \\ -2r \end{pmatrix} \begin{pmatrix} \nu_1 + \nu_2 + g_1 + g_4 \\ \nu_1 + \nu_2 - g_1 - g_4 \\ \nu_1 - \nu_2 \\ g_1 - g_4 \\ g_2 + g_3 \\ g_2 - g_3 \end{pmatrix}. \tag{7.75}$$

Note that unless $b_w = \pm r$, all of the parameters of the covariance matrix are suppressed to zero; The modes become maximally mixed and uncorrelated. The effect of this dynamics is to modify the rates at which the parameters decay. In the limiting case where $b_w = \pm r$ the final state may still have some correlations. For example if $b_w = -r$ then the sum, $\nu_1 + \nu_2 + g_1 + g_4$, is preserved resulting in the final state

$$\Gamma(\infty) = \begin{pmatrix} 0 & k & k & 0 \\ -k & 0 & 0 & k \\ -k & 0 & 0 & k \\ 0 & -k & -k & 0 \end{pmatrix}, \tag{7.76}$$

where $k = \frac{1}{4}(\nu_1 + \nu_2 + g_1 + g_4)|_{t=0}$.

The $b_1$ term provides similar phenomenology, shielding either the sum $\nu_1 + \nu_2 + g_3 - g_2$ or $\nu_1 + \nu_2 - g_3 + g_2$.

***Non-orthogonal, passive and state-dependent***

For $N = 2$ the multi-mode, non-orthogonal, passive, state-dependent dynamics are given by,

$$A_{\text{NP}} = \begin{pmatrix} 0_2 & b_x\, X + b_z\, Z \\ b_x\, X + b_z\, Z & 0_2 \end{pmatrix}. \tag{7.77}$$

Since this dynamics is non-orthogonal we must introduce a certain amount of noise to make it completely positive. Restricting our attention to the $b_x$ term we have,

$$A = \begin{pmatrix} -r\, \mathbb{1}_2 & b_x\, X \\ b_x\, X & -r\, \mathbb{1}_2 \end{pmatrix}, \tag{7.78}$$

where $r \geq |b_x|$ is required for complete positivity.

Using equation (5.97) we can associate this term with Lindblad operators which are linear in the Majorana operators.

$$\hat{L}_1 = \sqrt{r - b_w}\ (\hat{x}_1 + \hat{p}_2), \quad \hat{L}_2 = \sqrt{r - b_w}\ (\hat{p}_1 + \hat{x}_2), \tag{7.79}$$

$$\hat{L}_3 = \sqrt{r + b_w}\ (\hat{x}_1 - \hat{p}_2), \quad \hat{L}_4 = \sqrt{r + b_w}\ (\hat{p}_1 - \hat{x}_2). \tag{7.80}$$

Computing and diagonalizing $\mathcal{A}$ we find,

$$\frac{\mathrm{d}}{\mathrm{d}t} \begin{pmatrix} \nu_1 + \nu_2 \\ \nu_1 - \nu_2 + g_1 - g_4 \\ \nu_1 - \nu_2 - g_1 + g_4 \\ g_4 + g_1 \\ g_2 + g_3 \\ g_2 - g_3 \end{pmatrix} = \text{diag} \begin{pmatrix} -2r \\ -2(r - b_x) \\ -2(r + b_x) \\ -2r \\ -2r \\ -2r \end{pmatrix} \begin{pmatrix} \nu_1 + \nu_2 \\ \nu_1 - \nu_2 + g_1 - g_4 \\ \nu_1 - \nu_2 - g_1 + g_4 \\ g_4 + g_1 \\ g_2 + g_3 \\ g_2 - g_3 \end{pmatrix}. \tag{7.81}$$

Once again, unless $b_x = \pm r$, all the parameters are suppressed to zero. The effect of this dynamics is to modify the rates at which the parameters decay. In the limiting case where $b_x = \pm r$ the final state may still have excitations and correlations. For example if $b_x = -r$ then the sum $\nu_1 - \nu_2 + g_1 - g_4$ is preserved resulting in the state

$$\Gamma(\infty) = \begin{pmatrix} 0 & k & k & 0 \\ -k & 0 & 0 & -k \\ -k & 0 & 0 & -k \\ 0 & k & k & 0 \end{pmatrix}, \tag{7.82}$$

where $k = \frac{1}{4}(\nu_1 - \nu_2 + g_1 - g_4)|_{t=0}$.

The $b_z$ term provides similar phenomenology, shielding either the sum $\nu_1 - \nu_2 + g_2 + g_3$ or $\nu_1 - \nu_2 - g_2 - g_3$.

***Non-orthogonal, passive and state-independent dynamics***

The final type of dynamics identified by the partition described above is given by

$$C_{\mathrm{NP}}^{\mathrm{S}} = \begin{pmatrix} 0 & 0 & c_1 & c_2 \\ 0 & 0 & c_3 & c_4 \\ -c_1 & -c_3 & 0 & 0 \\ -c_2 & -c_4 & 0 & 0 \end{pmatrix}. \tag{7.83}$$

This dynamics adds directly to the $g_1$, $g_2$, $g_3$, and $g_4$ correlations.

Since this dynamics is non-orthogonal we must introduce some noise to make it completely positive. Taking

$$A = \begin{pmatrix} -r\,\mathbb{1}_2 & 0 \\ 0 & -r\,\mathbb{1}_2 \end{pmatrix}, \qquad C = \begin{pmatrix} 0 & 0 & c_1 & c_2 \\ 0 & 0 & c_3 & c_4 \\ -c_1 & -c_3 & 0 & 0 \\ c_2 & -c_4 & 0 & 0 \end{pmatrix} \tag{7.84}$$

we compute $\mathcal{A}$ and $\mathcal{C}$ to find

$$\frac{\mathrm{d}}{\mathrm{d}t}\begin{pmatrix} \nu_1 \\ \nu_2 \\ g_1 \\ g_2 \\ g_3 \\ g_4 \end{pmatrix} = \mathrm{diag}\begin{pmatrix} -2r \\ -2r \\ -2r \\ -2r \\ -2r \\ -2r \end{pmatrix}\begin{pmatrix} \nu_1 \\ \nu_2 \\ g_1 \\ g_2 \\ g_3 \\ g_4 \end{pmatrix} + \begin{pmatrix} 0 \\ 0 \\ c_1 \\ c_2 \\ c_3 \\ c_4 \end{pmatrix}. \tag{7.85}$$

The solution to these equations have both $\nu_1$ and $\nu_2$ decaying to zero at a rate $2r$, while the correlation $g_i$ decays to $g_i(\infty) = c_i/2r$ at a rate $2r$.

Note that as we discussed in Section 7.2 our classification scheme is invariant under a change of local basis. Using this freedom we can take a representative scenario with $c_2 = 0$ and $c_3 = 0$. In this case we can assign equation (5.97) to this type of dynamics with Lindblad operators that are linear in the Majorana operators.

$$\hat{L}_1 = \sqrt{r - c_1/2}\,(\hat{x}_1 - \mathrm{i}\,\hat{x}_2), \quad \hat{L}_2 = \sqrt{r + c_1/2}\,(\hat{x}_1 + \mathrm{i}\,\hat{x}_2), \tag{7.86}$$

$$\hat{L}_3 = \sqrt{r - c_4/2}\,(\hat{p}_1 - \mathrm{i}\,\hat{p}_2), \quad \hat{L}_4 = \sqrt{r + c_4/2}\,(\hat{p}_1 + \mathrm{i}\,\hat{p}_2). \tag{7.87}$$

| Single-mode? (else Multi-mode) | Orthogonal? (else Non-orthogonal) | Passive? (else Active) | State-Dependent? (else Independent) | Name of dynamics |
|---|---|---|---|---|
| Yes | Yes | Yes | Yes | $A^{\mathrm{S}}_{\mathrm{OP}}$: Free Evolution |
| Yes | Yes | Yes | No | Not Possible |
| Yes | Yes | No | Yes | Not Possible |
| Yes | Yes | No | No | Not Possible |
| Yes | No | Yes | Yes | $A^{\mathrm{S}}_{\mathrm{NP}}$: Correlation Shielding |
| Yes | No | Yes | No | Not Possible |
| Yes | No | No | Yes | $A^{\mathrm{S}}_{\mathrm{NA}}$: Noise |
| Yes | No | No | No | $C^{\mathrm{S}}_{\mathrm{NA}}$: Purifying |
| No | Yes | Yes | Yes | $A^{\mathrm{M}}_{\mathrm{OP}}$: Multi-mode Rotation |
| No | Yes | Yes | No | Not Possible |
| No | Yes | No | Yes | $A^{\mathrm{M}}_{\mathrm{OA}}$: Multi-mode Counter Rotation |
| No | Yes | No | No | Not Possible |
| No | No | Yes | Yes | $A^{\mathrm{M}}_{\mathrm{NA}}$: Multi-mode Active Corr. Shielding |
| No | No | Yes | No | $C^{\mathrm{M}}_{\mathrm{NP}}$: Correlating |
| No | No | No | Yes | $A^{\mathrm{M}}_{\mathrm{NP}}$: Multi-mode Passive Corr. Shielding |
| No | No | No | No | Not Possible |

Table 7.2: The partition performed in Sec. 7.3.1 results in nine distinct types of open fermionic Gaussian dynamics. Examples of each (and justifications for their names) are presented in the chapter.

## 7.5 Comparison with Bosonic Gaussian Dynamics

The mathematical structures underlying bosonic and fermionic GQM are very similar, but lead to vastly different phenomenology. Additional comparisons of bosonic and fermionic Gaussian systems can be found in [44] and [28].

Fundamentally their differences begin with how their (anti-)commutation relations are described on the system's phase space. In the fermionic/bosonic case we have

$$\{\hat{r}_n, \hat{r}_m\} = \delta_{nm}\hat{\mathbb{1}} \quad \text{vs.} \quad [\hat{r}_n, \hat{r}_m] = \Omega_{nm}\hat{\mathbb{1}}.$$

For fermionic systems symmetric combinations of Majorana operators are associated with the identity matrix on phase space whereas for bosonic systems antisymmetric combinations of quadrature operators are associated with the symplectic matrix $\Omega$.

In either case, Gaussian states are fully described by the system's first and second moments. In the fermionic case, non-trivial linear combinations of the Majorana operators are unphysical so all first moments vanish. Moreover the symmetric part of the second moments are fixed by the commutation relations. Thus all that is left is the antisymmetric covariance matrix $\Gamma_{nm} = \langle \mathrm{i}[\hat{r}_n, \hat{r}_m]\rangle$. In the bosonic case, the system may have non-trivial first moments (allowing for displaced/coherent states) and the symmetric part of the system's second moments are non-trivial, that is the system's covariance matrix $\sigma_{nm} = \langle \hat{r}_n, \hat{r}_m\rangle$. The overall difference is that fermionic Gaussian states are more restricted then bosonic ones.

In either case, the complete positivity condition is stated as the following matrix inequality for both bosonic and fermionic sytems:

$$-\mathbb{1}_{2N} \leq \mathrm{i}\Gamma \leq \mathbb{1}_{2N} \quad \text{vs.} \quad \mathrm{i}\Omega \leq \sigma. \tag{7.88}$$

One critical thing to note here is that in the fermionic case the two-sided bound in (7.88) above implies that the space of allowed states is compact, whereas in the bosonic case the state space is unbounded.

In either case, the unitary Gaussian transformations can be seen as linear transformations on the system's quadrature/Majorana operators. And in either case these turn out to be the transformations that preserve the system's (anti-)commutation relations. In the fermionic case these are orthogonal transformations (i.e. transformations that preserve the identity) and in the bosonic case they are symplectic transformations (i.e. transformations that preserve the symplectic form). An important difference between these groups is that the special orthogonal transformations form a compact group whereas the symplectic transformations do not.

Ultimately, fermionic Gaussian dynamics are notably more restricted than bosonic dynamics. The fermionic state space is smaller in several ways: its first moments all vanish (meaning no displaced states are possible), its covariance matrix is antisymmetric (which necessarily has less degrees of freedom than a symmetric matrix of the same dimension) and the state space itself is bounded/compact. As for the dynamics, comparing the fermionic partition performed here to the bosonic one performed in [58] we find two less types of dynamics are possible. Furthermore, due to the compactness of the state space, fermionic Gaussian dynamics must either be cyclic or evolve to a fixed point, there is no infinite direction for the state to head off towards. This is in contrast to the bosonic case where the state may be squeezed, displaced or heated to an arbitrary degree without converging to a fixed point.

## 7.6 Conclusion

We have introduced a classification of the generators of open fermionic Gaussian dynamics. Specifically we divided the generators of the dynamics along four lines:

1. unitary and non-unitary
2. active and passive
3. single-mode and multi-mode
4. state-dependent and state-independent

Of the potential sixteen types of dynamics expected of such a division, we find that seven of them vanish, leaving only nine types of fermionic Gaussian dynamics.

We have provided illustrative examples of each of these types of dynamics. Our analysis of the complete positivity of these dynamics indicates that the presence of any non-unitary effects necessitates the presence of noise in the dynamics. Since this noise is active (it involved particle flux with the environment), completely positive fermionic Gaussian dynamics is either unitary or involve particle exchange with its environment.

We have also provided comparison with a similar partitioning of bosonic Gaussian dynamics [58]. Overall, fermionic Gaussian states and transformation are more restricted than bosonic ones. For a finite number of modes, there are less degrees of freedom for both Gaussian states and transformations if the modes are fermionic as compared to if

they are bosonic. As we discussed these restrictions ultimately stem from the system's (anti-)commutation relations.

Work that applies this partition to the dynamics of quantum systems that are bombarded by a rapid succession of fermionic ancillae is in progress.

# Chapter 8

# Conclusion

## 8.1 Summary

In this thesis, we have investigated some leading problems in quantum physics as related to quantum computing and quantum information processing.

First is the problem of quantum decoherence; an effect that is attributed to quantum states that are in macroscopic superposition. Such states are characterized by quantum coherence and quantum entanglement–fundamental properties in quantum physics that characterize quantum devices thereby distinguishing them from their classical counterparts. An example in quantum optics is the quantum superposition of coherent states (SCS) that have equal amplitude but are 180 degrees out-of-phase. If we are able to harness these quantum superposition states to detect their various quantum effects and features, we are certain of developments and innovations in our communication and quantum technologies. Unfortunately, superposition states are very fragile; due to constant interactions with the environment, they easily lose their quantum coherence and quantum entanglement and rapidly decohere to a statistical mixture of coherent states (a counterpart of the quantum superposition of coherent states).

The loss of coherence in a quantum superposition of states is referred to as *decoherence*. Decoherence is the major reason we cannot observe superposition in our macroscopic world or even generate quantum superpositions of states such as the SCS. It follows that for applications in quantum information processing and testing quantum theories, we require quantum SCS that have high fidelity and large amplitude respectively. So far researchers have been able to generate SCS that only have small amplitudes. A recent proposal shows

that employing the effect of squeezing would help generate SCS that have large amplitudes and high fidelity. A detection mechanism that will probe and display the quantum effects in quantum superposition states is necessary.

In this regard and assuming we have access to a squeezed superposition of coherent states (SSCS), I presented a scheme that probes the quantum SSCS stored in a cavity. I do so without significantly modifying the quantum states. This scheme is the mode-invisibility measurement scheme which was presented first in [97] to probe a Fock state of light nondestructively. I showed that the mode-invisibility technique provides (at least in principle) a good measurement scheme for observing the quantum nature of a superposition of coherent states. I demonstrated this explicitly for the even, odd, and Yuker-Stoler cat states respectively. For small values of the magnitude $\alpha$ of the coherent state parameter, I find it straightforward to distinguish these states. The distinguishability of the three cat states is enhanced by squeezing. Interestingly, oscillations are present in the interferometric phase difference only when squeezing is introduced and absent without squeezing. Therefore our method also offers a scheme to distinguish between cat states and squeezed cat states.

In contrast to the several ways in which the nonclassical properties of coherent states have been investigated, our method provides a measure for studying the behaviour of a superposed cat state, most importantly distinguishing between them in a non-destructive way. Of course the natural question is how to realize this mode-invisibility technique in the laboratory and use it to study the decoherence properties of these cat states. We leave this project for future study.

More so I have demonstrated the utility of the mode-invisibility measurement technique for non-destructively probing the Bell cat state (that is entangled generalized qubit/cat state) in a cavity mode. In this state, the effect of the qubit-field coupling and probe-field coupling comes to play. For realistic physical parameters, and provided that the amplitude of the cavity field is not too large, the technique works very well, especially in the regime where the probe-cavity field coupling is approximately equal to the qubit-cavity field coupling. However the method breaks down once the amplitude of the cavity field is sufficiently large. I also investigated the dynamics of the qubit state and the von Neumann entropy of the combined system Bell cat state.

The second problem I investigated belongs to the field of quantum information processing with a link to quantum thermodynamics - this is the problem of work extraction from quantum systems, precisely from non-interacting fermionic systems. Passive states are those states for which work cannot be extracted via unitary transformations, that is those states whose average energy cannot be lowered through a unitary operation acting

on them. However some passive states may have extractable work if several copies of the system are processed through a unitary process acting on the global system– a state may be passive given only a single copy but can become active for $n$ copies. Completely passive states remain passive no matter how many copies of the system are available (an example is the thermal Gibb's state [106, 81], while those states that become active for some $k \geq n$ copies of the system are termed $k$-activable [125]. I showed that a fermionic mode in thermal state is k-activable, that is a fermionic mode in thermal state although passive, can be activated to yield work given three or more copies of the system. This number is sufficient and yields an upper bound on the number of copies needed.

On the other hand, although work can be extracted from non-passive states the unitary transformation required for this process is difficult to realize. Given that Gaussian unitaries are easily generated, one may consider extracting work via the restricted class of Gaussian unitaries, this introduces us to the notion of Gaussian passivity [22] which allows work to be extracted from quantum systems via Gaussian unitary operations. In the bosonic setting, the idea of extracting work from passive but not completely passive states via Gaussian unitary transformations have been established [22]. I extended the idea of Gaussian passivity to a system non-interacting fermionic modes in thermal states. I characterize general quantum states in fermionic systems according to their ability to yield work (or not) under such transformations. Overall, fermionic Gaussian transformations are more restricted than general unitary transformations for work extraction.

Lastly I studied the dynamics of open fermionic quantum systems. An open quantum system is one that is in constant interaction with its environment via exchange of energy or particles. This practically implies that the operation of any realistic quantum information devices (quantum computer for example) would be accompanied by noise and by loss of quantum information into the environment. Hence it is important to investigate how our quantum system in a realistic setting, would behave. In this regard I investigated the dynamics of an open Markovian non-interacting fermionic system. I have introduced a classification of the generators of open fermionic Gaussian dynamics. Specifically I divided the generators of the dynamics along four lines:

1. unitary and non-unitary
2. active and passive
3. single-mode and multi-mode
4. state-dependent and state-independent

Of the potential sixteen types of dynamics expected of such a division, we find that seven of them vanish, leaving only nine types of fermionic Gaussian dynamics.

I have provided illustrative examples of each of these types of dynamics. I have also provided comparison with a similar partitioning of bosonic Gaussian dynamics [58]. Overall, fermionic Gaussian states and transformation are more restricted than bosonic ones. For a finite number of modes, there are less degrees of freedom for both Gaussian states and transformations if the modes are fermionic as compared to if they are bosonic. As we discussed these restrictions ultimately stem from the system's (anti-)commutation relations.

## 8.2 Outlook

Some recommendations and possible future work are listed in this section.

### Exploring the mode-invisibility measurement scheme

We note here that the initial idea of the mode invisibility measurement scheme is to probe a given state of light without significantly perturbing it. This opens up new ideas to investigate some problems in quantum optics. I will list these possibilities for future work below.

#### *Quantum information processing*

Quantum superpositions of coherent states or what we have called the Schrödinger's cat states have a range of applications that extend from precision measurement, to quantum lithography and quantum information processing. Over the years, physicists have not only made critical observations of the superposition principle, but have in fact started working towards harnessing superposed states to build quantum computers required to fully implement quantum algorithms at increased power and speed.

With the aim of realizing a quantum computer, proposals to encode and implement a CNOT quantum gate using a superposition of coherent states in a realistic superconducting cavity-QED system have been made. Encoding based on superposition of states offer advantages over the traditional method of encoding based on number state. One is that the generation of superposition of coherent states in optical cavities are easily achievable

unlike generation of number states. Another is that superposition of coherent states are less prone to irreversible errors imposed by the environment than are number states.

Although encoding based on superposition of coherent states offers some advantages, we note that the slightest bit of perturbation may cause the system to decohere, such that the superposition is lost. Hence it is necessary to shield the quantum system from external noise in the surrounding environment.

We have seen that the mode invisibility measurement scheme will be useful for the purpose described above since it probes a system leaving it significantly unperturbed. Not only does it leave the system significantly unperturbed, it also acquires strong information about the system of interest. The main playground in this measurement scheme has been the elimination of the rotating wave terms in a system's interaction Hamiltonian with a detector. However such a term characterizes the Jaynes-Cummings interaction Hamiltonian. Since most light-matter interactions are described by the Jaynes-Cummings model, as such the rotating wave approximation in the Jaynes-Cummings model should be revisited.

### *Detection of weak force*

A research proposal for sensitive force detection using superpositions of coherent states have been proposed [92]. Here the weak force is modelled as a displacement operation on a coherent state. When the displacement operator $D(\beta)$ is applied on the even cat state

$$|\Psi\rangle_{\text{cat}} = \frac{1}{\sqrt{2}}(|\alpha\rangle + |-\alpha\rangle) \tag{8.1}$$

it displaces it by

$$|\Psi\rangle = \cos\theta|+\rangle + \sin\theta|-\rangle, \qquad \theta = -\text{Im}[\alpha\beta^*] \tag{8.2}$$

where $|\pm\rangle = \frac{1}{\sqrt{2}}(|\alpha\rangle \pm |-\alpha\rangle)$. The task is to find an optimal measurement scheme to estimate $\theta$ and hence the force parameter $\epsilon$. The maximum sensitivity is achieved when $\theta$ is maximized for a given displacement, that is when $\beta$ is purely imaginary. Setting $\beta = \text{i}\epsilon$, one obtains $\theta = \epsilon\alpha$.

Using the MI scheme, we propose to measure $\theta$ by considering a detection of the displaced state (8.2). Given that the MI scheme measures the average photon number in the cat states non-destructively, any disturbance in the measurement will display the presence of an external influence on the even cat state.

***Generation of Schrödinger cat states***

Another application of the MI scheme would be in generation of Schrödinger's cat state. Many schemes have successfully generated quantum superposition of coherent states with small amplitudes (called Schrödinger's kitten). Realizing Schrödinger's cat state that is superposition of coherent states with large amplitudes have been challenging.

We propose to generate one based on the ideas of MI scheme. This would involve obtaining an effective Hamiltonian in the limit where the necessary approximations are allowed.

## Building quantum heat machines

We have seen that for three fermionic modes, a product of three fermionic thermal states at different temperatures is non-passive. This shows that the minimum number of baths required to construct a heat engine in the fermionic setting is three.

Within thermodynamics, heat engines are devices that operate in a thermal context so as to extract ordered energy in the form of work. The traditional setup involves an engine that operates cyclically between two temperatures $T_{\text{hot}}, T_{\text{cold}}$ and performs a quantity of mechanical work. The engine operates according to the second law of thermodynamics, where it absorbs heat from the hot reservoir with temperature $T_{\text{hot}}$, converts some of this energy to mechanical work and pumps it into the cold reservoir with temperature $T_{\text{cold}}$. The largest possible efficiency is given by the Carnot formula: $\eta = 1 - \frac{T_{\text{cold}}}{T_{\text{hot}}}$, occurs for the reversible Carnot engine and provides a fundamental thermodynamic bound on the amount of ordered energy that can be obtained.

A future work would be to construct quantum heat engines that involves an engine operating cyclically between three temperatures in the fermionic setting.

# References


[1] Sumiyoshi Abe, A R Usha Devi, and A K Rajagopal. The thermostatistical aspect of werner-type states and quantum entanglement. *Journal of Physics A: Mathematical and Theoretical*, 43(4):045303, 2010.

[2] G. S. Agarwal. Vacuum-field rabi oscillations of atoms in a cavity. *Journal of the Optical Society of America B*, 2(3):480–485, 1985.

[3] Yakir Aharonov and Leonard Susskind. Charge superselection rule. *Phys. Rev.*, 155:1428–1431, Mar 1967.

[4] A. E Allahverdyan, R Balian, and Th. M Nieuwenhuizen. Maximal work extraction from finite quantum systems. 67(4):565–571, 2004.

[5] L. Allen and J. H. Eberly. *Optical Resonance and Two-level Atoms*. John Wley & Sons, Inc, 1975.

[6] M. R. Andrews, C. G. Townsend, H. J. Miesner, D. S. Durfee, D. M. Kurn, and W. Ketterle. Observation of interference between two bose condensates. *Science*, 275(5300):637, 01 1997.

[7] Alain Aspect, Philippe Grangier, and Gérard Roger. Experimental realization of einstein-podolsky-rosen-bohm *Gedankenexperiment* : A new violation of bell's inequalities. *Phys. Rev. Lett.*, 49:91–94, Jul 1982.

[8] G Badurek, H Rauch, J Summhammer, U Kischko, and A Zeilinger. Direct verification of the quantum spin-state superposition law. 16(6):1133–1139, 1983.

[9] Charles H. Bennett, Herbert J. Bernstein, Sandu Popescu, and Benjamin Schumacher. Concentrating partial entanglement by local operations. *Phys. Rev. A*, 53:2046–2052, Apr 1996.

[10] Charles H. Bennett, Gilles Brassard, Claude Crépeau, Richard Jozsa, Asher Peres, and William K. Wootters. Teleporting an unknown quantum state via dual classical and einstein-podolsky-rosen channels. *Phys. Rev. Lett.*, 70:1895–1899, Mar 1993.

[11] Charles H. Bennett, David P. DiVincenzo, John A. Smolin, and William K. Wootters. Mixed-state entanglement and quantum error correction. *Phys. Rev. A*, 54:3824–3851, Nov 1996.

[12] P.R. Berman and N.D. *Cavity Quantum Electrodynamics*. Academic Press, 1994.

[13] S. Bose, I. Fuentes-Guridi, P. L. Knight, and V. Vedral. Subsystem purity as an enforcer of entanglement. *Physical Review Letters*, 87(5):050401–, 07 2001.

[14] Alonso Botero and Benni Reznik. Modewise entanglement of gaussian states. *Phys. Rev. A*, 67:052311, May 2003.

[15] Alonso Botero and Benni Reznik. Bcs-like modewise entanglement of fermion gaussian states. *Physics Letters A*, 331(1):39 – 44, 2004.

[16] V. B. Braginsky and F. Ya Khalili. Quantum Non-Demolition Measurements: The Route from Toys to Tools. *Rev. Mod. Phys.*, 68:565–582, 1996.

[17] Fernando G. S. L. Brandão, Michał Horodecki, Jonathan Oppenheim, Joseph M. Renes, and Robert W. Spekkens. Resource theory of quantum states out of thermal equilibrium. *Physical Review Letters*, 111(25):250404–, 12 2013.

[18] Sergey Bravyi. 2005. arXiv:quant-ph/0507282.

[19] Sergey Bravyi and Robert König. Classical simulation of dissipative fermionic linear optics. *Quantum Information & Computation*, 12(11-12):925–943, 2012.

[20] Sergey B. Bravyi and Alexei Yu. Kitaev. Fermionic quantum computation. *Annals of Physics*, 298(1):210 – 226, 2002.

[21] Stephan Briaudeau, Solomon Saltiel, Gerard Nienhuis, Daniel Bloch, and Martial Ducloy. Coherent doppler narrowing in a thin vapor cell: Observation of the dicke regime in the optical domain. *Phys. Rev. A*, 57:R3169–R3172, May 1998.

[22] Eric G Brown, Nicolai Friis, and Marcus Huber. Passivity and practical work extraction using gaussian operations. *New Journal of Physics*, 18(11):113028, 2016.

[23] M. Brune, E. Hagley, J. Dreyer, X. Maitre, A. Maali, C. Wunderlich, J. M. Raimond, and S. Haroche. Observing the progressive decoherence of the "meter" in a quantum measurement. *Phys. Rev. Lett.*, 77:4887–4890, Dec 1996.

[24] M. Brune, S. Haroche, V. Lefevre, J. M. Raimond, and N. Zagury. Quantum nondemolition measurement of small photon numbers by rydberg-atom phase-sensitive detection. *Phys. Rev. Lett.*, 65:976–979, Aug 1990.

[25] M. Brune, S. Haroche, and J. M. Raimond. Manipulation of Photons in a cavity by Dispersive Atom-Field Coupling: Quantum-Nondemolition Measurements and Generation of "Schrödinger Cat" States. *A.J. P.*, 45(7):5193–5214, 1992.

[26] M. Brune, S. Haroche, J. M. Raimond, L. Davidovich, and N. Zagury. Manipulation of photons in a cavity by dispersive atom-field coupling: Quantum-nondemolition measurements and generation of "schrödinger cat" states. *Phys. Rev. A*, 45:5193–5214, Apr 1992.

[27] V. Bužek, A. Vidiella-Barranco, and P. L. Knight. Superpositions of coherent states: Squeezing and dissipation. *Phys. Rev. A*, 45:6570–6585, May 1992.

[28] E. T. Campbell. Decoherence in open majorana systems. 2015. arXiv:quant-ph/1502.05626.

[29] Carlton M. Caves. Quantum-mechanical noise in an interferometer. *Phys. Rev. D*, 23:1693–1708, Apr 1981.

[30] Alex W. Chin, Susana F. Huelga, and Martin B. Plenio. Quantum metrology in non-markovian environments. *Phys. Rev. Lett.*, 109:233601, Dec 2012.

[31] J. I. Cirac, M. Lewenstein, K. Mølmer, and P. Zoller. Quantum superposition states of bose-einstein condensates. *Physical Review A*, 57(2):1208–1218, 02 1998.

[32] J F Corney and P D Drummond. Gaussian operator bases for correlated fermions. 39(2):269–297, 2005.

[33] Paulina Corona-Ugalde, Marvellous Onuma-Kalu, and Robert B. Mann. Mode invisibility as a nondestructive probe of entangled qubit-cat states. *Phys. Rev. A*, 96:033845, Sep 2017.

[34] L. Davidovich, M. Brune, J. M. Raimond, and S. Haroche. Mesoscopic quantum coherences in cavity qed: Preparation and decoherence monitoring schemes. *Phys. Rev. A*, 53:1295–1309, Mar 1996.

[35] L. Davidovich, M. Orszag, and N. Zagury. Quantum nondemolition measurements of vibrational populations in ionic traps. *Phys. Rev. A*, 54:5118–5125, Dec 1996.

[36] C. DAVISSON and L. H. GERMER. The scattering of electrons by a single crystal of nickel. *Nature*, 119(2998):558–560, 1927.

[37] LOUIS DE BROGLIE. Waves and quanta. *Nature*, 112(2815):540–540, 1923.

[38] Fernando de Melo, Piotr Ćwikliński, and Barbara M Terhal. The power of noisy fermionic quantum computation. *New Journal of Physics*, 15(1):013015, jan 2013.

[39] Samuel Deléglise, Igor Dotsenko, Clément Sayrin, Julien Bernu, Michel Brune, Jean-Michel Raimond, and Serge Haroche. Reconstruction of non-classical cavity field states with snapshots of their decoherence. *Nature*, 455:510 EP –, 09 2008.

[40] R. H. Dicke. Coherence in spontaneous radiation processes. *Physical Review*, 93(1):99–110, 01 1954.

[41] David P. DiVincenzo and Barbara M. Terhal. Fermionic linear optics revisited. *Foundations of Physics*, 35(12):1967–1984, Dec 2005.

[42] V. V. Dodonov, I. A. Malkin, and V. I. Man'ko. Even and odd coherent states and excitations of a singular oscillator. *Physica*, 72(3):597–615, 1974.

[43] J. H. Eberly, N. B. Narozhny, and J. J. Sanchez-Mondragon. Periodic spontaneous collapse and revival in a simple quantum model. *Physical Review Letters*, 44(20):1323–1326, 05 1980.

[44] J. Eisert and T. Prosen. Noise-driven quantum criticality. 2010. arXiv:quant-ph/1012.5013.

[45] Jens Eisert, Viktor Eisler, and Zoltán Zimborás. Entanglement negativity bounds for fermionic gaussian states. *Phys. Rev. B*, 97:165123, Apr 2018.

[46] Viktor Eisler and Zoltán Zimborás. On the partial transpose of fermionic gaussian states. *New Journal of Physics*, 17(5):053048, 2015.

[47] Stephen R. Friberg, Susumu Machida, and Yoshihisa Yamamoto. Quantum-nondemolition measurement of the photon number of an optical soliton. *Phys. Rev. Lett.*, 69:3165–3168, Nov 1992.

[48] Nicolai Friis, Marcus Huber, and Martí Perarnau-Llobet. Energetics of correlations in interacting systems. *Physical Review E*, 93(4):042135–, 04 2016.

[49] Unruh W. G. Analysis of quantum-nondemolition measurement. *Phys. Rev. D*, 18:1764–1772, Sep 1978.

[50] C C Gerry and P. L. Knight. *Introductory Quantum Optics*. Cambridge University Press, 2005.

[51] Christopher C. Gerry. Generation of schr\"odinger cats and entangled coherent states in the motion of a trapped ionby a dispersive interaction. *Physical Review A*, 55(3):2478–2481, 03 1997.

[52] A Gilchrist, Kae Nemoto, W J Munro, T C Ralph, S Glancy, Samuel L Braunstein, and G J Milburn. Schrödinger cats and their power for quantum information processing. *Journal of Optics B: Quantum and Semiclassical Optics*, 6(8):S828, 2004.

[53] Roy J. Glauber. Coherent and incoherent states of the radiation field. *Phys. Rev.*, 131:2766–2788, Sep 1963.

[54] M. Gluza, M. Kliesch, J. Eisert, and L. Aolita. Fidelity witnesses for fermionic quantum simulations. *Phys. Rev. Lett.*, 120:190501, May 2018.

[55] P. Grangier, J. A. Levenson, and J P Poizat. Generation of optical 'schrodinger cats' from photon number states. *Nature*, 448:784–786, 2007.

[56] Philippe Grangier, Juan Ariel Levenson, and Jean-Philippe Poizat. Quantum nondemolition measurements in optics. *Nature*, 396:537–542, 1998.

[57] Eliska Greplová and Géza Giedke. Degradability of fermionic gaussian channels. *Phys. Rev. Lett.*, 121:200501, Nov 2018.

[58] Daniel Grimmer, Eric Brown, Achim Kempf, Robert B Mann, and Eduardo Martín-Martínez. A classification of open gaussian dynamics. *Journal of Physics A: Mathematical and Theoretical*, 51(24):245301, 2018.

[59] S. Haroche and J. M. Raimond. *Exploring the Quantum Atoms, Cavities, and Photons*. Oxford University Press, 2006.

[60] Serge Haroche. Nobel Lecture: Controlling Photons in a Box and Exploring the Quantum to Classical Boundary. *Reviews of Modern Physics*, 85:1083–1099, 2013.

[61] Silas Hoffman, Constantin Schrade, Jelena Klinovaja, and Daniel Loss. Universal quantum computation with hybrid spin-majorana qubits. *Phys. Rev. B*, 94:045316, Jul 2016.

[62] Alexander Holevo. *Probalistic and Statistical Aspect of Quantum Theory.* Edizioni Della Normale, 2011.

[63] C. K. Hong and L. Mandel. Higher-order squeezing of a quantum field. *Physical Review Letters*, 54(4):323–325, 01 1985.

[64] Ryszard Horodecki, Paweł Horodecki, Michał Horodecki, and Karol Horodecki. Quantum entanglement. *Rev. Mod. Phys.*, 81:865–942, Jun 2009.

[65] Birger Horstmann, J. Ignacio Cirac, and Géza Giedke. Noise-driven dynamics and phase transitions in fermionic systems. *Phys. Rev. A*, 87:012108, Jan 2013.

[66] Karen V. Hovhannisyan, Martí Perarnau-Llobet, Marcus Huber, and Antonio Acín. Entanglement generation is not necessary for optimal work extraction. *Phys. Rev. Lett.*, 111:240401, Dec 2013.

[67] S. F. Huelga, C. Macchiavello, T. Pellizzari, A. K. Ekert, M. B. Plenio, and J. I. Cirac. Improvement of frequency standards with quantum entanglement. *Phys. Rev. Lett.*, 79:3865–3868, Nov 1997.

[68] Randall G. Hulet and Daniel Kleppner. Rydberg atoms in "circular" states. *Phys. Rev. Lett.*, 51:1430–1433, Oct 1983.

[69] T. Hyart, B. van Heck, I. C. Fulga, M. Burrello, A. R. Akhmerov, and C. W. J. Beenakker. Flux-controlled quantum computation with majorana fermions. *Phys. Rev. B*, 88:035121, Jul 2013.

[70] E. T. Jaynes and F. W. Cummings. Comparison of quantum and semiclassical radiation theories with application to the beam maser. *Proceedings of the IEEE*, 51(1):89–109, 1963.

[71] Robert H. Jonsson, Eduardo Martin-Martinez, and Achim Kempf. Quantum Signalling in Cavity qed. 2013. arXiv:1306.4275 [quant-ph].

[72] F. C. Khanna, J. M. C. Malbouisson, A. E. Santana, and E. S. Santos. Maximum entanglement in squeezed boson and fermion states. *Phys. Rev. A*, 76:022109, Aug 2007.

[73] Tien D. Kieu. The second law, maxwell's demon, and work derivable from quantum heat engines. *Phys. Rev. Lett.*, 93:140403, Sep 2004.

[74] H.J Kimble and D. F. Walls. Squeezed States of the Electromagnetic Field: Introduction to Feature Issue. *J. Opt. Soc. Am. J. B.*, 4:1449, 1987.

[75] P. L. Knight. Squeezed light au - loudon, r. *Journal of Modern Optics*, 34(6-7):709–759, 06 1987.

[76] Kamil Korzekwa, Matteo Lostaglio, Jonathan Oppenheim, and David Jennings. The extraction of work from quantum coherence. *New Journal of Physics*, 18(2):023045, 2016.

[77] Christina V. Kraus, Michael M. Wolf, J. Ignacio Cirac, and Géza Giedke. Pairing in fermionic systems: A quantum-information perspective. *Phys. Rev. A*, 79:012306, Jan 2009.

[78] J. R. Kukliński and J. L. Madajczyk. Strong squeezing in the jaynes-cummings model. *Physical Review A*, 37(8):3175–3178, 04 1988.

[79] Amine Laghaout, Jonas S. Neergaard-Nielsen, Ioannes Rigas, Christian Kragh, Anders Tipsmark, and Ulrik L. Andersen. Amplification of realistic schrödinger-cat-state-like states by homodyne heralding. *Phys. Rev. A*, 87:043826, Apr 2013.

[80] Peter J. Leek. Storing quantum information in schrödinger's cats. *Science*, 342(6158):568–569, 2013.

[81] A. Lenard. Thermodynamical proof of the gibbs formula for elementary quantum systems. *Journal of Statistical Physics*, 19(6):575–586, Dec 1978.

[82] M. Lewenstein, B. Kraus, J. I. Cirac, and P. Horodecki. Optimization of entanglement witnesses. *Phys. Rev. A*, 62:052310, Oct 2000.

[83] R. Loudon and P. L. Knight. Squeezed Light. *Journal of Modern Optics*, 34:6–7,709–759, 1987.

[84] L. Mandel. Sub-poissonian photon statistics in resonance fluorescence. *Optics Letters*, 4(7):205–207, 1979.

[85] P. Marek, H. Jeong, and M. S. Kim. Generating "squeezed" superpositions of coherent states using photon addition and subtraction. *Physical Review A*, 78(6):063811–, 12 2008.

[86] E Martín-Martínez, Ivette Fuentes, and Robert B. Mann. Berry Phase Quantum Thermometer. *New J. Phys.*, 15(053036):1–12, 2013.

[87] Eduardo Martín-Martínez, Ivette Fuentes, and Robert B. Mann. Using berry's phase to detect the unruh effect at lower accelerations. *Phys. Rev. Lett.*, 107:131301, Sep 2011.

[88] Eduardo Martín-Martínez, Miguel Montero, and Marco del Rey. Wavepacket detection with the unruh-dewitt model. *Phys. Rev. D*, 87:064038, Mar 2013.

[89] W.J. Munro Robert Mann Marvellous Onuma-Kalu, Kae Nemoto. Taming an optical schrödinger's cat - a quantum non-demolition approach. 2017. arXiv:1706.09448.

[90] Pierre Meystre. Theoretical developments in cavity quantum optics: a brief review. *Physics Reports*, 219(3):243 – 262, 1992.

[91] C. Moura Alves and D. Jaksch. Multipartite entanglement detection in bosons. *Phys. Rev. Lett.*, 93:110501, Sep 2004.

[92] W. J. Munro, K. Nemoto, G. J. Milburn, and S. L. Braunstein. Weak-force detection with superposed coherent states. *Phys. Rev. A*, 66:023819, Aug 2002.

[93] Michael A. Nielson and Isaac L. Chuang. *Quantum Computation and Quantum Information*. Campbridge University Press, 2010.

[94] G. Nougues, A. Rauschenbeute, S. Osnaghi, M. Brune, J. M. Raimond, and S. Haroche. Seeing a Single Photon Without Destroying It. *Nature*, 400:239–242, 1999.

[95] Marvellous Onuma-Kalu, Daniel Grimmer, Robert B Mann, and Eduardo Martín-Martínez. A classification of markovian fermionic gaussian master equations. 52(43):435302, 2019.

[96] Marvellous Onuma-Kalu and Robert B. Mann. Work extraction using gaussian operations in noninteracting fermionic systems. *Phys. Rev. E*, 98:042121, Oct 2018.

[97] Marvellous Onuma-Kalu, Robert B. Mann, and Eduardo Martín-Martínez. Mode invisibility and single-photon detection. *Phys. Rev. A*, 88:063824, Dec 2013.

[98] Marvellous Onuma-Kalu, Robert B. Mann, and Eduardo Martín-Martínez. Mode invisibility as a quantum nondemolition measurement of coherent light. *Physical Review A*, 90(3):033847–, 09 2014.

[99] Michał Oszmaniec, Jan Gutt, and Marek Kuś. Classical simulation of fermionic linear optics augmented with noisy ancillas. *Phys. Rev. A*, 90:020302, Aug 2014.

[100] J. G. Peixoto de Faria and M. C. Nemes. Dissipative dynamics of the jaynes-cummings model in the dispersive approximation: Analytical results. *Phys. Rev. A*, 59:3918–3925, May 1999.

[101] Martí Perarnau-Llobet, Karen V. Hovhannisyan, Marcus Huber, Paul Skrzypczyk, Nicolas Brunner, and Antonio Acín. Extractable work from correlations. *Phys. Rev. X*, 5:041011, Oct 2015.

[102] M. B. Plenio and S. F. Huelga. Entangled light from white noise. *Phys. Rev. Lett.*, 88:197901, Apr 2002.

[103] M. B. Plenio, S. F. Huelga, A. Beige, and P. L. Knight. Cavity-loss-induced generation of entangled atoms. *Phys. Rev. A*, 59:2468–2475, Mar 1999.

[104] J. Ph. Poizat and P. Grangier. Experimental realization of a quantum optical tap. *Phys. Rev. Lett.*, 70:271–274, Jan 1993.

[105] Tomaž Prosen. Third quantization: a general method to solve master equations for quadratic open fermi systems. *New Journal of Physics*, 10(4):043026, apr 2008.

[106] W. Pusz and S. L. Woronowicz. Passive states and kms states for general quantum systems. *Communications in Mathematical Physics*, 58(3):273–290, Oct 1978.

[107] J M Raimond, M Brune, and Serge Haroche. Manipulating Quantum Entanglement with Atoms and Photons in a Cavity. *Rev. Mod. Phys.*, 73:565–582, 2001.

[108] T. C. Ralph, A. Gilchrist, G. J. Milburn, W. J. Munro, and S. Glancy. Quantum computation with optical coherent states. *Phys. Rev. A*, 68:042319, Oct 2003.

[109] Gerhard Rempe, Herbert Walther, and Norbert Klein. Observation of quantum collapse and revival in a one-atom maser. *Physical Review Letters*, 58(4):353–356, 01 1987.

[110] Benedikt Richter, Krzysztof Lorek, Andrzej Dragan, and Yasser Omar. Effect of acceleration on localized fermionic gaussian states: From vacuum entanglement to maximally entangled states. *Phys. Rev. D*, 95:076004, Apr 2017.

[111] Ángel Rivas, Susana F. Huelga, and Martin B. Plenio. Entanglement and non-markovianity of quantum evolutions. *Phys. Rev. Lett.*, 105:050403, Jul 2010.

[112] Ángel Rivas, Susana F Huelga, and Martin B Plenio. Quantum non-markovianity: characterization, quantification and detection. *Reports on Progress in Physics*, 77(9):094001, aug 2014.

[113] J F Roch, G Roger, P Grangier, J M Courty, and S Reynaud. Quantum Nondemolition Measurements in Optics – a review and some recent experimental results. *Appl. Phys, B.*, 55:291–297, 1992.

[114] R. H. Romer and R. H. Dicke. New technique for high-resolution microwave spectroscopy. *Phys. Rev.*, 99:532–536, Jul 1955.

[115] J.J. Sakurai. *Modern Quantum Mechanics*. Cambridge University Press, 2017.

[116] D. Sarkisyan, T. Varzhapetyan, A. Sarkisyan, Yu. Malakyan, A. Papoyan, A. Lezama, D. Bloch, and M. Ducloy. Spectroscopy in an extremely thin vapor cell: Comparing the cell-length dependence in fluorescence and in absorption techniques. *Phys. Rev. A*, 69:065802, Jun 2004.

[117] W. Schleich, M. Pernigo, and Fam Le Kien. Nonclassical state from two pseudoclassical states. *Phys. Rev. A*, 44:2172–2187, Aug 1991.

[118] E. Schrödinger. Die gegenwärtige situation in der quantenmechanik. *Naturwissenschaften*, 23(48):807–812, 1935.

[119] Marlan O. Scully and Suhail M.Zubairy. *Quantum Optics*. Cambridge University Press, 1997.

[120] Haroche Serge and Raimond Jean-Michel. *Exploring the Quantum Atoms, Cavities, and Photons*. Oxford University Press, 2006.

[121] Raymond A. Serway and Jerry S. Faughn. *College Physics*. Number 1. Saunders college publishing, 1984.

[122] W. Shuai, Z. Xiao-Yan, and F. Hong-Yi. Oscillation Behaviour in the Photon-Number Distribution of Squeezed Coherent States. *Chin. Phys. B.*, 21(5), 2012.

[123] Erik Sjöqvist, Arun K. Pati, Artur Ekert, Jeeva S. Anandan, Marie Ericsson, Daniel K. L. Oi, and Vlatko Vedral. Geometric phases for mixed states in interferometry. *Phys. Rev. Lett.*, 85:2845–2849, Oct 2000.

[124] Paul Skrzypczyk, Anthony J. Short, and Sandu Popescu. Work extraction and thermodynamics for individual quantum systems. *Nature Communications*, 5(1):4185, 2014.

[125] Paul Skrzypczyk, Ralph Silva, and Nicolas Brunner. Passivity, complete passivity, and virtual temperatures. *Physical Review E*, 91(5):052133–, 05 2015.

[126] Carlo Sparaciari, David Jennings, and Jonathan Oppenheim. Energetic instability of passive states in thermodynamics. *Nature Communications*, 8(1):1895, 2017.

[127] Carlo Sparaciari, Jonathan Oppenheim, and Tobias Fritz. Resource theory for work and heat. *Physical Review A*, 96(5):052112–, 11 2017.

[128] Barbara M. Terhal. Bell inequalities and the separability criterion. *Physics Letters A*, 271(5–6):319 – 326, 2000.

[129] The Royal Swedish Academy of Siences. Particle Control in Quantum World, October 2012.

[130] Kip S. Thorne, Ronald W. P. Drever, Carlton M. Caves, Mark Zimmermann, and Vernon D. Sandberg. Quantum nondemolition measurements of harmonic oscillators. *Phys. Rev. Lett.*, 40:667–671, Mar 1978.

[131] Henning Vahlbruch, Moritz Mehmet, Karsten Danzmann, and Roman Schnabel. Detection of 15 db squeezed states of light and their application for the absolute calibration of photoelectric quantum efficiency. *Physical Review Letters*, 117(11):110801–, 09 2016.

[132] V. Vedral and M. B. Plenio. Entanglement measures and purification procedures. *Phys. Rev. A*, 57:1619–1633, Mar 1998.

[133] Anna Vershynina. Complete criterion for convex-gaussian-state detection. *Phys. Rev. A*, 90:062329, Dec 2014.

[134] B. Vlastakis, A. Petrenko, N. Offek, L. Sun, Z. Leghtas, K. Sliwa, Y. Liu, M. Hatridge, J. Blumoff, L. Frunzio, M. Mirrahimi, L. Jiang, M. H. Devoret, and R. J. Schoelkopf. Characterizing entanglement of an artificial atom and a cavity cat state with bell's inequality. *Nature Communications*, 9970, Oct 2015.

[135] Christian Weedbrook, Stefano Pirandola, Raúl García-Patrón, Nicolas J. Cerf, Timothy C. Ralph, Jeffrey H. Shapiro, and Seth Lloyd. Gaussian quantum information. *Rev. Mod. Phys.*, 84:621–669, May 2012.

[136] David J. Wineland. Nobel lecture: Superposition, entanglement, and raising schr\"odinger's cat. *Reviews of Modern Physics*, 85(3):1103–1114, 07 2013.

[137] B. Yurke, W. Schleich, and D. F. Walls. Quantum superpositions generated by quantum nondemolition measurements. *Phys. Rev. A*, 42:1703–1711, Aug 1990.

[138] B. Yurke and D. Stoler. Generating quantum mechanical superpositions of macroscopically distinguishable states via amplitude dispersion. *Phys. Rev. Lett.*, 57:13–16, Jul 1986.

[139] Wojciech H. Zurek, Salman Habib, and Juan Pablo Paz. Coherent states via decoherence. *Phys. Rev. Lett.*, 70:1187–1190, Mar 1993.

[140] Wojciech Hubert Zurek. Decoherence, einselection, and the quantum origins of the classical. *Reviews of Modern Physics*, 75(3):715–775, 05 2003.